

https://dspace.org/

Group invariant solutions for a pre-existing fluid-driven fracture in permeable rock

Fareo, Adewunmi Gideon

2009-05-22T12:18:35Z
http://hdl.handle.net/10539/6973

Downloaded from a DSpace repository. https://dspace.org/

Group Invariant Solutions for a Pre-Existing Fluid-Driven Fracture in Permeable Rock



ADEWUNMI GIDEON FAREO

A dissertation submitted to the Faculty of Science, University of the Witwatersrand, Johannesburg, South Africa, in fulfilment of the requirements for the degree of Master of Science.

Declaration

I declare that this dissertation is my own unaided work. It is being submitted for the degree of Masters of Science at the University of the Witwatersrand, Johannesburg. It has not been submitted before for any degree or examination at any other university.

Fareo Adewunmi Gideon

23nd day of February 2008

Abstract

The propagation of a two-dimensional fluid-driven pre-existing fluid-filled fracture in permeable rock by the injection of a viscous, incompressible Newtonian fluid is considered. The fluid flow in the fracture is laminar. By the application of lubrication theory, a partial differential equation relating the half-width of the fracture to the fluid pressure and leak-off velocity is obtained. The leak-off velocity is an unspecified function whose form is derived from the similarity solution. The model is closed by the adoption of the PKN formulation in which the fluid pressure is proportional to the fracture half-width. The constant of proportionality depends on the material properties of the rock through its Young modulus and Poisson ratio . The group invariant solutions obtained describe hydraulic fracturing in a permeable rock. Results are also obtained for the case in which the rock is impermeable. Applications in which the rate of fluid injection into the fracture and the pressure at the fracture entry are independent of time are analysed. The limiting solution in which the fracture length and fracture half-width grow exponentially with time is derived. Approximate power law solutions for large values of time for the fracture length and volume are derived. Finally, the case in which the fluid is injected by a pump working at a constant rate is investigated. The results are illustrated by computer generated graphs.

Acknowledgements

My uttermost appreciation goes to God Almighty who has made it possible for me to complete my Master's dissertation.

I am very grateful to my supervisor, Prof David Paul Mason for his support throughtout my academic programme. His diligent lifestyle has taught me that nothing else does it better. He showed me ways to approach a research problem and the need to be persistent so as to obtain results. His encouragement and confidence in me is a source of synergy which has driven me throughout my academic programme.

A special thanks also goes to Prof Momoniat and Prof Fazer for their attention granted me whenever I needed it and also their interest in the progress of my work. I would also like to thank Prof Grae Worster for his help and encouragement.

I gratefully acknowledge the financial assistance that was provided by the African Institute for Mathematical Sciences(AIMS), CapeTown and the School of Computational and Applied Mathematics of the University of the Witwatersrand, Johannesburg.

Contents

1 INTRODUCTION **1**

1.1 Introduction 1

1.2 Hydraulic fracturing 1

1.2.1 Lubrication theory and elasticity equations 3

1.3 Dynamics of fracture width 3

1.4 Literature review 4

1.5 Fracture geometry models 5

1.5.1 The PKN model 5

1.5.2 The KGD or plane strain model 6

1.5.3 The Penny-shape or radial model. 6

1.6 Mathematical method of solution 8

1.7 Numerical methods 9

1.8 Outline of research work 9

2 BACKGROUND **11**

2.1 Introduction 11

2.2 Lie point symmetries 11

2.3 Lie's equations 12

2.4 Group invariant solutions 13

2.5 Thin fluid film approximation 14

3 TWO DIMENSIONAL HYDRAULIC FRACTURE IN PERMEABLE ROCK **16**

3.1 Introduction 16

3.2 Thin fluid film equations for the flow in a two-dimensional fracture 17
3.3 Mathematical formulation 20
3.4 Governing equations 21
3.4.1 Fluid problem: Lubrication theory 21
3.4.2 Initial and boundary conditions 22
3.5 Nonlinear diffusion equation with leak-off term 26
3.6 Lie point symmetries and general properties of group invariant solutions . . . 29
3.7 Special values for the ratio $\frac{c_3}{c_2}$ 36
3.7.1 Length of the fracture 36
3.7.2 Total volume of the fracture 37
3.7.3 Pressure at the fracture entry 37
3.7.4 Rate of working of the pressure at the fracture entry 38
3.7.5 Rate of fluid injection into the fracture 38
3.7.6 Rate of fluid leak-off at the fluid/rock interface 39
3.7.7 Balance law for flux of fluid 39

4 LEAK-OFF VELOCITY PROPORTIONAL TO FRACTURE HALF-WIDTH 41
4.1 Introduction 41
4.2 Leak-off velocity proportional to half-width of fracture 42
4.3 Exact solution for zero fluid injection rate at fracture entry 45
4.4 Discussion of results for $\beta = \frac{1}{3}\left(\frac{c_2}{c_3} - 5\right)$ 47
4.4.1 Fracture length and volume 49
4.4.2 Fracture half-width and leak-off velocity 52
4.5 Exact solution for non-zero fluid injection rate at fracture entry 62
4.6 Discussion of results for $\beta = \frac{1}{3}\left(\frac{c_2}{c_3} - 1\right)$ 65
4.6.1 Fracture length and volume 65
4.6.2 Fracture half-width and leak-off velocity 69
4.7 Transformation of boundary value problem into two initial value problems . . 77
4.8 Numerical solution 82
4.9 Numerical Results 86

4.9.1 Physical significance of curves 86
4.9.2 Graphical results for fixed $\frac{c_3}{c_2}$ and varying values of β 90
4.9.3 Graphical results for fixed β and varying values of $\frac{c_3}{c_2}$ 98
4.10 Conclusion 106

5 LEAK-OFF VELOCITY PROPORTIONAL TO GRADIENT OF FRACTURE HALF-WIDTH 109

5.1 Introduction 109
5.2 Leak-off velocity proportional to gradient of fluid-rock interface 110
5.3 Exact analytical solutions: Case 1 112
5.3.1 Fracture length and volume 117
5.3.2 Fracture half-width and leak-off velocity 118
5.4 Exact analytical solutions: Case 2 125
5.5 Discussion of results for $\beta = 1 - \frac{c_2}{c_3}$ 127
5.5.1 Fracture length and volume 129
5.5.2 Fracture half-width and leak-off velocity 130
5.6 Transformation of boundary value problem to two initial value problems 138
5.7 Numerical solution 143
5.8 Numerical Results 144
5.8.1 Graphical results for fixed $\frac{c_3}{c_2}$ and varying values of β 147
5.8.2 Graphical results for fixed β and varying values of $\frac{c_3}{c_2}$ 155
5.9 Conclusions 162

6 Conclusions 164

Appendix A 168

Appendix B 175

Bibliography 181

List of Figures

1.5.1 The PKN model. 6

1.5.2 The KGD model. 7

1.5.3 The penny-shaped or radial model. Q_0 is the fluid flux. 7

2.5.1 Thin film of viscous incompressible fluid of characteristic thickness H and characteristic lenght L 15

3.2.1 A crack propagating in an elastic permeable medium(the coordinate direction y points into the page). The leak-off velocity, v_n, is perpendicular to the interface. 17

3.4.1 Tangent plane at a point on the surface, $z = h(x,t)$. 23

3.4.2 Tangent plane at a point on the surface, $z = -h(x,t)$. 23

4.4.1 Graph of $\beta = \frac{\frac{5}{3}\left(\frac{1}{5}-\frac{c_3}{c_2}\right)}{\frac{c_3}{c_2}}$ plotted against $\frac{c_3}{c_2}$ for the range $-2 < \frac{c_3}{c_2} < 2$. 49

4.4.2 Leak-off velocity proportional to fracture half-width: Graph of fracture length $L(t)$ given by (4.3.16) and (4.3.24) plotted against t for a selection of values of the parameter $\frac{c_3}{c_2}$ and for $\frac{V_0}{I} = 1$. 50

4.4.3 Leak-off velocity proportional to fracture half-width: Total volume of the fracture $\frac{V(t)}{V_0}$ given by (4.3.15) and (4.3.23) plotted against t for a selection of values of the parameter $\frac{c_3}{c_2}$ and for $\frac{V_0}{I} = 1$. 51

4.4.4 (a) Fracture half-width, $h(x,t)$, given by (4.3.17) and (b) leak-off velocity at the fluid/rock interface, $v_n(x,t)$, given by (4.3.18), plotted against x for a range of values of t and for $\frac{c_3}{c_2} = 0.0008$, $\beta = 415$. 54

4.4.5 (a) Fracture half-width, $h(x,t)$, given by (4.3.17) and (b) leak-off velocity at the fluid/rock interface, $v_n(x,t)$, given by (4.3.18), plotted against x for a range of values of t and for $\frac{c_3}{c_2} = 0.1$, $\beta = 1.66$. 55

4.4.6 Fracture halfwidth, $h(x,t)$, given by (4.3.17) plotted against x for a range of values of t and for $\frac{c_3}{c_2} = 0.2$, $\beta = 0$. The leak-off velocity at the fluid/rock interface, $v_n(x,t)$, given by (4.3.18) is zero. 56

4.4.7 (a) Fracture half-width, $h(x,t)$, given by (4.3.17) and (b) leak-off velocity at the fluid/rock interface, $v_n(x,t)$, given by (4.3.18), plotted against x for a range of values of t and for $\frac{c_3}{c_2} = 0.5$, $\beta = -1$. 57

4.4.8 (a) Fracture half-width, $h(x,t)$, given by (4.3.17) and (b) leak-off velocity at the fluid/rock interface, $v_n(x,t)$, given by (4.3.18), plotted against x for a range of values of t and for $\frac{c_3}{c_2} = 2$, $\beta = -1.5$. 58

4.4.9 (a) Fracture half-width, $h(x,t)$, given by (4.3.17) and (b) leak-off velocity at the fluid/rock interface, $v_n(x,t)$, given by (4.3.18), plotted against x for a range of values of t and for $\frac{c_3}{c_2} = 5$, $\beta = -1.6$. 59

4.4.10 (a) Fracture half-width, $h(x,t)$, given by (4.3.25) and (b) leak-off velocity at the fluid/rock interface, $v_n(x,t)$, given by (4.3.26), plotted against x for a range of values of t and for $\frac{c_3}{c_2} = \infty$, $\beta = -1.66$. 60

4.4.11 (a) Fracture half-width, $h(x,t)$, given by (4.3.17) and (b) leak-off velocity at the fluid/rock interface, $v_n(x,t)$, given by (4.3.18), plotted against x for a range of values of t and for $\frac{c_3}{c_2}$ = -1, β = -2. 61

4.6.1 Graph of $\beta = \frac{\left(1-\frac{c_3}{c_2}\right)}{3\frac{c_3}{c_2}}$ against $\frac{c_3}{c_2}$ for the range $-2 < \frac{c_3}{c_2} < 2$. 66

4.6.2 Leak-off velocity proportional to fracture half-width: Graph of fracture length, $L(t)$, given by (4.5.18) and (4.5.25) plotted against t for $V_0 = 1$ and a selection of values of the parameter $\frac{c_3}{c_2}$. 67

4.6.3 Leak-off velocity proportional to fracture half-width: Total volume of the fracture, $\frac{V}{V_0}(t)$, given by (4.5.17) and (4.5.24) plotted against t for $V_0 = 1$ and a selection of values of $\frac{c_3}{c_2}$. 68

4.6.4 (a) Fracture half-width, $h(x,t)$, given by (4.5.19) and (b) leak-off velocity at the fluid/rock interface, $v_n(x,t)$, given by (4.5.20), plotted against x for a range of values of t and for $\frac{c_3}{c_2} = 10^{-5}$, $\beta = 33333$. 71

4.6.5 (a) Fracture half-width, $h(x,t)$, given by (4.5.19) and (b) leak-off velocity at the fluid/rock interface, $v_n(x,t)$, given by (4.5.20), plotted against x for a range of values of t and for $\frac{c_3}{c_2} = 0.5$, $\beta = 0.33$. 72

4.6.6 Fracture half-width, $h(x,t)$, given by (4.5.19) plotted against x for a range of values of t and for $\frac{c_3}{c_2} = 1$, $\beta = 0$. The leak-off velocity at the fluid/rock interface, $v_n(x,t)$, given by (4.5.20), is zero. 73

4.6.7 (a) Fracture half-width, $h(x,t)$, given by (4.5.19) and (b) leak-off velocity at the fluid/rock interface, $v_n(x,t)$, given by (4.5.20), plotted against x for a range of values of t and for $\frac{c_3}{c_2} = 2$, $\beta = -0.166$. 74

4.6.8 (a) Fracture half-width, $h(x,t)$, given by (4.5.26) and (b) leak-off velocity at the fluid/rock interface, $v_n(x,t)$, given by (4.5.27), plotted against x for a range of values of t and for $\frac{c_3}{c_2} = \infty$, $\beta = -0.33$. 75

4.6.9 (a) Fracture half-width, $h(x,t)$, given by (4.5.19) and (b) leak-off velocity at the fluid/rock interface, $v_n(x,t)$, given by (4.5.20), plotted against x for a range of values of t and for $\frac{c_3}{c_2} = -1$, $\beta = -0.66$. 76

4.9.1 Curves for the analytical solutions and the limiting curve 89

4.9.2 Graphs for $\frac{c_3}{c_2} = 0.1$ and a selection of values of β : (a) Fracture length $L(t)$ plotted against time; (b) Fracture half-width $h(x,t)$ plotted against x at time $t = 50$; (c) Leak-off fluid velocity $v_n(x,t)$ plotted against x at time $t = 50$. 93

4.9.3 Graphs for $\frac{c_3}{c_2} = 0.2$ and a selection of values of β : (a) Fracture length $L(t)$ plotted against time; (b) Fracture half-width $h(x,t)$ plotted against x at time $t = 50$; (c) Leak-off fluid velocity $v_n(x,t)$ plotted against x at time $t = 50$. 94

4.9.4 Graphs for $\frac{c_3}{c_2} = 0.5$ and a selection of values of β : (a) Fracture length $L(t)$ plotted against time; (b) Fracture half-width $h(x,t)$ plotted against x at time $t = 50$; (c) Leak-off fluid velocity $v_n(x,t)$ plotted against x at time $t = 50$. 95

4.9.5 Graphs for $\frac{c_3}{c_2} = 0.8$ and a selection of values of β : (a) Fracture length $L(t)$ plotted against time; (b) Fracture half-width $h(x,t)$ plotted against x at time $t = 50$; (c) Leak-off fluid velocity $v_n(x,t)$ plotted against x at time $t = 50$. 96

4.9.6 Graphs for $\frac{c_3}{c_2} = 1$ and a selection of values of β : (a) Fracture length $L(t)$ plotted against time; (b) Fracture half-width $h(x,t)$ plotted against x at time $t = 50$; (c) Leak-off fluid velocity $v_n(x,t)$ plotted against x at time $t = 50$. 97

4.9.7 Graphs for $\beta = -2$ and a selection of values of $\frac{c_3}{c_2}$: (a) Fracture length $L(t)$ plotted against time; (b) Fracture half-width $h(x,t)$ plotted against x at time $t = 50$; (c) Leak-off fluid velocity $v_n(x,t)$ plotted against x at time $t = 50$. 100

4.9.8 Graphs for $\beta = -1$ and a selection of values of $\frac{c_3}{c_2}$: (a) Fracture length $L(t)$ plotted against time; (b) Fracture half-width $h(x,t)$ plotted against x at time $t = 50$; (c) Leak-off fluid velocity $v_n(x,t)$ plotted against x at time $t = 50$. 101

4.9.9 Graphs for $\beta = 0$ and a selection of values of $\frac{c_3}{c_2}$: (a) Fracture length $L(t)$ plotted against time ; (b) Fracture half-width $h(x,t)$ plotted against x at time $t = 50$. The leak-off velocity $v_n(x,t) = 0$ 102

4.9.10 Graphs for $\beta = 1$ and a selection of values of $\frac{c_3}{c_2}$: (a) Fracture length $L(t)$ plotted against time; (b) Fracture half-width $h(x,t)$ plotted against x at time $t = 50$; (c) Leak-off fluid velocity $v_n(x,t)$ plotted against x at time $t = 50$. 103

4.9.11 Graphs for $\beta = 2$ and a selection of values of $\frac{c_3}{c_2}$: (a) Fracture length $L(t)$ plotted against time; (b) Fracture half-width $h(x,t)$ plotted against x at time $t = 50$; (c) Leak-off fluid velocity $v_n(x,t)$ plotted against x at time $t = 50$. 104

4.9.12 Graphs for $\beta = 5$ and a selection of values of $\frac{c_3}{c_2}$: (a) Fracture length $L(t)$ plotted against time; (b) Fracture half-width $h(x,t)$ plotted against x at time $t = 50$; (c) Leak-off fluid velocity $v_n(x,t)$ plotted against x at time $t = 50$. 105

5.3.1 Curves for the analytical solutions and the limiting curve. 116

5.3.2 Leak-off velocity proportional to gradient of fracture half-width: Graph of fracture length $L(t)$ given by (5.3.16) plotted against t for a selection of values of the parameter $\frac{c_3}{c_2}$ and for $\frac{V_0}{I} = 1$. 117

5.3.3 Leak-off velocity proportional to gradient of fracture half-width: Graph of fracture volume $\frac{V(t)}{V_0}$ given by (5.3.15) plotted against t for a selection of values of the parameter $\frac{c_3}{c_2}$ and for $\frac{V_0}{I} = 1$. 118

5.3.4 (a) Fracture half-width, $h(x,t)$, given by (5.3.17) and (b) leak-off velocity at the fluid/rock interface, $v_n(x,t)$, given by (5.3.18), plotted against x for a range of values of t and for $\frac{c_3}{c_2} = 0.1$, $\beta = 1.66$. 120

5.3.5 (a) Fracture half-width, $h(x,t)$, given by (5.3.17) plotted against x for a range of values of t and for $\frac{c_3}{c_2} = 0.2$, $\beta = 0$. The leak-off velocity at the fluid/rock interface, $v_n(x,t)$, given by (5.3.18) is zero. 121

5.3.6 (a) Fracture half-width, $h(x,t)$, given by (5.3.17) and (b) leak-off velocity at the fluid/rock interface, $v_n(x,t)$, given by (5.3.18), plotted against x for a range of values of t and for $\frac{c_3}{c_2} = 0.3$, $\beta = -0.55$. 122

5.3.7 (a) Fracture half-width, $h(x,t)$, given by (5.3.17) and (b) leak-off velocity at the fluid/rock interface, $v_n(x,t)$, given by (5.3.18), plotted against x for a range of values of t and for $\frac{c_3}{c_2} = 0.4$, $\beta = -0.833$. 123

5.3.8 (a) Fracture half-width, $h(x,t)$, given by (5.3.17) and (b) leak-off velocity at the fluid/rock interface, $v_n(x,t)$, given by (5.3.18), plotted against x for a range of values of t and for $\frac{c_3}{c_2} = 0.499$, $\beta = -0.99$. 124

5.5.1 Leak-off velocity proportional to gradient of fracture half-width and $\beta = 1 - \frac{c_2}{c_3}$. Rate of fluid injection at entry, $q_1(t)$, given by (5.5.1) plotted against t for $\frac{c_3}{c_2} = 0.51, 0.6, 0.8, 1, 2$ and for $V_0 = 1$ and $\Lambda = 1$. 128

5.5.2 Leak-off velocity proportional to gradient of fracture half-width and $\beta = 1 - \frac{c_2}{c_3}$. Rate of fluid leak-off at fluid/rock interface, $q_2(t)$, given by (5.5.2) plotted against t for $\frac{c_3}{c_2} = 0.51, 0.6, 0.8, 1, 2$ and for $V_0 = 1$ and $\Lambda = 1$. 128

5.5.3 Leak-off velocity proportional to gradient of fracture half-width: Graph of fracture length $L(t)$ given by (5.4.14) plotted against t for a selection of values of the parameter $\frac{c_3}{c_2}$ and for $V_0 = 1$. 130

5.5.4 Leak-off velocity proportional to gradient of fracture half-width: Total volume of the fracture $\frac{V(t)}{V_0}$ given by (5.4.15) plotted against t for a selection of values of the parameter $\frac{c_3}{c_2}$ and for $V_0 = 1$. 131

5.5.5 (a) Fracture half-width, $h(x,t)$, given by (5.4.16) and (b) leak-off velocity at the fluid/rock interface, $v_n(x,t)$, given by (5.4.17), plotted against x for a range of values of t and for $\frac{c_3}{c_2} = 0.51$, $\beta = -0.96$. 133

5.5.6 (a) Fracture half-width, $h(x,t)$, given by (5.4.16) and (b) leak-off velocity at the fluid/rock interface, $v_n(x,t)$, given by (5.4.17), plotted against x for a range of values of t and for $\frac{c_3}{c_2} = 0.6$, $\beta = -0.66$. 134

5.5.7 (a) Fracture half-width, $h(x,t)$, given by (5.4.16) and (b) leak-off velocity at the fluid/rock interface, $v_n(x,t)$, given by (5.4.17), plotted against x for a range of values of t and for $\frac{c_3}{c_2} = 0.7$, $\beta = -0.42$. 135

5.5.8 (a) Fracture half-width, $h(x,t)$, given by (5.4.16) and (b) leak-off velocity at the fluid/rock interface, $v_n(x,t)$, given by (5.4.17), plotted against x for a range of values of t and for $\frac{c_3}{c_2} = 0.8$, $\beta = -0.25$. 136

5.5.9 (a) Fracture half-width, $h(x,t)$, given by (5.4.16) and (b) leak-off velocity at the fluid/rock interface, $v_n(x,t)$, given by (5.4.17), plotted against x for a range of values of t and for $\frac{c_3}{c_2} = 0.9$, $\beta = -0.11$. 137

5.5.10 (a) Fracture half-width, $h(x,t)$, given by (5.4.16) plotted against x for a range of values of t and for $\frac{c_3}{c_2} = 1.0$, $\beta = 0$. The leak-off velocity $v_n = 0$ and the rock is impermeable. 138

5.8.1 Graphs for $\frac{c_3}{c_2} = 0.1$ and a selection of values of β : (a) Fracture length $L(t)$ plotted against time; (b) Fracture half-width $h(x,t)$ plotted against x at time $t = 50$; (c) Leak-off fluid velocity $v_n(x,t)$ plotted against x at time $t = 50$. 149

5.8.2 Graphs for $\frac{c_3}{c_2} = 0.125$ and a selection of values of β : (a) Fracture length $L(t)$ plotted against time; (b) Fracture half-width $h(x,t)$ plotted against x at time $t = 50$; (c) Leak-off fluid velocity $v_n(x,t)$ plotted against x at time $t = 50$. 150

5.8.3 Graphs for $\frac{c_3}{c_2} = 0.2$ and a selection of values of β : (a) Fracture length $L(t)$ plotted against time; (b) Fracture half-width $h(x,t)$ plotted against x at time $t = 50$; (c) Leak-off fluid velocity $v_n(x,t)$ plotted against x at time $t = 50$. 151

5.8.4 Graphs for $\frac{c_3}{c_2} = 0.5$ and a selection of values of β : (a) Fracture length $L(t)$ plotted against time; (b) Fracture half-width $h(x,t)$ plotted against x at time $t = 50$; (c) Leak-off fluid velocity $v_n(x,t)$ plotted against x at time $t = 50$. 152

5.8.5 Graphs for $\frac{c_3}{c_2} = 0.8$ and a selection of values of β : (a) Fracture length $L(t)$ plotted against time; (b) Fracture half-width $h(x,t)$ plotted against x at time $t = 50$; (c) Leak-off fluid velocity $v_n(x,t)$ plotted against x at time $t = 50$. 153

5.8.6 Graphs for $\frac{c_3}{c_2} = 1$ and a selection of values of β : (a) Fracture length $L(t)$ plotted against time; (b) Fracture half-width $h(x,t)$ plotted against x at time $t = 50$; (c) Leak-off fluid velocity $v_n(x,t)$ plotted against x at time $t = 50$. 154

5.8.7 Graphs for $\beta = -0.9$ and a selection of values of $\frac{c_3}{c_2}$: (a) Fracture length $L(t)$ plotted against time; (b) Fracture half-width $h(x,t)$ plotted against x at time $t = 50$; (c) Leak-off fluid velocity $v_n(x,t)$ plotted against x at time $t = 50$. 157

5.8.8 Graphs for $\beta = -0.5$ and a selection of values of $\frac{c_3}{c_2}$: (a) Fracture length $L(t)$ plotted against time; (b) Fracture half-width $h(x,t)$ plotted against x at time $t = 50$; (c) Leak-off fluid velocity $v_n(x,t)$ plotted against x at time $t = 50$. 158

5.8.9 Graphs for $\beta = 0$ and a selection of values of $\frac{c_3}{c_2}$: (a) Fracture length $L(t)$ plotted against time; (b) Fracture half-width $h(x,t)$ plotted against x at time $t = 50$. The leak-off velocity, $v_n(x,t)$, is zero for all values of $\frac{c_3}{c_2}$ and the rock is impermeable. . 159

5.8.10 Graphs for $\beta = 1$ and a selection of values of $\frac{c_3}{c_2}$: (a) Fracture length $L(t)$ plotted against time; (b) Fracture half-width $h(x,t)$ plotted against x at time $t = 50$; (c) Leak-off fluid velocity $v_n(x,t)$ plotted against x at time $t = 50$. 160

5.8.11 Graphs for $\beta = 5$ and a selection of values of $\frac{c_3}{c_2}$: (a) Fracture length $L(t)$ plotted against time; (b) Fracture half-width $h(x,t)$ plotted against x at time $t = 50$; (c) Leak-off fluid velocity $v_n(x,t)$ plotted against x at time $t = 50$. 161

Chapter 1

INTRODUCTION

1.1 Introduction

A particular class of fractures in rock develops as a result of internal pressurisation by a viscous fluid. These fractures are either man-made hydraulic fractures created by injecting a viscous fluid from a bore hole into the subsurface reservoir rock in order to increase production from oil and gas reservoirs or natural fractures such as kilometers-long volcanic dykes driven by magma coming from the upper mantle beneath the Earth's crust or fissures in rocks in mining opened up by the use of ultra high pressure water.

The problem of a pre-existing fluid-driven fracture propagating in rock, either permeable or not, arises in hydraulic fracturing, a technique widely used in the petroleum and mining industries, as well as in the formation of sills and dykes and in magma transport in the Earth's crust by means of magma-driven fractures. In this dissertation, we will investigate the problem of a pre-existing fluid-driven fracture propagating in permeable rock.

1.2 Hydraulic fracturing

Hydraulic fracturing is a technique which was first introduced in the 1940's and has proved to be a very useful and standard technique for the enhancement of the production of oil and natural gas from a reservoir rock and for the opening up of fissures in rocks in mining. It occurs naturally in the formation of intrusive dykes and sills in the Earth's crust[1]. In this technique,

ultra high pressure fluid, usually water with some additive substances to increase viscosity, is injected into the underground reservoir rock. For tensile cracks to form, the pressure created by the fluid must exceed the fracture toughness of the rock. Hence, new fractures are created and existing ones are opened up. Sand grains, aluminium pellets, glass beads, or similar materials are carried in suspension by the fluid into the fractures. These are called propping agents or proppants. When the pressure is released at the surface, the fracturing fluid returns to the wellbore as the fractures partially close on the proppants, leaving paths with increased permeability for fluid flow.

In the mining industry, the use of explosives, usually dynamite, to break unmined rock poses several problems which include:

- the creation of solid particles of small dimensions (radius $1\mu m$) in the working atmosphere which are very harmful to the lungs as they are too small to be ejected by coughing and too large to pass through the alveoli,
- high level of destructiveness in which a great deal of chemical energy is wasted in the form of noise and vibrations,
- the blasting site has to be cleared of personnel during the blasting operation.

In the petroleum industry, the process of hydrocarbon recovery from the subsurface reservoir rock involves the flow of oil and gas from the reservoir into the wellbore and then to the surface. This process of hydraulic fracturing consists of pumping a fluid into the wellbore in order to enlarge a pre-existing fracture and facilitate the flow of oil and gas through the rock formation. The main concept in hydraulic fracturing is to induce a crack in the rock formation to facilitate the flow of oil and gas through the formation. Hence hydraulic fracturing has proved to be an alternative method for the breaking of rocks in the mining industry and in the opening up of fissures for hydrocarbon recovery in the petroleum industry.

Modelling hydraulic fracturing of rocks requires consideration of both fluid and solid mechanics.

- On the one hand, the lubrication equations to characterize the flow of fluid in the thin fracture and

- on the other, the elasticity equations to describe the deformation and propagation of the fracture.

1.2.1 Lubrication theory and elasticity equations

Lubrication theory is the analysis of fluid in thin layers. For an incompressible fluid, it becomes applicable in the governing of fluid flow in the fracture on the assumption that the ratio of the fracture half-width, H, to the length of the fracture, L, is much less than one. This concept is dealt with extensively in Chapter 2.

The elasticity equations which control the rock deformation produced by the internal fluid pressure in the fracture are also applicable because many investigators[2] have shown that rocks behave elastically over some range of stress. Obviously, if the compressive stress applied on a rock exceeds some limiting value, the rock will fail in tension. In a similar manner, there are some limiting shear stresses that can be imposed upon rocks. The shear conditions that will lead to failure have been discussed in Hubbert and Willis[3]. When fracturing hydraulically, and when pressure due to the injected fluid is applied rapidly, most rocks will fail in a brittle or ductile manner. A rock behaves in a ductile manner if it is able to support an increasing load as it deforms. When the load supported by the rock decreases as the strain increases, the rock is then said to be in a brittle state. A rock exhibits either of these two types of behaviour in a range of stresses which depend essentially on the mineralogy, microstructure, and also on factors such as temperature[4].

1.3 Dynamics of fracture width

Under static conditions, fractures will be very narrow. If fluid is injected at reasonable pump-rates into narrow fractures under high injection pressure, the fracture walls are forced apart. As the fracture width increases, the pressure necessary to keep the fracture propagating will have to increase, otherwise the fracture width will remain small. This is easily seen from the PKN model which states that

$$p = \Lambda h(x,t), \tag{1.3.1}$$

where Λ is a constant that is determined from the material properties of the rock[5]. Also,

$$p = p_f - \sigma_0 \tag{1.3.2}$$

is the net pressure of the fluid, p_f, the internal fluid pressure and σ_0 is the far-field compressive stress perpendicular to the fracture and $h(x,t)$ is the half-width of the fracture. One of the important possible predictions of the PKN theory is the behaviour to be expected when there is no fluid injection into the fracture at the fracture entry. This is investigated in this dissertation.

1.4 Literature review

In the last half century a significant amount of work has been done in the mathematical modelling of hydraulic fractures in rocks. Some of the work involves modelling fluid-driven fracture in permeable rock while some is in impermeable rock. These models, which aim at calculating the net fluid pressure, leak-off, opening, size and shape of the fracture given the properties of the rock, injection rate and fluid characteristics, have to account for the primary physical mechanisms involved, namely, deformation of the rock, fracturing or creation of new surfaces in the rock, flow of viscous fluid in the fracture and leak-off of the fracturing fluid into the permeable rock.

A number of significant contributions have been made to the solution of the fluid-driven fracture problem in the past fifty years. Some of these are analytical models with analytical solutions while others are numerical models with numerical solutions.

Earlier work on mathematical modelling of hydraulic fractures involved finding approximate solutions for simple fracture geometries[1, 6, 7, 8]. Recent work has been concerned with developing numerical algorithms to simulate three dimensional propagation of hydraulic fractures[9, 10]. One of the first analytical solutions was developed by Perkins and Kern[6]. Their model, called the PK model, adapted the classic plane strain crack solution of Sneddon and Elliot[11]. An extension of the work by Perkins and Kern was made by Nordgren[7] and is called the PKN model. In the PKN model, the effect of fluid loss into the surrounding rock mass was investigated.

Another model, known as the KGD model was developed by Khristianovic and Zheltov[8]

and also by Geertsma and de Klerk[12]. The geometry and properties of these models are discussed in Section 1.5 that follows.

A major contribution was made by Spence and Sharp [13] towards the mathematical modelling of fluid-driven fractures. They initiated the work on self-similar solutions and scaling for a KGD crack propagating in an elastic, impermeable medium with finite toughness. The toughness of a rock is a quantitative value that represents its resistance to fracture when exposed to a high strain rate impact stress.

A new direction of analytical study is based on the application of Lie group analysis to the investigation of problems arising from pre-existing fluid-driven fracturing of rock. The group invariant solution for a pre-existing fluid-driven fracture in an impermeable rock has been derived using the Lie point symmetries of the nonlinear partial differential equation for the half-width of the fracture[5]. The research work of this dissertation investigates applying Lie group analysis to the problem of a pre-existing fluid driven fracture in permeable rock.

1.5 Fracture geometry models

A number of fracture geometry models have previously been proposed for the process of hydraulic fracturing in rock. These models are two-dimensional and they arose in the early 1960's from the need to have analytical solutions to the complex solid and fluid mechanics interaction, given the properties of the rock, injection rate and fluid characteristics. These analytical solutions are for the fluid pressure, leak-off, opening, size and shape of the fracture. It is worth noting that most models proposed in hydraulic fracturing consider planar fractures rather than kinked or curved ones[14, 15, 16].

1.5.1 The PKN model

This model was developed by Perkins and Kern[6] and Norgren[7]. It makes the assumption that the fracture has a constant height and an elliptical cross-section as shown in Figure 1.5.1. It also assumes that the fluid flow and fracture propagation are one-dimensional in a direction perpendicular to the elliptic cross-section. The fluid pressure is taken to be constant in the

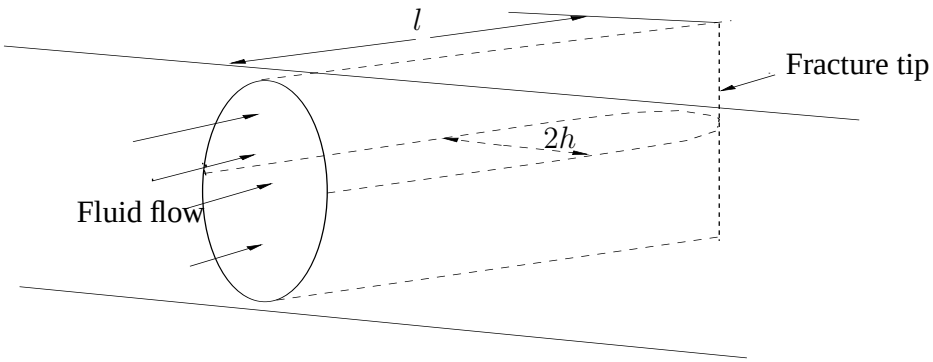


Figure 1.5.1: The PKN model.

vertical plane perpendicular to the direction of propagation and it is also assumed that the fluid pressure in the fracture decreases towards the fracture tip so that, at the tip, the fluid pressure equals the compressive stress.

1.5.2 The KGD or plane strain model

This model was developed by Khristianovic and Zheltov[8] and Geertsma and de Klerk[12]. This model assumes that the fracture deformation and propagation evolve in a situation of plane strain. Fluid flow in the fracture and the fracture propagation are assumed to be one-dimensional and fracture height is constant, each horizontal plane deforming independently, as shown in Figure 1.5.2.

1.5.3 The Penny-shape or radial model.

In this model, the fracture propagates within a given plane and is symmetrical with respect to the point at which fluid is injected as shown in Figure 1.5.3.

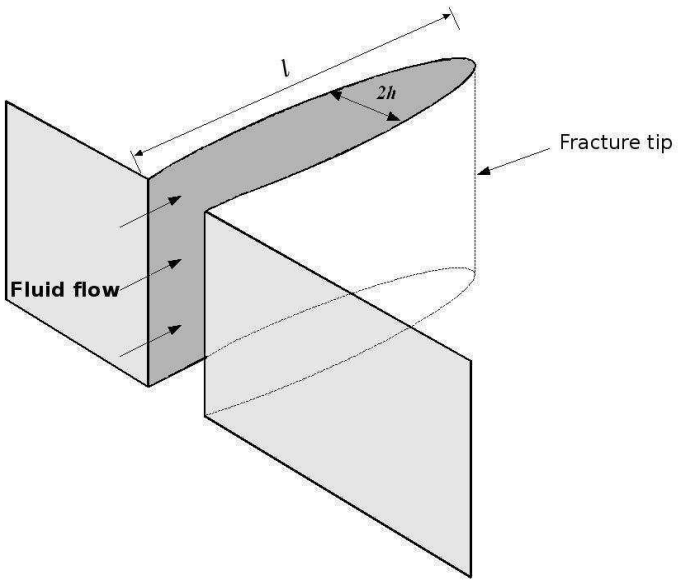


Figure 1.5.2: The KGD model.

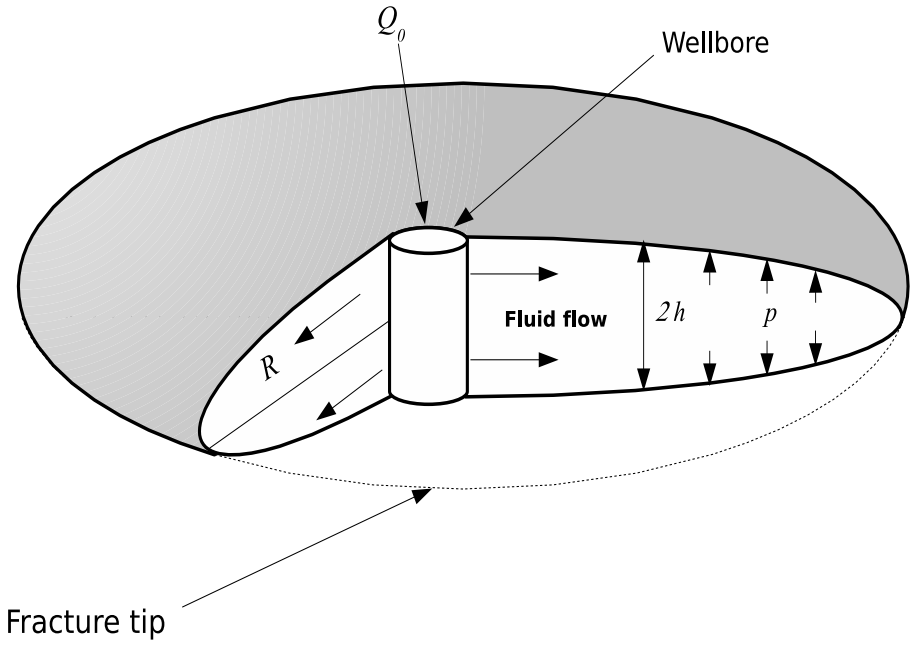


Figure 1.5.3: The penny-shaped or radial model. Q_0 is the fluid flux.

1.6 Mathematical method of solution

Modelling the problem of a pre-existing fluid-driven fracture in impermeable rock using the PKN theory results in a nonlinear partial differential equation. This equation is a nonlinear diffusion equation.

In this dissertation, we investigate the case when the rock in question is permeable. This implies that the fluid injected into the fracture leaks off into the surrounding rock. The leak-off plays a crucial role in the overall reaction of the rock to the pressure of the fluid being injected. For the case in which the rock is permeable, the nonlinear diffusion equation contains a leak-off term, $\boldsymbol{v_n}$. This further complicates the solution of the nonlinear partial differential equation which now has two dependent variables and two independent variables.

A good way of obtaining analytical solutions of this nonlinear diffusion equation is to use Lie group analysis. In this technique, we derive the Lie point symmetries of the partial differential equation. The existence of these Lie point symmetries leads to the leak-off velocity, $\boldsymbol{v_n}$, satisfying a first order linear partial differential equation. The fluid flow in the fracture obeys the Navier-Stokes and mass conservation equations. Lubrication theory is used to simplify the equation governing the fluid motion in the fracture[17]. This simplification stems from the fact that the characteristic half-width, H, of the fracture, is small compared to the characteristic length, L, of the fracture; that is

$$\frac{H}{L} << 1. \tag{1.6.1}$$

It is also assumed that

$$Re\left(\frac{H}{L}\right)^2 << 1, \tag{1.6.2}$$

which implies that the inertia term in the Navier-Stokes equation can be neglected. In (1.6.2), Re is the Reynolds number defined by

$$Re = \frac{UL}{\nu}, \tag{1.6.3}$$

where U is the characteristic fluid velocity in the direction of propagation of the fracture and ν is the kinematic viscosity of the fluid. Lubrication theory is developed in Chapter 2. The invariant solutions for a pre-existing fluid-driven fracture in permeable rock are obtained using the Lie point symmetry method.

1.7 Numerical methods

The initial value solver ODE 45 in MATLAB and the computer algebra package, MATHEMATICA, with the built-in numerical differential equation solver, NDSolve, are used to numerically solve the system of two initial value problems encountered in this research. The two initial value problems are obtained by transformations derived from a scaling analysis of the original boundary value problem.

1.8 Outline of research work

Two related problems will be considered and their analytic and numerical solutions analysed. The problems are hydraulic fracture in permeable rock when the leak-off velocity at the fluid/rock interface is proportional to the fracture half-width and secondly when the leak-off velocity at the fluid/rock interface is proportional to the gradient of the fracture half-width.

In Chapter 2 a concise outline of the theory of group analysis of differential equations, the mathematical method of solution of the partial differential equation derived in this research work, is made. The thin fluid film theory is briefly introduced and reviewed and the approximations to the Navier-Stokes equation are explained.

Chapter 3 commences with the presentation of a two-dimensional PKN fracture model for a permeable rock. The initial fracture shape is unspecified and is only determined from the group invariant and numerical solutions obtained. By using the thin fluid film approximations of lubrication theory, the Navier-Stokes equation is reduced to a lubrication equation. A nonlinear diffusion equation for the half-width $h(x,t)$ of the fracture is derived using the thin film approximation and the PKN formulation (1.3.1). This equation contains a term which is the leak-off velocity, v_n. The Lie point symmetries of the partial differential equation are derived and a condition on v_n for the Lie point symmetries to exist is obtained. The general form of the group invariant solution for $h(x,t)$, $v_n(x,t)$ and $p(x,t)$ is derived. The partial differential equation reduces to a nonlinear second order ordinary differential equation in two dependent variables when the similarity form of $h(x,t)$ and $v_n(x,t)$ are substituted into it. Lastly, the physical significance of some special values of the ratio $\frac{c_3}{c_2}$ which features in the

group invariant solutions is discussed.

In Chapter 4 analysis is given for the problem of a fluid-driven fracture in permeable rock when the leak-off velocity, v_n, is proportional to the fracture half-width h. Exact solutions are obtained for some special cases and discussion is given on the physical significance of these cases. The general numerical solution is obtained and discussed.

In Chapter 5, a corresponding analysis is given for the problem of a fluid-driven fracture in permeable rock when the leak-off velocity is proportional to the gradient of the fracture half-width. Exact solutions are also obtained and discussed for some special cases and the general numerical solution is derived.

Finally, the general conclusions and a summary of the results are given in Chapter 6.

Chapter 2

BACKGROUND

2.1 Introduction

This chapter presents the main results from the theory of Lie group analysis of differential equations that will be used in solving the nonlinear partial and ordinary differential equations derived in this research. The theory of Lie group analysis of differential equations which has extensively been dealt with in several books[18, 19, 20, 21, 22] was initiated by the 19th century Norwegian mathematician, Sophus Lie (1842-1899). It is a systematic way of obtaining exact solutions of linear and nonlinear ordinary and partial differential equations.

A concise introduction is also given of the theory of thin fluid films, also known as lubrication theory. Lubrication theory describes the fluid flow inside the thin layer fracture.

2.2 Lie point symmetries

We consider the nonlinear second order partial differential equation

$$F(t, x, h, h_t, h_x, h_{tx}, h_{tt}, h_{xx}) = 0, \tag{2.2.1}$$

in the two independent variables x and t and dependent variable h, which is the fracture half-width, where a subscript denotes partial differentiation.

The Lie point symmetry generators

$$X = \xi^1(t, x, h)\frac{\partial}{\partial t} + \xi^2(t, x, h)\frac{\partial}{\partial x} + \eta(t, x, h)\frac{\partial}{\partial h} \tag{2.2.2}$$

of equation (2.2.1) are derived by solving the determining equation,

$$X^{[2]}F(t,x,h,h_t,h_x,h_{tx},h_{tt},h_{xx})\Big|_{F=0}=0, \tag{2.2.3}$$

for $\xi^1(t,x,h)$, $\xi^2(t,x,h)$ and $\eta(t,x,h)$, where $X^{[2]}$, called the second prolongation of X, is given by

$$X^{[2]}=X+\zeta_1\frac{\partial}{\partial h_t}+\zeta_2\frac{\partial}{\partial h_x}+\zeta_{11}\frac{\partial}{\partial h_{tt}}+\zeta_{12}\frac{\partial}{\partial h_{tx}}+\zeta_{22}\frac{\partial}{\partial h_{xx}}, \tag{2.2.4}$$

where

$$\zeta_i=D_i(\eta)-h_kD_i(\xi^k), \qquad i=1,2, \tag{2.2.5}$$

$$\zeta_{ij}=D_j(\zeta_i)-h_{ik}D_j(\xi^k), \qquad i,j=1,2, \tag{2.2.6}$$

with summation over the repeated index k from 1 to 2. The total derivatives with respect to the independent variables t and x in (2.2.5) and (2.2.6) are

$$D_1=D_t=\frac{\partial}{\partial t}+h_t\frac{\partial}{\partial h}+h_{tt}\frac{\partial}{\partial h_t}+h_{xt}\frac{\partial}{\partial h_x}+\dots\ , \tag{2.2.7}$$

$$D_2=D_x=\frac{\partial}{\partial x}+h_x\frac{\partial}{\partial h}+h_{tx}\frac{\partial}{\partial h_t}+h_{xx}\frac{\partial}{\partial h_x}+\dots .\ . \tag{2.2.8}$$

The partial differential equation obtained in the pre-existing fluid-driven fracture problem is second order and therefore we only need the second prolongation of X. The unknown functions $\xi^1(t,x,h)$, $\xi^2(t,x,h)$ and $\eta(t,x,h)$ in the Lie point symmetry do not depend on the derivatives of h. The derivatives of h in the determining equation are independent. Hence, the coefficient of each derivative of h in the determining equation (2.2.3) must be zero.

The determining equation (2.2.3) can therefore be separated according to derivatives of h and the coefficient of each derivative set to zero. Solving this overdetermined system of equations produces expressions for $\xi^1(t,x,h)$, $\xi^2(t,x,h)$ and $\eta(t,x,h)$. These solutions contain constants. By setting all the constants to zero except one in turn, we obtain all the Lie point symmetry generators X_i, $i=1,2,...,n$. We also obtain a linear partial differential equation for the leak-off velocity $\boldsymbol{v_n}$ which must be satisfied for the Lie point symmetries to exist.

2.3 Lie's equations

The one parameter group of transformations

$$\overline{x}^i=f^i(x,a), \qquad i=1,2,\dots,n \tag{2.3.1}$$

where a is the group parameter, generated by the Lie point symmetry

$$X = \xi^i \frac{\partial}{\partial x^i} \tag{2.3.2}$$

where there is summation over the repeated index i, is obtained by solving the Lie equations

$$\frac{d\overline{x}^i}{da} = \xi^i(\overline{x}), \tag{2.3.3}$$

subject to the initial conditions

$$\overline{x}^i\big|_{a=0} = x^i. \tag{2.3.4}$$

Lie equations will be used in Chapters 4 and 5 to derive the coordinate transformation which will transform a boundary value problem to two initial value problems.

2.4 Group invariant solutions

The symmetry generators obtained are of the form

$$X_i = \xi_i^1(t,x,h)\frac{\partial}{\partial t} + \xi_i^2(t,x,h)\frac{\partial}{\partial x} + \eta_i(t,x,h)\frac{\partial}{\partial h} \tag{2.4.1}$$

for $i = 1, 2, ...n$, where n is the number of admitted Lie point symmetries. Since a constant multiple of a Lie point symmetry is also a Lie point symmetry, any linear combination of Lie point symmetries is also a Lie point symmetry. Denote by X_c this linear combination:

$$X_c = c_1X_1 + c_2X_2 + c_3X_3 + ... + c_nX_n, \tag{2.4.2}$$

where $c_i, i = 1, 2, ...n$, are constants.

The group invariant solution, $h = \phi(t,x)$, of the nonlinear partial differential equation is obtained by solving the equation

$$X_c(h - \phi(t,x))\Big|_{h=\phi(t,x)} = 0. \tag{2.4.3}$$

The group invariant solution is then substituted into the nonlinear partial differential equation. This substitution reduces the partial differential equation to an ordinary differential equation in a new variable, called the similarity variable.

In the analysis of the fluid-driven fracturing of a permeable rock, the time rate of change of mass of fluid in the fracture is the net difference between the rate at which mass of fluid is entering the fracture and the rate at which mass of fluid is leaked-off into the rock formation. The fracturing fluid is incompressible, hence the volume of a fluid element is also conserved and the balance law can be expressed in terms of volume of fluid instead of mass of fluid. When the balance law is expressed in terms of the similarity variable a condition is obtained on the ratios of the unknown constants $c_i, i = 1, 2, ..., n$. The ratios of the constants c_i in the linear combination (2.4.2) are further obtained from the boundary condition at the fracture tip and the given initial total volume V_0 of the fracture.

2.5 Thin fluid film approximation

In the analysis of a fluid-driven fracture of rock, the relevant equations are the Navier-Stokes and continuity equations for a homogenous, viscous, incompressible Newtonian fluid which in vectorial form are

$$\frac{\partial \underline{v}}{\partial t} + (\underline{v} \cdot \underline{\nabla})\underline{v} = \frac{-1}{\rho}\underline{\nabla} p + \nu \nabla^2 \underline{v} + \underline{F}, \tag{2.5.1}$$

$$\underline{\nabla} \cdot \underline{v} = 0, \tag{2.5.2}$$

where $\underline{v}$ is the fluid velocity, p, the fluid pressure, ν, the kinematic viscosity of the fluid and $\underline{F}$, the body force per unit mass. Consider a thin film of viscous incompressible fluid in the region between two elastic half-spaces, bounded above by $z = h(t, x)$ and below by $z = -h(t, x)$, as shown in Figure 2.5.1. We choose L to be a suitable characteristic length of the fracture and H a suitable characteristic half-width of the fracture. Let U be the characteristic fluid velocity in the fracture in the x-direction. Under the consideration that the characteristic half-width, H, of the fracture is small compared to the characteristic length L of the fracture, the thin fluid film approximation[17] is given by (1.6.1) and (1.6.2) where Re, the Reynolds number, is defined by $Re = \frac{UL}{\nu}$. The thin film approximation removes the time derivative $\frac{\partial \underline{v}}{\partial t}$ and the nonlinear term $(\underline{v} \cdot \underline{\nabla})\underline{v}$ from the Navier-Stokes equation [17]. It is important to note that the thin film approximation applies even for high Reynolds number flow provided (1.6.2) is satisfied.

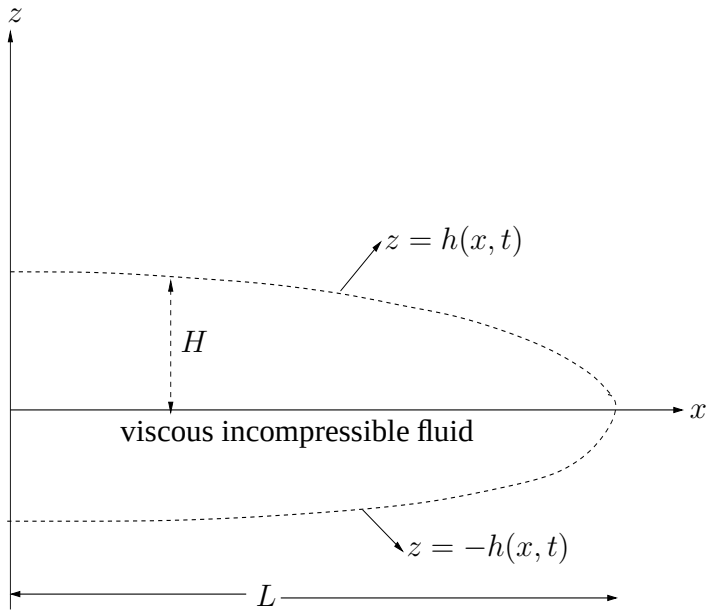


Figure 2.5.1: Thin film of viscous incompressible fluid of characteristic thickness H and characteristic lenght L

In summary, the Navier-Stokes equation is linear in the thin fluid film approximation. The linearity of the Navier-Stokes equation in the thin fluid film approximation does not imply that the problem of a fluid-driven fracture of rock is linear. Nonlinearity of the problem enters from the boundary condition at the fluid-rock interface.

Chapter 3

TWO DIMENSIONAL HYDRAULIC FRACTURE IN PERMEABLE ROCK

3.1 Introduction

In this chapter, we will consider a two-dimensional PKN fluid-driven fracture model for permeable rock. It is worth noting that the permeability of the rock implies that the injected fluid leaks off into the surrounding rock formation. A review of hydraulic fracture modelling has been given by Mendelsohn[23]. The fluid used to drive the fracture is a viscous incompressible Newtonian fluid.

One of the objectives of this chapter is to enumerate the assumptions on which our model depends in Section 3.3. Using these assumptions, we will formulate the mathematics underlying the fluid-driven fracture. The thin fluid film equations for the fluid flow in the two-dimensional fracture are derived. In Section 3.5, we derive the nonlinear diffusion equation in the dependent variable $h(x,t)$ and leak-off term $v_n(x,t)$. The symmetries of the nonlinear diffusion equation are obtained in Section 3.6. These symmetries exist provided the leak-off velocity satisfies a first order linear partial differential equation. Finally in Section 3.7, we discuss the special values for the parameter $\frac{c_3}{c_2}$ that are of clear physical significance.

3.2 Thin fluid film equations for the flow in a two-dimensional fracture

In this section, we will derive the two-dimensional thin fluid film equations for the flow of the injected viscous incompressible fluid in the fracture. Consider the flow in the region be-

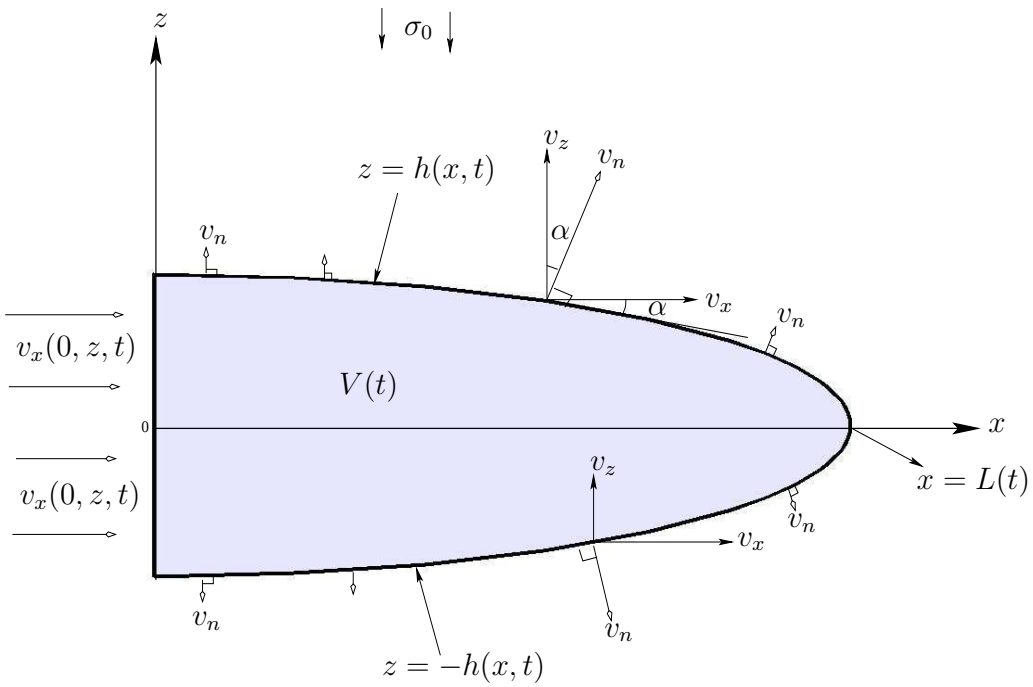


Figure 3.2.1: A crack propagating in an elastic permeable medium(the coordinate direction y points into the page). The leak-off velocity, v_n, is perpendicular to the interface.

tween the two boundaries $z = h(x,t)$ and $z = -h(x,t)$ where $h(x,t)$ is the half-width of the fracture. The cartesian coordinate system is as shown in Figure 3.2.1. The fluid flow is independent of y and obeys the two-dimensional Navier-Stokes equation for an incompressible fluid:

$$\frac{\partial \underline{v}}{\partial t} + (\underline{v} \cdot \underline{\nabla})\underline{v} = -\frac{1}{\rho}\underline{\nabla} p + \nu \nabla^2 \underline{v} \tag{3.2.1}$$

and the conservation of mass equation

$$\underline{\nabla}.\underline{v} = 0, \tag{3.2.2}$$

where $\underline{v} = (v_x(x,z,t), 0, v_z(x,z,t))$ denotes the fluid velocity, $p(x,z,t)$, the fluid pressure, ρ, the density of the fluid which is a constant and ν, the kinematic viscosity. The body force per unit mass is neglected. The fluid flow is symmetrical about the line $z = 0$.

In order to simplify equations (3.2.1) and (3.2.2), we first introduce the characteristic quantities and justification is then made of their choice:

characteristic length in x-direction =L

characteristic lenght in z-direction = H

characteristic fluid velocity in x-direction = U

characteristic fluid velocity in z-direction $W = \frac{H}{L}U$

characteristic fluid pressure $P = \frac{\mu U L}{H^2}$

characteristic time T=$\frac{L}{U}$.

We now justify the expression for the characteristic velocity in the z- direction. The continuity equation, (3.2.2), written in cartesian coordinates, is

$$\frac{\partial v_x}{\partial x} + \frac{\partial v_z}{\partial z} = 0. \tag{3.2.3}$$

The order of magnitude of terms in (3.2.3) is

$$\frac{U}{L} + \frac{W}{L} \sim 0 \tag{3.2.4}$$

and therefore

$$W = \frac{H}{L}U. \tag{3.2.5}$$

To justify the expression for the characteristic fluid pressure, consider the x-component of the Navier-Stokes equation

$$\rho\frac{Dv_x}{Dt} = -\frac{\partial p}{\partial x} + \mu\left(\frac{\partial^2 v_x}{\partial x^2} + \frac{\partial^2 v_x}{\partial z^2}\right). \tag{3.2.6}$$

The order of magnitude of the terms in (3.2.6) is

$$\rho\frac{U}{T} \sim -\frac{P}{L} + \mu\left(\frac{U}{L^2} + \frac{U}{H^2}\right). \tag{3.2.7}$$

Since equation (1.6.1) is satisfied,

$$\frac{U}{H^2} \gg \frac{U}{L^2}. \tag{3.2.8}$$

Therefore, the viscous term can be approximated by $\frac{\nu U}{H^2}$ and equation (3.2.7) becomes

$$\rho\frac{U^2}{L} \sim -\frac{P}{L} + \frac{\mu U}{H^2}, \tag{3.2.9}$$

where $T = \frac{L}{U}$. Now

$$\frac{\text{inertia term}}{\text{viscous term}} = \frac{\frac{\rho U^2}{L}}{\frac{\mu U}{H^2}} = \text{Re}\left(\frac{H}{L}\right)^2 \ll 1 \tag{3.2.10}$$

by (1.6.2) and (3.2.9) reduces to

$$P \sim \mu\frac{UL}{H^2}, \tag{3.2.11}$$

which is the characteristic fluid pressure.

Introduce the dimensionless variables:

$\overline{t}=\frac{Ut}{L}$, $\overline{x}=\frac{x}{L}$, $\overline{z}=\frac{z}{H}$, $\overline{v}_x=\frac{v_x}{U}$, $\overline{v}_z=\frac{v_z L}{UH}$, $\overline{p}=\frac{H^2 p}{\mu LU}$

and write the mass conservation equation and each component of the Navier-Stokes equation in dimensionless form. This gives:

the mass conservation equation:

$$\frac{\partial\overline{v}_x}{\partial\overline{x}} + \frac{\partial\overline{v}_z}{\partial\overline{z}} = 0, \tag{3.2.12}$$

the x-component of Navier-Stokes equation:

$$Re\left(\frac{H}{L}\right)^2\left(\frac{\partial\overline{v}_x}{\partial\overline{t}} + \overline{v}_x\frac{\partial\overline{v}_x}{\partial\overline{x}} + \overline{v}_z\frac{\partial\overline{v}_x}{\partial\overline{z}}\right) = -\frac{\partial\overline{p}}{\partial\overline{x}} + \left(\frac{H}{L}\right)^2\frac{\partial^2\overline{v}_x}{\partial\overline{x}^2} + \frac{\partial^2\overline{v}_x}{\partial\overline{z}^2}, \tag{3.2.13}$$

the z-component of Navier-Stokes equation:

$$Re\left(\frac{H}{L}\right)^4\left(\frac{\partial\overline{v}_z}{\partial\overline{t}} + \overline{v}_x\frac{\partial\overline{v}_z}{\partial\overline{x}} + \overline{v}_z\frac{\partial\overline{v}_z}{\partial\overline{z}}\right) = -\frac{\partial\overline{p}}{\partial\overline{z}} + \left(\frac{H}{L}\right)^4\frac{\partial^2\overline{v}_z}{\partial\overline{x}^2} + \left(\frac{H}{L}\right)^2\frac{\partial^2\overline{v}_z}{\partial\overline{z}^2}. \tag{3.2.14}$$

The motivation for putting the Navier-Stokes and mass conservation equations in dimensionless form arises from the need to know which terms can be neglected in the thin fluid film approximation of the concerned equations.

Impose the thin fluid film approximation, (1.6.1) and (1.6.2). Equations (3.2.12) to (3.2.14) reduce to

$$\frac{\partial\overline{v}_x}{\partial\overline{x}} + \frac{\partial\overline{v}_z}{\partial\overline{z}} = 0, \tag{3.2.15}$$

$$\frac{\partial\overline{p}}{\partial\overline{x}} = \frac{\partial^2\overline{v}_x}{\partial\overline{z}^2}, \tag{3.2.16}$$

$$\frac{\partial\overline{p}}{\partial\overline{z}} = 0. \tag{3.2.17}$$

The two-dimensional continuity equation (3.2.15) is unaltered by the thin film approximation. Equations (3.2.16) and (3.2.17) are the x-component and z- component of the Navier-Stokes equation in the thin fluid film approximation in dimensionless form.

3.3 Mathematical formulation

We consider the two-dimensional PKN model of a pre-existing fluid-filled hydraulic fracture propagating in a permeable linear elastic medium and driven by a viscous incompressible Newtonian fluid as shown in Figure 3.2.1. The case when the fracture is driven by a non-Newtonian fluid is of importance and will be considered in future work. The fracture is driven by a fluid injected into it at the rate $\frac{dV}{dt}$ per unit length in the y direction at the entry to the fracture. The injected fluid causes the fracture to propagate along the x-axis, perpendicular to the compressive stress of magnitude σ_0. As the fracture is being propagated in the permeable medium, fluid is being leaked-off into the rock formation through the interface between the rock and the injected fluid.

To build a mathematical model for the rock fracturing process, it will be necessary to consider both the mechanics of the fluid inside the fracture and the way that this interacts with the elasticity of the surrounding rock. We begin by making the following assumptions for our model:

- The rock is a permeable medium and there is fluid leak-off into it. The fluid leak-off into the rock mass is in the direction perpendicular to the fluid/rock interface.
- The rock is a linearly elastic material which assumes small displacement gradients.
- The fracture propagates along the positive x-direction, is one-sided, $0 \leq x \leq L(t)$, identical in every plane y=constant and has length $L(t)$ and half-width $h(x,t)$.
- In every plane y= constant, the fracture is symmetrical about the x-axis. The upper surface is $y = h(x,t)$ and the lower surface is y=-$h(x,t)$.
- The fracture is completely filled with the injected fluid. That is, the fluid front concides with the tip of the fracture and there is no fluid lag.

- The flow of fluid inside the fracture is laminar.
- The flow of fluid inside the fracture is modelled using lubrication theory.

3.4 Governing equations

3.4.1 Fluid problem: Lubrication theory

The coordinate system is as chosen in Figure 3.2.1. The fluid flow in the fracture is independent of the y-coordinate and obeys the two-dimensional Navier-Stokes equation for an incompressible fluid. For a thin fracture whose length is much greater than its width, the thin fluid film approximation, (1.6.1) and (1.6.2), is satisfied. The fluid flow in the fracture is then governed by the dimensionless equations (3.2.15) to (3.2.17). These thin fluid film equations are valid as long as the thin fluid film approximations, (1.6.1) and (1.6.2), hold through-out the process of the hydraulic fracturing. Lubrication theory breaks down when equations (1.6.1) and (1.6.2) no longer hold.
The fluid variables are

$$v_x = v_x(x,z,t), \qquad v_y = 0, \qquad v_z = v_z(x,z,t), \qquad p = p(x,z,t). \tag{3.4.1}$$

By dropping the overhead bars for simplicity, the thin film equations of lubrication theory in dimensionless form, (3.2.15) to (3.2.17), become

$$\frac{\partial p}{\partial x} = \frac{\partial^2 v_x}{\partial z^2}, \qquad \frac{\partial p}{\partial z} = 0, \qquad \frac{\partial v_x}{\partial x} + \frac{\partial v_z}{\partial z} = 0. \tag{3.4.2}$$

Fracture problem: Elasticity equation

Under the linear theory of elasticity, if an elastic half-space $z > 0$ is subjected to the normal traction $\sigma_{zz} = -p_f(x,t)$ on the internal face of the fracture, then for a fracture that propagates in the positive $x-$direction, the pressure is related to the half-width of the fracture by the plane strain elastic equation of the form

$$p(x,t) = p_f(x,t) - \sigma_0 = -\left(\frac{E}{\pi(1-\nu)}\right)\int_0^{L(t)} \frac{h_s(s,t)}{s-x} ds, \tag{3.4.3}$$

where E is the Young's modulus and ν is the Poisson ratio of the rock. At the fluid-rock interface, it is assumed that there is a no-slip condition so that the shear traction is negligible. Equation (3.4.3) is a non-trivial singular integral equation which describes the normal surface stresses resulting from the deformation of the interface of the elastic material from a planar state.

An alternative to this classical two-dimensional modelling is the PKN theory discussed in Sections 1.3 and 1.5 and which is used throughout this dissertation. The PKN theory is adopted in this dissertation because of its simplicity, unlike the plane strain equation (3.4.3) which is difficult to solve analytically when coupled with other equations of hydraulic fracture.

The elastic constitutive law for the two-dimensional model of a fluid driven fracture propagating in a permeable linear elastic medium in PKN theory[5] is given as

$$p = \Lambda h(x,t), \tag{3.4.4}$$

where[6]

$$\Lambda = \frac{EH^3}{(1-\sigma^2)\mu ULB}. \tag{3.4.5}$$

In (3.4.5) E and σ are the Young's modulus and Poisson ratio of the rock, B is the breadth in the $y-$direction of the fracture, μ the dynamic viscosity and H, L and U are the characteristic quantities defined earlier. Also,

$$p = p_f - \sigma_0 \tag{3.4.6}$$

is the net pressure of the fluid that will be determined, p_f is the internal fluid pressure in the fracture and σ_0 is the far field compressive stress perpendicular to the fracture.

3.4.2 Initial and boundary conditions

At the solid boundary of the fracture, the boundary conditions are the no-slip condition for a viscous fluid and the leak-off condition.

Denote by $v_n(x,t)$ the fluid velocity at the interface, measured relative to the interface in the direction perpendicular to the interface. The velocity $v_n(x,t)$ is referred to as the leak-off velocity.

From Figures 3.4.1 and 3.4.2, we obtain the following boundary conditions at $z = \pm h(x,t)$.

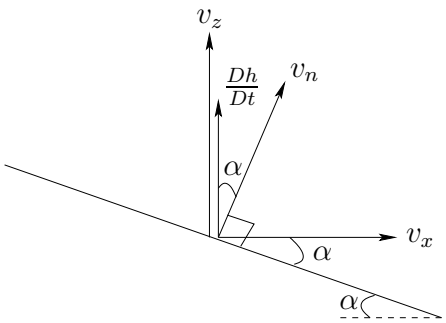


Figure 3.4.1: Tangent plane at a point on the surface, $z = h(x,t)$.

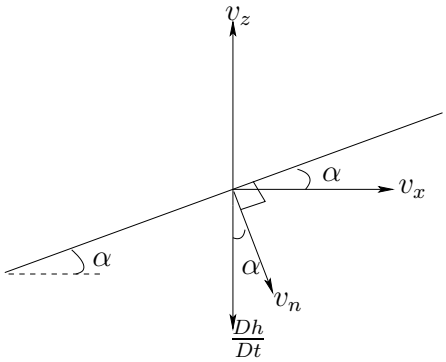


Figure 3.4.2: Tangent plane at a point on the surface, $z = -h(x,t)$.

No slip condition:

Tangential component of the fluid velocity at the boundary equals the tangential component of the velocity of the boundary.

$$z = h(x,t): \qquad v_x(x,h,t)\cos\alpha = -\frac{Dh}{Dt}\sin\alpha, \tag{3.4.7}$$

$$z = -h(x,t): \qquad v_x(x,-h,t)\cos\alpha = -\frac{Dh}{Dt}\sin\alpha, \tag{3.4.8}$$

where $\frac{D}{Dt}$ denotes the material time derivative.

Leak-off condition:

Normal component of the fluid velocity at the boundary equals the normal component of the velocity of the boundary + normal component of the velocity of fluid relative to the boundary.

$$z = h(x,t): \qquad v_z(x,h,t)\cos\alpha = \frac{Dh}{Dt}\cos\alpha + v_n(x,t), \tag{3.4.9}$$

$$z = -h(x,t): \qquad v_z(x,-h,t)\cos\alpha = -\frac{Dh}{Dt}\cos\alpha - v_n(x,t). \tag{3.4.10}$$

Now

$$\tan\alpha = -\frac{\partial h}{\partial x} = \bigcirc\left(\frac{H}{L}\right) \tag{3.4.11}$$

and in the thin film approximation $\frac{H}{L} << 1$. Thus α is small and

$$\tan\alpha = \bigcirc(\alpha) = \bigcirc\left(\frac{H}{L}\right), \quad \sin\alpha = \bigcirc(\alpha) = \bigcirc\left(\frac{H}{L}\right), \quad \cos\alpha = \bigcirc(1) \tag{3.4.12}$$

and the boundary conditions (3.4.7) to (3.4.10) reduce to the following conditions.

No-slip condition:

$$z = h(x,t): \qquad v_x(x,h,t) = 0, \tag{3.4.13}$$

$$z = -h(x,t): \qquad v_x(x,-h,t) = 0. \tag{3.4.14}$$

Leak-off condition:

$$z = h(x,t): \qquad v_z(x,h,t) = \frac{Dh}{Dt} + v_n(x,t), \tag{3.4.15}$$

$$z = -h(x,t): \qquad v_z(x,-h,t) = -\frac{Dh}{Dt} - v_n(x,t). \tag{3.4.16}$$

The thin film approximation $\frac{H}{L} << 1$ is a good approximation except near the tip of the fracture. The boundary conditions (3.4.13) to (3.4.16) will therefore be valid except near the fracture tip where the thin film approximation breaks down. Equations (3.4.15) and (3.4.16) are expressed in dimensionless form. The leak-off velocity v_n has been made dimensionless by division by the characteristic velocity in the z-direction $\frac{H}{L}U$. By expanding the material time derivative, (3.4.15) becomes

$$\begin{aligned} v_z(x,h,t) &= \frac{\partial h}{\partial t} + v_x(x,h,t)\frac{\partial h}{\partial x} + v_n(x,t) \\ &= \frac{\partial h}{\partial t} + v_n(x,t), \end{aligned} \tag{3.4.17}$$

since $v_x(x,h,t) = 0$ from the no slip boundary condition (3.4.13). Similarly, the boundary condition (3.4.16) becomes

$$v_z(x,-h,t) = -\frac{\partial h}{\partial t} - v_n(x,t). \tag{3.4.18}$$

Initial conditions:

In the model, the rock has a pre-existing fracture. Hence, the initial fracture shape is such that

$$t = 0: \qquad h(x,0) = h_o(x). \tag{3.4.19}$$

In general, it will not be possible for a similarity solution to satisfy condition (3.4.19). We will investigate the initial condition $h(x,0)$ given by the similarity solution in Chapters 4 and 5.

The initial dimensionless length and volume of the fracture is also specified:

$$t = 0: \qquad L(0) = 1, \tag{3.4.20}$$

$$t = 0: \qquad V(0) = 1. \tag{3.4.21}$$

This is equivalent to taking the characteristic length of the fracture to be the initial dimensional length and the characteristic volume of the fracture to be the initial dimensional volume.

Condition at the fracture tip:

$$x = L(t): \qquad h(L(t), t) = 0. \tag{3.4.22}$$

The mathematical formulation is summarized as follows:

Governing equations:

$$\frac{\partial p}{\partial x} = \frac{\partial^2 v_x}{\partial z^2}, \tag{3.4.23}$$

$$\frac{\partial p}{\partial z} = 0, \tag{3.4.24}$$

$$\frac{\partial v_x}{\partial x} + \frac{\partial v_z}{\partial z} = 0. \tag{3.4.25}$$

Boundary conditions:

$$z = h(x, t): \qquad v_x(x, h, t) = 0, \tag{3.4.26}$$

$$z = -h(x, t): \qquad v_x(x, -h, t) = 0, \tag{3.4.27}$$

$$z = h(x, t): \qquad v_z(x, h, t) = \frac{\partial h}{\partial t}(x, t) + v_n(x, t), \tag{3.4.28}$$

$$z = -h(x, t): \qquad v_z(x, -h, t) = -\frac{\partial h}{\partial t}(x, t) - v_n(x, t). \tag{3.4.29}$$

Initial conditions:

$$t = 0: \qquad h(x, 0) = h_o(x), \tag{3.4.30}$$

$$t = 0: \qquad L(0) = 1, \tag{3.4.31}$$

$$t = 0: \qquad V(0) = 1. \tag{3.4.32}$$

condition at the fracture tip:

$$x = L(t): \qquad h(L(t), t) = 0. \tag{3.4.33}$$

Using equations (3.4.23) to (3.4.25) and boundary conditions (3.4.26) to (3.4.29), a nonlinear partial differential equation relating the half-width of the fracture $h(x, t)$ to the fluid pressure $p(x, t)$ and leak-off velocity $v_n(x, t)$ will be derived in the next section.

3.5 Nonlinear diffusion equation with leak-off term

We will now derive the nonlinear diffusion equation for the half-width of the fracture $h(x,t)$. This equation also contains a term describing fluid leak-off at the fluid/rock interface.

We first obtain an expression for $v_x(x,z,t)$. By integrating equation (3.4.23) twice with respect to z and applying the no slip boundary conditions (3.4.26) and (3.4.27) at the interface between the fluid and the solid boundary, we obtain

$$v_x(x,z,t) = -\frac{1}{2}\left(h^2(x,t) - z^2\right)\frac{\partial p}{\partial x}. \tag{3.5.1}$$

The continuity equation (3.4.25) is integrated with respect to z across the two-dimensional fracture. This gives

$$v_z(x,h,t) - v_z(x,-h,t) + \int_{-h}^{h} \frac{\partial v_x}{\partial x}(x,z,t)dz = 0. \tag{3.5.2}$$

Using boundary conditions (3.4.28) and (3.4.29), equation (3.5.2) becomes

$$\frac{\partial h}{\partial t} + v_n(x,t) + \frac{1}{2}\int_{-h}^{h} \frac{\partial v_x}{\partial x}(x,z,t)dz = 0. \tag{3.5.3}$$

The partial derivative inside the integral is taken outside the integral using Leibnitz formula for differentiation under the integral sign[24]:

$$\frac{\partial}{\partial x}\int_{-h(x,t)}^{h(x,t)} v_x(x,z,t)dz = \int_{-h(x,t)}^{h(x,t)} \frac{\partial v_x}{\partial x}(x,z,t)dz + v_x(x,h,t)\frac{\partial h}{\partial x} - v_x(x,-h,t)\left(-\frac{\partial h}{\partial x}\right) \tag{3.5.4}$$

which using the no-slip boundary conditions (3.4.26) and (3.4.27), simplifies to

$$\frac{\partial}{\partial x}\int_{-h(x,t)}^{h(x,t)} v_x(x,z,t)dz = \int_{-h(x,t)}^{h(x,t)} \frac{\partial v_x}{\partial x}(x,z,t)dz. \tag{3.5.5}$$

Using (3.5.5), equation (3.5.3) becomes

$$\frac{\partial h}{\partial t} + \frac{1}{2}\frac{\partial}{\partial x}\int_{-h}^{h} v_x(x,z,t)dz = -v_n(x,t). \tag{3.5.6}$$

Equation (3.5.6) has the form of a conservation equation with a sink term. We now substitute equation (3.5.1) into equation (3.5.6) to obtain:

$$\frac{\partial h}{\partial t} - \frac{1}{4}\frac{\partial}{\partial x}\left[\frac{\partial p}{\partial x}(x,t)\int_{-h}^{h}(h^2(x,t) - z^2)dz\right] = -v_n(x,t). \tag{3.5.7}$$

This gives the nonlinear partial differential equation

$$\frac{\partial h}{\partial t} = \frac{1}{3}\frac{\partial}{\partial x}\left(h^3\frac{\partial p}{\partial x}\right) - v_n. \tag{3.5.8}$$

Using equation (3.4.4), we obtain the nonlinear diffusion equation

$$\frac{\partial h}{\partial t} = \frac{\Lambda}{3}\frac{\partial}{\partial x}\left(h^3\frac{\partial h}{\partial x}\right) - v_n. \tag{3.5.9}$$

We will now derive the equation relating the rate of change of total volume of the fracture per unit length in the y-direction to the resultant area flux into the fracture at the entry and at the fluid-rock interface.

The total volume of the fracture, $V(t)$, per unit length in the y-direction is

$$V(t) = 2\int_0^{L(t)} h(x,t)dx. \tag{3.5.10}$$

Equation (3.5.10) is dimensionless. The total volume V(t) was made dimensionless by division by the characteristic volume per unit length in the $y-$ direction, HL. The injected fluid is incompressible. Therefore, per unit length in the y-direction,

the time rate of change of the total volume of the fracture = the rate of fluid flow into the fracture at the entry to the fracture - rate of fluid leak-off at the fluid-rock interface.

At $x = 0$, the rate of fluid flow into the fracture per unit length in the y-direction, which is the area flux into the fracture per unit length in the y-direction, is

$$q_1 = \int_{-h(0,t)}^{h(0,t)} v_x(0,z,t)dz = 2\int_0^{h(0,t)} v_x(0,z,t)dz. \tag{3.5.11}$$

The rate of flow of leaked-off fluid into the rock mass per unit length in the y-direction, which is the area flux of the leaked-off fluid per unit length in the y-direction, is

$$q_2 = 2\int_0^{L(t)} v_n(x,t)dx. \tag{3.5.12}$$

Hence, per unit length in the y-direction, the rate of increase of the total volume of the fracture, $\frac{dV}{dt}$, is

$$\begin{aligned}\frac{dV}{dt} &= q_1 - q_2 \\ &= 2\int_0^{h(0,t)} v_x(0,z,t)dz - 2\int_0^{L(t)} v_n(x,t)dx.\end{aligned} \tag{3.5.13}$$

We substitute (3.5.1) evaluated at $x = 0$ into equation (3.5.13) and integrate to obtain

$$\frac{dV}{dt} = -\frac{2}{3}h^3(0,t)\frac{\partial p}{\partial x}(0,t) - 2\int_0^{L(t)} v_n(x,t)dx. \tag{3.5.14}$$

Applying equation (3.4.4) we obtain

$$\frac{dV}{dt} = -\frac{2\Lambda}{3}h^3(0,t)\frac{\partial h}{\partial x}(0,t) - 2\int_0^{L(t)} v_n(x,t)dx. \tag{3.5.15}$$

A statement of the problem is as follows: Solve for $h(x,t)$, $v_n(x,t)$ and $L(t)$ the partial differential equation

$$\frac{\partial h}{\partial t} = \frac{\Lambda}{3}\frac{\partial}{\partial x}\left(h^3\frac{\partial h}{\partial x}\right) - v_n, \tag{3.5.16}$$

subject to the boundary condition

$$h(L(t),t) = 0 \tag{3.5.17}$$

and the initial condition

$$L(0) = 1 \tag{3.5.18}$$

and the balance law

$$\frac{dV}{dt} = -\frac{2\Lambda}{3}h^3(0,t)\frac{\partial h}{\partial x}(0,t) - 2\int_0^{L(t)} v_n(x,t)dx, \tag{3.5.19}$$

where

$$V(t) = 2\int_0^{L(t)} h(x,t)dx. \tag{3.5.20}$$

Once $h(x,t)$ has been obtained, $p(x,t)$ is given by

$$p(x,t) = \Lambda h(x,t). \tag{3.5.21}$$

Problem (3.5.16) to (3.5.21) is not a closed problem since equation (3.5.16) is not sufficient to determine the leak-off term $v_n(x,t)$. Further modelling will be required for $v_n(x,t)$ in order to have a well posed closed problem. However, in this dissertation, Lie group analysis is used to determine the form of $v_n(x,t)$.

We will derive a group invariant solution for $h(x,t)$, $v_n(x,t)$ and $L(t)$. The first step in achieving this goal is to investigate the Lie point symmetries of equation (3.5.16).

3.6 Lie point symmetries and general properties of group invariant solutions

We will use a linear combination of the Lie point symmetries of the nonlinear diffusion equation

$$\frac{\partial h}{\partial t} = \frac{\Lambda}{3}\frac{\partial}{\partial x}\left(h^3\frac{\partial h}{\partial x}\right) - v_n \tag{3.6.1}$$

to construct a group invariant solution for $h(x,t)$, $v_n(x,t)$, $L(t)$, $p(x,t)$ and $V(t)$. We will first outline in a concise manner the derivation of the Lie point symmetries of (3.6.1) and then establish some general properties of the group invariant solution. The complete derivation of the Lie point symmetries of equation (3.6.1) is presented in Appendix A.

The Lie point symmetries

$$X = \xi^1(t,x,h)\frac{\partial}{\partial t} + \xi^2(t,x,h)\frac{\partial}{\partial x} + \eta(t,x,h)\frac{\partial}{\partial h} \tag{3.6.2}$$

of equation (3.6.1) are derived by solving the determining equation[19]

$$X^{[2]}\left(h_t - \frac{\Lambda}{3}h^3h_{xx} - \Lambda h^2h_x^2 + v_n\right)\Big|_{eq(3.6.1)} = 0 \tag{3.6.3}$$

for ξ^1, ξ^2 and η where $X^{[2]}$ is the second prolongation of the Lie point symmetry generator X. The subscripts in equation (3.6.3) denote partial differentiation. It can be verified that

$$\begin{aligned} X &= (c_1 + c_2t)\frac{\partial}{\partial t} + (c_4 + c_3x)\frac{\partial}{\partial x} + \frac{1}{3}(2c_3 - c_2)h\frac{\partial}{\partial h} \\ &= c_1X_1 + c_2X_2 + c_3X_3 + c_4X_4, \end{aligned} \tag{3.6.4}$$

where

$$X_1 = \frac{\partial}{\partial t}, \tag{3.6.5}$$

$$X_2 = t\frac{\partial}{\partial t} - \frac{1}{3}h\frac{\partial}{\partial h}, \tag{3.6.6}$$

$$X_3 = x\frac{\partial}{\partial x} + \frac{2}{3}h\frac{\partial}{\partial h}, \tag{3.6.7}$$

$$X_4 = \frac{\partial}{\partial x}, \tag{3.6.8}$$

and c_1, c_2, c_3 and c_4 are constants, provided the fluid leak-off velocity, $v_n(x,t)$, satisfies the first order linear partial differential equation

$$(c_1 + c_2 t)\frac{\partial v_n}{\partial t} + (c_4 + c_3 x)\frac{\partial v_n}{\partial x} = \frac{2}{3}(c_3 - 2c_2)v_n. \tag{3.6.9}$$

Now, $h(x,t)$ is a group invariant solution of (3.6.1) provided

$$X\left(h - \phi(x,t)\right)\Big|_{h=\phi} = 0, \tag{3.6.10}$$

that is, provided

$$(c_1 + c_2 t)\frac{\partial \phi}{\partial t} + (c_4 + c_3 x)\frac{\partial \phi}{\partial x} = \frac{1}{3}(2c_3 - c_2)\phi. \tag{3.6.11}$$

The system of first order differential equations of the characteristic curves of (3.6.11) are

$$\frac{dt}{c_1 + c_2 t} = \frac{dx}{c_4 + c_3 x} = \frac{d\phi}{\frac{1}{3}(2c_3 - c_2)\phi} \tag{3.6.12}$$

It is equivalently rewritten as

$$\frac{dt}{c_1 + c_2 t} = \frac{dx}{c_4 + c_3 x}, \quad \frac{dt}{c_1 + c_2 t} = \frac{d\phi}{\frac{1}{3}(2c_3 - c_2)\phi}. \tag{3.6.13}$$

On integrating each of the differential equations in (3.6.13), one arrives at the following two independent first integrals, respectively:

$$I_1 = \frac{c_4 + c_3 x}{(c_1 + c_2 t)^{\frac{c_3}{c_2}}}, \qquad I_2 = \frac{\phi}{(c_1 + c_2 t)^{\frac{2c_3 - c_2}{3c_2}}}. \tag{3.6.14}$$

The constants I_1 and I_2 form a basis of invariants of (3.6.11) since they are independent. The general form of the solution of (3.6.11) is

$$I_2 = f(I_1), \tag{3.6.15}$$

where f is an arbitrary function. Hence

$$\phi(x,t) = (c_1 + c_2 t)^{\frac{2c_3 - c_2}{3c_2}} f(\xi), \tag{3.6.16}$$

where

$$\xi = \frac{c_4 + c_3 x}{(c_1 + c_2 t)^{\frac{c_3}{c_2}}}. \tag{3.6.17}$$

But since $\phi(x,t) = h(x,t)$, it follows that

$$h(x,t) = (c_1 + c_2 t)^{\frac{2c_3 - c_2}{3c_2}} f(\xi), \tag{3.6.18}$$

where $f(\xi)$ is an arbitrary function of ξ.

Consider now the fluid leak-off velocity, $v_n(x,t)$. We note that the existence of the group invariant solution (3.6.18) requires that $v_n(x,t)$ satisfies equation (3.6.9). The differential equations of the characteristic curves of (3.6.9) are

$$\frac{dt}{c_1 + c_2 t} = \frac{dx}{c_4 + c_3 x} = \frac{dv_n}{\frac{2}{3}(c_3 - 2c_2)v_n}, \tag{3.6.19}$$

which may equivalently be written as

$$\frac{dt}{c_1 + c_2 t} = \frac{dx}{c_4 + c_3 x}, \qquad \frac{dt}{c_1 + c_2 t} = \frac{dv_n}{\frac{2}{3}(c_3 - 2c_2)v_n}. \tag{3.6.20}$$

We integrate the two differential equations in (3.6.20) to obtain the basis of invariants

$$I_3 = \frac{c_4 + c_3 x}{(c_1 + c_2 t)^{\frac{c_3}{c_2}}}, \qquad I_4 = \frac{v_n}{(c_1 + c_2 t)^{\frac{2(c_3 - 2c_2)}{3c_2}}}, \tag{3.6.21}$$

respectively.

The general form of the solution of (3.6.19) is

$$I_4 = g(I_3), \tag{3.6.22}$$

where g is an arbitrary function. Hence

$$v_n(x,t) = (c_1 + c_2 t)^{\frac{2(c_3 - 2c_2)}{3c_2}} g(\xi) \tag{3.6.23}$$

and ξ is as defined by equation (3.6.17).

We have suceeded in obtaining the general form of the group invariant solution for the fracture half-width, $h(x,t)$, and velocity of leak-off fluid, $v_n(x,t)$. We now express the problem in terms of the variable ξ and the functions $f(\xi)$ and $g(\xi)$.

Consider first the partial differential equation (3.6.1). We substitute (3.6.18) and (3.6.23) for $h(x,t)$ and $v_n(x,t)$ into equation (3.6.1). The partial differential equation (3.6.1) becomes the second order nonlinear ordinary differential equation

$$\frac{\Lambda}{3} c_3^2 \frac{d}{d\xi}\left(f^3 \frac{df}{d\xi}\right) + c_3 \frac{d}{d\xi}(\xi f) + \frac{c_3}{3}\left(\frac{c_2}{c_3} - 5\right) f - g = 0. \tag{3.6.24}$$

Equation (3.6.24) does not depend on c_4. We can therefore choose $c_4 = 0$ in (3.6.17) so that $\xi = 0$ when $x = 0$.

Consider next the boundary condition (3.4.22),

$$h(L(t), t) = 0. \tag{3.6.25}$$

From equation (3.6.18), the boundary condition (3.6.25) becomes

$$f(\xi) = 0 \quad \text{at} \quad \xi = \frac{c_3 L(t)}{(c_1 + c_2 t)^{\frac{c_3}{c_2}}}. \tag{3.6.26}$$

But the fracture half-width, $h(x, t)$ is not a zero function. For instance at time $t = 0$, $h(x, t)$ satisfies the initial condition (3.4.19). Therefore, from (3.6.26), f cuts the ξ-axis at $\xi = \frac{c_3 L(t)}{(c_1+c_2 t)^{\frac{c_3}{c_2}}}$ which must be a constant. Thus

$$\frac{c_3 L(t)}{(c_1 + c_2 t)^{\frac{c_3}{c_2}}} = \text{constant} = A \tag{3.6.27}$$

and therefore

$$L(t) = \frac{A}{c_3}(c_1 + c_2 t)^{\frac{c_3}{c_2}}. \tag{3.6.28}$$

But from (3.4.31), the initial condition is $L(0) = 1$. Thus

$$A = c_3 c_1^{-\frac{c_3}{c_2}}. \tag{3.6.29}$$

The length of the fracture, $L(t)$, as a function of time is therefore derived as

$$L(t) = \left(1 + \frac{c_2}{c_1} t\right)^{\frac{c_3}{c_2}}. \tag{3.6.30}$$

For large times, $L(t)$ becomes the power law

$$L(t) = \left(\frac{c_2}{c_1}\right)^{\frac{c_3}{c_2}} t^{\frac{c_3}{c_2}}. \tag{3.6.31}$$

The boundary condition (3.6.26) becomes

$$f(c_3 c_1^{-\frac{c_3}{c_2}}) = 0 \tag{3.6.32}$$

and the variable ξ, given by (3.6.17) can be expressed in terms of $L(t)$ as

$$\xi = c_3 c_1^{-\frac{c_3}{c_2}} \frac{x}{L(t)}. \tag{3.6.33}$$

Consider next the balance law (3.5.15). Substituting (3.6.18) and (3.6.23) into (3.5.15) and using (3.6.30) for $L(t)$ gives

$$\frac{dV}{dt} = -\frac{2\Lambda}{3}c_3(c_1+c_2t)^{\frac{5}{3}\frac{c_3}{c_2}-\frac{4}{3}}f^3(0)\frac{df}{d\xi}(0) - \frac{2}{c_3}(c_1+c_2t)^{\frac{5}{3}\frac{c_3}{c_2}-\frac{4}{3}}\int_0^{c_3c_1^{-\frac{c_3}{c_2}}} g(\xi)d\xi. \quad (3.6.34)$$

In order to evaluate the left hand side of (3.6.34), consider the total volume, $V(t)$, of the fracture per unit length in the y-direction which is given by (3.5.20). Using (3.6.17) and (3.6.18) for ξ and $h(x,t)$ respectively and (3.6.30) for $L(t)$, (3.5.20) becomes

$$V(t) = \frac{2}{c_3}(c_1+c_2t)^{\frac{5}{3}\frac{c_3}{c_2}-\frac{1}{3}}\int_0^{c_3c_1^{-\frac{c_3}{c_2}}} f(\xi)d\xi. \quad (3.6.35)$$

Differentiating equation (3.6.35) with respect to t gives

$$\frac{dV}{dt} = \frac{2}{3}\left(5-\frac{c_2}{c_3}\right)(c_1+c_2t)^{\frac{5}{3}\frac{c_3}{c_2}-\frac{4}{3}}\int_0^{c_3c_1^{-\frac{c_3}{c_2}}} f(\xi)d\xi. \quad (3.6.36)$$

Substituting (3.6.36) into (3.6.34) yields

$$\Lambda c_3 f^3(0)\frac{df}{d\xi}(0) = \left(\frac{c_2}{c_3}-5\right)\int_0^{c_3c_1^{-\frac{c_3}{c_2}}} f(\xi)d\xi - \frac{3}{c_3}\int_0^{c_3c_1^{-\frac{c_3}{c_2}}} g(\xi)d\xi. \quad (3.6.37)$$

Lastly, from (3.6.35) the total volume $V(t)$ of the fracture per unit length in the y-direction can be expressed as

$$V(t) = V_0\left(1+\frac{c_2}{c_1}t\right)^{\frac{5}{3}(\frac{c_3}{c_2}-\frac{1}{5})}, \quad (3.6.38)$$

where

$$V_0 = \frac{2}{c_3}c_1^{\frac{5}{3}(\frac{c_3}{c_2}-\frac{1}{5})}\int_0^{c_3c_1^{-\frac{c_3}{c_2}}} f(\xi)d\xi. \quad (3.6.39)$$

A summary of the mathematical formulation is as follows:

$$\frac{\Lambda}{3}c_3^2\frac{d}{d\xi}\left(f^3\frac{df}{d\xi}\right)+c_3\frac{d}{d\xi}\left(\xi f\right)+\frac{c_3}{3}\left(\frac{c_2}{c_3}-5\right)f-g=0, \tag{3.6.40}$$

$$f\left(c_3c_1^{-\frac{c_3}{c_2}}\right)=0, \tag{3.6.41}$$

$$\Lambda c_3f^3(0)\frac{df}{d\xi}(0)=\left(\frac{c_2}{c_3}-5\right)\int_0^{c_3c_1^{-\frac{c_3}{c_2}}}f(\xi)d\xi-\frac{3}{c_3}\int_0^{c_3c_1^{-\frac{c_3}{c_2}}}g(\xi)d\xi, \tag{3.6.42}$$

$$V_0=\frac{2}{c_3}c_1^{\frac{5}{3}\frac{c_3}{c_2}-\frac{1}{3}}\int_0^{c_3c_1^{-\frac{c_3}{c_2}}}f(\xi)d\xi, \tag{3.6.43}$$

$$\frac{c_2}{c_1}=\frac{c_2}{c_3}\frac{c_3}{c_1}, \tag{3.6.44}$$

$$V(t)=V_0\left(1+\frac{c_2}{c_1}t\right)^{\frac{5}{3}\frac{c_3}{c_2}-\frac{1}{3}}, \tag{3.6.45}$$

$$L(t)=\left(1+\frac{c_2}{c_1}t\right)^{\frac{c_3}{c_2}}, \tag{3.6.46}$$

$$h(x,t)=(c_1+c_2t)^{\frac{2c_3-c_2}{3c_2}}f(\xi)=c_1^{\frac{2}{3}\frac{c_3}{c_2}-\frac{1}{3}}\left(1+\frac{c_2}{c_1}t\right)^{\frac{2}{3}\frac{c_3}{c_2}-\frac{1}{3}}f(\xi), \tag{3.6.47}$$

$$v_n=(c_1+c_2t)^{\frac{2(c_3-2c_2)}{3c_2}}g(\xi)=c_1^{\frac{2}{3}\frac{c_3}{c_2}-\frac{4}{3}}\left(1+\frac{c_2}{c_1}t\right)^{\frac{2}{3}\frac{c_3}{c_2}-\frac{4}{3}}g(\xi), \tag{3.6.48}$$

$$p=\Lambda h(x,t), \tag{3.6.49}$$

$$\xi=c_3c_1^{-\frac{c_3}{c_2}}\frac{x}{L(t)}. \tag{3.6.50}$$

We now make a change of variables in order to simplify equations (3.6.40) to (3.6.50).

Let

$$u=\frac{x}{L(t)}. \tag{3.6.51}$$

The range of u is $0\leq u\leq 1$. From (3.6.50),

$$\xi=c_3c_1^{-\frac{c_3}{c_2}}u. \tag{3.6.52}$$

Also let

$$f(\xi)=c_3^{\frac{1}{3}}c_1^{-\frac{2}{3}\frac{c_3}{c_2}}F(u), \tag{3.6.53}$$

$$g(\xi) = c_3^{\frac{4}{3}} c_1^{-\frac{2}{3}\frac{c_3}{c_2}} G(u). \tag{3.6.54}$$

Equations (3.6.40) to (3.6.50) expressed in terms of u, $F(u)$ and $G(u)$ become :

$$\Lambda \frac{d}{du}\left(F^3 \frac{dF}{du}\right) + 3\frac{d}{du}\left(uF(u)\right) + \left(\frac{c_2}{c_3} - 5\right) F(u) - 3G(u) = 0, \tag{3.6.55}$$

$$F(1) = 0, \tag{3.6.56}$$

$$\Lambda F^3(0)\frac{dF}{du}(0) = \left(\frac{c_2}{c_3} - 5\right)\int_0^1 F(u)du - 3\int_0^1 G(u)du, \tag{3.6.57}$$

$$V_0 = 2\left(\frac{c_3}{c_1}\right)^{\frac{1}{3}} \int_0^1 F(u)du, \tag{3.6.58}$$

$$\frac{c_2}{c_1} = \frac{c_2}{c_3}\frac{c_3}{c_1}, \tag{3.6.59}$$

$$V(t) = V_0\left(1 + \frac{c_2}{c_1}t\right)^{\frac{5}{3}\frac{c_3}{c_2} - \frac{1}{3}}, \tag{3.6.60}$$

$$L(t) = \left(1 + \frac{c_2}{c_1}t\right)^{\frac{c_3}{c_2}}, \tag{3.6.61}$$

$$h(x,t) = \left(\frac{c_3}{c_1}\right)^{\frac{1}{3}}\left(1 + \frac{c_2}{c_1}t\right)^{\frac{2}{3}\frac{c_3}{c_2} - \frac{1}{3}} F(u), \tag{3.6.62}$$

$$v_n(x,t) = \left(\frac{c_3}{c_1}\right)^{\frac{4}{3}}\left(1 + \frac{c_2}{c_1}t\right)^{\frac{2}{3}\frac{c_3}{c_2} - \frac{4}{3}} G(u), \tag{3.6.63}$$

$$p(x,t) = \Lambda h(x,t), \tag{3.6.64}$$

where $0 \leq u \leq 1$. This completes the mathematical formulation of the problem.
We see that the solution depends on the ratios $\frac{c_1}{c_2}$, $\frac{c_2}{c_3}$, $\frac{c_3}{c_1}$ of the constants and not on the constants separately. This is because only the ratio of the constants in (3.6.4) can be determined since a constant multiple of a Lie point symmetry is also a Lie point symmetry.

In order to solve the system of equations (3.6.55) to (3.6.64), the ratio $\frac{c_2}{c_3}$, the initial total volume V_0 and $G(u)$, or a relation between $G(u)$ and $F(u)$, need to be given. Equation (3.6.55) is then an ordinary differential equation for $F(u)$ subject to the boundary conditions (3.6.56) and (3.6.57). The ratio $\frac{c_3}{c_1}$ is obtained from (3.6.58) and the ratio $\frac{c_2}{c_1}$ from (3.6.59). The solutions for $V(t)$, $L(t)$, $h(x,t)$, $v_n(x,t)$ and $p(x,t)$ are then given by (3.6.60) to (3.6.64).

In Chapters 4 and 5 we will consider the solution for two special relations between $G(u)$ and $F(u)$ and for a range of values of $\frac{c_3}{c_2}$.

3.7 Special values for the ratio $\frac{c_3}{c_2}$

When analysing the results it is more convenient to work with the ratio $\frac{c_3}{c_2}$ than with $\frac{c_2}{c_3}$. We investigate here the values taken by $\frac{c_3}{c_2}$ when a range of physical conditions are imposed on the fluid-driven fracture. The constants c_3 and c_1 are assumed to be positive while c_2 takes on all values on the real line.

The results derived here do not depend on the choice for $G(u)$ or the relation between $G(u)$ and $F(u)$.

3.7.1 Length of the fracture

The length of the fracture, $L(t)$, is given by (3.6.61). As $\frac{c_3}{c_2} \to 0$, the length $L(t)$ of the fracture tends to unity. Consider the limit $\frac{c_3}{c_2} \to \infty$. Then rewriting (3.6.61) as

$$L(t) = \exp\left[\frac{c_3}{c_2} ln\left(1 + \frac{c_2}{c_3}\frac{c_3}{c_1}t\right)\right] \tag{3.7.1}$$

and using the expansion

$$ln(1+\epsilon) = \epsilon - \frac{\epsilon^2}{2} + \frac{\epsilon^3}{3} + \bigcirc(\epsilon^4), \tag{3.7.2}$$

as $\epsilon \to 0$, it follows that in the limit $\frac{c_3}{c_2} = \infty$,

$$L(t) = \exp\left(\frac{c_3}{c_1}t\right). \tag{3.7.3}$$

As $t \to \infty$ and for all values of $\frac{c_3}{c_2}$ the fracture length, $L(t)$, behaves as the power law

$$\left(\frac{c_2}{c_1}\right)^{\frac{c_3}{c_2}} t^{\frac{c_3}{c_2}}. \tag{3.7.4}$$

The speed of propagation of the fracture is

$$\frac{dL}{dt} = \frac{c_3}{c_2}\left(1 + \frac{c_2}{c_1}t\right)^{\frac{c_3}{c_2}-1}. \tag{3.7.5}$$

The fracture propagates at constant speed if

$$\frac{c_3}{c_2} = 1. \tag{3.7.6}$$

The speed of propagation of the fracture has an exponential time-dependence in the limit $\frac{c_3}{c_2} \to \infty$ given by

$$\frac{dL}{dt} = \frac{c_3}{c_1}\exp\left(\frac{c_3}{c_1}t\right). \tag{3.7.7}$$

3.7.2 Total volume of the fracture

The total volume of the fracture per unit length in the y-direction, $V(t)$, is given by (3.6.60). The total volume of the fracture remains constant if

$$\frac{c_3}{c_2} = 0.2. \tag{3.7.8}$$

In the limit $\frac{c_3}{c_2} = \infty$, $V(t)$ has exponential time-dependence given by

$$V(t) = V_0\exp\left(\frac{5}{3}\frac{c_3}{c_1}t\right). \tag{3.7.9}$$

As $t \to \infty$ and for all values of $\frac{c_3}{c_2}$ the fracture volume, $V(t)$, behaves as the power law

$$V_0\left(\frac{c_2}{c_1}\right)^{\frac{5}{3}\frac{c_3}{c_2}-\frac{1}{3}} t^{\left(\frac{5}{3}\frac{c_3}{c_2}-\frac{1}{3}\right)}. \tag{3.7.10}$$

Also

$$\frac{dV}{dt} = \frac{5}{3}\frac{c_2}{c_1}\left(\frac{c_3}{c_2}-\frac{1}{5}\right)V_0\left(1+\frac{c_2}{c_1}t\right)^{\frac{5}{3}\frac{c_3}{c_2}-\frac{4}{3}}. \tag{3.7.11}$$

The rate of change of the total volume of the fracture per unit length in the y-direction is constant if

$$\frac{c_3}{c_2} = 0.8. \tag{3.7.12}$$

3.7.3 Pressure at the fracture entry

From (3.6.64) and (3.6.62) the pressure at the fracture entry, $x = 0$, is

$$p(0,t) = \Lambda\left(\frac{c_3}{c_1}\right)^{\frac{1}{3}}\left(1+\frac{c_2}{c_1}t\right)^{\frac{2}{3}\frac{c_3}{c_2}-\frac{1}{3}} F(0). \tag{3.7.13}$$

The pressure at the entry to the fracture remains constant if

$$\frac{c_3}{c_2} = 0.5. \tag{3.7.14}$$

For values of $\frac{c_3}{c_2} < 0.5$ the pumping pressure at the fracture entry, $x = 0$, is a decreasing function of time while for values of $\frac{c_3}{c_2} > 0.5$, the pumping pressure at the fracture entry is an increasing function of time.

3.7.4 Rate of working of the pressure at the fracture entry

The rate of working of the pressure at the fracture entry per unit length in the y-direction, $W(t)$, is

$$W(t) = p(0,t)\frac{dV}{dt}. \tag{3.7.15}$$

Using (3.7.11) and (3.7.13) we obtain

$$p(0,t)\frac{dV}{dt} = \frac{5}{3}\Lambda\frac{c_2}{c_1}\left(\frac{c_3}{c_2} - \frac{1}{5}\right)\left(\frac{c_3}{c_1}\right)^{\frac{1}{3}} V_0\left(1 + \frac{c_2}{c_1}t\right)^{\frac{7}{3}\frac{c_3}{c_2} - \frac{5}{3}} F(0). \tag{3.7.16}$$

Thus, the rate of working of the pressure at the fracture entry per unit length in the y-direction (which we can interpret as the rate of working of the pump) is constant if

$$\frac{c_3}{c_2} = \frac{5}{7} = 0.7143. \tag{3.7.17}$$

3.7.5 Rate of fluid injection into the fracture

The rate of fluid injection into the fracture per unit length in the y-direction, q_1, is given by (3.5.11):

$$q_1 = 2\int_0^{h(0,t)} v_x(0,z,t)dz. \tag{3.7.18}$$

But from (3.5.1) evaluated at $x = 0$,

$$v_x(0,z,t) = -\frac{1}{2}\left(h^2(0,t) - z^2\right)\frac{\partial p}{\partial x}(0,t). \tag{3.7.19}$$

Substituting (3.7.19) into (3.7.18) gives

$$q_1 = -\frac{2}{3}h^3(0,t)\frac{\partial p}{\partial x}(0,t). \tag{3.7.20}$$

Using (3.6.64) and (3.6.62), (3.7.20) becomes

$$q_1 = -\frac{2}{3}\Lambda \left(\frac{c_3}{c_1}\right)^{\frac{4}{3}} \left(1+\frac{c_2}{c_1}t\right)^{\frac{5}{3}\frac{c_3}{c_2}-\frac{4}{3}} F^3(0)\frac{dF}{du}(0). \tag{3.7.21}$$

Thus the rate of fluid injection into the fracture is independent of time if

$$\frac{c_3}{c_2} = 0.8. \tag{3.7.22}$$

3.7.6 Rate of fluid leak-off at the fluid/rock interface

The rate of fluid leak-off at the interface between the fluid and rock per unit length in the y-direction, q_2, is given by (3.5.12):

$$q_2 = 2\int_0^{L(t)} v_n(x,t)dx. \tag{3.7.23}$$

Using (3.6.63), (3.7.23) becomes

$$q_2 = 2\left(\frac{c_3}{c_1}\right)^{\frac{4}{3}} \left(1+\frac{c_2}{c_1}t\right)^{\frac{5}{3}\frac{c_3}{c_2}-\frac{4}{3}} \int_0^1 G(u)du. \tag{3.7.24}$$

Thus the rate of fluid leak-off at the fluid-rock interface is independent of time if

$$\frac{c_3}{c_2} = 0.8. \tag{3.7.25}$$

3.7.7 Balance law for flux of fluid

By considering the balance law for the flux of fluid into the fracture a useful expression for the rate of fluid injection can be obtained. From (3.5.13), per unit length in the y-direction,

rate of fluid injection into the fracture = rate of change of the total volume of the fracture + rate of fluid leak-off at the fluid-rock interface.

Thus

$$q_1 = \frac{dV}{dt} + q_2 \tag{3.7.26}$$

and using (3.7.11), (3.6.58) for V_0 and (3.7.24), (3.7.26) becomes

$$q_1 = \frac{2}{3}\left(\frac{c_3}{c_1}\right)^{\frac{4}{3}} \left(1+\frac{c_2}{c_1}t\right)^{\frac{5}{3}\frac{c_3}{c_2}-\frac{4}{3}} \left[3\int_0^1 G(u)du + \left(5-\frac{c_2}{c_3}\right)\int_0^1 F(u)du\right]. \tag{3.7.27}$$

Equation (3.7.27) for the rate of fluid injection into the fracture will be useful for interpreting the results. The results derived in this section are summarized in Table (3.7.1).

Length of the fracture is constant	$\frac{c_3}{c_2} = 0$
Total volume of the fluid in the fracture is constant	$\frac{c_3}{c_2} = 0.2$
Pressure at the fracture entry is constant	$\frac{c_3}{c_2} = 0.5$
Rate of working of the pressure at the fracture entry is constant	$\frac{c_3}{c_2} = 0.714$
Rate of fluid injection into the fracture is constant	$\frac{c_3}{c_2} = 0.8$
Rate of fluid leak-off at the fluid/rock interface is constant	$\frac{c_3}{c_2} = 0.8$
Rate of change of the total volume of the fracture is constant	$\frac{c_3}{c_2} = 0.8$
Speed of propagation of the fracture is constant	$\frac{c_3}{c_2} = 1.0$

Table 3.7.1: Physical significance of values of the ratio $\frac{c_3}{c_2}$.

Chapter 4

LEAK-OFF VELOCITY PROPORTIONAL TO FRACTURE HALF-WIDTH

4.1 Introduction

In order to solve the boundary value problem (3.6.55) to (3.6.64), either $G(u)$ must be given or a relation between $G(u)$ and $F(u)$ stated. In this chapter, we begin by specifying a form for $G(u)$ which is in direct proportion to $F(u)$. The constant of proportionality is β and it plays an important role in this chapter and in subsequent chapters. Equations (4.2.4) to (4.2.13) which are now in terms of the dependent variable $F(u)$ are solved for special cases which yield exact solutions. We have identified two special cases of exact solutions. The first case which yields exact solutions corresponds to the condition in which the net flow of viscous incompressible fluid into the fracture at the fracture entry is zero. The second case of exact solutions corresponds to a condition in which the net flow of viscous incompressible fluid into the fracture at the fracture entry is positive. Another possible physical condition is when there is fluid extraction out of the fracture at the fracture entry. No exact solution has been found for this condition.

In Section 4.3, analytical solutions are obtained for the case when the rate of fluid injection

into the fracture at the fracture entry is zero while in Section 4.5, analytical solutions for which the rate of fluid injection is positive at the fracture entry are obtained. The results for the two cases of analytical solutions are discussed and analysed in Sections 4.4 and 4.6. Numerical analysis of the boundary value problem (4.2.4) to (4.2.13) commences in Section 4.7 with the transformation of the boundary value problem into two intial value problems which are easier to solve.

4.2 Leak-off velocity proportional to half-width of fracture

Consider the case where $G(u)$ is proportional to $F(u)$:

$$G(u) = \beta F(u), \tag{4.2.1}$$

where β is a constant. It follows from (3.6.62) and (3.6.63) that

$$v_n = \beta \frac{c_3}{(c_1 + c_2 t)} h(x,t) = \beta \frac{c_3}{c_1} \frac{h(x,t)}{L(t)^{\frac{c_2}{c_3}}}. \tag{4.2.2}$$

For large times,

$$v_n \sim \beta \frac{h(x,t)}{\frac{c_2}{c_3} t}. \tag{4.2.3}$$

Hence, $v_n(x,t)$ is proportional to the half-width of the fracture, $h(x,t)$. It follows immediately from (4.2.2) that v_n vanishes at the fracture tip since $h(x,t)$ vanishes there. From (4.2.2), the case $\beta > 0$ describes fluid leak-off into the rock mass and $\beta < 0$ describes fluid inflow into the fracture at the fluid-rock interface. The case $\beta = 0$ represents no leak-off of fluid into the rock mass and this means that the rock is impermeable.

The boundary value problem is then stated as follows:

$$\Lambda \frac{d}{du}\left(F^3 \frac{dF}{du}\right) + 3\frac{d}{du}\left(uF(u)\right) + \left(\frac{c_2}{c_3} - 5 - 3\beta\right) F(u) = 0, \tag{4.2.4}$$

$$F(1) = 0, \tag{4.2.5}$$

$$\Lambda F^3(0)\frac{dF}{du}(0) = \left(\frac{c_2}{c_3} - 5 - 3\beta\right)\int_0^1 F(u)du, \tag{4.2.6}$$

$$V_0 = 2\left(\frac{c_3}{c_1}\right)^{\frac{1}{3}} \int_0^1 F(u)du, \tag{4.2.7}$$

$$\frac{c_2}{c_1} = \frac{c_2}{c_3}\frac{c_3}{c_1}, \tag{4.2.8}$$

$$V(t) = V_0\left(1 + \frac{c_2}{c_1}t\right)^{\frac{5}{3}\frac{c_3}{c_2} - \frac{1}{3}}, \tag{4.2.9}$$

$$L(t) = \left(1 + \frac{c_2}{c_1}t\right)^{\frac{c_3}{c_2}}, \tag{4.2.10}$$

$$h(x,t) = \left(\frac{c_3}{c_1}\right)^{\frac{1}{3}}\left(1 + \frac{c_2}{c_1}t\right)^{\frac{2}{3}\frac{c_3}{c_2} - \frac{1}{3}} F(u), \tag{4.2.11}$$

$$v_n(x,t) = \beta\left(\frac{c_3}{c_1}\right)^{\frac{4}{3}}\left(1 + \frac{c_2}{c_1}t\right)^{\frac{2}{3}\frac{c_3}{c_2} - \frac{4}{3}} F(u), \tag{4.2.12}$$

$$p(x,t) = \Lambda h(x,t), \tag{4.2.13}$$

where

$$u = \frac{x}{L(t)}, \qquad 0 \le u \le 1. \tag{4.2.14}$$

Firstly, we determine how $F(u)$ behaves as $u \to 1$. The asymptotic behaviour of $F(u)$ as $u \to 1$ is required in the numerical solution for $F(u)$. We seek a solution having asymptotic series expansion of the form

$$F(u) \sim \sum_{n=1}^{\infty} a_n (b-u)^{s_n} \quad \text{as} \quad u \to 1, \tag{4.2.15}$$

where b, a_n, s_n are constants and $a_n \neq 0$ for some $n \geq 1$ and $s_n > 0$ with $s_1 < s_2 < s_3 \cdots$. Using boundary condition (4.2.5), we obtain $b = 1$. Hence, (4.2.15) becomes:

$$F(u) \sim \sum_{n=1}^{\infty} a_n (1-u)^{s_n}, \qquad \text{as} \qquad u \to 1. \tag{4.2.16}$$

The asymptotic sequence of functions $\{(1-u)^{s_n}\}$ is such that

$$\frac{(1-u)^{s_{n+1}}}{(1-u)^{s_n}} \to 0 \quad \text{as} \quad u \to 1. \tag{4.2.17}$$

Therefore, we approximate $F(u)$ by the first and leading term of the series. Thus

$$F(u) \sim a_1(1-u)^{s_1}. \tag{4.2.18}$$

We substitute (4.2.18) for $F(u)$ into the differential equation (4.2.4) to obtain

$$a_1^4 \Lambda s_1(4s_1-1)(1-u)^{4s_1-2} - 3a_1 s_1(1-u)^{s_1-1} + (\frac{c_2}{c_3} - 2 - 3\beta + 3s_1)a_1(1-u)^{s_1} \sim 0, \tag{4.2.19}$$

as $u \to 1$. In order that the dominant terms in (4.2.19) balance each other

$$4s_1 - 2 = s_1 - 1, \tag{4.2.20}$$

which implies that

$$s_1 = \frac{1}{3}. \tag{4.2.21}$$

Substituting equation (4.2.21) into (4.2.19) gives

$$\frac{1}{9}\Lambda a_1^4(1-u)^{-\frac{2}{3}} - a_1(1-u)^{-\frac{2}{3}} + (\frac{c_2}{c_3} - 1 - 3\beta)a_1(1-u)^{\frac{1}{3}} \sim 0 \tag{4.2.22}$$

as $u \to 1$, and therefore

$$\frac{1}{9}\Lambda a_1^4 - a_1 + \left(\frac{c_2}{c_3} - 1 - 3\beta\right) a_1(1-u) \sim 0 \tag{4.2.23}$$

as $u \to 1$. Hence, setting $u = 1$ in (4.2.23), we obtain

$$a_1 = \left(\frac{9}{\Lambda}\right)^{\frac{1}{3}}. \tag{4.2.24}$$

Thus, the asymptotic solution of (4.2.4) as $u \to 1$ is

$$F(u) \sim \left(\frac{9}{\Lambda}\right)^{\frac{1}{3}} (1-u)^{\frac{1}{3}}. \tag{4.2.25}$$

The asymptotic solution (4.2.25) for $F(u)$ is true for all the values of $\frac{c_2}{c_3}$ and β.

We now consider two special cases which yield exact analytical solutions for the differential equation (4.2.4).

4.3 Exact solution for zero fluid injection rate at fracture entry

We first consider the special case when

$$\frac{c_2}{c_3} - 5 - 3\beta = 0. \tag{4.3.1}$$

The differential equation (4.2.4) reduces to

$$\Lambda \frac{d}{du}\left(F^3 \frac{dF}{du}\right) + 3\frac{d}{du}\left(uF(u)\right) = 0, \tag{4.3.2}$$

subject to the boundary conditions (4.2.5) and (4.2.6):

$$F(1) = 0. \tag{4.3.3}$$

$$\frac{dF}{du}(0) = 0. \tag{4.3.4}$$

In (4.2.6), $F(0) \neq 0$ and finite because $h(0,t) \neq 0$ and finite in (4.2.11). Integrate (4.3.2) with respect to u:

$$\Lambda F^3 \frac{dF}{du} + 3uF(u) = A, \tag{4.3.5}$$

where A is a constant. To obtain A impose the boundary condition (4.3.4) at $u = 0$. Since $F(0)$ is finite, $A = 0$ and (4.3.5) becomes

$$F^2 \frac{dF}{du} = -\frac{3}{\Lambda}u, \tag{4.3.6}$$

which is variables separable differential equation. Integrating (4.3.6) gives

$$F^3(u) = -\frac{9}{2\Lambda}u^2 + B, \tag{4.3.7}$$

where B is a constant. Imposing the boundary condition (4.3.3) at $u = 1$ gives

$$B = \frac{9}{2\Lambda} \tag{4.3.8}$$

and therefore

$$F(u) = \left(\frac{9}{2\Lambda}\right)^{\frac{1}{3}} \left(1 - u^2\right)^{\frac{1}{3}}. \tag{4.3.9}$$

Substituting (4.3.9) into (4.2.7) gives

$$\frac{c_3}{c_1} = \frac{\Lambda}{36}\left(\frac{V_0}{I}\right)^3, \tag{4.3.10}$$

where

$$I = \int_0^1 (1-u^2)^{\frac{1}{3}} du = 0.8413 \tag{4.3.11}$$

and therefore from (4.2.8)

$$\frac{c_2}{c_1} = \frac{c_2}{c_3}\left(\frac{V_0}{I}\right)^3 \frac{\Lambda}{36}. \tag{4.3.12}$$

Also from (4.2.14),

$$u = \frac{x}{L(t)}. \tag{4.3.13}$$

The solution can be expressed in terms of either β or $\frac{c_2}{c_3}$. We will express the solution in terms of $\frac{c_2}{c_3}$. From (4.3.1),

$$\beta = \frac{1}{3}\left(\frac{c_2}{c_3} - 5\right) \tag{4.3.14}$$

and from (4.2.9) to (4.2.13),

$$V(t) = V_0\left[1 + \frac{c_2}{c_3}\left(\frac{V_0}{I}\right)^3 \frac{\Lambda t}{36}\right]^{\frac{5}{3}(\frac{c_3}{c_2}-\frac{1}{5})}, \tag{4.3.15}$$

$$L(t) = \left[1 + \frac{c_2}{c_3}\left(\frac{V_0}{I}\right)^3 \frac{\Lambda t}{36}\right]^{\frac{c_3}{c_2}}, \tag{4.3.16}$$

$$h(x,t) = \frac{V_0}{2I}\left[1 + \frac{c_2}{c_3}\left(\frac{V_0}{I}\right)^3 \frac{\Lambda t}{36}\right]^{\frac{2}{3}(\frac{c_3}{c_2}-\frac{1}{2})}\left[1 - \frac{x^2}{L^2(t)}\right]^{\frac{1}{3}}, \tag{4.3.17}$$

$$v_n(x,t) = \frac{\beta\Lambda}{72}\left(\frac{V_0}{I}\right)^4\left[1 + \frac{c_2}{c_3}\left(\frac{V_0}{I}\right)^3 \frac{\Lambda t}{36}\right]^{\frac{2}{3}(\frac{c_3}{c_2}-2)}\left[1 - \frac{x^2}{L^2(t)}\right]^{\frac{1}{3}}, \tag{4.3.18}$$

$$p(x,t) = \Lambda h(x,t). \tag{4.3.19}$$

By expressing β in terms of $\frac{c_2}{c_3}$, (4.3.18) becomes

$$v_n(x,t) = \left(\frac{c_2}{c_3} - 5\right)\frac{2\Lambda}{27}\left(\frac{V_0}{2I}\right)^4\left[1 + \frac{c_2}{c_3}\left(\frac{V_0}{I}\right)^3 \frac{\Lambda t}{36}\right]^{\frac{2}{3}(\frac{c_3}{c_2}-2)}\left[1 - \frac{x^2}{L^2(t)}\right]^{\frac{1}{3}}. \tag{4.3.20}$$

The solution for $h(x,t)$, $v_n(x,t)$ and $p(x,t)$ can be expressed in terms of $L(t)$:

$$h(x,t) = \frac{V_0}{2I}L(t)^{\frac{1}{3}(2-\frac{c_2}{c_3})}\left[1 - \frac{x^2}{L^2(t)}\right]^{\frac{1}{3}}, \tag{4.3.21}$$

$$v_n(x,t) = \left(\frac{c_2}{c_3} - 5\right)\frac{2\Lambda}{27}\left(\frac{V_0}{2I}\right)^4 L(t)^{\frac{4}{3}(\frac{1}{2}-\frac{c_2}{c_3})}\left[1 - \frac{x^2}{L^2(t)}\right]^{\frac{1}{3}} \tag{4.3.22}$$

and $p(x,t)$ is related to $h(x,t)$ by (4.3.19).

In the limit $\frac{c_3}{c_2} \to \infty$, $\beta \to -1.66$, $L(t)$, $h(x,t)$, $V(t)$, $v_n(x,t)$ and $p(x,t)$ have exponential time-dependence and (4.3.15) to (4.3.19) tend to

$$V(t) = V_0 \exp\left(\frac{5}{108}\left(\frac{V_0}{I}\right)^3 \Lambda t\right), \tag{4.3.23}$$

$$L(t) = \exp\left(\frac{1}{36}\left(\frac{V_0}{I}\right)^3 \Lambda t\right), \tag{4.3.24}$$

$$h(x,t) = \frac{V_0}{2I}\exp\left(\frac{1}{54}\left(\frac{V_0}{I}\right)^3 \Lambda t\right)\left[1 - \frac{x^2}{L(t)^2}\right]^{\frac{1}{3}}, \tag{4.3.25}$$

$$v_n(x,t) = -\frac{10\Lambda}{27}\left(\frac{V_0}{2I}\right)^4 \exp\left(\frac{1}{54}\left(\frac{V_0}{I}\right)^3 \Lambda t\right)\left[1 - \frac{x^2}{L(t)^2}\right]^{\frac{1}{3}} \tag{4.3.26}$$

and $p(x,t)$ and $h(x,t)$ are related by (4.3.19).

4.4 Discussion of results for $\beta = \frac{1}{3}\left(\frac{c_2}{c_3} - 5\right)$

Consider now the physical significance of the special case (4.3.14). Equation (4.3.14) defines a dividing curve between solutions of interest in the $\left(\frac{c_3}{c_2}, \beta\right)$ plane. The rate of fluid injection into the fracture at the fracture entry, q_1, is given by (3.7.27) and the rate of fluid leak-off at the fluid/rock interface, q_2, is given by (3.7.24). When $G(u) = \beta F(u)$, and after substituting (4.3.9), (4.3.10) and (4.3.12), equation (3.7.27) for the rate of fluid injection into the fracture at the fracture entry becomes

$$q_1 = \frac{\Lambda}{108}\left(\frac{V_0}{I}\right)^4\left[1 + \frac{1}{36}\left(\frac{V_0}{I}\right)^3 \frac{c_2}{c_3}\Lambda t\right]^{\frac{5}{3}\frac{c_3}{c_2}-\frac{4}{3}}\left(3\beta + 5 - \frac{c_2}{c_3}\right)I. \tag{4.4.1}$$

and equation (3.7.24) for the rate of fluid leak-off at the fluid/rock interface becomes

$$q_2 = \frac{\Lambda}{36}\left(\frac{V_0}{I}\right)^4\left[1 + \frac{1}{36}\left(\frac{V_0}{I}\right)^3 \frac{c_2}{c_3}\Lambda t\right]^{\frac{5}{3}\frac{c_3}{c_2}-\frac{4}{3}}\beta I. \tag{4.4.2}$$

When condition (4.3.14) is substituted into (4.4.1), we obtain

$$q_1 = 0. \tag{4.4.3}$$

This implies that the rate of fluid injection into the fracture at the fracture entry vanishes for all values of $\frac{c_3}{c_2}$ and β that satisfiy (4.3.14). This occurs when the net flow of viscous fluid into and out of the fracture at the fracture entry is zero. Physically this could correspond to the case in which pumping has ceased and the entrance to the fracture sealed. The fracture then relaxes and evolves due to leak-off or inflow at the fluid/rock interface. For the case in which

$$\beta < \frac{1}{3}\left(\frac{c_2}{c_3} - 5\right), \tag{4.4.4}$$

we have a negative net flux and the rate of fluid injection at the fracture entry

$$q_1 < 0. \tag{4.4.5}$$

Physically, (4.4.4) describes fluid suction out of the fracture. The condition

$$\beta > \frac{1}{3}\left(\frac{c_2}{c_3} - 5\right) \tag{4.4.6}$$

describes fluid injection into the fracture.

Condition (4.3.14) can be solved for β in terms of $\frac{c_3}{c_2}$ to give

$$\beta = \frac{\frac{5}{3}\left(\frac{1}{5} - \frac{c_3}{c_2}\right)}{\frac{c_3}{c_2}} \tag{4.4.7}$$

and for $\frac{c_3}{c_2}$ in terms of β as

$$\frac{c_3}{c_2} = \frac{1}{5 + 3\beta}. \tag{4.4.8}$$

The graph of β against $\frac{c_3}{c_2}$ given by equation (4.4.7) is plotted in Figure 4.4.1. For values of β above the curve there is fluid injection into the fracture at the entry to the fracture while for values of β below the curve fluid is extracted at the fracture entry. We will investigate the whole range $-\infty < \frac{c_3}{c_2} < \infty$ to determine the results produced by the solution. Table (3.7.1) shows that the range of values of practical interest is $0 < \frac{c_3}{c_2} \leq 1$. In the graphical results that follow, we have redefined

$$t' = \Lambda t. \tag{4.4.9}$$

and for simplicity dropped the dash.

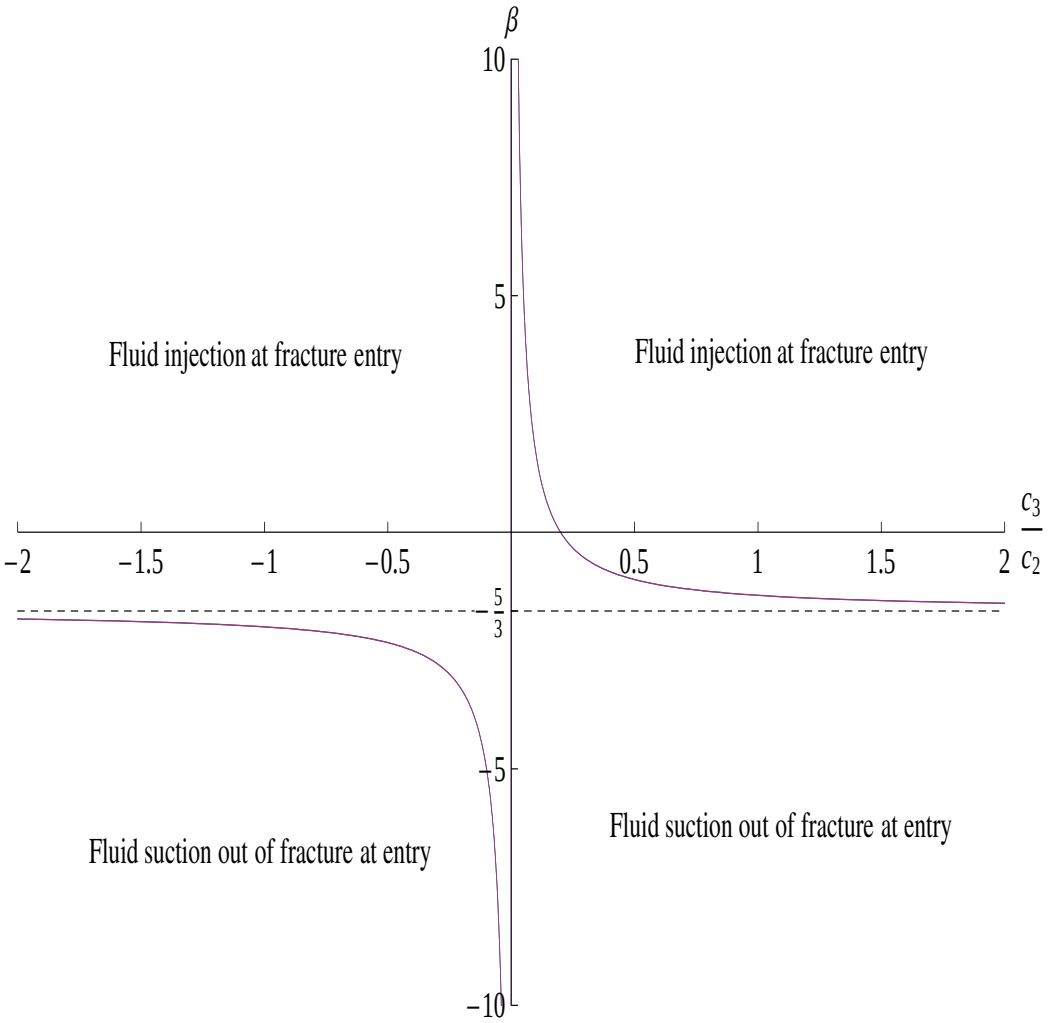


Figure 4.4.1: Graph of $\beta = \frac{\frac{5}{3}\left(\frac{1}{5} - \frac{c_3}{c_2}\right)}{\frac{c_3}{c_2}}$ plotted against $\frac{c_3}{c_2}$ for the range $-2 < \frac{c_3}{c_2} < 2$.

4.4.1 Fracture length and volume

Consider first the length of the fracture $L(t)$ given by (4.3.16) and (4.3.24) and plotted in Figure 4.4.2. As $\frac{c_3}{c_2}$ increases from 0 to 0.2, β decreases from $+\infty$ to 0 and there is fluid leak-off at the fluid-rock interface. At $\frac{c_3}{c_2} = 0.2$, $\beta = 0$ and there is no fluid leak-off. As $\frac{c_3}{c_2}$ increases from 0.2 to $+\infty$, β decreases from 0 to $-\frac{5}{3}$ and fluid enters the fracture at the fluid-rock interface. For $0 < \frac{c_3}{c_2} < \infty$, $L(t)$ is an increasing function of time and $L(t) \to \infty$ as $t \to \infty$. As $\frac{c_3}{c_2}$ increases from $-\infty$ to 0, β decreases from $-\frac{5}{3}$ to $-\infty$. Since $\frac{c_3}{c_2} < 0$, $\frac{c_2}{c_1} < 0$

and it follows that $L(t) \to +\infty$ in the finite time

$$t = -\frac{c_3}{c_2}\left(\frac{I}{V_0}\right)^3 \frac{36}{\Lambda}. \tag{4.4.10}$$

In Figure 4.4.2, $L(t) \to \infty$ in finite time $t' = \Lambda t$ = 36 when $\frac{c_3}{c_2} = -1$ and $\frac{V_0}{I} = 1$. The length of the fracture increases for $-\infty < \frac{c_3}{c_2} < \infty$ except at $\frac{c_3}{c_2} = 0$ even though there is no fluid injection at the entry to the fracture. Finally for $\frac{c_3}{c_2} = \infty$, $L(t) \to \infty$ exponentially as $t \to \infty$.

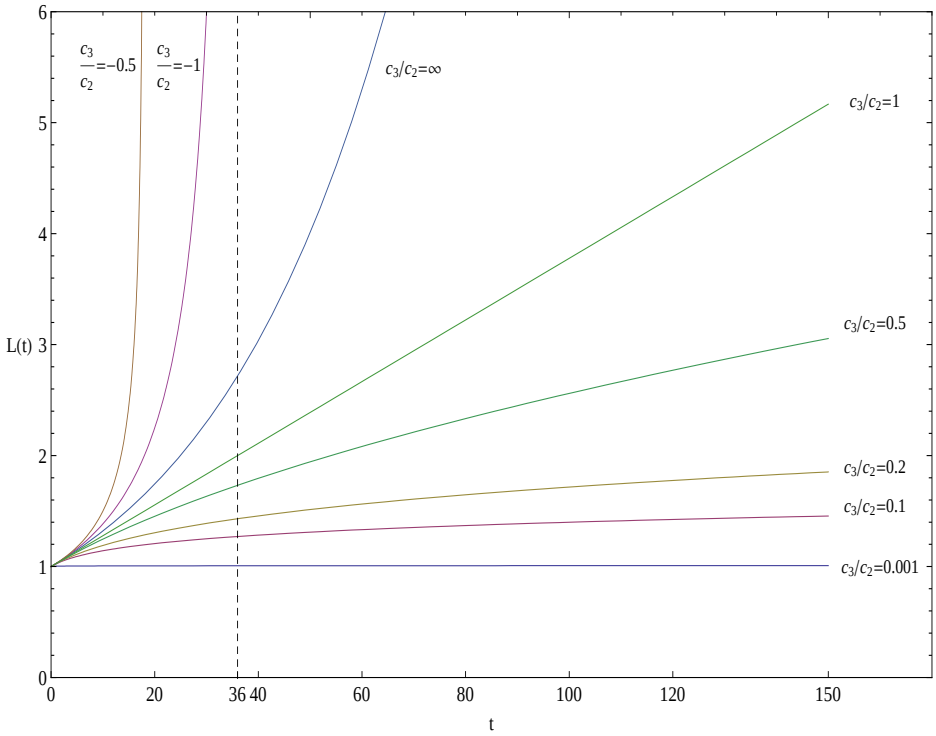


Figure 4.4.2: Leak-off velocity proportional to fracture half-width: Graph of fracture length $L(t)$ given by (4.3.16) and (4.3.24) plotted against t for a selection of values of the parameter $\frac{c_3}{c_2}$ and for $\frac{V_0}{I} = 1$.

Consider next the total volume of the fracture $V(t)$ given by (4.3.15) and (4.3.23) and plotted in Figure 4.4.3. For the analytical solutions considered in this section, the rate of fluid injection into the fracture at the fracture entry is zero. Hence the total volume of the fracture $V(t)$ can only change due to leak-off or inflow at the fluid-rock interface. For $0 < \frac{c_3}{c_2} < 0.2$, $\beta > 0$ and there is leak-off at the fluid-rock interface. The time rate of change of fracture volume is negative, $\frac{dV}{dt} < 0$, and $V(t) \to 0$ as $t \to \infty$. For $\frac{c_3}{c_2} = 0.2$, the rock is impermeable and $V(t)$ is constant for all time. This compares with the length of the fracture, $L(t)$, which still increases when $\frac{c_3}{c_2} = 0.2$. For $0.2 < \frac{c_3}{c_2} < \infty$, $\beta < 0$ and the fluid enters the fracture at the fluid-rock interface. Then $V(t)$ is an increasing function of time, $\frac{dV}{dt} > 0$ and $V(t) \to \infty$ as $t \to \infty$. We have a time dependent exponential solution when $\frac{c_3}{c_2} = \infty$. As $\frac{c_3}{c_2}$ increases from $-\infty$ to 0, β decreases from $-\frac{5}{3}$ to $-\infty$ and fluid enters the fracture at the fluid-rock interface. Since $\frac{c_3}{c_2} < 0$ and $\frac{c_2}{c_1} < 0$, $V(t) \to \infty$ in the finite time (4.4.10).

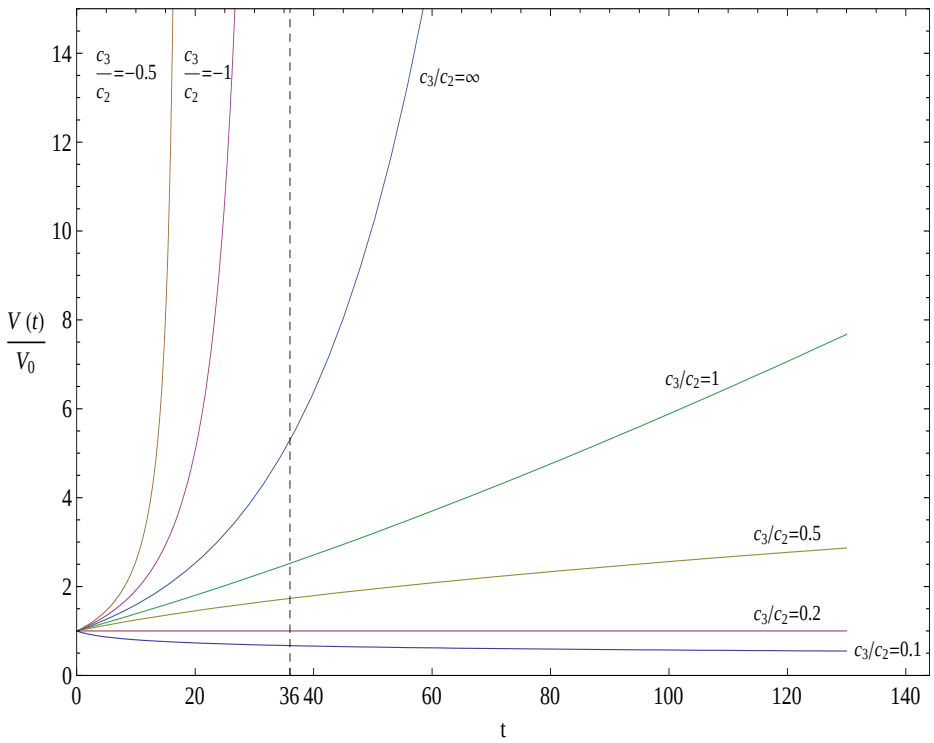


Figure 4.4.3: Leak-off velocity proportional to fracture half-width: Total volume of the fracture $\frac{V(t)}{V_0}$ given by (4.3.15) and (4.3.23) plotted against t for a selection of values of the parameter $\frac{c_3}{c_2}$ and for $\frac{V_0}{I} = 1$.

4.4.2 Fracture half-width and leak-off velocity

Consider now $h(x,t)$ which is given by (4.3.17) and (4.3.25) and plotted in Figures 4.4.4a to 4.4.11a. The initial fracture shape $h(x,0)$ cannot be specified arbitrarily. Since $L(0) = 1$, it follows from (4.3.17) and (4.3.25) that

$$h(x,0) = \frac{V_0}{2I}\left(1-x^2\right)^{\frac{1}{3}}. \tag{4.4.11}$$

Also,

$$h(0,0) = \frac{V_0}{2I}. \tag{4.4.12}$$

Now consider the half-width of the fracture at $x = 0$. From (4.3.17) for $\frac{c_3}{c_2}$ finite,

$$h(0,t) = \frac{V_0}{2I}\left[1 + \frac{c_2}{c_3}\left(\frac{V_0}{I}\right)^3 \frac{\Lambda t}{36}\right]^{\frac{2}{3}\left(\frac{c_3}{c_2}-\frac{1}{2}\right)}, \tag{4.4.13}$$

and from (4.3.25) for $\frac{c_3}{c_2} = \infty$,

$$h(0,t) = \frac{V_0}{2I}\exp\left(\frac{1}{54}\left(\frac{V_0}{I}\right)^3 \Lambda t\right). \tag{4.4.14}$$

For $0 < \frac{c_3}{c_2} < \frac{1}{2}$, the width of the fracture at the entry, $h(0,t)$, decreases as t increases. When $\frac{c_3}{c_2} = \frac{1}{2}$, the width of the fracture at the entry, $h(0,t)$, remains constant. For $\frac{1}{2} < \frac{c_3}{c_2} \leq \infty$, $h(0,t)$ increases as t increases. For $-\infty < \frac{c_3}{c_2} < 0$, $h(0,t) \to \infty$ in the finite time given by (4.4.10). The results are illustrated in Figures 4.4.4a to 4.4.11a. Also from (4.3.17) and (4.3.25),

$$\frac{\partial h}{\partial x} = -\frac{V_0 x}{3I}\left[1 + \frac{1}{36}\frac{c_2}{c_3}\left(\frac{V_0}{I}\right)^3 \Lambda t\right]^{-\frac{4}{3}\left(\frac{c_3}{c_2}+\frac{1}{4}\right)}\left[1 - \frac{x^2}{L(t)^2}\right]^{-\frac{2}{3}}, \tag{4.4.15}$$

$$\frac{\partial h}{\partial x} = -\frac{V_0 x}{3I}\exp\left(-\frac{1}{27}\left(\frac{V_0}{I}\right)^3 \Lambda t\right)\left[1 - \frac{x^2}{L(t)^2}\right]^{-\frac{2}{3}}, \tag{4.4.16}$$

and therefore $\dfrac{\partial h}{\partial x} \to -\infty$ as $x \to L(t)$. The thin film approximation breaks down in the vicinity of the fracture tip, $x = L(t)$.

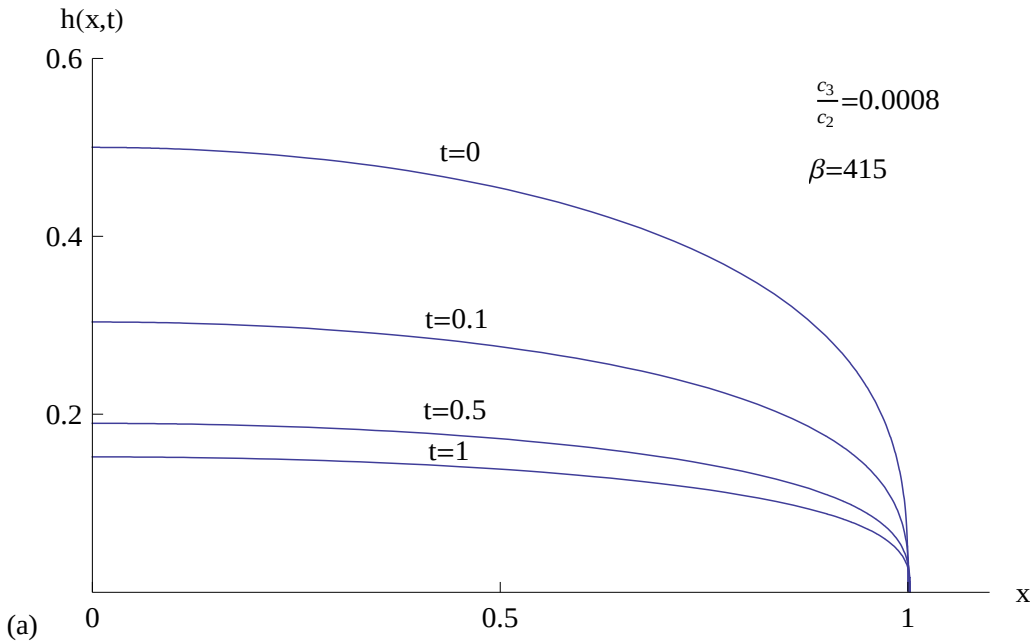
Finally, consider $v_n(x,t)$ which is given by (4.3.18) and (4.3.26) and is also plotted in Figures 4.4.4b to 4.4.11b. From (4.3.18) for $\frac{c_3}{c_2}$ finite

$$v_n(0,t) = \frac{\beta\Lambda}{72}\left(\frac{V_0}{I}\right)^4\left[1 + \frac{c_2}{c_3}\left(\frac{V_0}{I}\right)^3 \frac{\Lambda t}{36}\right]^{\frac{2}{3}\left(\frac{c_3}{c_2}-2\right)} \tag{4.4.17}$$

and for $\frac{c_3}{c_2} = \infty$,

$$v_n(0,t) = -\frac{10\Lambda}{27}\left(\frac{V_0}{2I}\right)^4 \exp\left(\frac{1}{54}\left(\frac{V_0}{I}\right)^3 \Lambda t\right). \tag{4.4.18}$$

For $0 < \frac{c_3}{c_2} < 0.2$, $v_n > 0$ and there is leak-off of fluid at the fluid/rock interface. Also $v_n(0,t)$ decreases as t increases. For $0.2 < \frac{c_3}{c_2} < \infty$, $v_n(x,t) < 0$ and there is fluid inflow at the fluid/rock interface. For $0 \leq \frac{c_3}{c_2} < 2$, the magnitude of $v_n(0,t)$ decreases as t increases except at $\frac{c_3}{c_2} = 0.2$ where v_n vanishes. When $\frac{c_3}{c_2} = 2$, the magnitude of $v_n(0,t)$ remains constant and when $2 < \frac{c_3}{c_2} < \infty$ the magnitude of the inflow at the fluid/rock interface increases as t increases. For $-\infty < \frac{c_3}{c_2} < 0$, $\beta < 0$ and there is fluid inflow at the fluid/rock interface. Also $v_n(x,t) \to -\infty$ in the finite time (4.4.10).



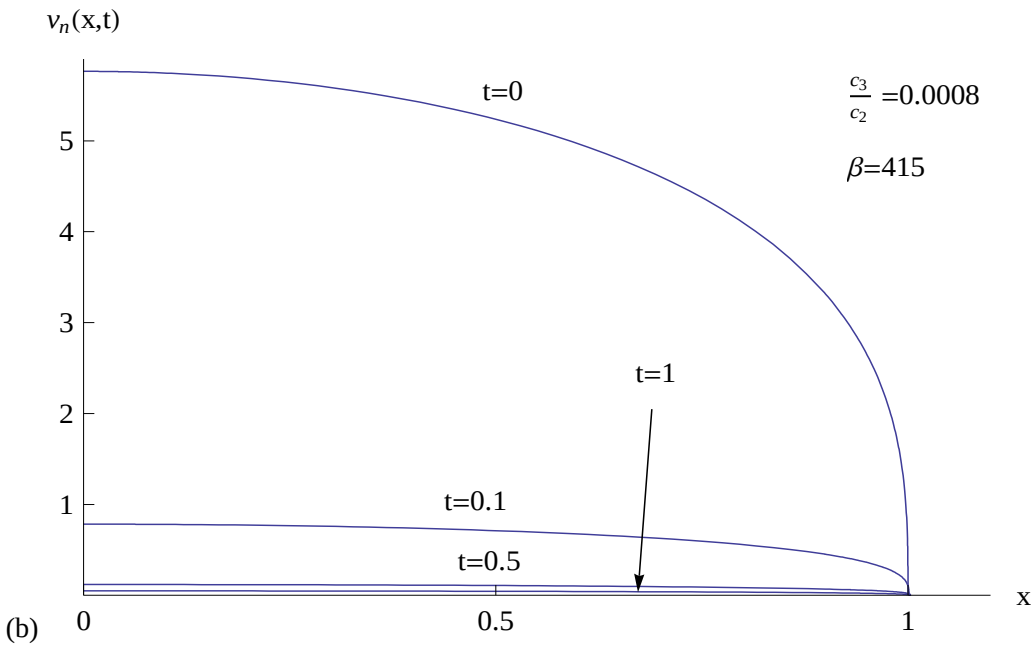
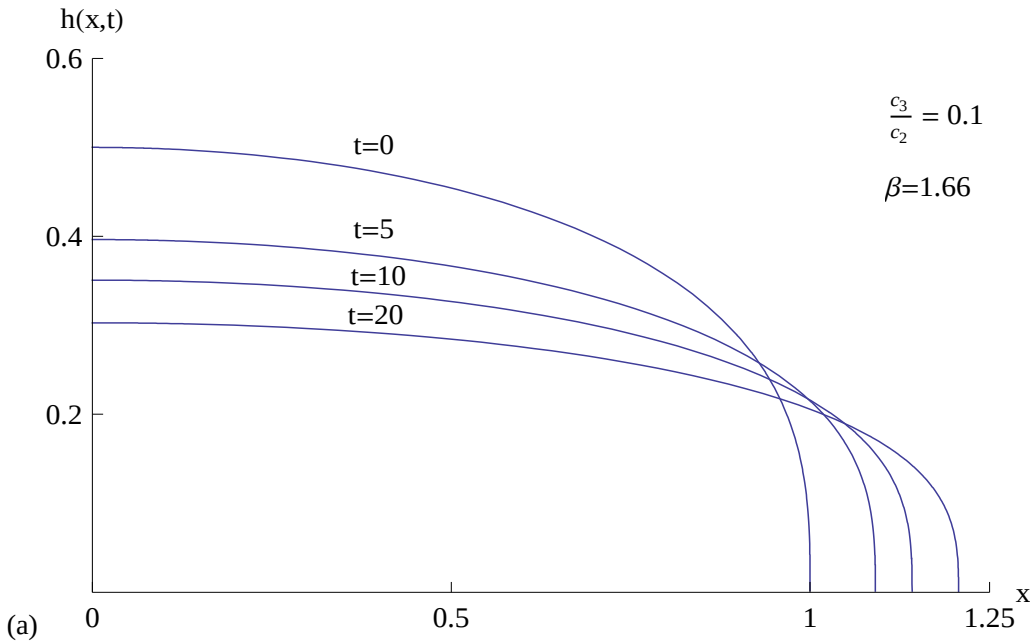
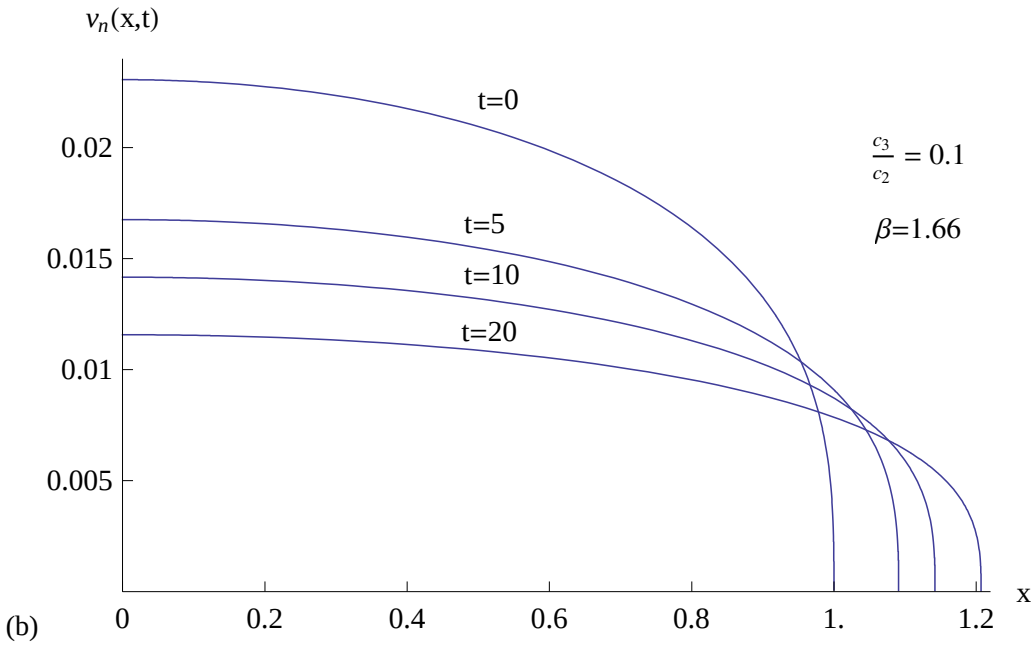


Figure 4.4.4: (a) Fracture half-width, $h(x,t)$, given by (4.3.17) and (b) leak-off velocity at the fluid/rock interface, $v_n(x,t)$, given by (4.3.18), plotted against x for a range of values of t and for $\frac{c_3}{c_2} = 0.0008$, $\beta = 415$.



(a)



(b)

Figure 4.4.5: (a) Fracture half-width, $h(x,t)$, given by (4.3.17) and (b) leak-off velocity at the fluid/rock interface, $v_n(x,t)$, given by (4.3.18), plotted against x for a range of values of t and for $\frac{c_3}{c_2} = 0.1$, $\beta = 1.66$.

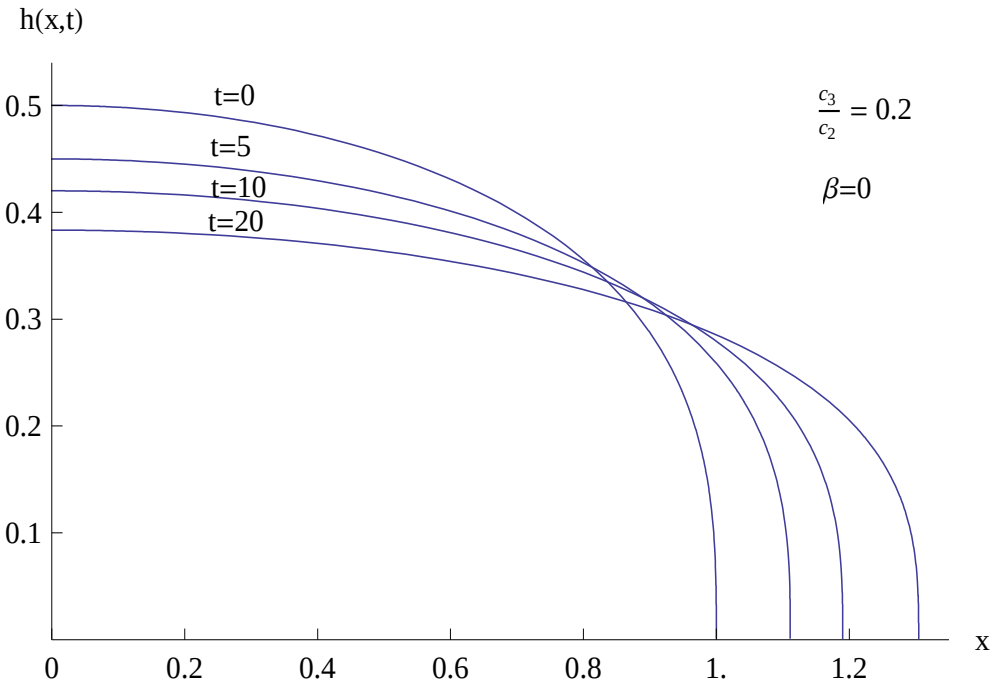


Figure 4.4.6: Fracture halfwidth, $h(x,t)$, given by (4.3.17) plotted against x for a range of values of t and for $\frac{c_3}{c_2} = 0.2$, $\beta = 0$. The leak-off velocity at the fluid/rock interface, $v_n(x,t)$, given by (4.3.18) is zero.

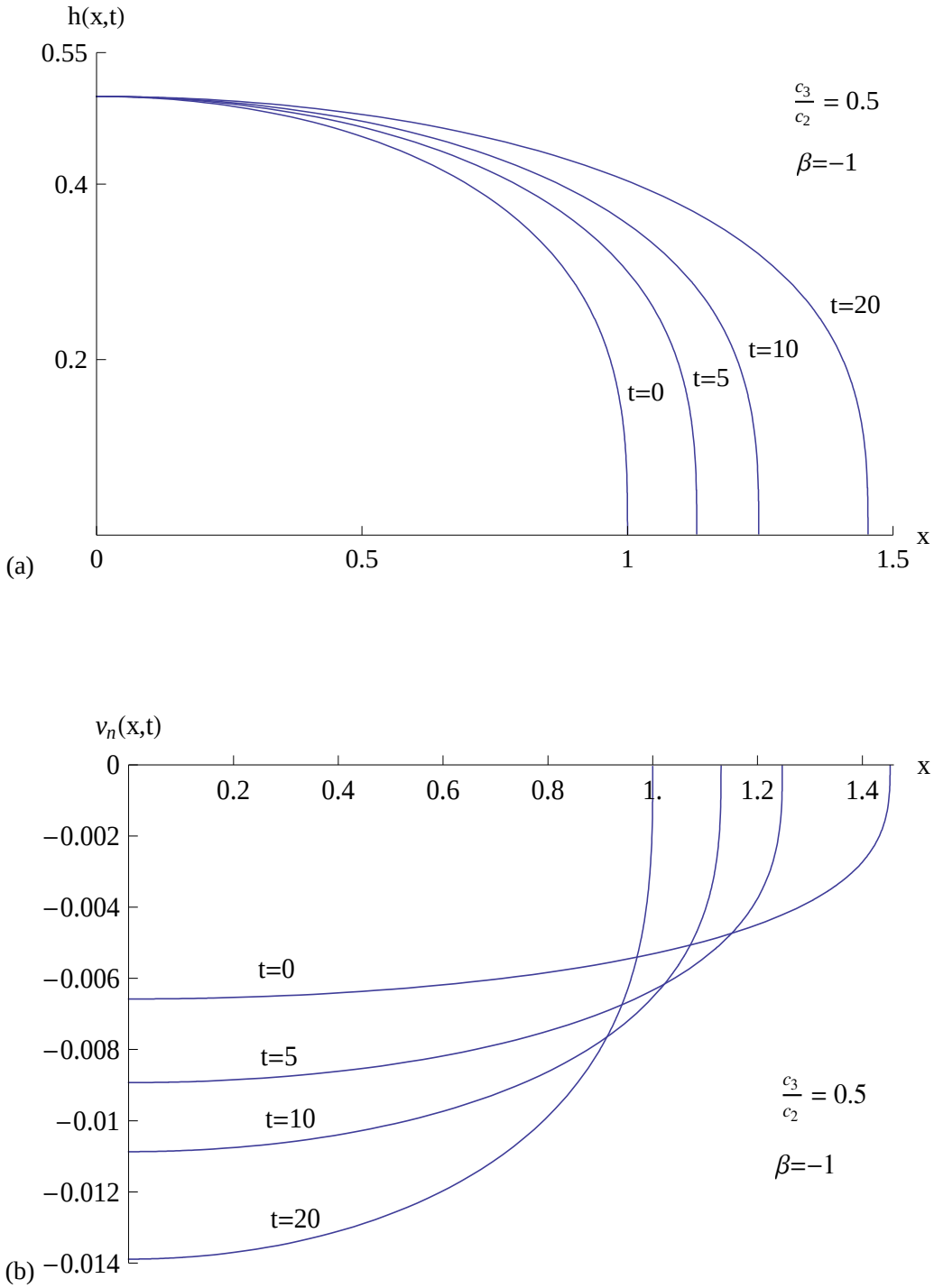


Figure 4.4.7: (a) Fracture half-width, $h(x,t)$, given by (4.3.17) and (b) leak-off velocity at the fluid/rock interface, $v_n(x,t)$, given by (4.3.18), plotted against x for a range of values of t and for $\frac{c_3}{c_2} = 0.5$, $\beta = -1$.

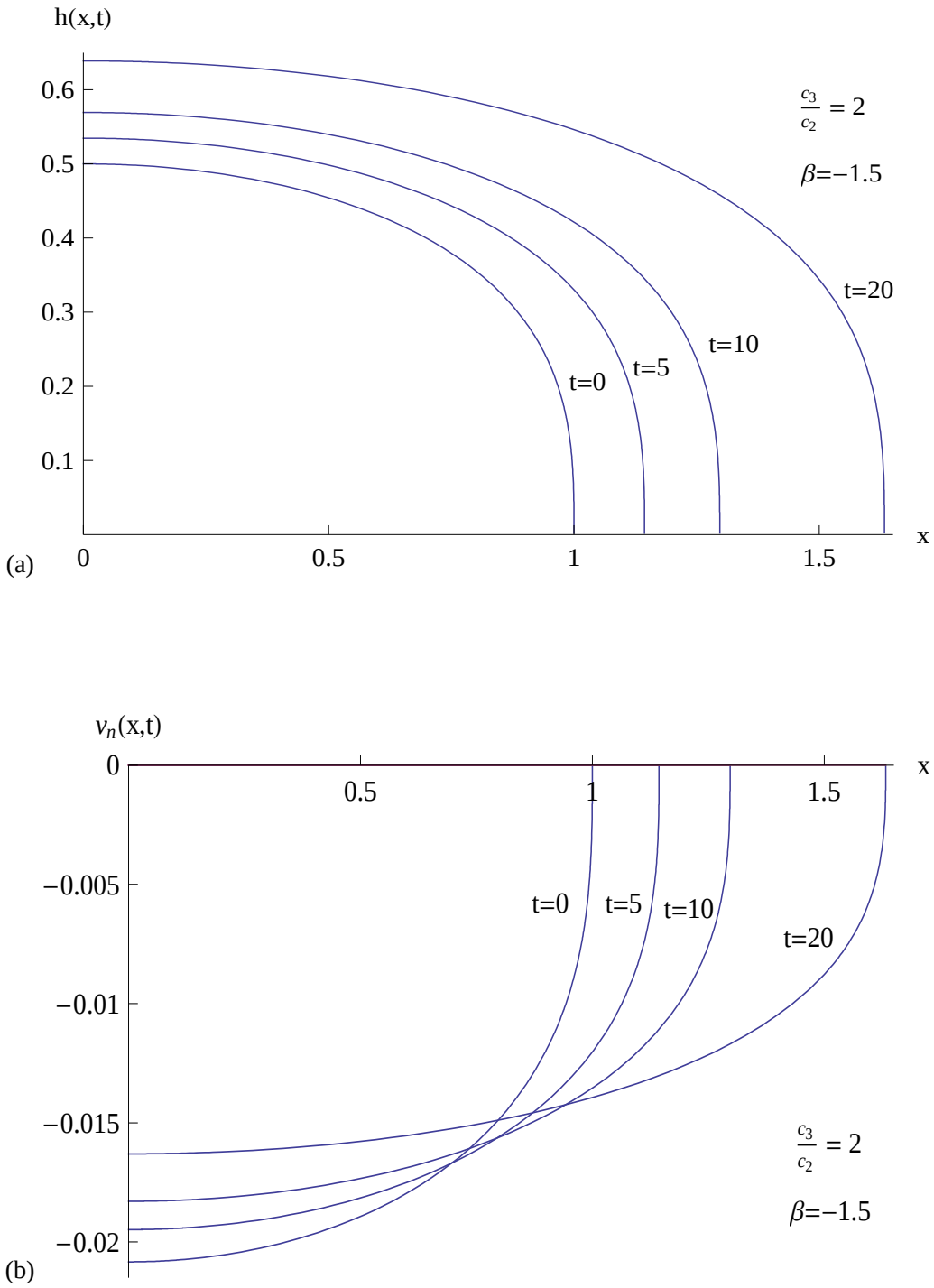


Figure 4.4.8: (a) Fracture half-width, $h(x,t)$, given by (4.3.17) and (b) leak-off velocity at the fluid/rock interface, $v_n(x,t)$, given by (4.3.18), plotted against x for a range of values of t and for $\frac{c_3}{c_2} = 2$, $\beta = -1.5$.

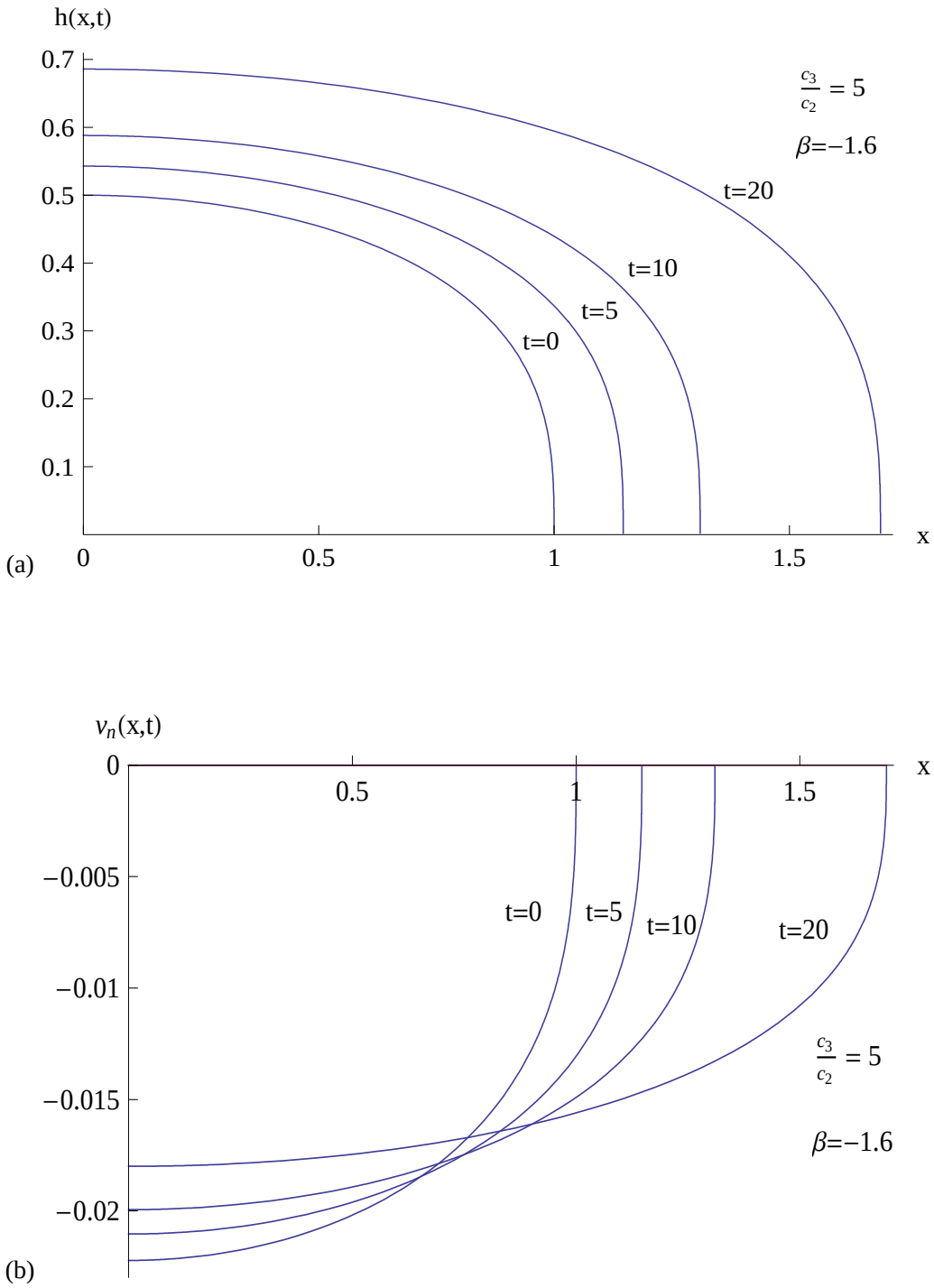


Figure 4.4.9: (a) Fracture half-width, $h(x,t)$, given by (4.3.17) and (b) leak-off velocity at the fluid/rock interface, $v_n(x,t)$, given by (4.3.18), plotted against x for a range of values of t and for $\frac{c_3}{c_2} = 5$, $\beta = -1.6$.

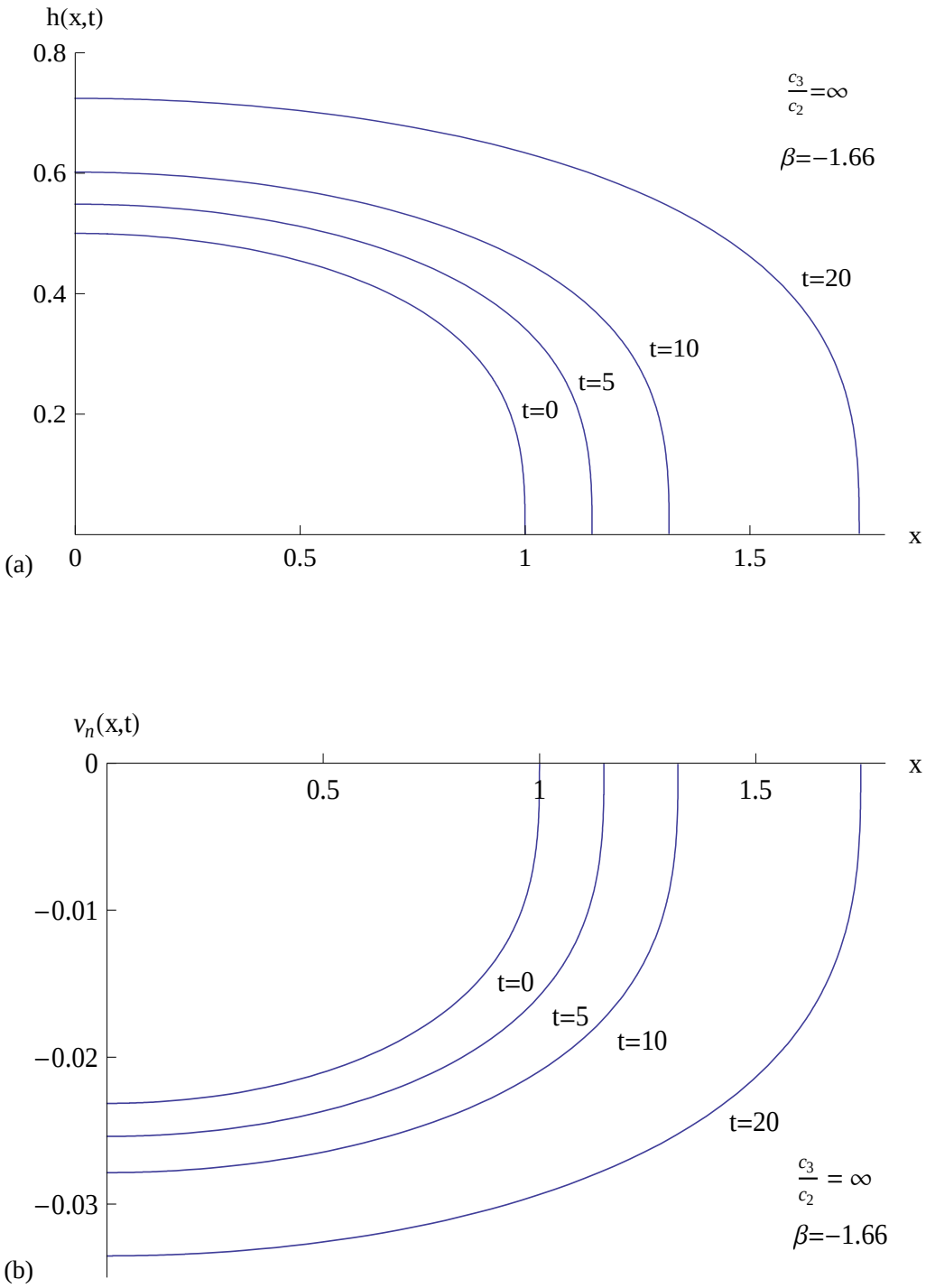


Figure 4.4.10: (a) Fracture half-width, $h(x,t)$, given by (4.3.25) and (b) leak-off velocity at the fluid/rock interface, $v_n(x,t)$, given by (4.3.26), plotted against x for a range of values of t and for $\frac{c_3}{c_2}=\infty$, $\beta=-1.66$.

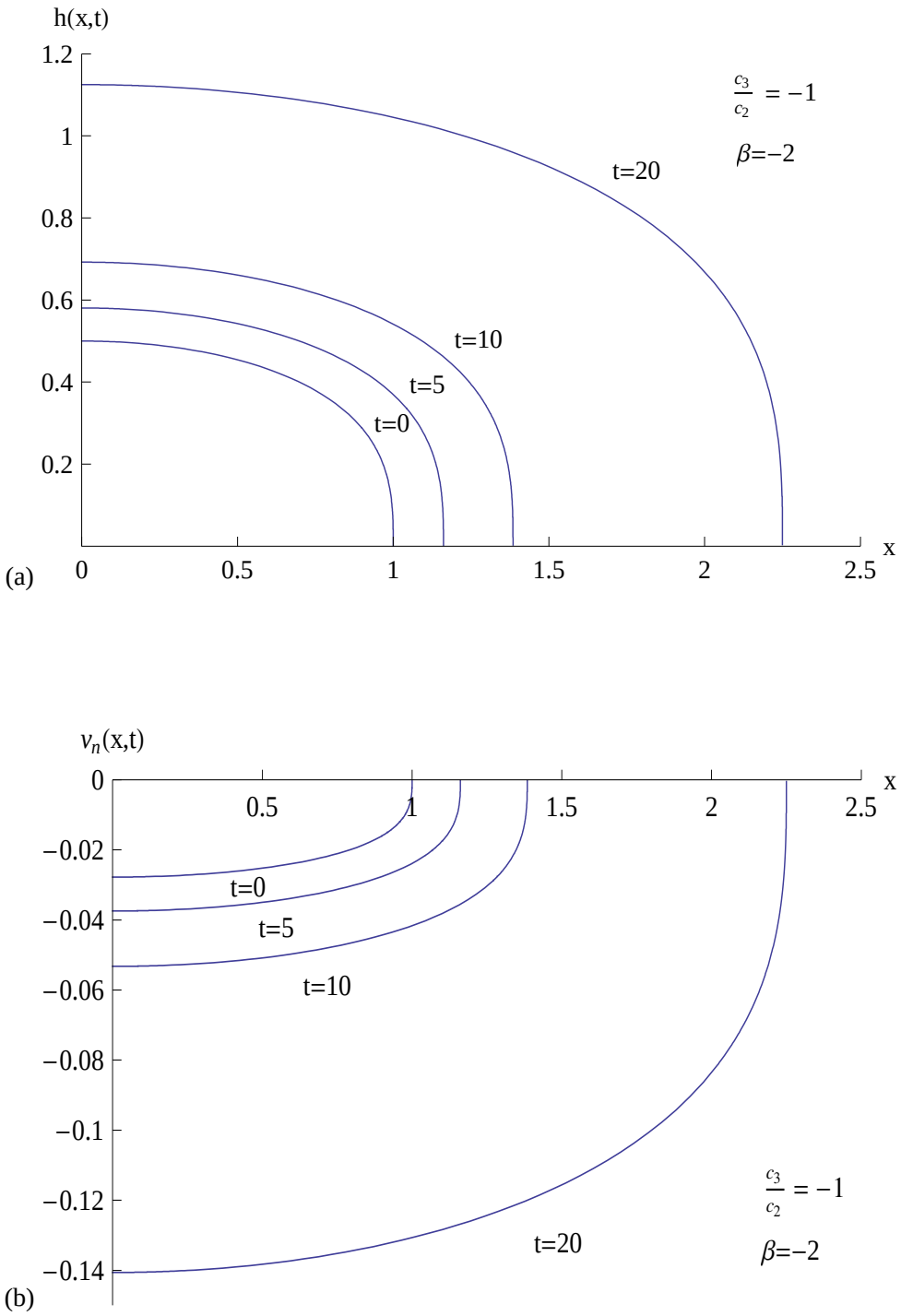


Figure 4.4.11: (a) Fracture half-width, $h(x,t)$, given by (4.3.17) and (b) leak-off velocity at the fluid/rock interface, $v_n(x,t)$, given by (4.3.18), plotted against x for a range of values of t and for $\frac{c_3}{c_2}$ = -1, β = -2.

4.5 Exact solution for non-zero fluid injection rate at fracture entry

We now look for a solution of (4.2.4) subject to (4.2.5) and (4.2.6) which is of the form

$$F(u) = a(\alpha - u)^{\sigma}, \tag{4.5.1}$$

where a, α and σ are constants to be determined such that $a \neq 0$ and $\sigma > 0$. The value of α for which $F(u)$ satisfies (4.2.5) is $\alpha = 1$. Equation (4.5.1) becomes

$$F(u) = a(1 - u)^{\sigma}. \tag{4.5.2}$$

Substituting (4.5.2) into (4.2.4), we obtain

$$\Lambda a^4 \sigma(4\sigma - 1)(1-u)^{4\sigma-2} - 3a\sigma(1-u)^{\sigma-1} + a\left(\frac{c_2}{c_3} + 3\sigma - 2 - 3\beta\right)(1-u)^{\sigma} = 0. \tag{4.5.3}$$

Equation (4.5.3) will be satisfied if

$$\Lambda a^4 \sigma(4\sigma - 1)(1-u)^{4\sigma-2} - 3a\sigma(1-u)^{\sigma-1} = 0 \tag{4.5.4}$$

and

$$\frac{c_2}{c_3} + 3\sigma - 2 - 3\beta = 0. \tag{4.5.5}$$

Equating the powers of $1 - u$ in (4.5.4) gives

$$\sigma = \frac{1}{3}. \tag{4.5.6}$$

When σ is substituted into (4.5.4) and (4.5.5), we obtain

$$\frac{\Lambda}{9}a^4 - a = 0, \tag{4.5.7}$$

$$\frac{c_2}{c_3} - 1 - 3\beta = 0. \tag{4.5.8}$$

Solving (4.5.7) gives

$$a = \left(\frac{9}{\Lambda}\right)^{\frac{1}{3}}. \tag{4.5.9}$$

Hence, the solution of the form (4.5.1) is

$$F(u) = \left(\frac{9}{\Lambda}\right)^{\frac{1}{3}} (1-u)^{\frac{1}{3}}, \tag{4.5.10}$$

provided that (4.5.8) is satisfied.

We note that the boundary condition (4.2.6) was not used to obtain (4.5.10), but it must be satisfied for (4.5.10) to be a solution of the problem. We will now show that (4.2.6) is satisfied. Substituting (4.5.10) into the left hand side of (4.2.6) gives

$$\Lambda F^3(0)\frac{dF}{du}(0) = -3\left(\frac{9}{\Lambda}\right)^{\frac{1}{3}}, \tag{4.5.11}$$

while substituting (4.5.10) into the right hand side gives

$$\left(\frac{c_2}{c_3} - 5 - 3\beta\right)\int_0^1 F(u)du = \frac{3}{4}\left(\frac{c_2}{c_3} - 5 - 3\beta\right)\left(\frac{9}{\Lambda}\right)^{\frac{1}{3}}. \tag{4.5.12}$$

Hence, the boundary condition (4.2.6) is satisfied provided (4.5.8) holds.
By substituting (4.5.10) into (4.2.7) we obtain

$$\frac{c_3}{c_1} = \frac{8\Lambda V_0^3}{243}, \tag{4.5.13}$$

and hence from (4.2.8),

$$\frac{c_2}{c_1} = \frac{8\Lambda V_0^3}{243}\frac{c_2}{c_3}. \tag{4.5.14}$$

We also have from (4.2.14)

$$u = \frac{x}{L(t)}, \qquad 0 \le u \le 1. \tag{4.5.15}$$

The solution can be written either in terms of β or $\frac{c_2}{c_3}$. As in the first special solution we will express the results in terms of $\frac{c_2}{c_3}$. From (4.5.8),

$$\beta = \frac{1}{3}\left(\frac{c_2}{c_3} - 1\right). \tag{4.5.16}$$

From (4.2.9) to (4.2.13),

$$V(t) = V_0 \left[1 + \frac{8V_0^3}{243}\frac{c_2}{c_3}\Lambda t\right]^{\frac{5}{3}(\frac{c_3}{c_2}-\frac{1}{5})}, \tag{4.5.17}$$

$$L(t) = \left[1 + \frac{8V_0^3}{243}\frac{c_2}{c_3}\Lambda t\right]^{\frac{c_3}{c_2}}, \tag{4.5.18}$$

$$h(x,t) = \frac{2V_0}{3}\left[1 + \frac{8V_0^3}{243}\frac{c_2}{c_3}\Lambda t\right]^{\frac{2}{3}\left(\frac{c_3}{c_2}-\frac{1}{2}\right)}\left[1 - \frac{x}{L(t)}\right]^{\frac{1}{3}}, \tag{4.5.19}$$

$$v_n(x,t) = \frac{16}{2187}\left(\frac{c_2}{c_3} - 1\right)\Lambda V_0^4\left[1 + \frac{8V_0^3}{243}\frac{c_2}{c_3}\Lambda t\right]^{\frac{2}{3}(\frac{c_3}{c_2}-2)}\left[1 - \frac{x}{L(t)}\right]^{\frac{1}{3}}, \tag{4.5.20}$$

$$p(x,t) = \Lambda h(x,t). \tag{4.5.21}$$

The solution for $h(x,t)$, $v_n(x,t)$ and $p(x,t)$ can be expressed alternately in terms of $L(t)$:

$$h(x,t) = \frac{2}{3}V_0 L(t)^{\frac{1}{3}\left(2-\frac{c_2}{c_3}\right)}\left[1 - \frac{x}{L(t)}\right]^{\frac{1}{3}}, \tag{4.5.22}$$

$$v_n(x,t) = \frac{16}{2187}\left(\frac{c_2}{c_3} - 1\right)\Lambda V_0^4 L(t)^{\frac{4}{3}\left(\frac{1}{2}-\frac{c_2}{c_3}\right)}\left[1 - \frac{x}{L(t)}\right]^{\frac{1}{3}}, \tag{4.5.23}$$

and $p(x,t)$ is given by (4.5.21) and (4.5.22).

In the limit $\frac{c_3}{c_2} \to \infty$, we have $\beta \to -\frac{1}{3}$ and the group invariant solutions for $L(t)$, $V(t)$, $h(x,t)$, $v_n(x,t)$ and $p(x,t)$ have an exponential time-dependence given as

$$V(t) = V_0 \exp\left(\frac{40}{729}V_0^3\Lambda t\right), \tag{4.5.24}$$

$$L(t) = \exp\left(\frac{8V_0^3}{243}\Lambda t\right), \tag{4.5.25}$$

$$h(x,t) = \frac{2V_0}{3}\exp\left(\frac{16V_0^3}{729}\Lambda t\right)\left[1 - \frac{x}{L(t)}\right]^{\frac{1}{3}}, \tag{4.5.26}$$

$$v_n(x,t) = -\frac{16\Lambda V_0^4}{2187}\exp\left(\frac{16V_0^3}{729}\Lambda t\right)\left[1 - \frac{x}{L(t)}\right]^{\frac{1}{3}} \tag{4.5.27}$$

and $p(x,t)$ is given by (4.5.21) and (4.5.26). The constant Λ is as defined in (3.4.5).

4.6 Discussion of results for $\beta = \frac{1}{3}\left(\frac{c_2}{c_3} - 1\right)$

Consider now the physical significance of the special case

$$\beta = \frac{1}{3}\left(\frac{c_2}{c_3} - 1\right). \tag{4.6.1}$$

Unlike the condition (4.3.14), condition (4.6.1) does not make a physical quantity vanish, neither does it define a dividing curve between solutions in the $\left(\frac{c_3}{c_2}, \beta\right)$ plane. Substituting (4.2.1), (4.5.10), (4.5.13) and (4.5.14) firstly, into (3.7.27) and secondly, into (3.7.24) gives the rate of fluid injection at the fracture entry

$$q_1(t) = \frac{8}{729}\Lambda V_0^4 \left[1 + \frac{8}{243}V_0^3 \frac{c_2}{c_3}\Lambda t\right]^{\frac{5}{3}\left(\frac{c_3}{c_2} - \frac{4}{5}\right)} \tag{4.6.2}$$

and the rate of fluid leak-off at the fluid/rock interface

$$q_2(t) = \frac{8}{243}\beta\Lambda V_0^4 \left[1 + \frac{8}{243}V_0^3 \frac{c_2}{c_3}\Lambda t\right]^{\frac{5}{3}\left(\frac{c_3}{c_2} - \frac{4}{5}\right)} \tag{4.6.3}$$

respectively. Thus $q_1(t) > 0$ and fluid is always injected into the fracture at the fracture entry for the special case (4.6.1). The strength of the injected fluid either increases or decreases with time depending on the value taken by the parameter $\frac{c_3}{c_2}$ and it is constant when $\frac{c_3}{c_2} = 0.8$.

Condition (4.6.1) can be written as

$$\beta = \frac{1 - \frac{c_3}{c_2}}{3\frac{c_3}{c_2}} \tag{4.6.4}$$

and as

$$\frac{c_3}{c_2} = \frac{1}{1 + 3\beta}. \tag{4.6.5}$$

In Fig 4.6.1, β given by (4.6.4) is plotted against $\frac{c_3}{c_2}$. As with the special case (4.3.14) we investigate the whole range $-\infty < \frac{c_3}{c_2} < \infty$. Table 3.7.1 shows that the range of values of practical interest is $0 < \frac{c_3}{c_2} \leq 1$.

4.6.1 Fracture length and volume

Consider now the length of the fracture given by (4.5.18) and (4.5.25) and plotted in Figure 4.6.2 for a selection of values of $\frac{c_3}{c_2}$. For $0 < \frac{c_3}{c_2} < 1$, $L(t)$ increases even when there is leak-off

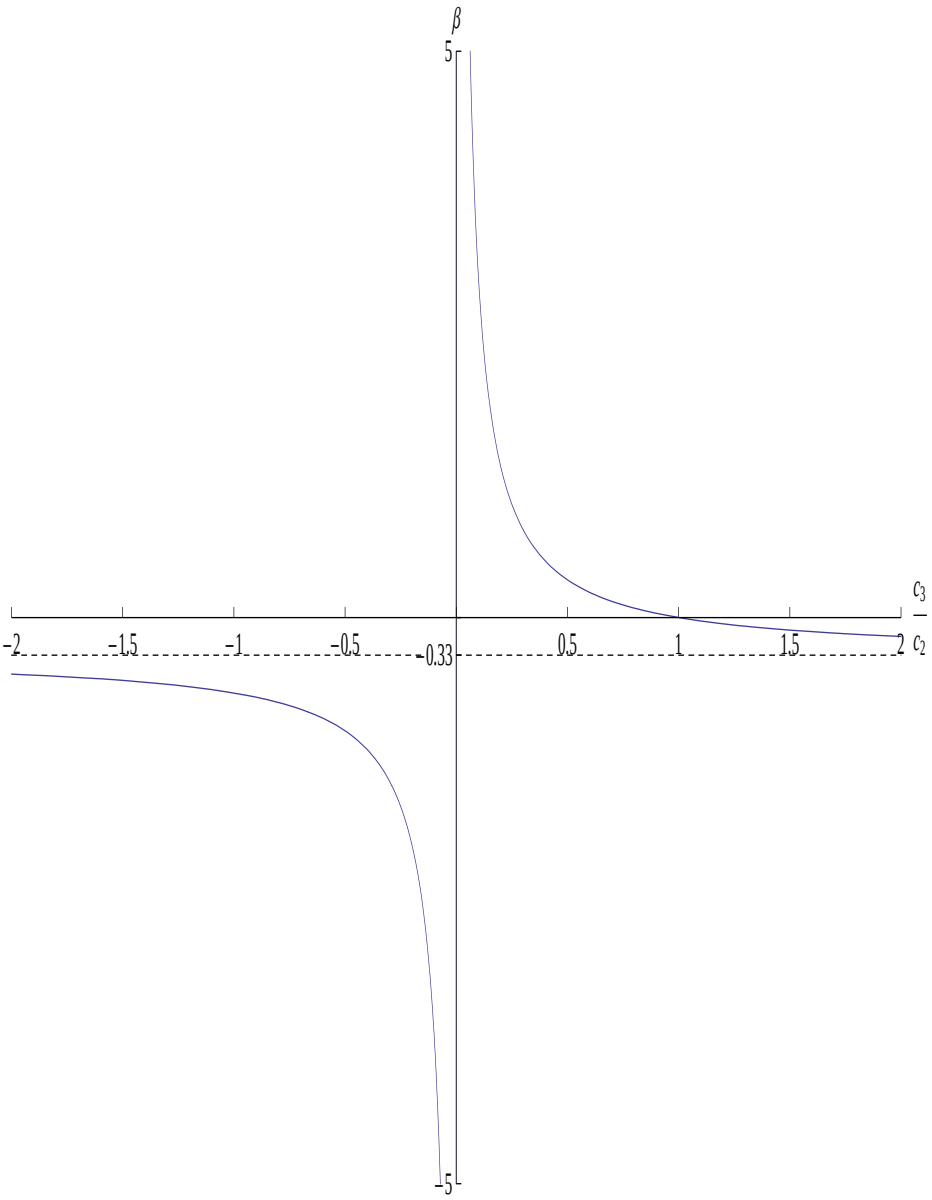


Figure 4.6.1: Graph of $\beta = \frac{\left(1-\frac{c_3}{c_2}\right)}{3\frac{c_3}{c_2}}$ against $\frac{c_3}{c_2}$ for the range $-2 < \frac{c_3}{c_2} < 2$.

at the fluid/rock interface. For $\frac{c_3}{c_2} = 1$, $\beta = 0$ and the rock is impermeable. The linear growth in $L(t)$ is due entirely to the fluid injection at the fracture entry:

$$q_1(t) = \frac{8}{729}\Lambda V_0^4 \left[1 + \frac{8}{243}V_0^3\Lambda t\right]^{\frac{1}{3}}, \tag{4.6.6}$$

the strenght of which increases at t increases. For $\frac{c_3}{c_2} < 0$, $L(t) \to \infty$ algebraically in the finite time

$$\Lambda t = \frac{243}{8V_0^3}\left(-\frac{c_3}{c_2}\right). \tag{4.6.7}$$

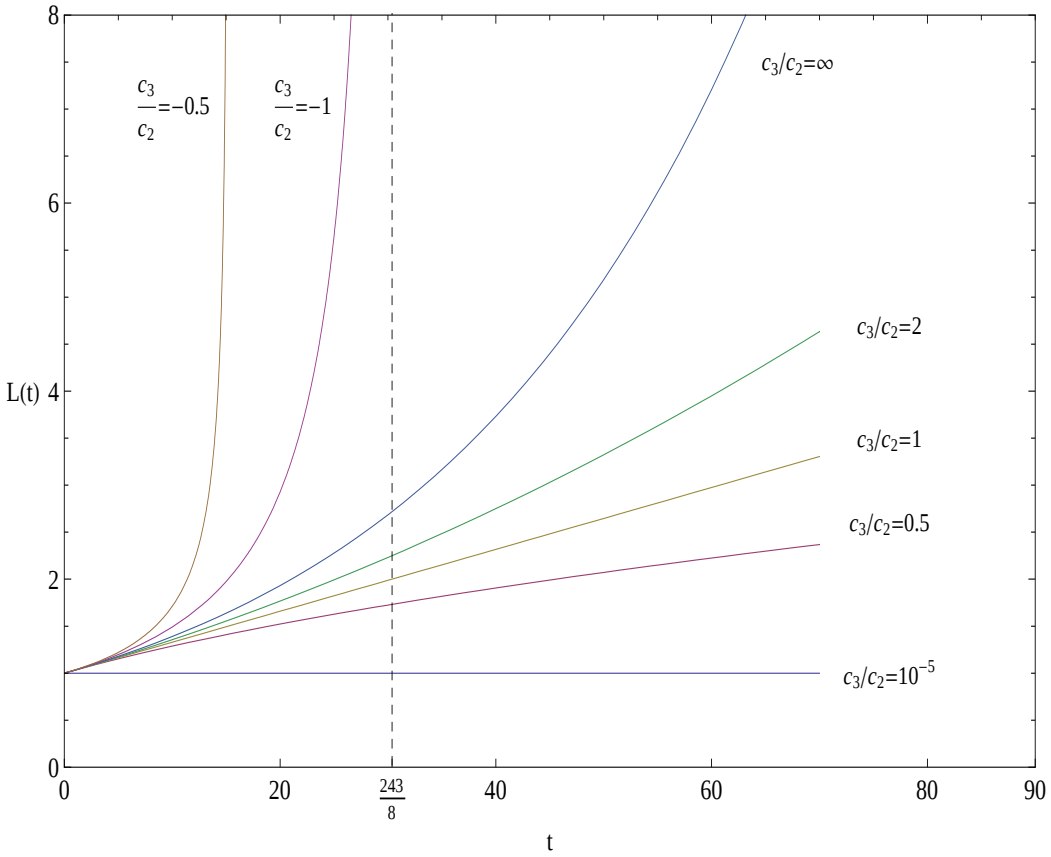


Figure 4.6.2: Leak-off velocity proportional to fracture half-width: Graph of fracture length, $L(t)$, given by (4.5.18) and (4.5.25) plotted against t for $V_0 = 1$ and a selection of values of the parameter $\frac{c_3}{c_2}$.

In Figure 4.6.3, the fracture volume $V(t)$ given by (4.5.17) and (4.5.24) is plotted against t for the same values of $\frac{c_3}{c_2}$ as used in Figure 4.4.3 for $V(t)$. When $0 < \frac{c_3}{c_2} < 0.2$, $V(t) \to 0$ as $t \to \infty$. When $\frac{c_3}{c_2} = 0.2$, $\beta = \frac{4}{3}$ and leak-off at the fluid/rock interface balances the decreasing inflow rate at the fracture entry so that $V(t)$ remains constant. When $\frac{c_3}{c_2} = +1$, $\beta = 0$ and the rock is impermeable. The rate of fluid injection, $q_1(t)$ increases with time and hence $V(t)$ increases. The fracture volume $V(t) \to \infty$ in the finite time (4.6.7) when $\frac{c_3}{c_2} < 0$.

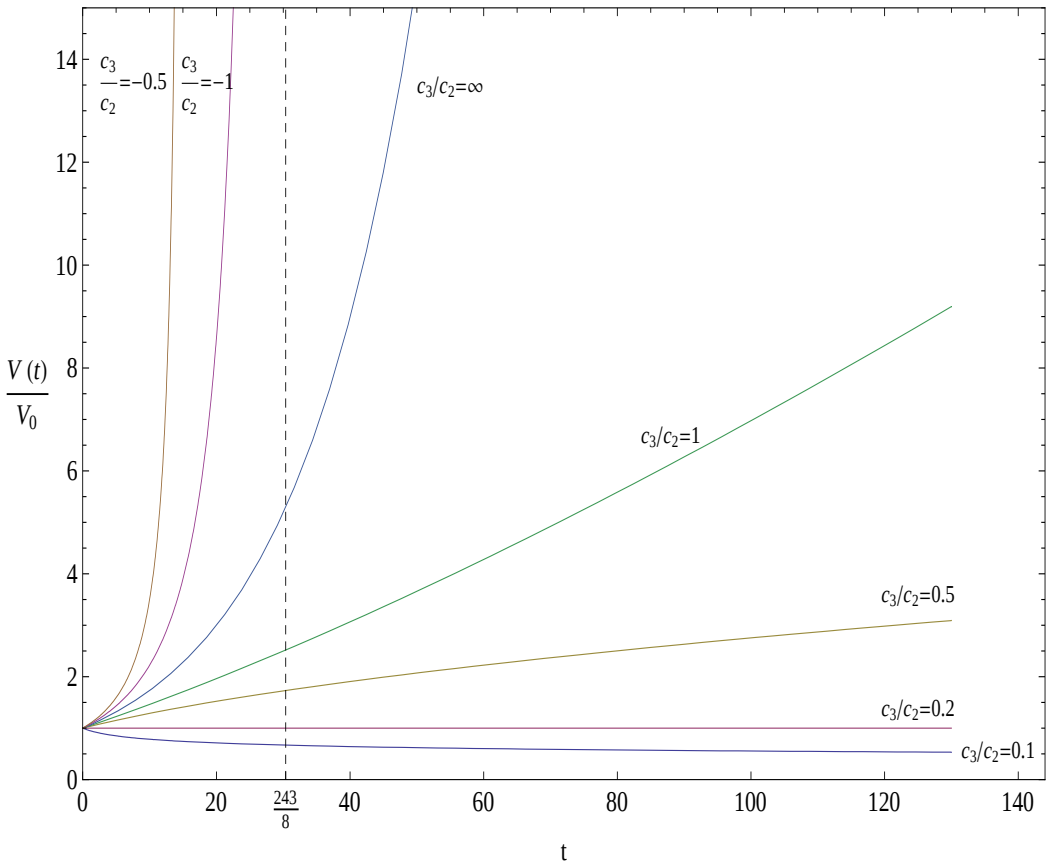


Figure 4.6.3: Leak-off velocity proportional to fracture half-width: Total volume of the fracture, $\frac{V}{V_0}(t)$, given by (4.5.17) and (4.5.24) plotted against t for $V_0 = 1$ and a selection of values of $\frac{c_3}{c_2}$.

4.6.2 Fracture half-width and leak-off velocity

Consider next $h(x,t)$ which is given by (4.5.19) and (4.5.26) and is plotted in Figures 4.6.4 to 4.6.9. For the second case of exact solution, the initial fracture shape $h(0,t)$ is

$$h(x,0) = \frac{2}{3} V_0 \left(1-x\right)^{\frac{1}{3}}. \tag{4.6.8}$$

From (4.5.19), when $\frac{c_3}{c_2}$ is finite,

$$h(0,t) = \frac{2V_0}{3}\left[1 + \frac{8V_0^3}{243}\frac{c_2}{c_3}\Lambda t\right]^{\frac{2}{3}\left(\frac{c_3}{c_2}-\frac{1}{2}\right)} \tag{4.6.9}$$

and for $\frac{c_3}{c_2} = \infty$,

$$h(0,t) = \frac{2V_0}{3}\exp\left(\frac{16V_0^3}{729}\Lambda t\right). \tag{4.6.10}$$

For $0 < \frac{c_3}{c_2} < \frac{1}{2}$, $\frac{1}{3} < \beta < \infty$, $h(0,t)$ decreases as t increases and the width of the fracture at the entry decreases as t increases. The maximum leak-off occurs always near the fracture entry where $h(x,t)$ is highest and its strenght decreases with time. For this range of $\frac{c_3}{c_2}$ the rate of fluid injection at the entry decreases with time. The pressure at the entry $p(0,t)$ required to induce fracture also decreases with time, a consequence from the PKN formulation (1.3.1). When $\frac{c_3}{c_2} = \frac{1}{2}$, $\beta = \frac{1}{3}$ and $h(0,t)$ remains constant. The pressure at the fracture entry $p(0,t)$ is constant from (1.3.1) even though the rate of fluid injection at the entry and leak-off at the interface decrease with time. These operating conditions result in the width of the fracture at the entry remaining constant. For the special case discussed in Section (4.4), there was no inflow at the fracture entry and $h(0,t)$ remained constant when $\frac{c_3}{c_2} = \frac{1}{2}$ and $L(t)$ increased due to inflow at the fluid/rock interface. For $\frac{1}{2} < \frac{c_3}{c_2} < \infty$, the fluid pressure $p(0,t)$ increases with time and hence $h(0,t)$ increases as t increases. For $-\infty < \frac{c_3}{c_2} < 0$, $h(0,t) \to \infty$ in the finite time (4.6.7).

From (4.5.19) and (4.5.26), the gradient of the fracture half-width is given for $0 < \frac{c_3}{c_2} < \infty$ by

$$\frac{\partial h}{\partial x} = -\frac{2V_0}{9}\left[1 + \frac{8V_0^3}{243}\frac{c_2}{c_3}\Lambda t\right]^{-\frac{1}{3}\left(\frac{c_3}{c_2}+1\right)}\left(1-\frac{x}{L(t)}\right)^{-\frac{2}{3}} \tag{4.6.11}$$

and in the limit $\frac{c_3}{c_2} = \infty$, by

$$\frac{\partial h}{\partial x} = -\frac{2V_0}{9}\exp\left(-\frac{8V_0^3}{729}\Lambda t\right)\left(1-\frac{x}{L(t)}\right)^{-\frac{2}{3}}. \tag{4.6.12}$$

At the fracture entry when $t = 0$ and for $-\infty < \frac{c_3}{c_2} \leq \infty$,

$$\frac{\partial h}{\partial x}(0,0) = -\frac{2V_0}{9}. \tag{4.6.13}$$

In the limit $t \to \infty$ and for $\frac{c_3}{c_2} > 0$,

$$\frac{\partial h}{\partial x}(0,\infty) \to 0. \tag{4.6.14}$$

As $x \to L(t)$, $\dfrac{\partial h}{\partial x} \to -\infty$. The thin film approximation (1.6.1) and (1.6.2) therefore breaks down in the neighbourhood of the fracture tip.

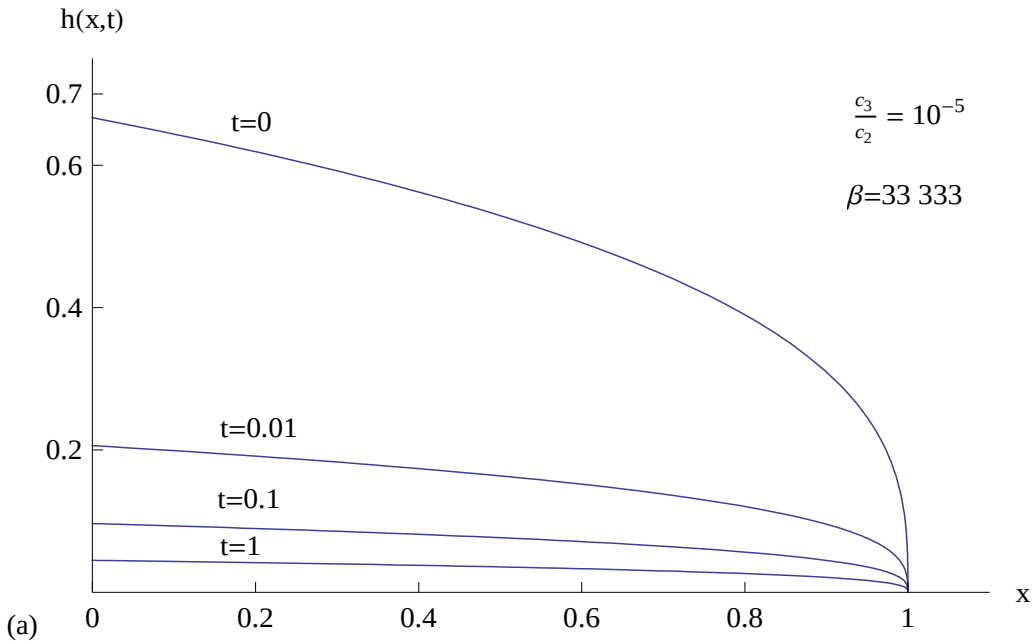
Lastly, consider $v_n(x,t)$ which is given by (4.5.20) and (4.5.27) and plotted in Figures 4.6.4 to 4.6.9. From (4.5.20), for $\frac{c_3}{c_2}$ finite,

$$v_n(0,t) = \frac{16}{2187}\Lambda V_0^4 \left(\frac{c_2}{c_3} - 1\right)\left[1 + \frac{8V_0^3}{243}\frac{c_2}{c_3}\Lambda t\right]^{\frac{2}{3}(\frac{c_3}{c_2}-2)} \tag{4.6.15}$$

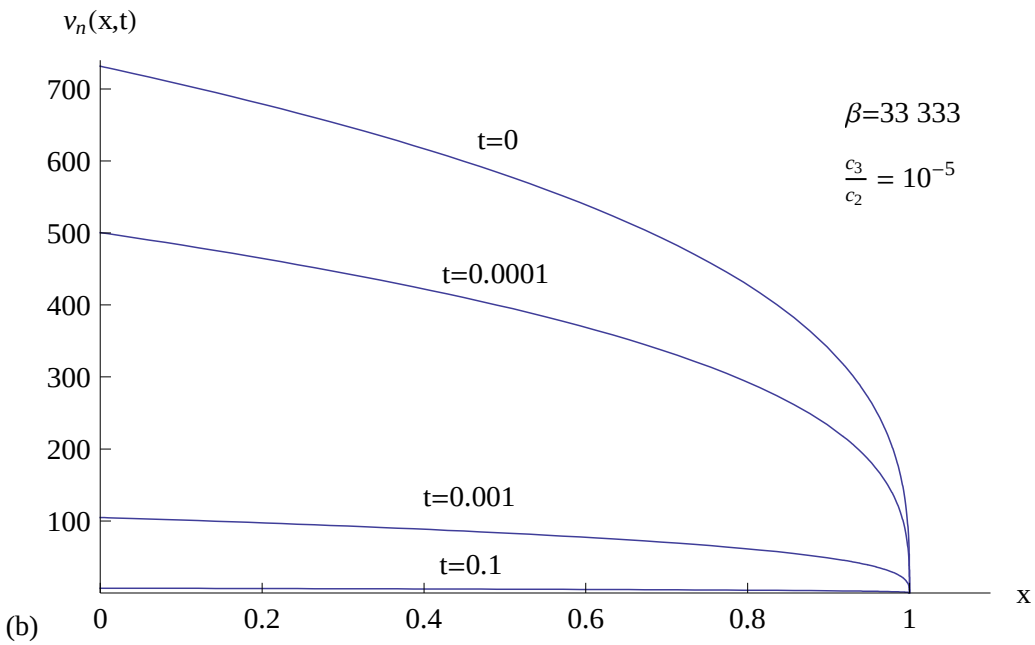
and for $\frac{c_3}{c_2} = \infty$,

$$v_n(0,t) = -\frac{16\Lambda V_0^4}{2187}\exp\left(\frac{16V_0^3}{729}\Lambda t\right). \tag{4.6.16}$$

For $0 < \frac{c_3}{c_2} < 1$, $v_n(x,t) > 0$, there is leak-off at the fluid/rock interface and v_n decreases as t increases. For $1 < \frac{c_3}{c_2} < \infty$, $v_n(x,t) < 0$ and there is inflow of fluid at the fluid/rock interface. For $0 < \frac{c_3}{c_2} < 2$, the magnitude of $v_n(0,t)$ decreases as t increases. When $\frac{c_3}{c_2} = 2$, the magnitude of $v_n(0,t)$ remains constant and when $2 < \frac{c_3}{c_2} < \infty$ the magnitude of $v_n(0,t)$ increases as t increases. For $-\infty < \frac{c_3}{c_2} < 0$, $\beta < 0$ and there is fluid inflow at the fluid/rock interface and $v_n(0,t) \to -\infty$ in the finite time (4.6.7).

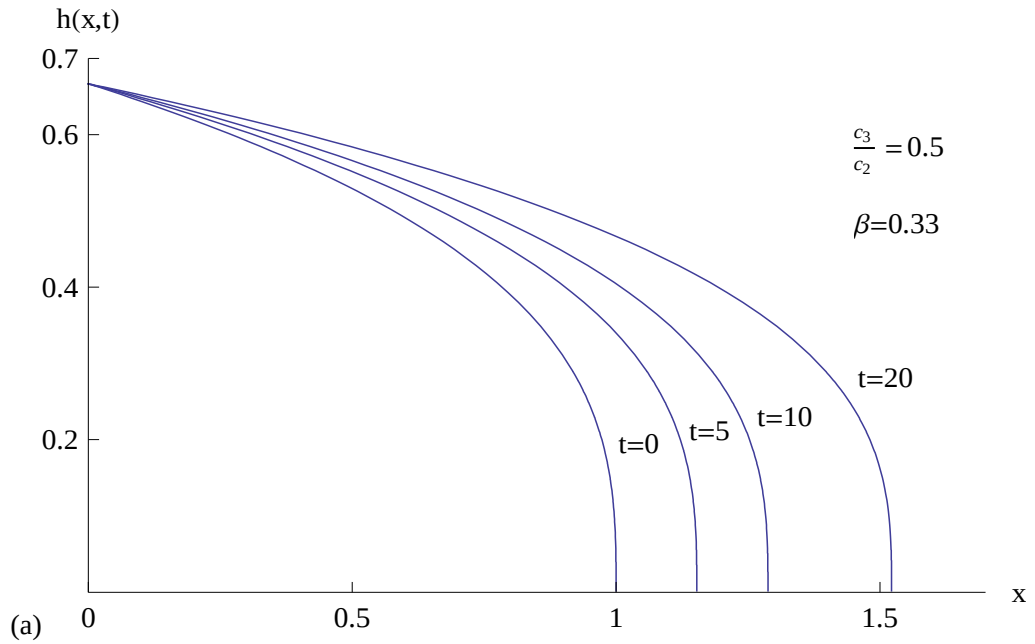


(a)



(b)

Figure 4.6.4: (a) Fracture half-width, $h(x,t)$, given by (4.5.19) and (b) leak-off velocity at the fluid/rock interface, $v_n(x,t)$, given by (4.5.20), plotted against x for a range of values of t and for $\frac{c_3}{c_2} = 10^{-5}$, $\beta = 33333$.



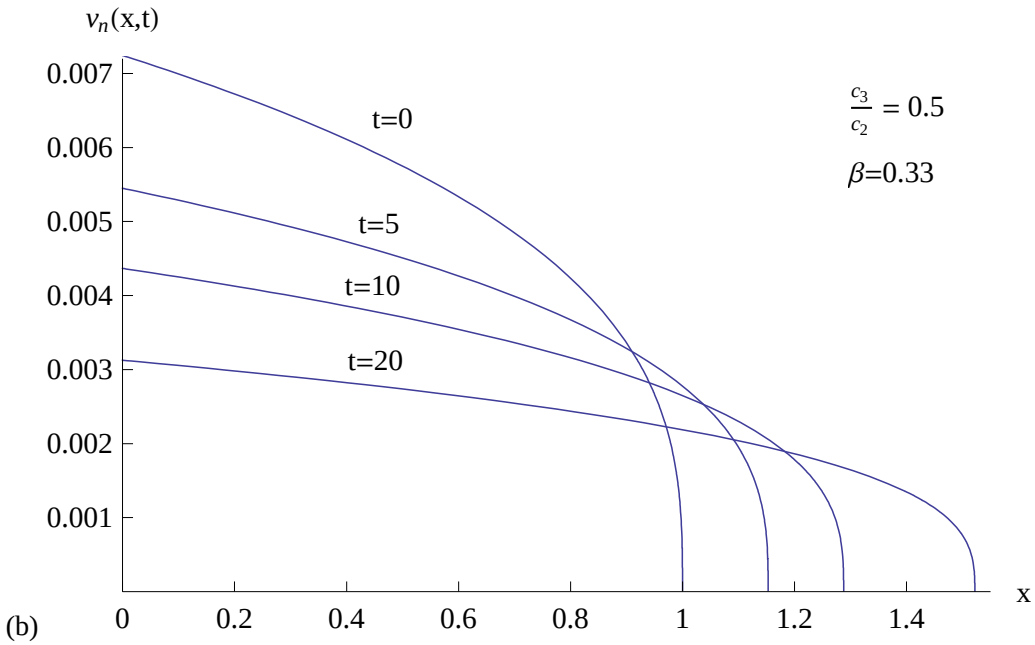


Figure 4.6.5: (a) Fracture half-width, $h(x,t)$, given by (4.5.19) and (b) leak-off velocity at the fluid/rock interface, $v_n(x,t)$, given by (4.5.20), plotted against x for a range of values of t and for $\frac{c_3}{c_2} = 0.5$, $\beta = 0.33$.

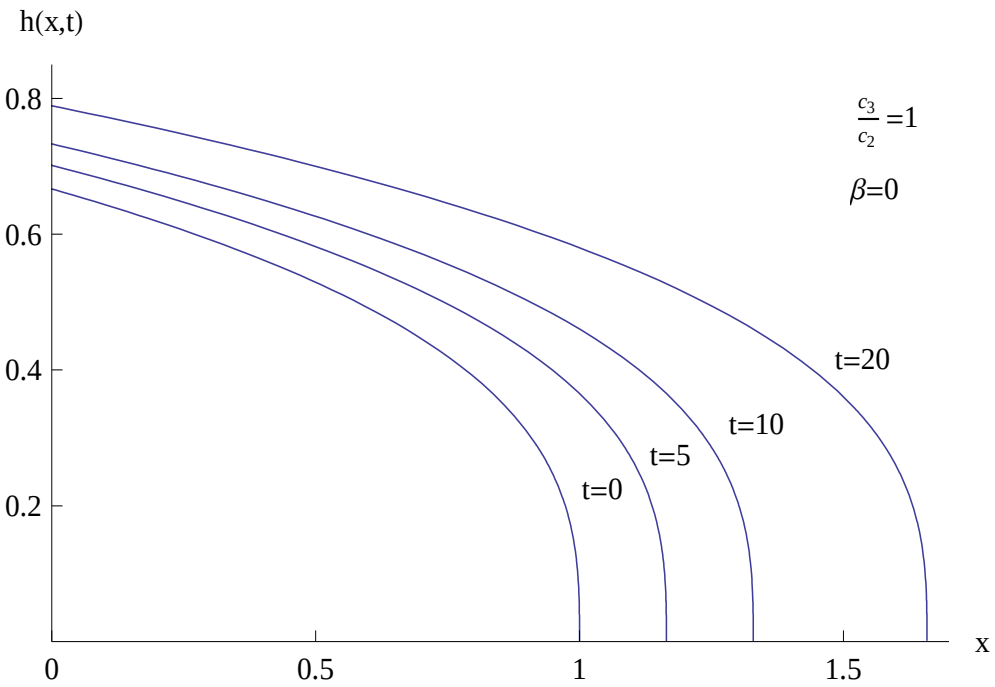


Figure 4.6.6: Fracture half-width, $h(x,t)$, given by (4.5.19) plotted against x for a range of values of t and for $\frac{c_3}{c_2} = 1$, $\beta = 0$. The leak-off velocity at the fluid/rock interface, $v_n(x,t)$, given by (4.5.20), is zero.

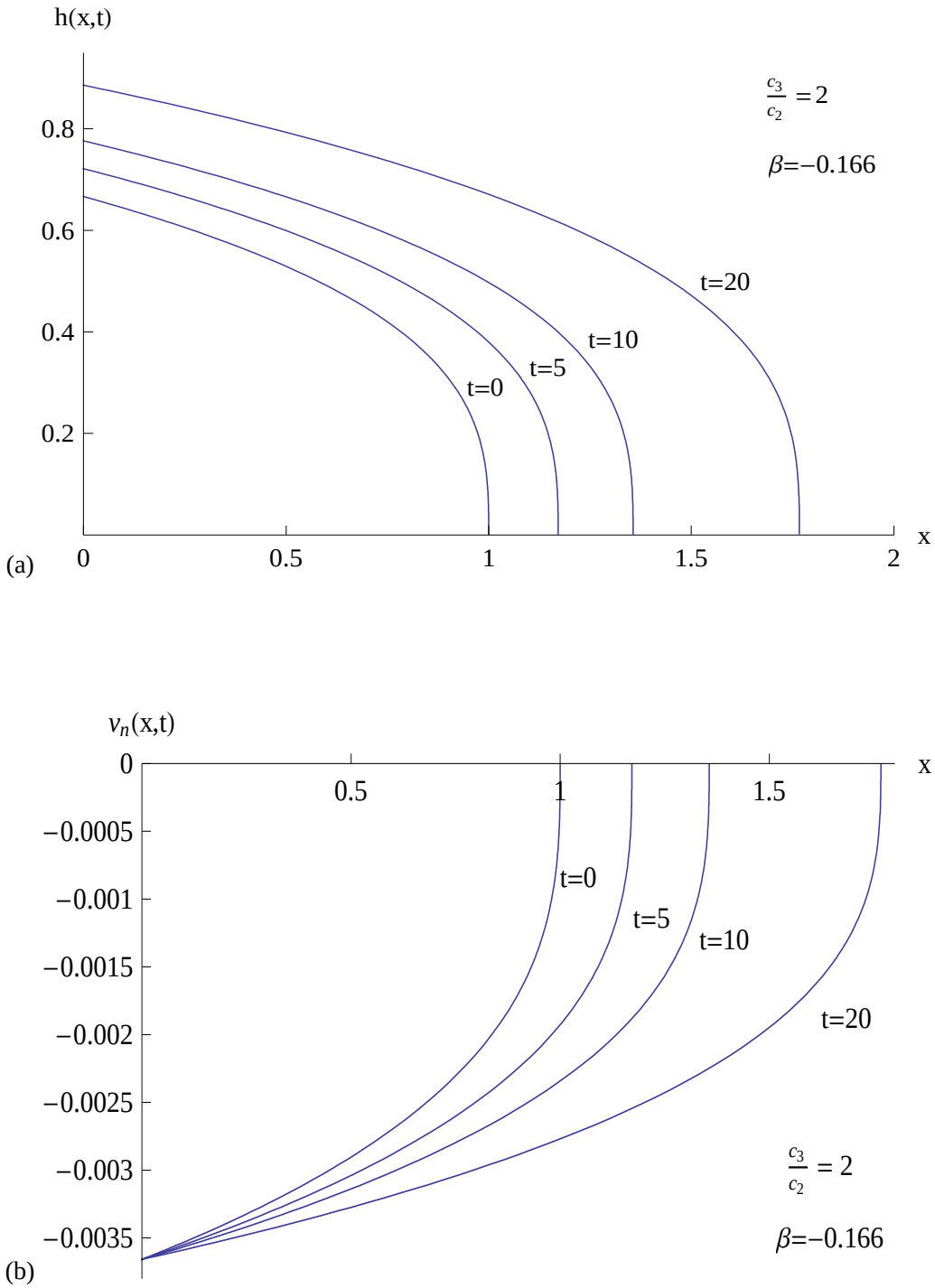


Figure 4.6.7: (a) Fracture half-width, $h(x,t)$, given by (4.5.19) and (b) leak-off velocity at the fluid/rock interface, $v_n(x,t)$, given by (4.5.20), plotted against x for a range of values of t and for $\frac{c_3}{c_2} = 2$, $\beta = -0.166$.

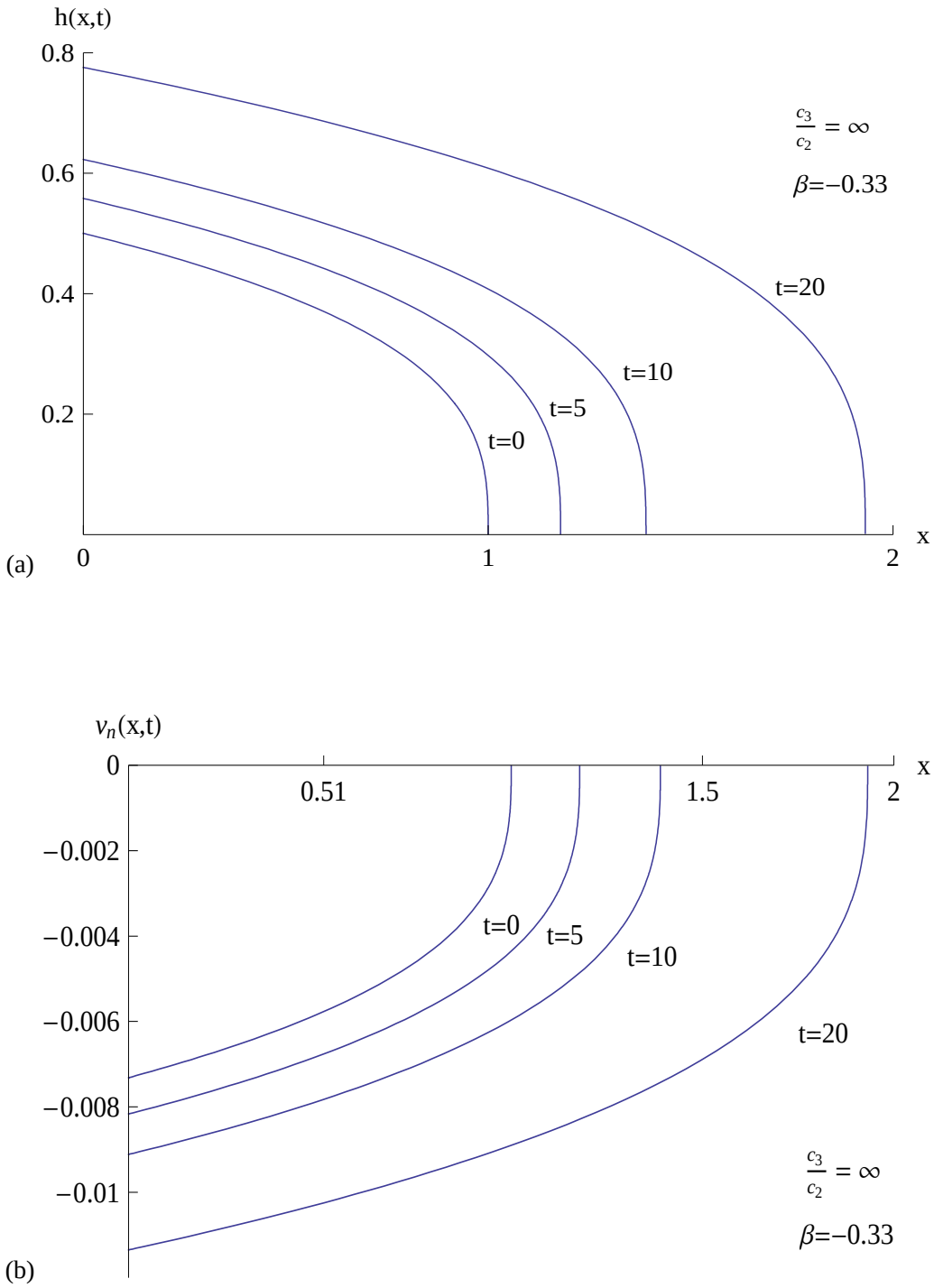


Figure 4.6.8: (a) Fracture half-width, $h(x,t)$, given by (4.5.26) and (b) leak-off velocity at the fluid/rock interface, $v_n(x,t)$, given by (4.5.27), plotted against x for a range of values of t and for $\frac{c_3}{c_2} = \infty$, $\beta = -0.33$.

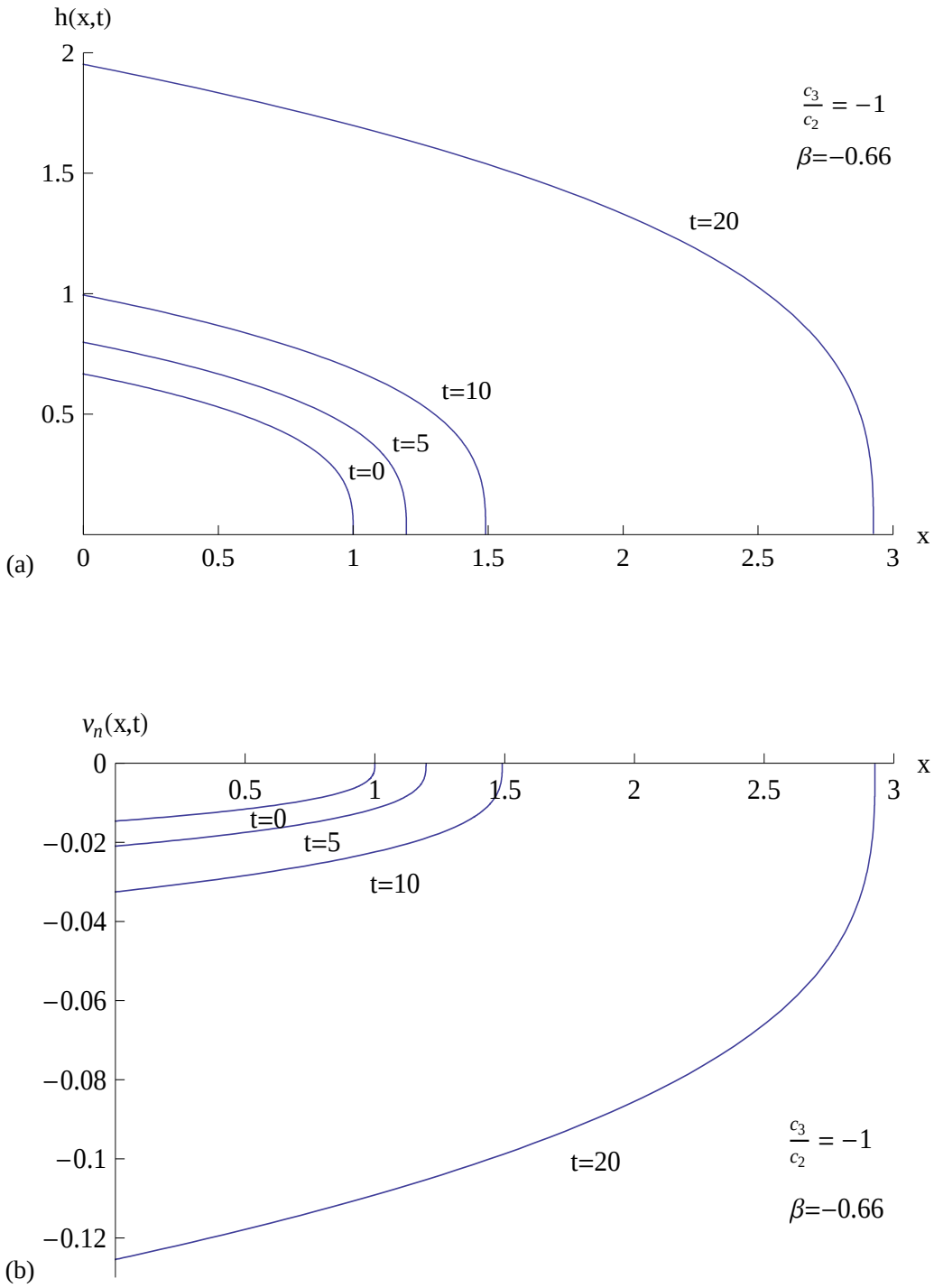


Figure 4.6.9: (a) Fracture half-width, $h(x,t)$, given by (4.5.19) and (b) leak-off velocity at the fluid/rock interface, $v_n(x,t)$, given by (4.5.20), plotted against x for a range of values of t and for $\frac{c_3}{c_2} = -1$, $\beta = -0.66$.

4.7 Transformation of boundary value problem into two initial value problems

When

$$\beta \neq \frac{1}{3}\left(\frac{c_2}{c_3} - 5\right) \quad \text{and} \quad \beta \neq \frac{1}{3}\left(\frac{c_2}{c_3} - 1\right) \tag{4.7.1}$$

the problem is solved numerically. In this section, we present a method of solving numerically the boundary value problem (4.2.4), (4.2.5) and (4.2.6) by transforming it to two initial value problems. This method will also be used in Chapter 5 to transform the boundary value problem derived there to two initial value problems. It is shown in Appendix B that any differential equation of the form

$$\Lambda \frac{d}{du}\left(F^3 \frac{dF}{du}\right) + A\frac{d}{du}\left(uF\right) + BF = 0 \tag{4.7.2}$$

admits only one Lie point symmetry generator and it exists only if $A \neq 0$. Equation (4.2.4) is of the form (4.7.2) with $A = 3$ and $B = \dfrac{c_2}{c_3} - 5 - 3\beta$. Equation (4.2.4) therefore cannot be integrated completely in general to give an analytical solution. It is solved numerically for a range of values of $\frac{c_3}{c_2}$ and β. It has been shown that invariance of a boundary value problem for an ordinary differential equation under a scaling transformation allows the boundary value problem to be transformed to two initial value problems which are easier to solve[25]. This method was first used to solve the Blasius boundary value problem for steady two-dimensional flow of an incompressible fluid past a flat plate placed edgewise to the stream[26]. Several extensions of the technique have been made[27, 28, 29].

The Lie point symmetry generator admitted by any differential equation of the form (4.7.2) is, from Appendix B,

$$X = 3u\frac{d}{du} + 2F\frac{d}{dF}. \tag{4.7.3}$$

The transformation $(u, F) \rightarrow (\overline{u}, \overline{F})$, generated by the Lie point symmetry (4.7.3) is derived by solving Lie's equations subject to initial conditions as described in Section 2.3. Lie's equations and the initial conditions for the transformation generated by the Lie point symmetry

(4.7.3) are

$$\frac{d\overline{u}}{da} = 3\overline{u}, \qquad \overline{u}(0) = u,$$

$$\frac{d\overline{F}}{da} = 2\overline{F}, \qquad \overline{F}(0) = F. \tag{4.7.4}$$

where a is the group parameter. The solution of (4.7.4) is

$$\overline{u} = e^{3a}u, \qquad \overline{F} = e^{2a}F. \tag{4.7.5}$$

Let $\lambda = e^{3a}$, then (4.7.5) becomes

$$\overline{u} = \lambda u, \quad \overline{F} = \lambda^{\frac{2}{3}}F. \tag{4.7.6}$$

The boundary value problem (4.2.4) to (4.2.6) is

$$\Lambda\frac{d}{du}\left(F^3\frac{dF}{du}\right) + 3\frac{d}{du}\left(uF(u)\right) + \left(\frac{c_2}{c_3} - 5 - 3\beta\right)F(u) = 0, \tag{4.7.7}$$

$$F(1) = 0, \tag{4.7.8}$$

$$\Lambda F^3(0)\frac{dF}{du}(0) = \left(\frac{c_2}{c_3} - 5 - 3\beta\right)\int_0^1 F(u)du. \tag{4.7.9}$$

Under the transformation (4.7.6), equations (4.7.7) to (4.7.9) become

$$\Lambda\frac{d}{d\overline{u}}\left(\overline{F}^3\frac{d\overline{F}}{d\overline{u}}\right) + 3\frac{d}{d\overline{u}}\left(\overline{u}\overline{F}(\overline{u})\right) + \left(\frac{c_2}{c_3} - 5 - 3\beta\right)\overline{F}(\overline{u}) = 0, \tag{4.7.10}$$

$$\overline{F}(\lambda) = 0, \tag{4.7.11}$$

$$\Lambda\overline{F}^3(0)\frac{d\overline{F}}{d\overline{u}}(0) = \left(\frac{c_2}{c_3} - 5 - 3\beta\right)\int_0^\lambda \overline{F}(\overline{u})d\overline{u}. \tag{4.7.12}$$

We see that the differential equation (4.7.7) is invariant under the transformation (4.7.6). This is the basic property of a transformation generated by a Lie point symmetry of a differential equation.

We now choose

$$\overline{F}(0) = 1. \tag{4.7.13}$$

Then from (4.7.6),

$$F(0) = \frac{1}{\lambda^{\frac{2}{3}}}. \tag{4.7.14}$$

The parameter λ is defined by (4.7.11). The boundary value problem, (4.7.7) to (4.7.9), can therefore be transformed into the following two initial value problems:

Initial Value Problem 1

$$\Lambda\frac{d}{d\overline{u}}\left(\overline{F}^3\frac{d\overline{F}}{d\overline{u}}\right)+3\frac{d}{d\overline{u}}\left(\overline{u}\overline{F}(\overline{u})\right)+\left(\frac{c_2}{c_3}-5-3\beta\right)\overline{F}(\overline{u})=0, \tag{4.7.15}$$

$$\overline{F}(0)=1, \tag{4.7.16}$$

$$\Lambda\frac{d\overline{F}}{d\overline{u}}(0)=\left(\frac{c_2}{c_3}-5-3\beta\right)\int_0^{\lambda}\overline{F}(\overline{u})d\overline{u}, \tag{4.7.17}$$

where $0\leq\overline{u}\leq\lambda$ and λ is defined by

$$\overline{F}(\lambda)=0. \tag{4.7.18}$$

Initial Value Problem 2

$$\Lambda\frac{d}{du}\left(F^3\frac{dF}{du}\right)+3\frac{d}{du}\left(uF(u)\right)+\left(\frac{c_2}{c_3}-5-3\beta\right)F(u)=0, \tag{4.7.19}$$

$$F(0)=\lambda^{-\frac{2}{3}}, \tag{4.7.20}$$

$$\Lambda\frac{dF}{du}(0)=\lambda^2\left(\frac{c_2}{c_3}-5-3\beta\right)\int_0^1 F(u)du, \tag{4.7.21}$$

where $0\leq u\leq 1$ and the parameter λ is obtained from Problem 1.

The Initial Value Problem 1 is used only to calculate λ. The solution $F(u)$ is obtained by solving the Initial Value Problem 2. The remainder of the solution is given by (4.2.7) to (4.2.13). Before we consider the numerical solution for general values of β and $\frac{c_3}{c_2}$ we will transform the boundary value problem for the two special cases for which an analytical solution has been found into two Initial Value Problems. These Initial Value Problems will be solved. It will give a check on the numerical method.

Special case: $\beta = \frac{1}{3}\left(\frac{c_2}{c_3} - 5\right)$

The boundary value problem (4.7.7) to (4.7.9) reduces to

$$\Lambda \frac{d}{du}\left(F^3 \frac{dF}{du}\right) + 3\frac{d}{du}(uF(u)) = 0, \tag{4.7.22}$$

$$F(1) = 0, \tag{4.7.23}$$

$$\frac{dF}{du}(0) = 0. \tag{4.7.24}$$

This boundary value problem can be transformed to the following two initial value problems:

Initial Value Problem 1:

$$\Lambda \frac{d}{d\overline{u}}\left(\overline{F}^3 \frac{d\overline{F}}{d\overline{u}}\right) + 3\frac{d}{d\overline{u}}\left(\overline{u}\overline{F}(\overline{u})\right) = 0, \tag{4.7.25}$$

$$\overline{F}(0) = 1, \tag{4.7.26}$$

$$\frac{d\overline{F}}{d\overline{u}}(0) = 0, \tag{4.7.27}$$

where $0 \leq \overline{u} \leq \lambda$ and λ is defined by

$$\overline{F}(\lambda) = 0. \tag{4.7.28}$$

Initial Value Problem 2 :

$$\Lambda \frac{d}{du}\left(F^3 \frac{dF}{du}\right) + 3\frac{d}{du}\left(uF(u)\right), \tag{4.7.29}$$

$$F(0) = \lambda^{-\frac{2}{3}}, \tag{4.7.30}$$

$$\frac{dF}{du}(0) = 0, \tag{4.7.31}$$

where $0 \leq u \leq 1$ and λ is obtained from Problem 1.

Solving the Initial Value Problem 1 for $\overline{F}(\overline{u})$ gives

$$\overline{F}(\overline{u}) = \left(\frac{9}{2\Lambda}\right)^{\frac{1}{3}}\left(\frac{2\Lambda}{9} - \overline{u}^2\right)^{\frac{1}{3}}. \tag{4.7.32}$$

Using (4.7.28), we obtain

$$\lambda = \frac{\sqrt{2\Lambda}}{3}. \tag{4.7.33}$$

The solution of the Initial Value Problem 2 is

$$F(u) = \left(\frac{9}{2\Lambda}\right)^{\frac{1}{3}} \left(1-u^2\right)^{\frac{1}{3}}. \tag{4.7.34}$$

Equation (4.7.34) agrees with (4.3.9) derived for $F(u)$ in Section 4.3.

Special case: $\beta = \frac{1}{3}\left(\frac{c_2}{c_3} - 1\right)$

For this special case the boundary value problem (4.7.7) to (4.7.9) is transformed to the following two Initial Value Problems:

Initial Value Problem 1

$$\Lambda \frac{d}{d\overline{u}}\left(\overline{F}^3 \frac{d\overline{F}}{d\overline{u}}\right) + 3\frac{d}{d\overline{u}}\left(\overline{u}\overline{F}\right) - 4\overline{F}(\overline{u}) = 0, \tag{4.7.35}$$

$$\overline{F}(0) = 1, \qquad \Lambda \frac{d\overline{F}}{d\overline{u}}(0) = -4\int_0^{\lambda} \overline{F}(\overline{u})d\overline{u}, \tag{4.7.36}$$

where $0 \leq \overline{u} \leq \lambda$ and λ is defined by

$$F(\lambda) = 0. \tag{4.7.37}$$

Initial Value Problem 2

$$\Lambda \frac{d}{du}\left(F^3 \frac{dF}{du}\right) + 3\frac{d}{du}\left(uF\right) - 4F(u) = 0, \tag{4.7.38}$$

$$F(0) = \lambda^{-\frac{2}{3}}, \qquad \Lambda \frac{dF}{du}(0) = -4\lambda^2 \int_0^1 F(u)du, \tag{4.7.39}$$

where $0 \leq u \leq 1$ and the parameter λ is obtained from Problem 1.

In order to solve Problem 1, look for a solution of (4.7.35) of the form

$$\overline{F}(\overline{u}) = A\left(B - \overline{u}\right)^n, \tag{4.7.40}$$

where A, B and n are constants to be determined such that $A \neq 0$ and $n > 0$. Using (4.7.36a) we have

$$AB^n = 1. \tag{4.7.41}$$

Substituting (4.7.40) into (4.7.35) and solving gives

$$n = \frac{1}{3}, \qquad A^3 = \frac{9B}{\Lambda} \tag{4.7.42}$$

and therefore using (4.7.41),

$$A = \left(\frac{9}{\Lambda}\right)^{\frac{1}{6}}, \qquad B = \left(\frac{\Lambda}{9}\right)^{\frac{1}{2}}. \tag{4.7.43}$$

Thus

$$\overline{F}(\overline{u}) = \left(\frac{9}{\Lambda}\right)^{\frac{1}{6}} \left[\left(\frac{\Lambda}{9}\right)^{\frac{1}{2}} - \overline{u}\right]^{\frac{1}{3}} \tag{4.7.44}$$

and hence from (4.7.37),

$$\lambda = \left(\frac{\Lambda}{9}\right)^{\frac{1}{2}}. \tag{4.7.45}$$

It can be verified that the boundary condition (4.7.36b) is identically satisfied by (4.7.44). The solution of the Initial Value Problem 2 is performed in a similar way by looking for a solution of (4.7.38) of the form (4.7.40). It is found out that

$$F(u) = \left(\frac{9}{\Lambda}\right)^{\frac{1}{3}} (1-u)^{\frac{1}{3}}. \tag{4.7.46}$$

Equation (4.7.46) agrees with (4.5.10) derived for $F(u)$ in Section 4.5.

4.8 Numerical solution

In order to transform Λ from the equations, redefine

$$t' = \Lambda t, \qquad v_n' = \frac{v_n}{\Lambda} \tag{4.8.1}$$

and then suppress the dash. The partial differential equation (3.6.1) becomes

$$\frac{\partial h}{\partial t} = \frac{1}{3}\frac{\partial}{\partial x}\left(h^3 \frac{\partial h}{\partial x}\right) - v_n. \tag{4.8.2}$$

The boundary value problem (4.2.4) to (4.2.6) becomes

$$\frac{d}{du}\left(F^3 \frac{dF}{du}\right) + 3\frac{d}{du}\left(uF(u)\right) + \left(\frac{c_2}{c_3} - 5 - 3\beta\right) F(u) = 0, \tag{4.8.3}$$

$$F(1) = 0, \tag{4.8.4}$$

$$F^3(0)\frac{dF}{du}(0) = \left(\frac{c_2}{c_3} - 5 - 3\beta\right) \int_0^1 F(u)du, \tag{4.8.5}$$

which is transformed into the two initial value problems (4.7.15) to (4.7.18) and (4.7.19) to (4.7.21) with $\Lambda = 1$:

Initial Value Problem 1

$$\frac{d}{d\overline{u}}\left(\overline{F}^3\frac{d\overline{F}}{d\overline{u}}\right)+3\frac{d}{d\overline{u}}\left(\overline{u}\overline{F}(\overline{u})\right)+\left(\frac{c_2}{c_3}-5-3\beta\right)\overline{F}(\overline{u})=0, \tag{4.8.6}$$

$$\overline{F}(0)=1, \tag{4.8.7}$$

$$\frac{d\overline{F}}{d\overline{u}}(0)=\left(\frac{c_2}{c_3}-5-3\beta\right)\int_0^{\lambda}\overline{F}(\overline{u})d\overline{u}, \tag{4.8.8}$$

where $0\leq\overline{u}\leq\lambda$ and λ is defined by

$$\overline{F}(\lambda)=0. \tag{4.8.9}$$

Initial Value Problem 2

$$\frac{d}{du}\left(F^3\frac{dF}{du}\right)+3\frac{d}{du}\left(uF(u)\right)+\left(\frac{c_2}{c_3}-5-3\beta\right)F(u)=0, \tag{4.8.10}$$

$$F(0)=\lambda^{-\frac{2}{3}}, \tag{4.8.11}$$

$$\frac{dF}{du}(0)=\lambda^{\frac{1}{3}}\frac{d\overline{F}}{d\overline{u}}(0), \tag{4.8.12}$$

where $0\leq u\leq 1$ and the parameter λ is obtained from Problem 1.

We present the numerical method employed to solve equations (4.8.6) to (4.8.9) of the Initial Value Problem 1 and (4.8.10) to (4.8.12) of the Initial Value Problem 2. The second order differential equation (4.8.6) can be transformed into the coupled system of first order differential equations

$$\frac{d\overline{F}}{d\overline{u}}=y_2, \tag{4.8.13}$$

$$\frac{dy_2}{d\overline{u}}=-\frac{1}{\overline{F}^3}\left[3\overline{F}^2y_2^2+3\overline{u}y_2+\left(\frac{c_2}{c_3}-2-3\beta\right)\overline{F}\right], \tag{4.8.14}$$

subject to the initial and boundary conditions

$$\overline{F}(0)=1,\quad y_2(0)=K_1,\quad \overline{F}(\lambda)=0 \tag{4.8.15}$$

where K_1 is to be determined. The second order differential equation (4.8.10) is transformed into the convenient set of coupled first order differential equations

$$\frac{dF}{du}=y_3, \tag{4.8.16}$$

$$\frac{dy_3}{du}=-\frac{1}{F^3}\left[3F^2y_3^2+3uy_3+\left(\frac{c_2}{c_3}-2-3\beta\right)F\right], \tag{4.8.17}$$

subject to the initial conditions

$$\overline{F}(0) = \lambda^{-\frac{2}{3}}, \quad y_3(0) = \lambda^{\frac{1}{3}} y_2(0). \tag{4.8.18}$$

The solution of the coupled system (4.8.16) to (4.8.17) subject to the initial conditions (4.8.18a) and (4.8.18b) is also the solution of the original boundary value problem (4.2.4) subject to the boundary conditions (4.2.5) and (4.2.6). The values of λ and $y_2(0)$ are obtained directly by solving (4.8.13)-(4.8.14) subject to (4.8.15a), (4.8.15b) and (4.8.15c) using the shooting method.

The algorithm for the shooting method is as follows

- STEP 1

  For fixed values of the parameters $\frac{c_3}{c_2}$ and β, solve the first order system (4.8.13) and (4.8.14) of the Initial Value Problem 1 subject to (4.8.15a), (4.8.15b) and (4.8.15c) for $\overline{F}$ and λ using the IVP solver-ODE 45 in MATLAB. The first step in determining $\overline{F}$ and λ involves integration of (4.8.13) and (4.8.14) backward from $\overline{u} = \lambda_*$ to $\overline{u} = 0$ with varying values of λ_* until the condition

  $$|\overline{F}_{\lambda_*}(0) - 1| < \varepsilon_1, \tag{4.8.19}$$

  where $\varepsilon_1 = 10^{-5}$ is satistied. Because of the singularity at $\overline{u} = \lambda$, it is necessary to commence the backward integration with the asymptotic representations for $\overline{F}(\overline{u})$ and $y_2(\overline{u})$ as initial conditions at an $\epsilon-$neighbourhood of the point $\overline{u} = \lambda$ where the solution $\overline{F}(\overline{u})$ faces singularity. These asymptotic representations can be derived directly from (4.2.25) using the transformation (4.7.6) with $\Lambda = 1$ as

  $$\overline{F} \sim (9\lambda)^{\frac{1}{3}} (\lambda - \overline{u})^{\frac{1}{3}}, \tag{4.8.20}$$

  $$y_2 \sim -\frac{1}{3}(9\lambda)^{\frac{1}{3}} (\lambda - \overline{u})^{-\frac{2}{3}}. \tag{4.8.21}$$

  When (4.8.19) is satisfied the value of the slope K_1 for the coupled first order system (4.8.13)-(4.8.14) then satisfies

  $$|\overline{F}'_{\lambda_*}(0) - K_1| < \varepsilon_2, \tag{4.8.22}$$

that is

$$\overline{F}'_{\lambda_*}(0) - \varepsilon_2 < K_1 < \overline{F}'_{\lambda_*}(0) + \varepsilon_2, \tag{4.8.23}$$

where ε_2 is taken to be 10^{-5}.

STEP 1 therefore provides us with an interval inside which we know that the slope K_1 lies and this ensures a faster rate of convergence of K_1.

- STEP 2

  Use the symbolic property of MATHEMATICA to solve the first order system (4.8.13) and (4.8.14) of IVP 1 on the domain $0 \leq u \leq \varpi$ where $\varpi > \lambda_*$, subject to the initial conditions

$$\overline{F}(0) = 1, \qquad \frac{d\overline{F}}{d\overline{u}}(0) = K_1, \tag{4.8.24}$$

  where K_1 is an iterate from $\overline{F}'_{\lambda_*}(0) - \varepsilon_2$ to $\overline{F}'_{\lambda_*}(0) + \varepsilon_2$.

  In order to ensure an accurate value of the slope K_1 used as initial condition, the step size for the iteration must be of order say 10^{-8}. This also ensures the accuracy of the value of λ obtained.

  For each iteration, solve for λ,

$$\overline{F}(\lambda) = 0.$$

- STEP 3

  If

$$\left| K_1 - (\frac{c_3}{c_2} - 5 - 3\beta) \int_0^{\lambda - 0.00001} \overline{F}(\overline{u}) d\overline{u} \right| < \varepsilon_3 \tag{4.8.25}$$

  where $\varepsilon_3 = 10^{-7}$, then the value of λ obtained in STEP 2 is the required value. Because there is a singularity at $\overline{u} = \lambda$, the upper limit in the integral is set equal to $\lambda - 0.000001$.

By obtaining λ in STEPS 1, 2 and 3, we now solve for $F(u)$ the coupled system (4.8.16) to (4.8.17) subject to known initial conditions (4.8.18a) and (4.8.18b). The initial condition (4.8.18b) must satisfy

$$\left| \frac{dF}{du}(0) - \lambda^{\frac{1}{3}} y_2(0) \right| < \varepsilon_4, \tag{4.8.26}$$

where $\varepsilon_4 = 10^{-6}$. During the numerical computation it turns out that the accurary of the shooting method at the fracture tip depends strongly on the value of the slope $\lambda^{\frac{1}{3}} y_2(0)$ used as

initial condition for the coupled system (4.8.16) to (4.8.17) which in turn depends on ε_3. Calculations made when $\varepsilon_3 = 10^{-9}$ and $\varepsilon_3 = 10^{-12}$ in (4.8.26) show that the overall properties of the solution $F(u)$ differed little from those for $\varepsilon_3 = 10^{-7}$ and solutions overlap on the domain $[0, 1)$ except in the neighbourhood of the fracture tip where $u = 1$. Calculations made with $\varepsilon_3 = 10^{-3}$ and $\varepsilon_3 = 10^{-5}$ in (4.8.26) show a good agreement between the numerical solution and the exact solution in the region away from the fracture tip but as the tip is approached the agreement begins to fail. Tables 4.8.1 and 4.8.2 show the numerical and analytical solutions for $F(u)$ for the two cases in Sections 4.3 and 4.5 in which exact solutions are known. The results shown are obtained for $\varepsilon_3 = 10^{-7}$ and solutions only agree to 3 decimal places in the fracture tip neighbourhood.

4.9 Numerical Results

In this section, we analyse the general results obtained from the numerical computation of the similarity dependent variable $F(u)$ for a range of values of the parameters β and $\frac{c_3}{c_2}$. It was discovered numerically while doing the calculations that for each value of the parameter $\frac{c_3}{c_2}$ there exists a minimum value for the leak-off parameter β. Below this value of β there is no solution of the Initial Value Problem (4.8.16) to (4.8.18). The set of values of the parameters $\frac{c_3}{c_2}$ and β in the $(\frac{c_3}{c_2}, \beta)$ plane for which a solution exists to the Initial Value Problem (4.8.16) to (4.8.18) is bounded below. This is shown in Fig 4.9.1.

4.9.1 Physical significance of curves

Consider the curve

$$\beta = \frac{5\left(\frac{1}{5} - \frac{c_3}{c_2}\right)}{3\frac{c_3}{c_2}}. \tag{4.9.1}$$

The set of values of the parameters $(\frac{c_3}{c_2}, \beta)$ satisfying (4.9.1) describes an operating condition in which there is no fluid injection or extraction at the fracture entry. That is, (4.9.1) is the curve for no injection or extraction of fluid at the fracture entry.

Special Case $\frac{c_2}{c_3} - 3\beta - 5$ =0		
u	Exact Solution	Numerical Solution
0.000	1.650960	1.650960
0.200	1.628650	1.628650
0.400	1.557750	1.557750
0.600	1.422760	1.422760
0.800	1.174460	1.174460
0.900	0.949122	0.949122
0.920	0.884168	0.884168
0.940	0.806099	0.806100
0.960	0.706604	0.706605
0.980	0.562733	0.562734
0.982	0.543496	0.543496
0.984	0.522747	0.522747
0.986	0.500157	0.500158
0.988	0.475266	0.475266
0.990	0.447392	0.447393
0.992	0.415461	0.415462
0.994	0.377598	0.377598
0.996	0.329972	0.329973
0.998	0.261987	0.261987
1.000	0.000000	0.000860

Table 4.8.1: Comparison of the numerical and analytical solutions for $F(u)$ for the special case $\frac{c_2}{c_3} - 3\beta - 5$ =0.

Special Case $\frac{c_2}{c_3} - 3\beta - 1$ =0		
u	Exact Solution	Numerical Solution
0.000	2.080080	2.080090
0.200	1.930980	1.930980
0.400	1.754410	1.754410
0.600	1.532620	1.532620
0.800	1.216440	1.216440
0.900	0.965489	0.965491
0.920	0.896281	0.896283
0.940	0.814325	0.814327
0.960	0.711379	0.711381
0.980	0.564622	0.564624
0.982	0.545136	0.545138
0.984	0.524148	0.524150
0.986	0.501330	0.501332
0.988	0.476220	0.476222
0.990	0.448140	0.448142
0.992	0.416017	0.416019
0.994	0.377976	0.377978
0.996	0.330193	0.330195
0.998	0.262074	0.262076
1.000	0.000000	0.001045

Table 4.8.2: Comparison of the numerical and analytical solutions for $F(u)$ for the special case $\frac{c_2}{c_3} - 3\beta - 1$ =0.

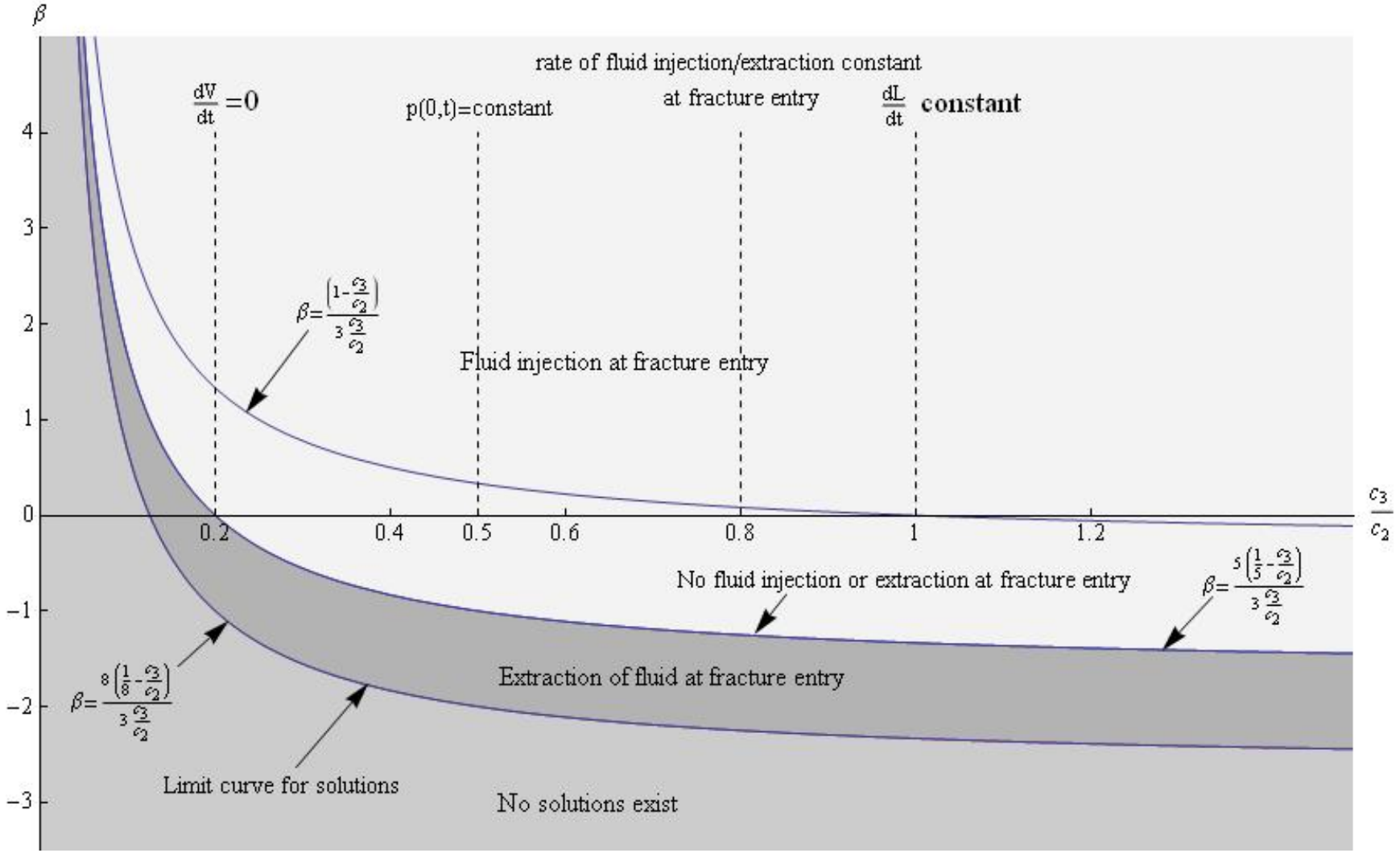


Figure 4.9.1: Curves for the analytical solutions and the limiting curve.

The limiting curve for solutions is described by

$$\beta_{min} = \frac{8\left(\frac{1}{8} - \frac{c_3}{c_2}\right)}{3\frac{c_3}{c_2}}, \tag{4.9.2}$$

where β_{min} is the minimum value of β for a given value of $\frac{c_3}{c_2}$. For

$$\beta_{min} < \frac{8\left(\frac{1}{8} - \frac{c_3}{c_2}\right)}{3\frac{c_3}{c_2}}, \tag{4.9.3}$$

there are no solutions. Equation (4.9.2) was found numerically. We are not able to give an analytical proof that there no solutions when (4.9.3) is satisfied or provide a physical explanation. In the region bounded by the curve (4.9.1) and (4.9.2), there is extraction of fluid at the fracture entry. Hence the solution of the Initial Value Problems 1 and 2 obtained using values of the parameters $\frac{c_3}{c_2}$ and β in this bounded region describes an operating condition in which there is fluid extraction out of the fracture at the fracture entry. This may have application in the extraction of oil from a fracture in permeable rock.

4.9.2 Graphical results for fixed $\frac{c_3}{c_2}$ and varying values of β

We present in this section the graphical results obtained for $h(x,t)$, $v_n(x,t)$ and $L(t)$ from the numerical solution of the two Initial Value Problems in Section 4.8 when the parameter $\frac{c_3}{c_2}$ is fixed and β is varied. For the two analytical solutions we investigated a wide range of values of $\frac{c_3}{c_2}$ and β because it was not difficult to produce graphs from the analytical results. It requires more work to derive the numerical results and therefore a smaller range of values of the parameters, β and $\frac{c_3}{c_2}$, will be considered. The values of the parameters used are those of clear physical significance. The results show how β affects the propagation of the fracture length and growth of the fracture half-width.

In Figure 4.9.2, $\frac{c_3}{c_2} = 0.1$ and from equation (4.9.2), $\beta_{min} = 0.66$. Therefore only the case in which fluid leaks off at the fluid/rock interface can be considered. The values of β considered in order of increasing leak-off are 0.66, 1, 1.66, 3 and 10. In Figure 4.9.2 (a), leak-off reduces the extent of propagation of the fracture length in a given time, with the fracture length propagating farthest when $\beta = 0.66$. For $\frac{c_3}{c_2} = 0.1$ and when $\beta = 1.66$, equation (4.9.1) is satisfied and we have the exact solution for which the rate of fluid injection into the fracture

at the entry, $q_1 = 0$. When $\beta = 3$, (4.6.1) is satisfied and we obtain the exact solution of Section 4.5 for which there is fluid injection into the fracture which increases with time. In Figure 4.9.2 (b), the gradient of the fracture half-width $\frac{\partial h}{\partial x} \to -\infty$ as $x \to L(t)$. The thin film approximation therefore breaks down in the neighbourhood of the fracture tip. In Figure 4.9.2 (c), the graph for $v_n(x,t)$ clearly reflects the underlying assumption that $v_n \propto h$. For low values of β, leak-off is approximately uniform over the fracture and an unexpected shape in which $\frac{\partial h}{\partial x}(0,t) > 0$ is obtained. For higher values of β, the expected shape is obtained. The case in which there is no leak-off cannot be analysed since solution does not exist when $\beta = 0$.

In Figure 4.9.3, $L(t)$, $h(x,t)$ and $v_n(x,t)$ are plotted for $\frac{c_3}{c_2} = 0.2$. When $\frac{c_3}{c_2} = 0.2$ the total volume of the fracture remains constant. There is no solution for $\beta < -1$ and the values of β used are those of significance and they are $\beta = -1, 0, 1.33, 5, 10$. When $\beta = 0$, there is no leak-off of fluid and equation (4.9.1) for which the rate of fluid injection into the fracture at the fracture entry, $q_1 = 0$, is satisfied. When $\beta = 1.33$, equation (4.6.1) for which the rate of fluid injection at the entry, q_1, is positive is satisfied. In Figure 4.9.3 (a), the rate of increase of the fracture length decreases as leak-off increases. Fluid injection at the fluid/rock interface also increases the fracture length. When there is leak-off, the fracture shape is as expected with $h(x,t)$ decreasing as x increases. Fluid injection at the interface gives an unexpected result in which $\frac{\partial h}{\partial x} > 0$ initially and the maximum width occurs near the mid-point of the fracture.

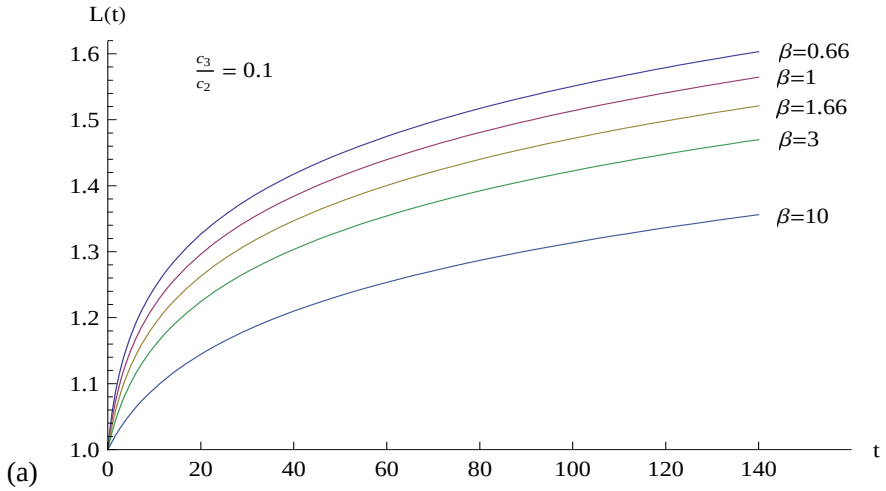
In Figure 4.9.4, $L(t)$, $h(x,t)$ and $v_n(x,t)$ are plotted for $\frac{c_3}{c_2} = 0.5$. When $\frac{c_3}{c_2} = 0.5$, the pressure at the entry, $p(0,t)$, is constant. No solution was found when $\beta < -2$. Solutions for $-2 \leq \beta < -1$ correspond to fluid extraction at the fracture entry and an unexpected shape is obtained. When $\beta = -1$, equation (4.9.1) for which the rate of fluid injection at the entry, q_1, is zero is satisfied and when $\beta = 0.33$, (4.6.1) for which the rate of fluid injection at entry, q_1, is positive is satisfied. Injection of fluid at the interface causes the fracture length to propagate further in a given time than when the rock is impermeable or when there is leak-off. This occurs even when fluid is extracted at the entry. In Figure 4.9.4 (a), fluid leak-off at the interface decreases the rate of propagation of the fracture length.

In Figure 4.9.5, $L(t)$, $h(x,t)$ and $v_n(x,t)$ are plotted for $\frac{c_3}{c_2} = 0.8$. When $\frac{c_3}{c_2} = 0.8$, the rate of fluid injection at the fracture entry is constant. No solution was found when $\beta < -2.25$.

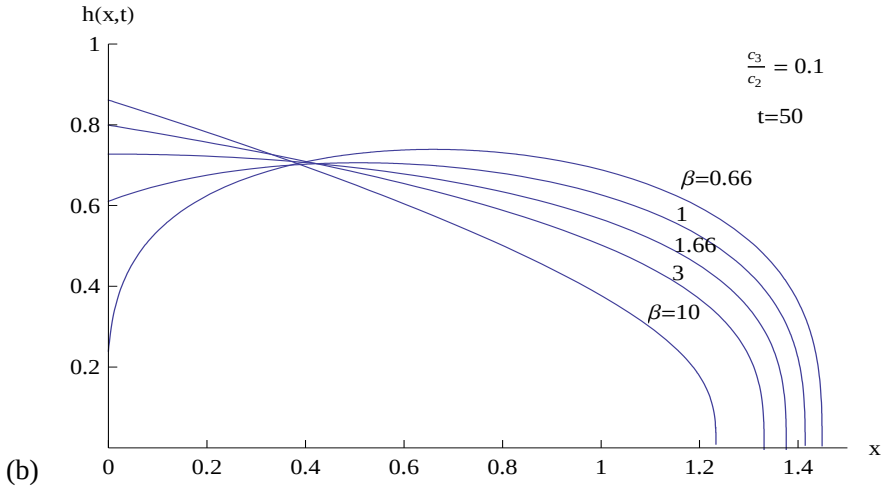
Equation (4.9.1) is satisfied when $\beta = -1.25$ and (4.6.1) is satisfied when $\beta = 0.083$. There is no fluid leak off into the rock mass when $\beta = 0$ while for $\beta = 5$ there is leak-off. Fluid injection at the interface increases the rate of propagation of the fracture length even although there is fluid extraction at the fracture entry. When there is fluid injection at the interface the unexpected shape of the fracture in which $h(x,t)$ first increases with x before decreasing is again obtained.

In Figure 4.9.6, $L(t)$, $h(x,t)$ and $v_n(x,t)$ are plotted for $\frac{c_3}{c_2} = 1$. When $\frac{c_3}{c_2} = 1$, the length of the fracture grows linearly with time for all values of β. The speed of propagation of the fracture, $\frac{dL}{dt}$, is constant. No solution exist when $\beta < -2.33$. When $\beta = -1.33$, there is no fluid injection at the entry and equation (4.9.1) is satisfied. For $\beta = 0$, there is no leak-off at the interface and equation (4.6.1) is also satisfied. Fluid injection through the interface increases the rate of propagation of the fracture length even if there is fluid extraction at the entry. The unexpected shape for the half-width of the fracture is obtained again.

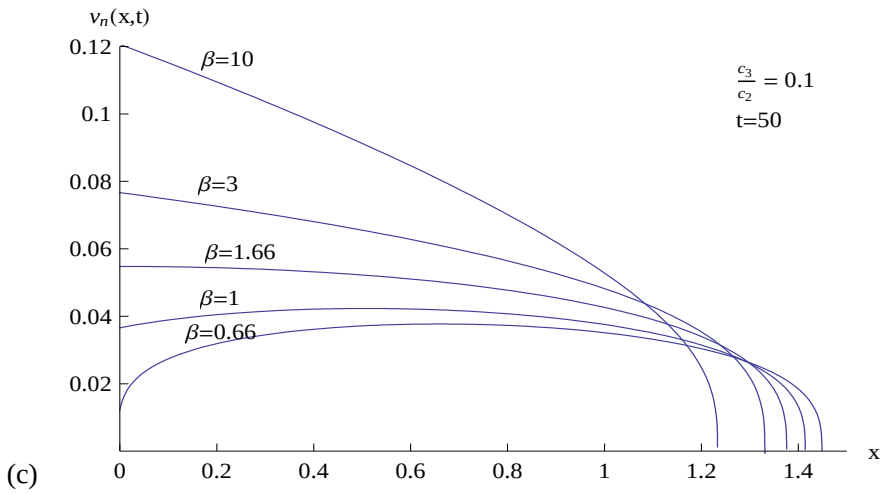
In all cases the maximum rate of growth of the length of the fracture occured for the limiting solution given by (4.9.2).



(a)

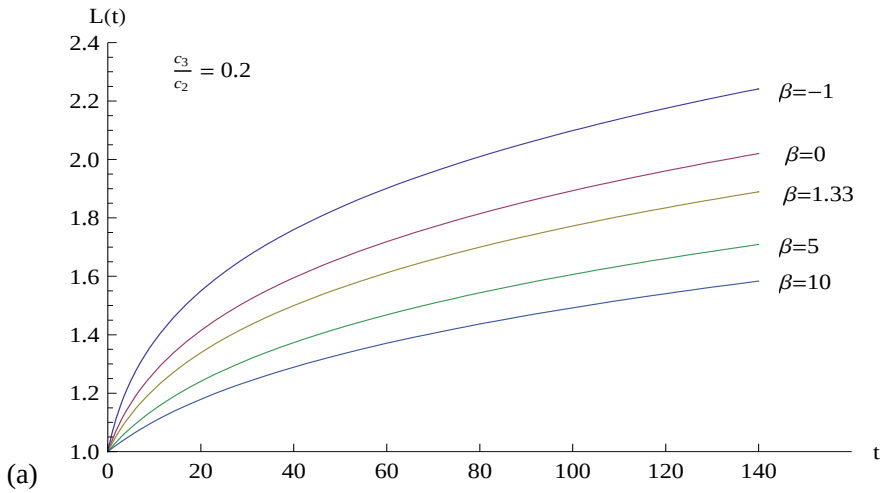


(b)

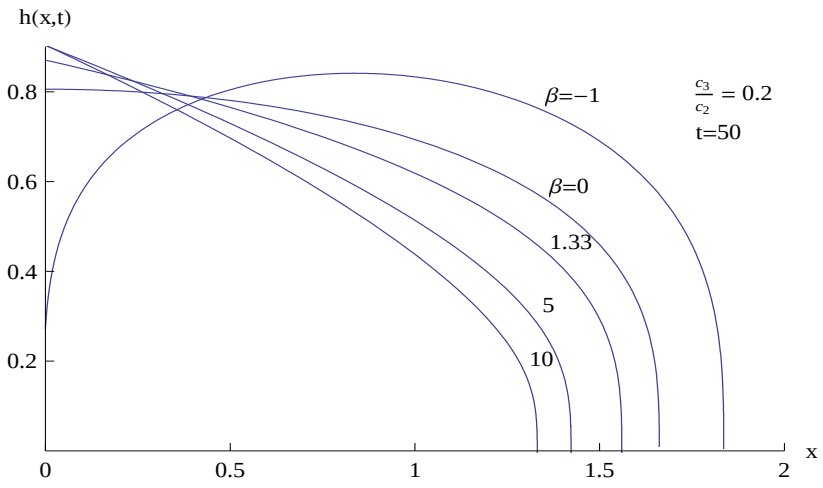


(c)

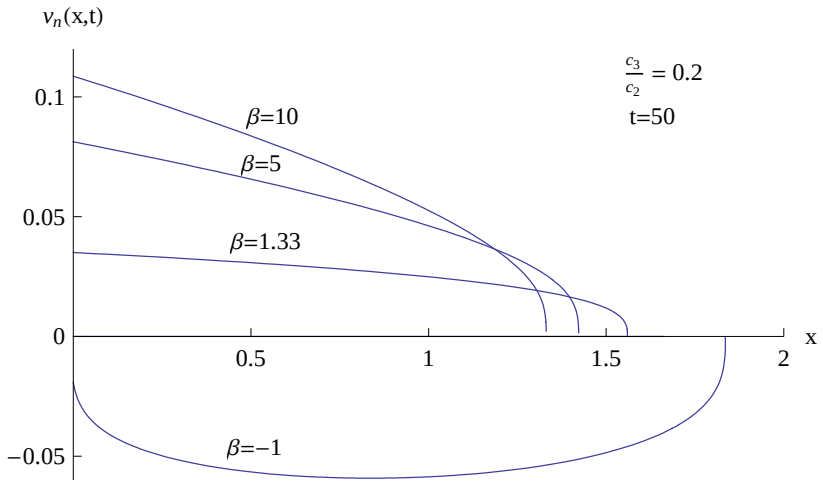
Figure 4.9.2: Graphs for $\frac{c_3}{c_2} = 0.1$ and a selection of values of β : (a) Fracture length $L(t)$ plotted against time; (b) Fracture half-width $h(x,t)$ plotted against x at time $t = 50$; (c) Leak-off fluid velocity $v_n(x,t)$ plotted against x at time $t = 50$.



(a)

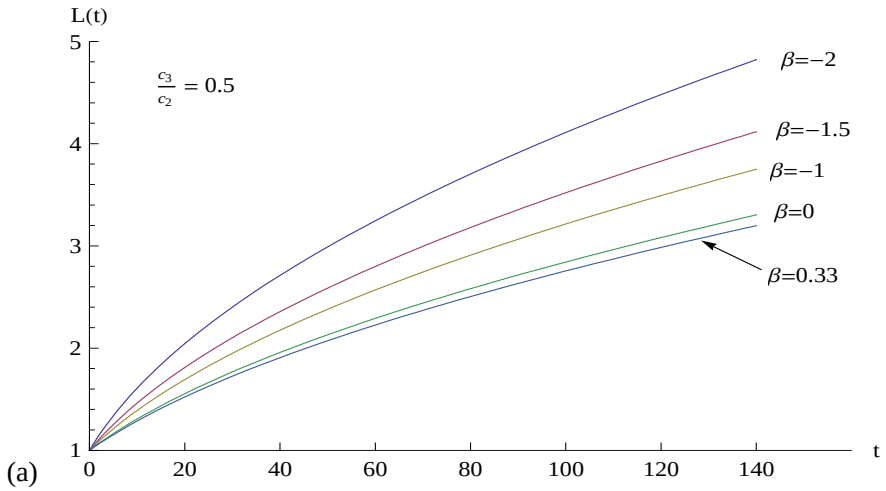


(b)

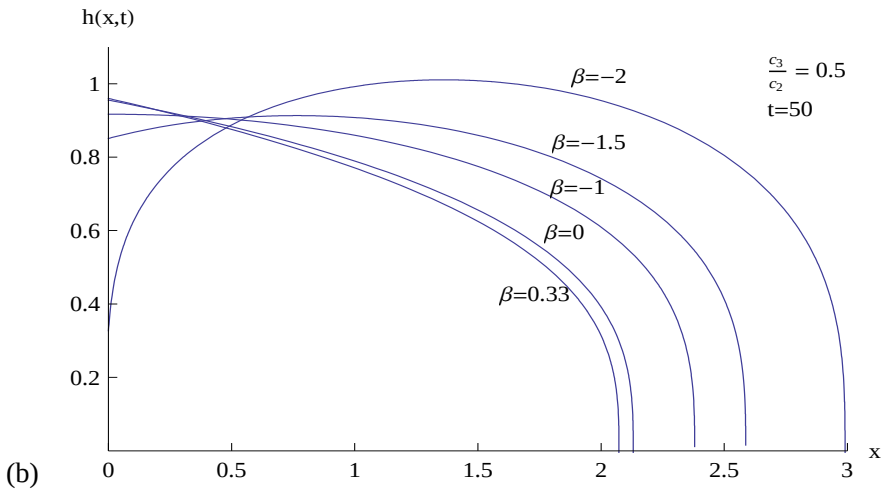


(c)

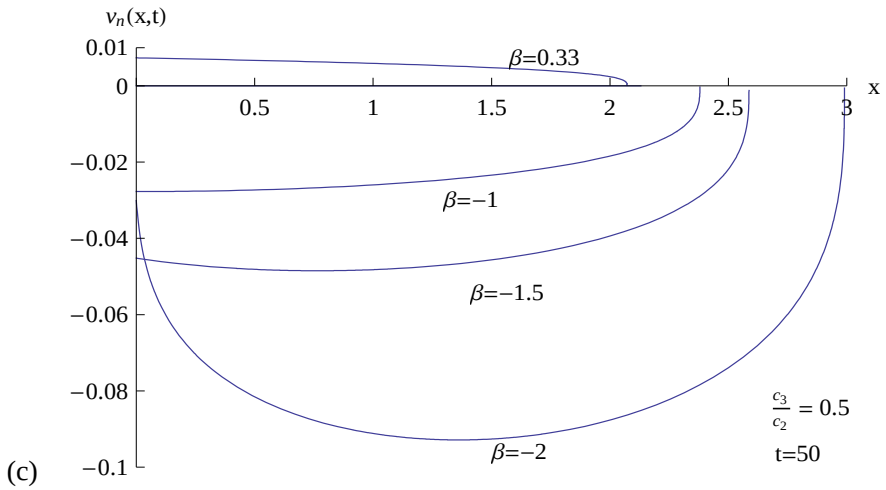
Figure 4.9.3: Graphs for $\frac{c_3}{c_2} = 0.2$ and a selection of values of β : (a) Fracture length $L(t)$ plotted against time; (b) Fracture half-width $h(x,t)$ plotted against x at time $t = 50$; (c) Leak-off fluid velocity $v_n(x,t)$ plotted against x at time $t = 50$.



(a)

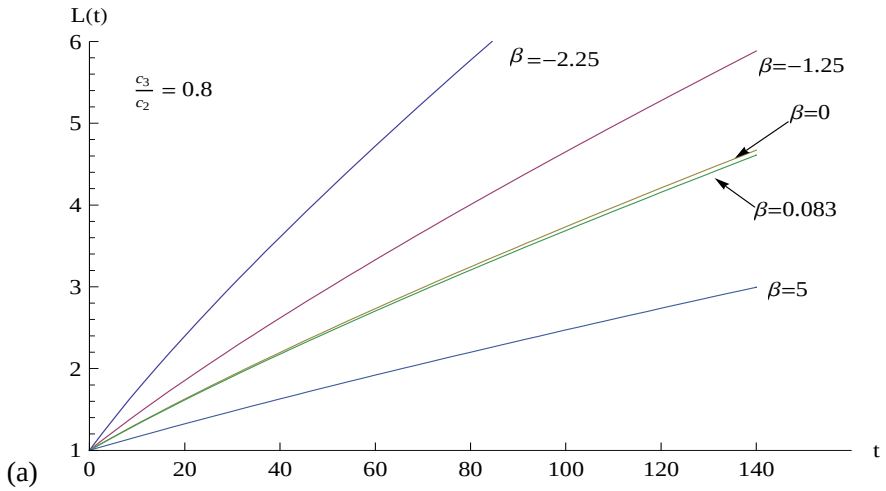


(b)

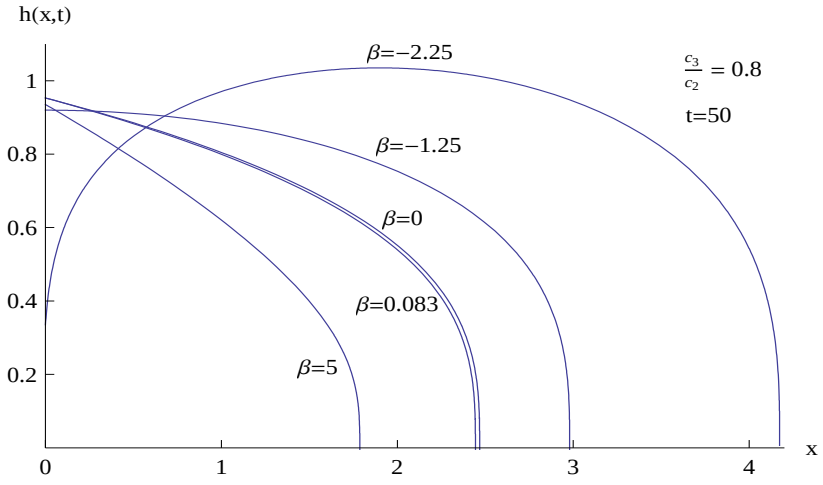


(c)

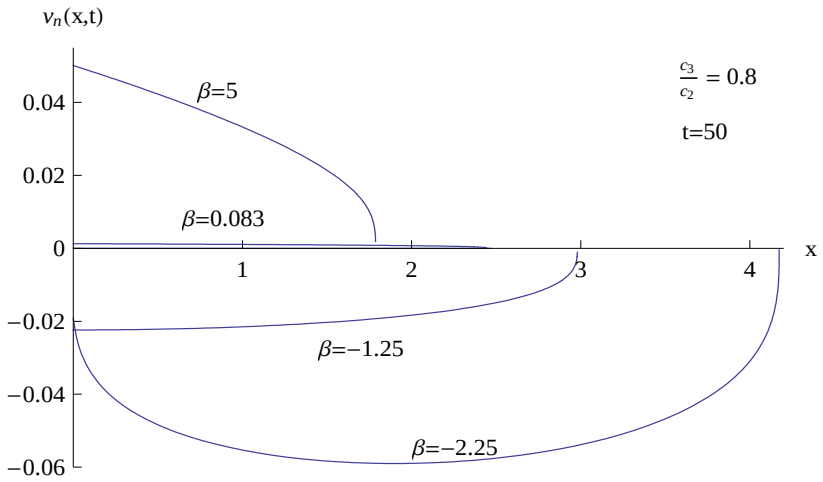
Figure 4.9.4: Graphs for $\frac{c_3}{c_2} = 0.5$ and a selection of values of β : (a) Fracture length $L(t)$ plotted against time; (b) Fracture half-width $h(x,t)$ plotted against x at time $t = 50$; (c) Leak-off fluid velocity $v_n(x,t)$ plotted against x at time $t = 50$.



(a)

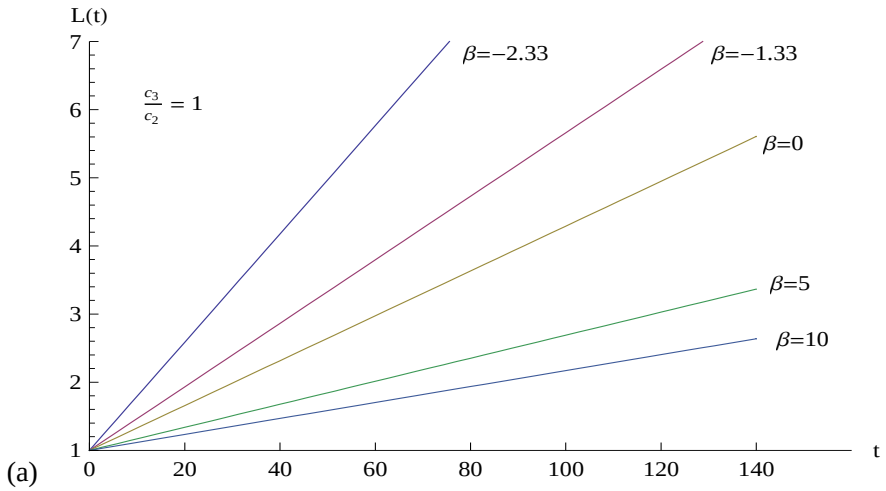


(b)

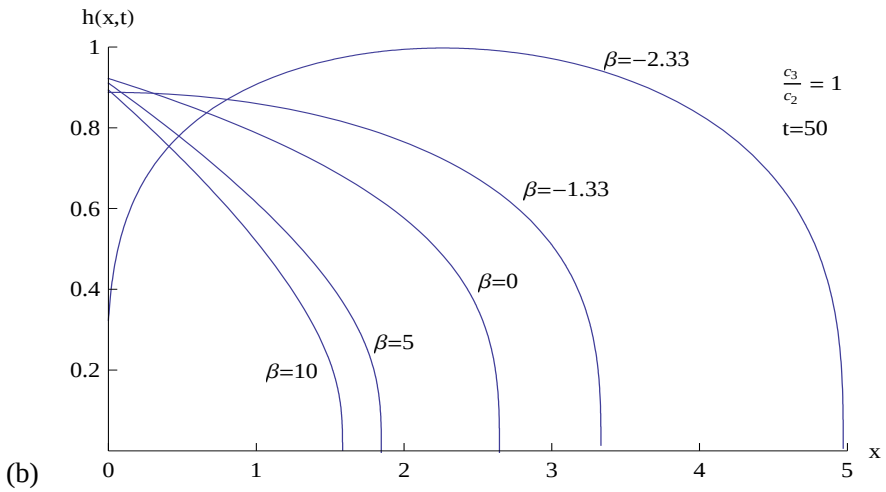


(c)

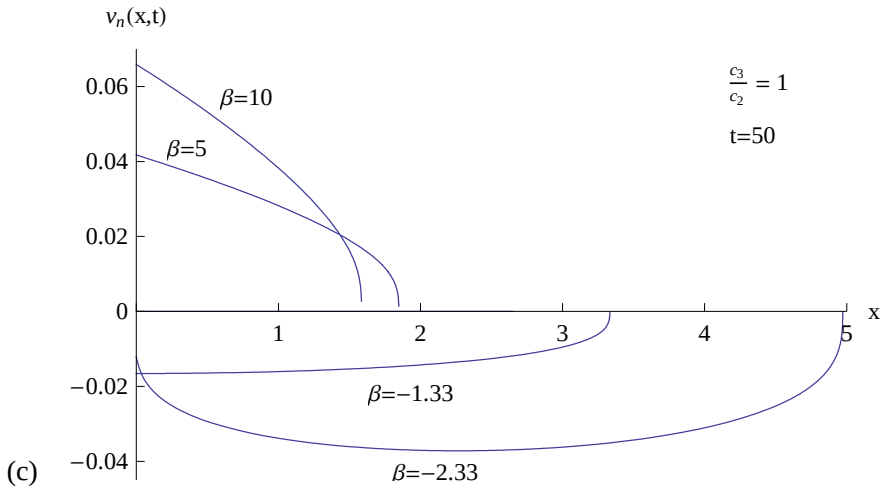
Figure 4.9.5: Graphs for $\frac{c_3}{c_2} = 0.8$ and a selection of values of β : (a) Fracture length $L(t)$ plotted against time; (b) Fracture half-width $h(x,t)$ plotted against x at time $t = 50$; (c) Leak-off fluid velocity $v_n(x,t)$ plotted against x at time $t = 50$.



(a)



(b)



(c)

Figure 4.9.6: Graphs for $\frac{c_3}{c_2} = 1$ and a selection of values of β : (a) Fracture length $L(t)$ plotted against time; (b) Fracture half-width $h(x,t)$ plotted against x at time $t = 50$; (c) Leak-off fluid velocity $v_n(x,t)$ plotted against x at time $t = 50$.

4.9.3 Graphical results for fixed β and varying values of $\frac{c_3}{c_2}$

We present in this section the graphical results obtained for $L(t)$, $h(x,t)$ and $v_n(x,t)$ when the parameter $\frac{c_3}{c_2}$ is varied and β is fixed. The values of $\frac{c_3}{c_2}$ used are those of physical significance in the range $0 < \frac{c_3}{c_2} < 1$. The results obtained show how the parameter $\frac{c_3}{c_2}$ affects the rate of propagation of the fracture length and growth of the fracture half-width.

In Figure 4.9.7, $\beta = -2$ and solution exists for $0.5 \leq \frac{c_3}{c_2} < \infty$. All solutions have fluid injection at the fluid/rock interface and extraction of fluid at the fracture entry. The maximum width of the fracture does not depend greatly on the parameter $\frac{c_3}{c_2}$ and occurs at the middle of the fracture, not at the entry since fluid extraction occurs there. The fracture length increases as $\frac{c_3}{c_2}$ increases, even although fluid extraction occurs at the entry. In Figure 4.9.7(c), the graph of $v_n(x,t)$, which is negative across the fracture for all values of $\frac{c_3}{c_2}$, verifies that fluid is always injected at the fluid/rock interface.

In Figure 4.9.8, $\beta = -1$ and the solution exists for $0.2 \leq \frac{c_3}{c_2} < \infty$. All solutions have fluid injection at the interface. For $0.2 \leq \frac{c_3}{c_2} < 0.5$, there is extraction of fluid at the entry. For $\frac{c_3}{c_2} = 0.2$ and $\frac{c_3}{c_2} = 0.35$, the half-width of the fracture initially increases with x before decreasing. For $0.5 < \frac{c_3}{c_2} < \infty$, there is fluid injection always at the entry to the fracture. When $\frac{c_3}{c_2} = 0.5$, equation (4.9.1) is satisfied and the rate of fluid injection at the entry, q_1, vanishes. Equation (4.6.1) is not satisfied for any value of $\frac{c_3}{c_2}$ when $\beta = -1$. The length of the fracture at a given time t increases as $\frac{c_3}{c_2}$ increases. It is greater when there is fluid injection at the entry $\left(\frac{c_3}{c_2} > 0.5\right)$ than when there is fluid extraction at the entry $(0.2 \leq \frac{c_3}{c_2} < 0.5)$.

In Figure 4.9.9, $\beta = 0$ and the solution exists for $0.125 \leq \frac{c_3}{c_2} < \infty$. All solutions have no fluid exchange at the interface. Hence the rock mass is impermeable. The fracture length increases as $\frac{c_3}{c_2}$ increases and the rate of increase is small when fluid extraction occurs at the entry. The shape of $h(x,t)$ when $0.125 \leq \frac{c_3}{c_2} < 0.2$ is due to fluid extraction at the entry. For $0.2 < \frac{c_3}{c_2} < \infty$, there is fluid injection at the entry and the maximum width always occurs at the entry to the fracture. When $\frac{c_3}{c_2} = 0.2$, there is no injection or extraction of fluid at the fracture entry.

In Figure 4.9.10, $\beta = 1$ and the solution exists for $0.091 \leq \frac{c_3}{c_2} < \infty$. All solutions have leak-off of fluid at the interface. Fluid extraction at the entry occurs for $0.091 \leq \frac{c_3}{c_2} < 0.125$.

Fluid injection at the entry occurs for $0.125 < \frac{c_3}{c_2} < \infty$. When $\frac{c_3}{c_2} = 0.125$, equation (4.9.1) is satisfied and $q_1 = 0$. For $\frac{c_3}{c_2} = 0.25$, equation (4.6.1) is satisfied and $q_1 > 0$. In Figure 4.9.10 (a), $L(t)$ increases as $\frac{c_3}{c_2}$ increases. The growth of $L(t)$ is stronger when there is injection of fluid at the entry than when fluid is being extracted at the entry.

In Figure 4.9.11, $\beta = 2$ and the solution exists for $0.0714 \leq \frac{c_3}{c_2} < \infty$. All solutions have leak-off of fluid at the interface. Fluid extraction occurs for $0.0714 < \frac{c_3}{c_2} < 0.091$. The shape of the fracture for $\frac{c_3}{c_2} = 0.0714$ again is due to the extraction of fluid at the entrance to the fracture. Injection of fluid at the entry occurs for $0.091 < \frac{c_3}{c_2} < \infty$ and a special case for which equation (4.6.1) is satisfied occurs when $\frac{c_3}{c_2} = 0.143$. Equation (4.9.1), for which $q_1 = 0$, is satisfied when $\frac{c_3}{c_2} = 0.091$. The fracture length $L(t)$ increases as $\frac{c_3}{c_2}$ increases. The leak-off velocity v_n is almost uniform as $\frac{c_3}{c_2}$ increases to unity.

In Figure 4.9.12, $\beta = 5$ and the solution exists for $0.043 \leq \frac{c_3}{c_2} < \infty$. All solutions have leak-off of fluid at the interface. Extraction of fluid at the entry occurs for $0.043 \leq \frac{c_3}{c_2} < 0.05$ while injection of fluid at the entry occurs for $0.05 < \frac{c_3}{c_2} < \infty$. The rate of fluid injection at the entry vanishes when $\frac{c_3}{c_2} = 0.05$. When $\frac{c_3}{c_2} = 0.0625$, equation (4.6.1) is satisfied and the exact solution, (4.5.17) to (4.5.21), applies.

In all cases the fracture length at a given time increases as $\frac{c_3}{c_2}$ increases to unity. This corresponds physically to the transition from fluid extraction at the fracture entry for small values of $\frac{c_3}{c_2}$ to fluid injection at the entry with increasing strength as $\frac{c_3}{c_2}$ increases.

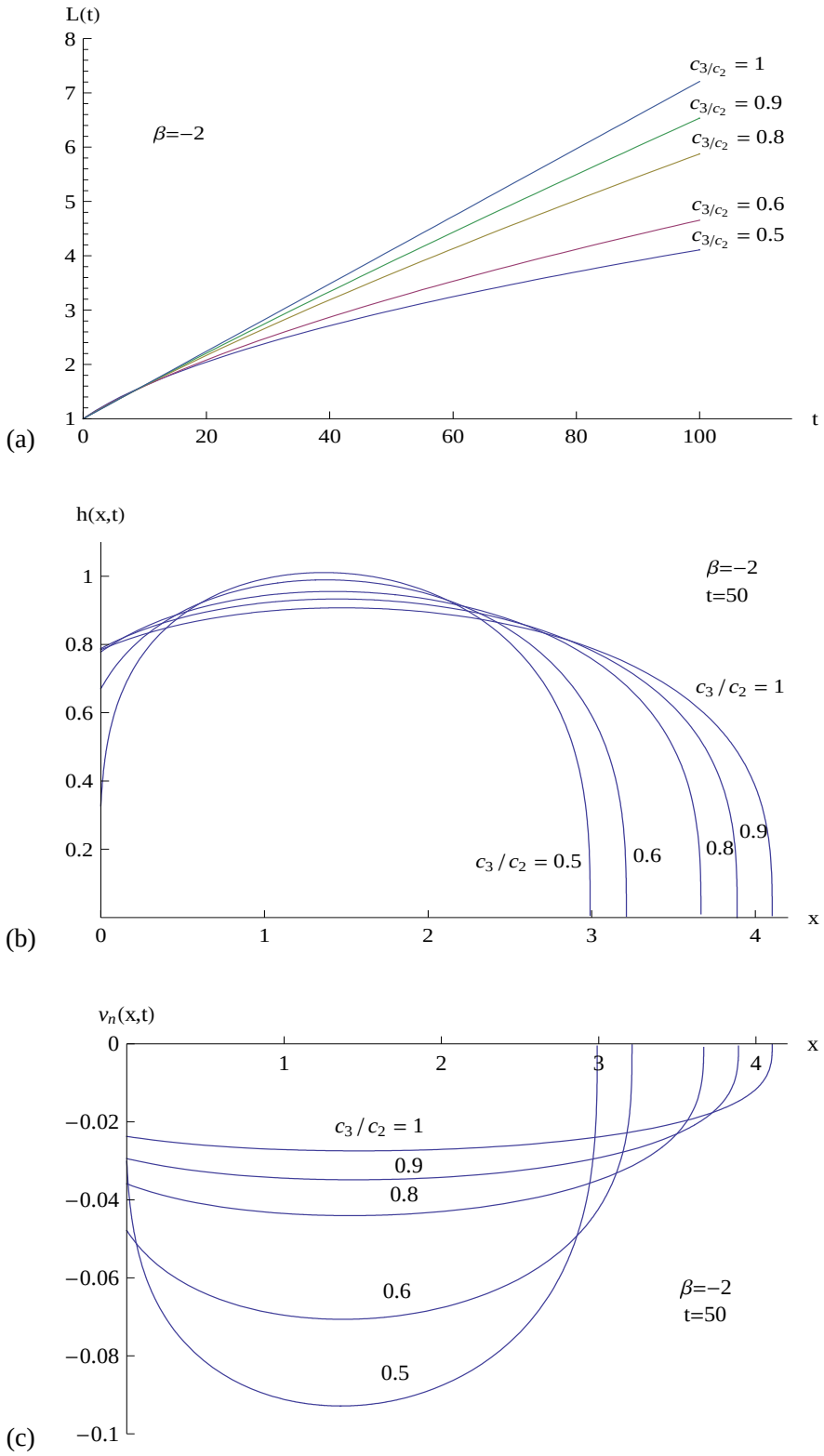


Figure 4.9.7: Graphs for $\beta = -2$ and a selection of values of $\frac{c_3}{c_2}$: (a) Fracture length $L(t)$ plotted against time; (b) Fracture half-width $h(x,t)$ plotted against x at time $t = 50$; (c) Leak-off fluid velocity $v_n(x,t)$ plotted against x at time $t = 50$.

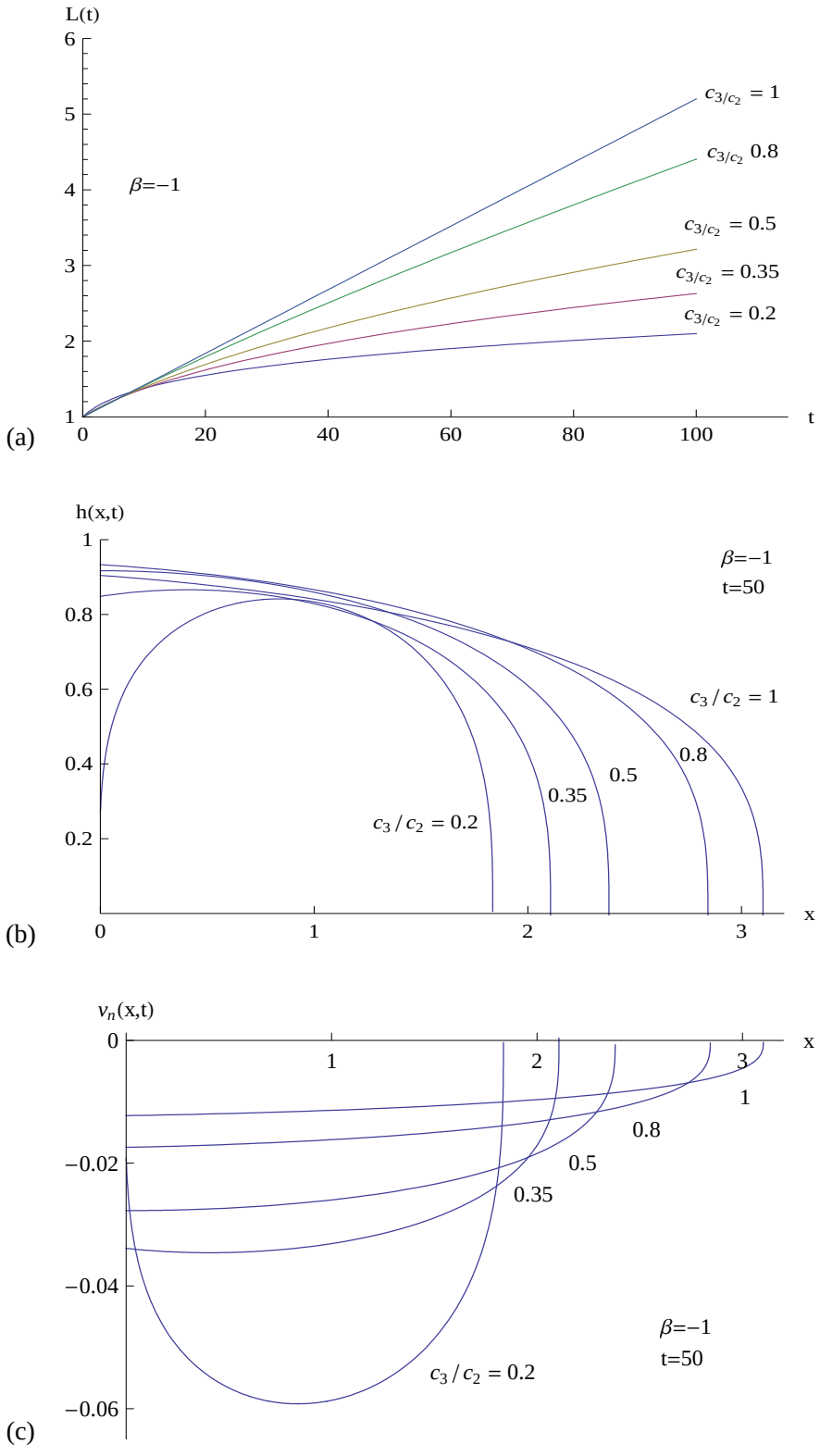


Figure 4.9.8: Graphs for $\beta = -1$ and a selection of values of $\frac{c_3}{c_2}$: (a) Fracture length $L(t)$ plotted against time; (b) Fracture half-width $h(x,t)$ plotted against x at time $t = 50$; (c) Leak-off fluid velocity $v_n(x,t)$ plotted against x at time $t = 50$.

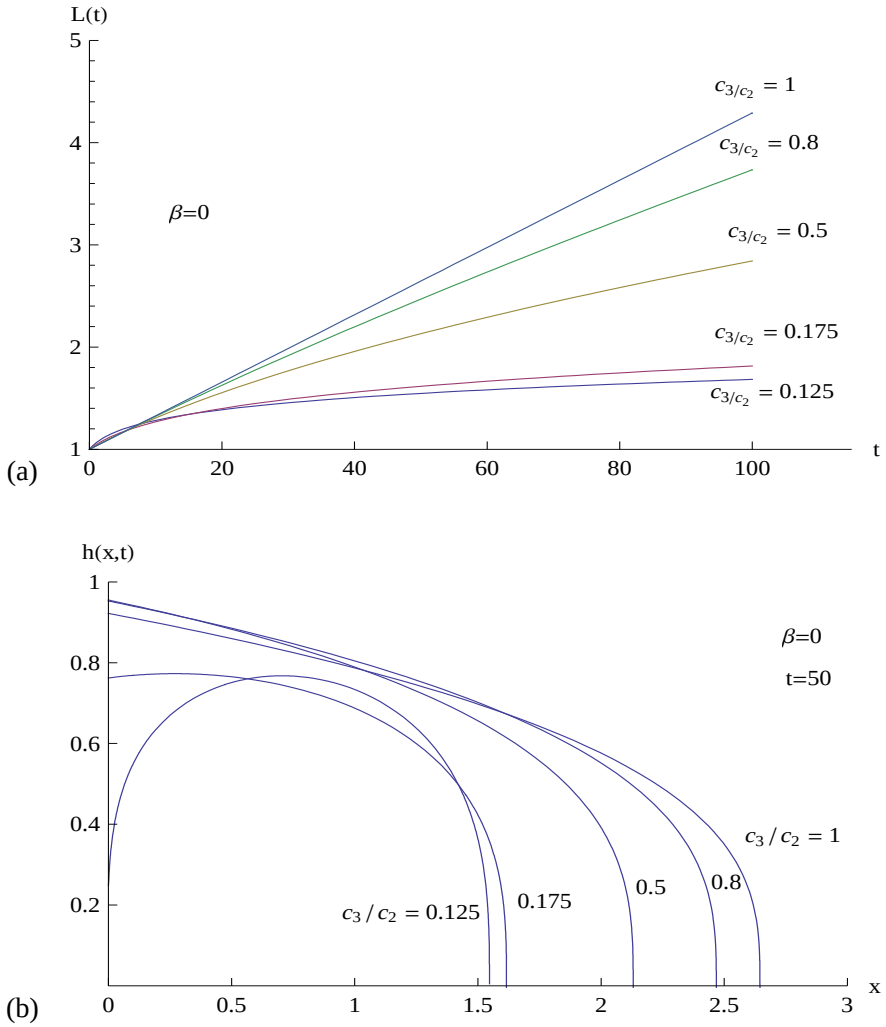
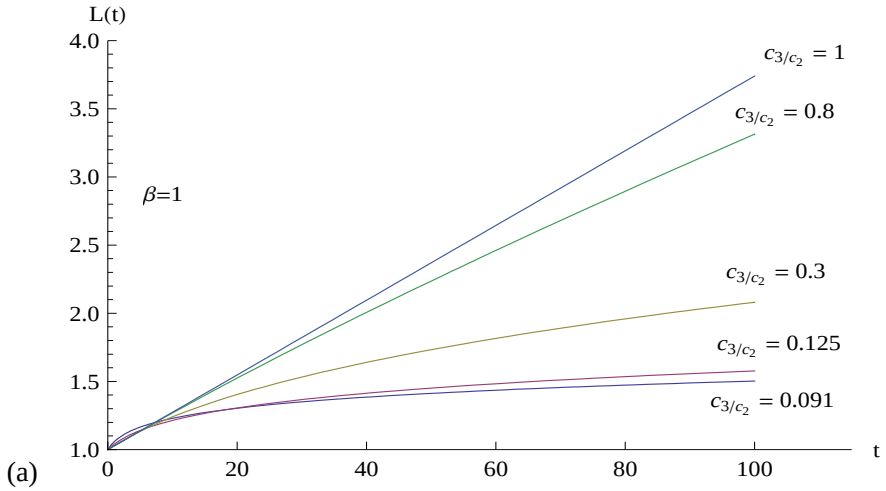
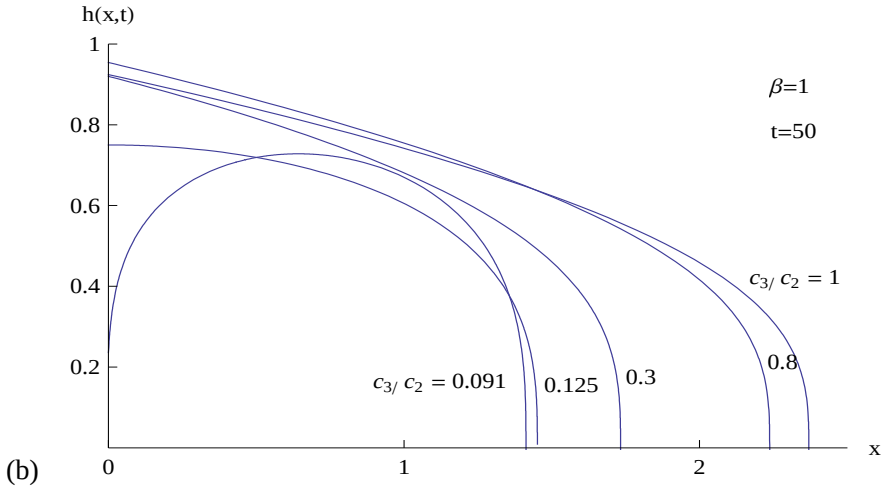


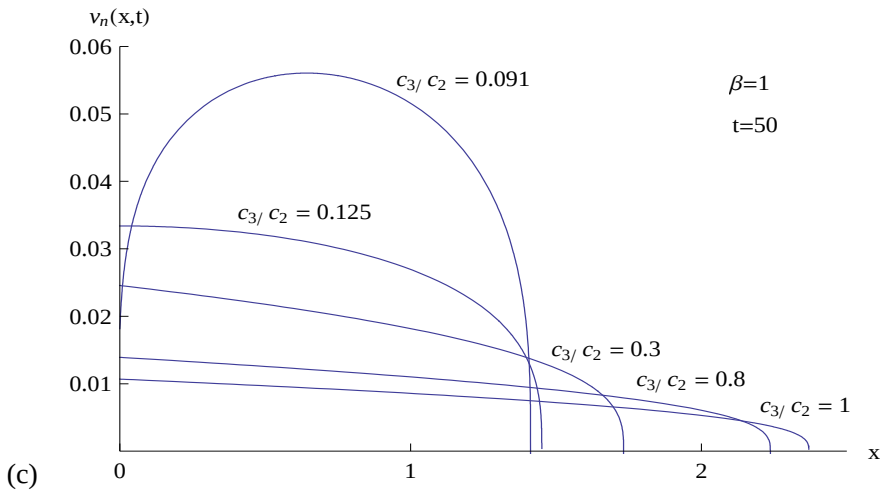
Figure 4.9.9: Graphs for $\beta = 0$ and a selection of values of $\frac{c_3}{c_2}$: (a) Fracture length $L(t)$ plotted against time ; (b) Fracture half-width $h(x,t)$ plotted against x at time $t = 50$. The leak-off velocity $v_n(x,t) = 0$



(a)

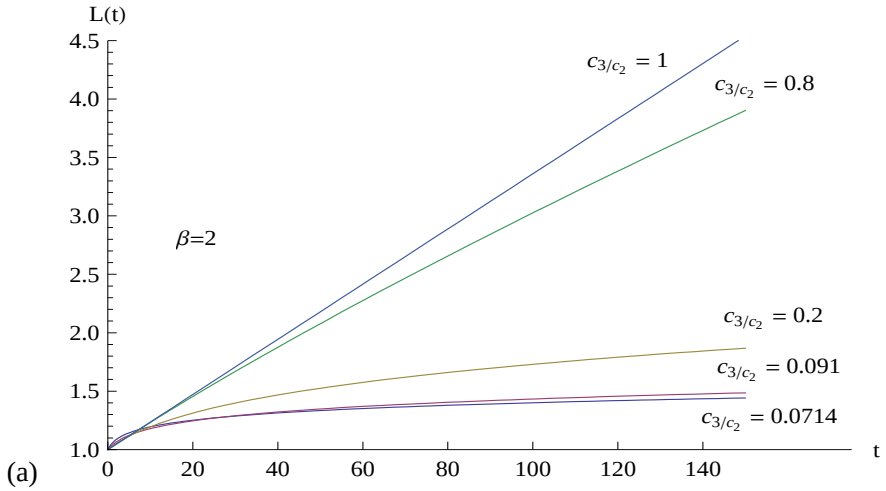


(b)

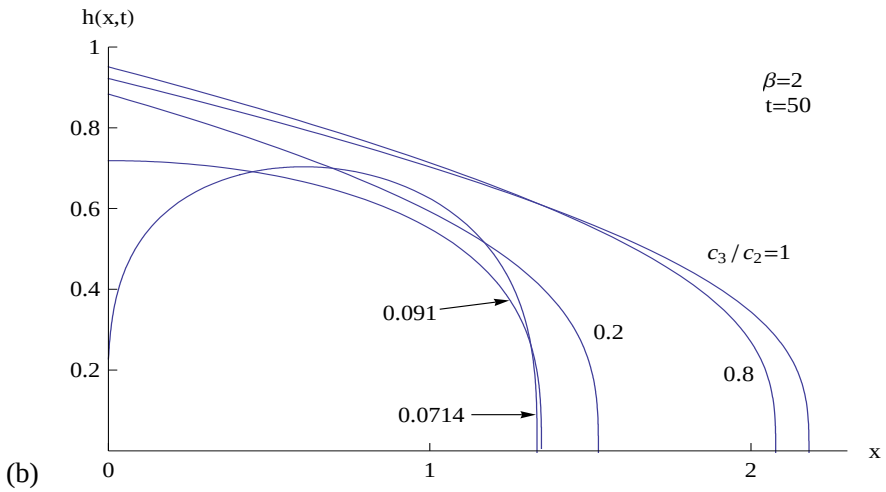


(c)

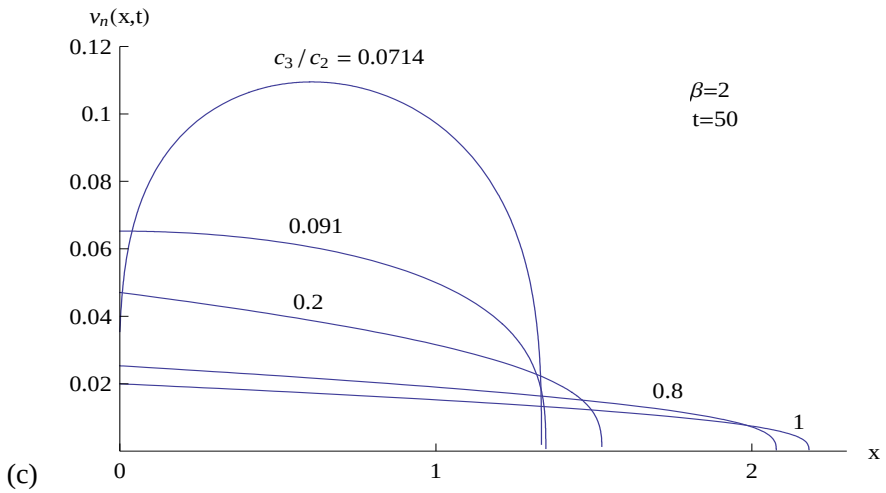
Figure 4.9.10: Graphs for $\beta = 1$ and a selection of values of $\frac{c_3}{c_2}$: (a) Fracture length $L(t)$ plotted against time; (b) Fracture half-width $h(x,t)$ plotted against x at time $t = 50$; (c) Leak-off fluid velocity $v_n(x,t)$ plotted against x at time $t = 50$.



(a)

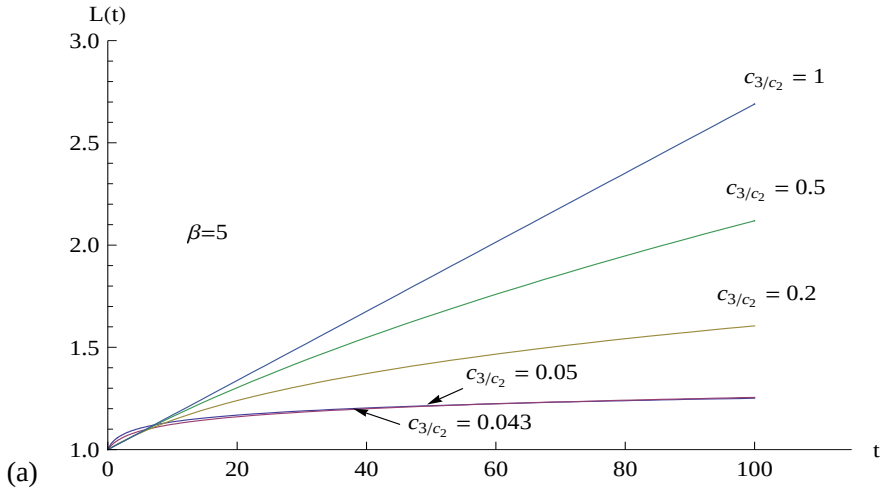


(b)

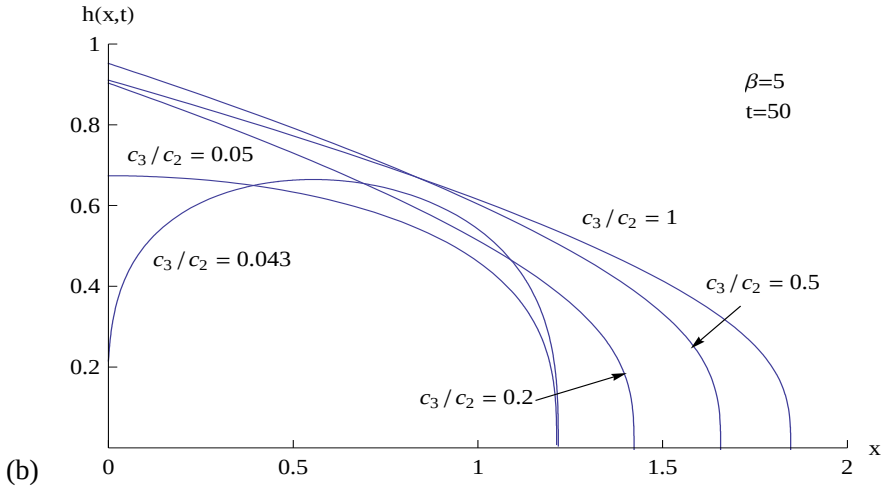


(c)

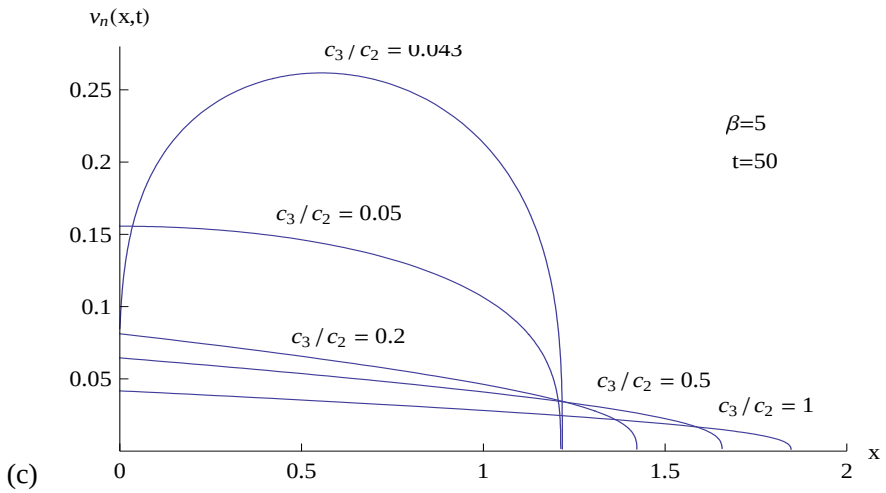
Figure 4.9.11: Graphs for $\beta = 2$ and a selection of values of $\frac{c_3}{c_2}$: (a) Fracture length $L(t)$ plotted against time; (b) Fracture half-width $h(x,t)$ plotted against x at time $t = 50$; (c) Leak-off fluid velocity $v_n(x,t)$ plotted against x at time $t = 50$.



(a)



(b)



(c)

Figure 4.9.12: Graphs for $\beta = 5$ and a selection of values of $\frac{c_3}{c_2}$: (a) Fracture length $L(t)$ plotted against time; (b) Fracture half-width $h(x,t)$ plotted against x at time $t = 50$; (c) Leak-off fluid velocity $v_n(x,t)$ plotted against x at time $t = 50$.

4.10 Conclusion

We have presented solutions to the fluid-driven fracture problem for the case in which the rock permeability is such that the velocity of fluid leak-off is proportional to the half-width of the fracture. The solutions contain the parameters $\frac{c_3}{c_2}$ and β. The leak-off parameter β determines the condition of flow at the fluid/rock interface. When $\beta > 0$, fluid leaks off into the rock mass at the interface and when $\beta < 0$, there is backward flow into the fracture at the interface. This may occur when the rock mass is saturated with fluid. For $\beta = 0$, there is no fluid exchange at the interface and the rock is impermeable.

Numerical and analytical solutions were found for the volume of the fracture, $V(t)$, fracture length, $L(t)$, fracture half-width, $h(x,t)$, leak-off velocity, $v_n(x,t)$ and the fluid presssure $p(x,t)$ for values of $\frac{c_3}{c_2}$ and β of physical significance in the range $-\infty < \frac{c_3}{c_2} < \infty$ and $-2.66 < \beta < \infty$. In the limit $\frac{c_3}{c_2} \to \infty$, time dependent exponential solutions were derived for $V(t)$, $L(t)$, $h(x,t)$, $v_n(x,t)$ and $p(x,t)$. For large times, approximate power law solutions can also be derived.

Three categories of solution were obtained that depend on the values of the parameters. The curve

$$\beta = \frac{5\left(\frac{1}{5} - \frac{c_3}{c_2}\right)}{3\frac{c_3}{c_2}} \tag{4.10.1}$$

partitions the $(\frac{c_3}{c_2}, \beta)$ plane into two parts. For values of $(\frac{c_3}{c_2}, \beta)$ above the curve (4.10.1), the rate of fluid injection into the fracture at the fracture entry is always positive. This could describe the process of hydraulic fracturing. Analytical group invariant solutions were obtained for the operating condition

$$\beta = \frac{\left(1 - \frac{c_3}{c_2}\right)}{3\frac{c_3}{c_2}} \tag{4.10.2}$$

in which fluid is always injected at the entry. For the values of $(\frac{c_3}{c_2}, \beta)$ below the curve (4.10.1), the rate of fluid injection is negative and fluid is always extracted from the fracture at the entry. The lower limit curve for solutions is

$$\beta = \frac{8\left(\frac{1}{8} - \frac{c_3}{c_2}\right)}{3\frac{c_3}{c_2}}. \tag{4.10.3}$$

An analytical proof of the curve (4.10.3) could not be established and its physical significance

could not be determined. Solutions with parameters in the range

$$\frac{8\left(\frac{1}{8}-\frac{c_3}{c_2}\right)}{3\frac{c_3}{c_2}} < \beta < \frac{5\left(\frac{1}{5}-\frac{c_3}{c_2}\right)}{3\frac{c_3}{c_2}} \tag{4.10.4}$$

could describe the process of extraction of fluid from a fracture in a permeable rock. Group invariant solutions and numerical solutions were obtained for this case. For the values of $(\frac{c_3}{c_2}, \beta)$ on the dividing curve (4.10.1), the rate of fluid injection at the entry, q_1, vanishes and we obtained analytical solutions for which there is no fluid injection or extraction at the entry. This could describe the evolution of a fluid-filled fracture, sealed at its entrance, in permeable rock.

The rate of fluid injection at the entry, q_1, is further controlled by the parameter $\frac{c_3}{c_2}$. For $\frac{c_3}{c_2} = 0.8$, q_1 is constant and fluid injection at the entry is constant. For $\frac{c_3}{c_2} < 0.8$, q_1 decreases as t increases and for $\frac{c_3}{c_2} > 0.8$, q_1 increases as t increases.

The graphical solutions in Sections 4.9.2 and 4.9.3 illustrate that the length of the fracture, $L(t)$, always increases even if there is leak-off of fluid at the interface and fluid extraction at the entry. Of interest is the behaviour that is observed when there is no fluid injection at the entry. The fracture relaxes to different final states depending on whether $\beta < 0$, $\beta = 0$ or $\beta > 0$. In particular, when $\beta \geq 0$ the fracture width will become narrower and the fracture length longer until the interface grips the propping material that holds the interface apart . Indeed, when $\beta > 0$, fluid will continue to leak off over the whole fracture area and particularly near the entry where $h(x,t)$ is maximum. This leak-off limits the additional length obtained when there is no fluid injection at the entry.

From Figures 4.9.2a to 4.9.6a, the speed of propagation $\frac{dL}{dt}$ increases as β decreases and its maximum value occurs always on the limiting solution curve. In fact fluid injection at the interface is always greatest and extraction of fluid at the fracture entry stongest for all values of β and $\frac{c_3}{c_2}$ on the limiting solution curve. When β is large and negative the maximum width of the fracture occurs at approximately the mid-point of the fracture. This is due to large negative values of β being associated with extraction of fluid at entry. This fluid extraction prevents the width of the fracture at the entry from increasing as much as at the mid-point. In all the solutions obtained, the graphs for the leak-off velocity, v_n, reflect that it is proportional to the fracture half-width, $h(x,t)$. From Figures 4.9.7a to 4.9.12a, the speed of propagation

of fracture length, $\frac{dL}{dt}$, increases as $\frac{c_3}{c_2}$ increases. Smaller values of $\frac{c_3}{c_2}$ are associated with extraction of fluid at the fracture entry while larger values are associated with injection of fluid at the entry. For all solutions obtained, the gradient of the fracture half-width, $\frac{\partial h}{\partial x}$, tends to $-\infty$ as $x \to L(t)$. Hence, the thin film approximation breaks down in the neighbourhood of the tip of the fracture, $x = L(t)$.

Finally, to check the accuracy of the numerical solution, we solved the two Initial Value Problems numerically for the special cases (4.3.1) and (4.5.8) which yield exact analytical solutions. We found that the numerical solution is in good agreement with the analytical solutions as shown in Tables 4.8.1 and 4.8.2. The solutions agree to five decimal places except at the fracture tip. In Table 4.8.1 the solutions at the fracture tip agree to three decimal places while the agreement at the fracture tip in Table 4.8.2 is to two decimal places.

Chapter 5

LEAK-OFF VELOCITY PROPORTIONAL TO GRADIENT OF FRACTURE HALF-WIDTH

5.1 Introduction

In this Chapter we consider the second special case in which $G(u)$ is proportional to $\frac{dF}{du}$. The leak-off velocity is therefore proportional to the gradient of the fluid/rock interface. The resulting boundary value problem for $F(u)$ is solved analytically for two special cases which yield exact solutions. For the first special case which is considered in Section 5.3, the rate of fluid injection into the fracture at the fracture entry is zero while for the second special case which is considered in Section 5.4, there is always inflow of fluid at the fracture entry. Numerical computation is used to obtain results in general and this begins with the transformation of the boundary value problem into two Initial Value Problems using the invariance of the boundary value problem under a scaling transformation. The algorithm outlined in Chapter 4 for solving the two initial value problems also applies in this Chapter.

5.2 Leak-off velocity proportional to gradient of fluid-rock interface

We now consider the case

$$G(u) = -\beta u \frac{dF}{du}, \tag{5.2.1}$$

where β is a constant. It follows from the similarity solution (3.6.61), (3.6.62) and (3.6.63) that

$$v_n = -\beta \frac{c_3}{c_1} \frac{x\frac{\partial h}{\partial x}}{(1+\frac{c_2}{c_1}t)} = -\beta \frac{c_3}{c_1} \frac{x\frac{\partial h}{\partial x}}{L(t)^{\frac{c_2}{c_3}}}. \tag{5.2.2}$$

Hence, v_n is proportional to the gradient of the fracture half-width. The boundary value problem (3.6.55) to (3.6.64) becomes

$$\Lambda \frac{d}{du}\left(F^3 \frac{dF}{du}\right) + 3(1+\beta)\frac{d}{du}(uF) + \left(\frac{c_2}{c_3} - 5 - 3\beta\right) F = 0, \tag{5.2.3}$$

$$F(1) = 0, \tag{5.2.4}$$

$$\Lambda F^3(0)\frac{dF}{du}(0) = \left(\frac{c_2}{c_3} - 5 - 3\beta\right)\int_0^1 F(u)du, \tag{5.2.5}$$

$$V_0 = 2\left(\frac{c_3}{c_1}\right)^{\frac{1}{3}} \int_0^1 F(u)du, \tag{5.2.6}$$

$$\frac{c_2}{c_1} = \frac{c_2}{c_3}\frac{c_3}{c_1}, \tag{5.2.7}$$

$$V(t) = V_0\left(1+\frac{c_2}{c_1}t\right)^{\frac{5}{3}\frac{c_3}{c_2}-\frac{1}{3}}, \tag{5.2.8}$$

$$L(t) = \left(1+\frac{c_2}{c_1}t\right)^{\frac{c_3}{c_2}}, \tag{5.2.9}$$

$$h(x,t) = \left(\frac{c_3}{c_1}\right)^{\frac{1}{3}}\left(1+\frac{c_2}{c_1}t\right)^{\frac{2}{3}\frac{c_3}{c_2}-\frac{1}{3}} F(u), \tag{5.2.10}$$

$$v_n(x,t) = -\beta\left(\frac{c_3}{c_1}\right)^{\frac{4}{3}}\left(1+\frac{c_2}{c_1}t\right)^{\frac{2}{3}\frac{c_3}{c_2}-\frac{4}{3}} u\frac{dF}{du}, \tag{5.2.11}$$

$$p(x,t) = \Lambda h(x,t), \tag{5.2.12}$$

where

$$u = \frac{x}{L(t)}, \qquad 0 \le u \le 1. \tag{5.2.13}$$

When $\frac{dF}{du} < 0$, $\beta > 0$ describes leak-off while $\beta < 0$ describes inflow at the fluid/rock interface. For the case $\frac{dF}{du} > 0$, $\beta > 0$ describes inflow at the fluid/rock interface while $\beta < 0$ describes leak-off. When $\frac{dF}{du} = 0$, there is no leak-off even for non-zero values of β.

We now seek to determine the asymptotic solution of the differential equation (5.2.3) subject to the boundary condition (5.2.4) as $u \to 1$. This asymptotic solution is required when deriving the numerical solution for $F(u)$. Look for an asymptotic solution of the form

$$F(u) \sim a(\eta - u)^n \qquad \text{as} \qquad u \to 1, \tag{5.2.14}$$

where a, η and n are constants to be determined. The boundary condition (5.2.4) gives $\eta = 1$ and therefore (5.2.14) becomes

$$F(u) \sim a(1 - u)^n \qquad \text{as} \qquad u \to 1. \tag{5.2.15}$$

We substitute (5.2.15) into (5.2.3) to obtain

$$\Lambda a^4 n(4n-1)(1-u)^{4n-2} - 3an(1+\beta)(1-u)^{n-1} + \left(\frac{c_2}{c_3} - 2 + 3n(1+\beta)\right) a(1-u)^n \sim 0, \tag{5.2.16}$$

as $u \to 1$. The dominant terms balance each other in (5.2.16) provided

$$4n - 2 = n - 1, \tag{5.2.17}$$

that is, provided

$$n = \frac{1}{3}. \tag{5.2.18}$$

Equation (5.2.16) becomes

$$\frac{\Lambda}{9}a^4 - (1+\beta)a + \left(\frac{c_2}{c_3} - 1 + \beta\right) a(1-u) \sim 0 \quad \text{as} \quad u \to 1. \tag{5.2.19}$$

Let $u \to 1$ in (5.2.19). This gives

$$a = \left(\frac{9(1+\beta)}{\Lambda}\right)^{\frac{1}{3}}. \tag{5.2.20}$$

Hence, the asymptotic solution is

$$F(u) \sim \left(\frac{9(1+\beta)}{\Lambda}\right)^{\frac{1}{3}} (1-u)^{\frac{1}{3}} \quad \text{as} \quad u \to 1. \tag{5.2.21}$$

Equation (5.2.21) is satisfied for all values of $\frac{c_2}{c_3}$ but requires $\beta > -1$. This compares with the asymptotic solution for $F(u)$ as $u \to 1$ when $G(u) = \beta F(u)$ in Chapter 4 which placed no condition on β.

In order to interpret the results we will require the rate of fluid injection into the fracture at the fracture entry, q_1, given by (3.7.27) and the rate of leak-off at the fluid/rock interface, q_2, which is given by (3.7.24). Using (5.2.1), equations (3.7.27) and (3.7.24) become

$$q_1 = \frac{2}{3}\left(\frac{c_3}{c_1}\right)^{\frac{4}{3}}\left(1+\frac{c_2}{c_1}t\right)^{\frac{5}{3}\frac{c_3}{c_2}-\frac{4}{3}}\left[-3\beta\int_0^1 u\frac{dF}{du}du + \left(5-\frac{c_2}{c_3}\right)\int_0^1 F(u)du\right], \quad (5.2.22)$$

$$q_2 = -2\beta\left(\frac{c_3}{c_1}\right)^{\frac{4}{3}}\left(1+\frac{c_2}{c_1}t\right)^{\frac{5}{3}\frac{c_3}{c_2}-\frac{4}{3}}\int_0^1 u\frac{dF}{du}du. \quad (5.2.23)$$

But, integrating by parts and using the boundary condition $F(1) = 0$ gives

$$\int_0^1 u\frac{dF}{du}(u)du = -\int_0^1 F(u)du. \quad (5.2.24)$$

Equations (5.2.22) and (5.2.23) become

$$q_1 = -\frac{2}{3}\left(\frac{c_2}{c_3}-5-3\beta\right)\left(\frac{c_3}{c_1}\right)^{\frac{4}{3}}\left(1+\frac{c_2}{c_1}t\right)^{\frac{5}{3}\frac{c_3}{c_2}-\frac{4}{3}}\int_0^1 F(u)du \quad (5.2.25)$$

and

$$q_2 = 2\beta\left(\frac{c_3}{c_1}\right)^{\frac{4}{3}}\left(1+\frac{c_2}{c_1}t\right)^{\frac{5}{3}\frac{c_3}{c_2}-\frac{4}{3}}\int_0^1 F(u)du. \quad (5.2.26)$$

We now consider two special cases for which an exact analytical solution of the differential equation (5.2.3) subject to boundary conditions (5.2.4) and (5.2.5) can be derived.

5.3 Exact analytical solutions: Case 1

We first consider the case

$$\frac{c_2}{c_3} - 5 - 3\beta = 0. \quad (5.3.1)$$

Equation (5.2.3) becomes

$$\Lambda\frac{d}{du}\left(F^3\frac{dF}{du}\right) + 3(1+\beta)\frac{d}{du}(uF) = 0, \quad (5.3.2)$$

subject to the boundary conditions

$$F(1) = 0, \tag{5.3.3}$$

$$\frac{dF}{du}(0) = 0. \tag{5.3.4}$$

In boundary condition (5.2.5), $F(0) \neq 0$ because if $F(0) = 0$ then from (5.2.10), $h(0,t) = 0$ which is not satisfied. Integrating (5.3.2) once with respect to u gives

$$\Lambda F^3(u)\frac{dF}{du} + 3(1+\beta)uF(u) = C \tag{5.3.5}$$

where C is a constant. Imposing the boundary condition (5.3.4) at $u = 0$ gives $C = 0$. Equation (5.3.5) becomes

$$F^2\frac{dF}{du} = -3\frac{(1+\beta)}{\Lambda}u, \tag{5.3.6}$$

which is variables separable. Thus

$$F^3(u) = -\frac{9(1+\beta)}{2\Lambda}u^2 + K, \tag{5.3.7}$$

where K is a constant. Since $F(1) = 0$ it follows that

$$K = \frac{9(1+\beta)}{2\Lambda} \tag{5.3.8}$$

and therefore

$$F(u) = \left(\frac{9(1+\beta)}{2\Lambda}\right)^{\frac{1}{3}}(1-u^2)^{\frac{1}{3}}, \tag{5.3.9}$$

provided $\beta > -1$. Using (5.3.1), the solution (5.3.9) can be written as

$$F(u) = \left(\frac{3}{2\Lambda}\left(\frac{c_2}{c_3} - 2\right)\right)^{\frac{1}{3}}\left(1-u^2\right)^{\frac{1}{3}}, \tag{5.3.10}$$

where $\frac{c_2}{c_3} > 2$ for a non-zero real solution to exist. When (5.3.1) is satisfied the solution exists provided $\beta > -1$ or $0 < \frac{c_3}{c_2} < 0.5$. This compares with the corresponding solution (4.3.9) when $G(u) = \beta F(u)$ which requires only that β and $\frac{c_3}{c_2}$ satisfy (5.3.1). Substituting (5.3.10) into (5.2.6) gives

$$\frac{c_3}{c_1} = \frac{\Lambda}{12\left(\frac{c_2}{c_3} - 2\right)}\left(\frac{V_0}{I}\right)^3, \tag{5.3.11}$$

where

$$I = \int_0^1 (1-u^2)^{\frac{1}{3}} du = 0.8413. \tag{5.3.12}$$

Thus from (5.2.7),

$$\frac{c_2}{c_1} = \frac{\Lambda}{24\left(\frac{1}{2} - \frac{c_3}{c_2}\right)} \left(\frac{V_0}{I}\right)^3 \tag{5.3.13}$$

and

$$u = \frac{x}{L(t)}. \tag{5.3.14}$$

The group invariant solution can be written either in terms of β or $\frac{c_3}{c_2}$. We will write the solution in terms of $\frac{c_3}{c_2}$. From (5.2.8) to (5.2.12),

$$V(t) = V_0 \left[1 + \frac{1}{24\left(\frac{1}{2} - \frac{c_3}{c_2}\right)} \left(\frac{V_0}{I}\right)^3 \Lambda t\right]^{\frac{5}{3}\left(\frac{c_3}{c_2} - \frac{1}{5}\right)}, \tag{5.3.15}$$

$$L(t) = \left[1 + \frac{1}{24\left(\frac{1}{2} - \frac{c_3}{c_2}\right)} \left(\frac{V_0}{I}\right)^3 \Lambda t\right]^{\frac{c_3}{c_2}}, \tag{5.3.16}$$

$$h(x,t) = \frac{V_0}{2I} \left[1 + \frac{1}{24\left(\frac{1}{2} - \frac{c_3}{c_2}\right)} \left(\frac{V_0}{I}\right)^3 \Lambda t\right]^{\frac{2}{3}\left(\frac{c_3}{c_2} - \frac{1}{2}\right)} \left[1 - \frac{x^2}{L(t)^2}\right]^{\frac{1}{3}}, \tag{5.3.17}$$

$$v_n(x,t) = \frac{10\Lambda}{27} \left(\frac{\frac{1}{5} - \frac{c_3}{c_2}}{\frac{1}{2} - \frac{c_3}{c_2}}\right) \left(\frac{V_0}{2I}\right)^4 \left[1 + \frac{1}{24\left(\frac{1}{2} - \frac{c_3}{c_2}\right)} \left(\frac{V_0}{I}\right)^3 \Lambda t\right]^{-\frac{4}{3}\left(\frac{c_3}{c_2} + 1\right)} \times x^2 \left(1 - \frac{x^2}{L(t)^2}\right)^{-\frac{2}{3}}, \tag{5.3.18}$$

$$p(x,t) = \Lambda h(x,t). \tag{5.3.19}$$

The solutions exist provided

$$0 < \frac{c_3}{c_2} < 0.5. \tag{5.3.20}$$

The results for $h(x,t)$, $v_n(x,t)$ and $p(x,t)$ can be expressed in terms of $L(t)$ as follows

$$h(x,t) = \frac{V_0}{2I} L(t)^{\frac{1}{3}\left(2 - \frac{c_2}{c_3}\right)} \left[1 - \frac{x^2}{L(t)^2}\right]^{\frac{1}{3}}, \tag{5.3.21}$$

$$v_n(x,t) = \frac{10\Lambda}{27} \left(\frac{\frac{1}{5} - \frac{c_3}{c_2}}{\frac{1}{2} - \frac{c_3}{c_2}}\right) \left(\frac{V_0}{2I}\right)^4 L(t)^{-\frac{4}{3}\left(\frac{c_2}{c_3} + 1\right)} x^2 \left[1 - \frac{x^2}{L(t)^2}\right]^{-\frac{2}{3}} \tag{5.3.22}$$

and $p(x,t)$ is given in terms of $h(x,t)$ by (5.3.19).

Consider now the physical significance of condition (5.3.1) when

$$G(u) = -\beta u \frac{dF}{du}. \tag{5.3.23}$$

From (5.2.22), when (5.3.1) is satisfied, $q_1 = 0$. Thus the rate of fluid injection into the fracture at the fracture entry is zero. Condition (5.3.1) therefore has the same physical significance as when $G(u) = \beta F(u)$. Figures 5.3.2 to 5.3.8 illustrate how a fracture of length $L(t)$ may relax after pumping at the entry has ceased and the entry to the fracture is sealed.

Condition (5.3.1) can be written as

$$\beta = \frac{\frac{5}{3}\left(\frac{1}{5} - \frac{c_3}{c_2}\right)}{\frac{c_3}{c_2}} \tag{5.3.24}$$

and also as

$$\frac{c_3}{c_2} = \frac{1}{5 + 3\beta}. \tag{5.3.25}$$

Equation (5.3.24) is plotted in the $\left(\frac{c_3}{c_2}, \beta\right)$ plane in Figure 5.3.1 together with other curves. Since the solution exists only for $\beta > -1$, it exists only for $0 < \frac{c_3}{c_2} < 0.5$. Unlike the special case $G(u) = \beta F(u)$, there is no solution for $\frac{c_3}{c_2} > 0.5$. Also the solutions for $L(t)$, $h(x,t)$ and $v_n(x,t)$ do not behave exponentially in time as $\frac{c_3}{c_2} \to \infty$ which compares with the exponential behaviour of the solutions for the special case $G(u) = \beta F(u)$ as $\frac{c_3}{c_2} \to \infty$. In the numerical results that follow, t is as defined in (4.4.9).

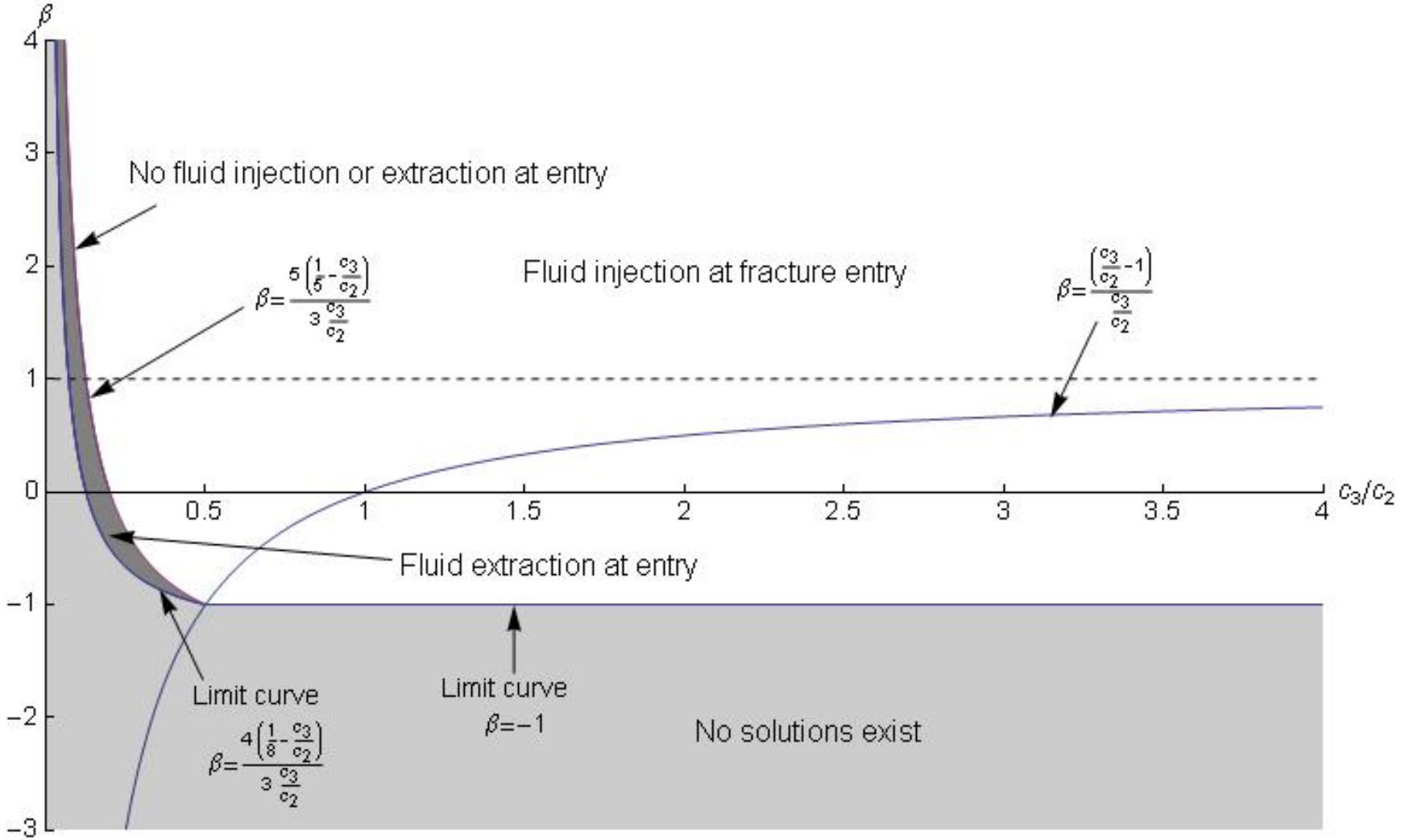


Figure 5.3.1: Curves for the analytical solutions and the limiting curve.

5.3.1 Fracture length and volume

Consider first the fracture length $L(t)$ given by (5.3.16) and plotted in Figure 5.3.2. We restrict our discussion to values of $\frac{c_3}{c_2}$ in the range $0 < \frac{c_3}{c_2} < 0.5$ for which the solution exists. For $0 < \frac{c_3}{c_2} < 0.2$, $0 < \beta < \infty$ and there is fluid leak-off at the interface. When $\frac{c_3}{c_2} = 0.2$, $\beta = 0$ and there is no fluid exchange at the interface. For $0.2 < \frac{c_3}{c_2} < 0.5$, $-1 < \beta < 0$ and fluid enters the fracture from the interface. The fracture length $L(t)$ is an increasing function of time for values of $\frac{c_3}{c_2}$ in the range $0 < \frac{c_3}{c_2} < 0.5$ and $L(t) \to \infty$ as $t \to \infty$. Even although the rate of fluid injection at the entry is zero, the fracture length grows for $0 < \frac{c_3}{c_2} < 0.5$. The length $L(t)$ increases as $\frac{c_3}{c_2}$ increases from 0 to 0.5 and $L(t) \to \infty$ as $\frac{c_3}{c_2} \to 0.5$ which is the limiting value of $\frac{c_3}{c_2}$ for solutions to exist.

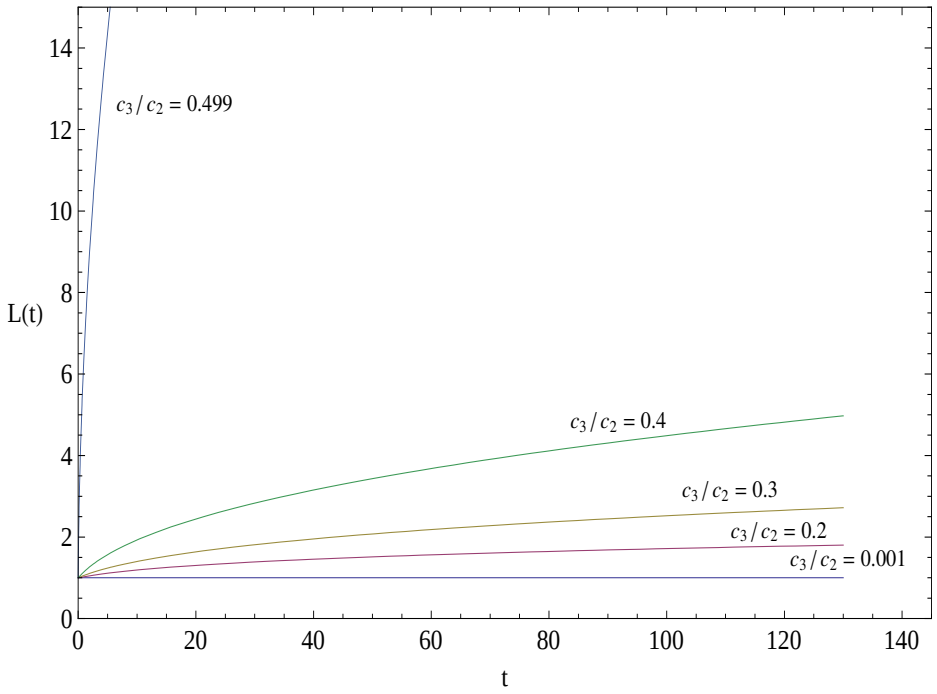


Figure 5.3.2: Leak-off velocity proportional to gradient of fracture half-width: Graph of fracture length $L(t)$ given by (5.3.16) plotted against t for a selection of values of the parameter $\frac{c_3}{c_2}$ and for $\frac{V_0}{I} = 1$.

Consider next the total volume of the fracture given by (5.3.15) and plotted in Figure 5.3.3. Since the fluid injection rate at the entry is zero, the fracture volume, $V(t)$, therefore changes

due to exchange of fluid at the fluid/rock interface. For $0 < \frac{c_3}{c_2} < 0.2$, $\beta > 0$ and there is leak-off at the fluid/rock interface. The time rate of change of fracture volume, $\frac{dV}{dt} < 0$ and $V(t) \to 0$ as $t \to \infty$. For $\frac{c_3}{c_2} = 0.2$, no fluid exchange occurs at the interface and $V(t)$ is constant for all time. Fluid enters the interface for $0.2 < \frac{c_3}{c_2} < 0.5$ and the fracture volume increases as t increases. Therefore $\frac{dV}{dt} > 0$ and $V(t) \to \infty$ as $t \to \infty$.

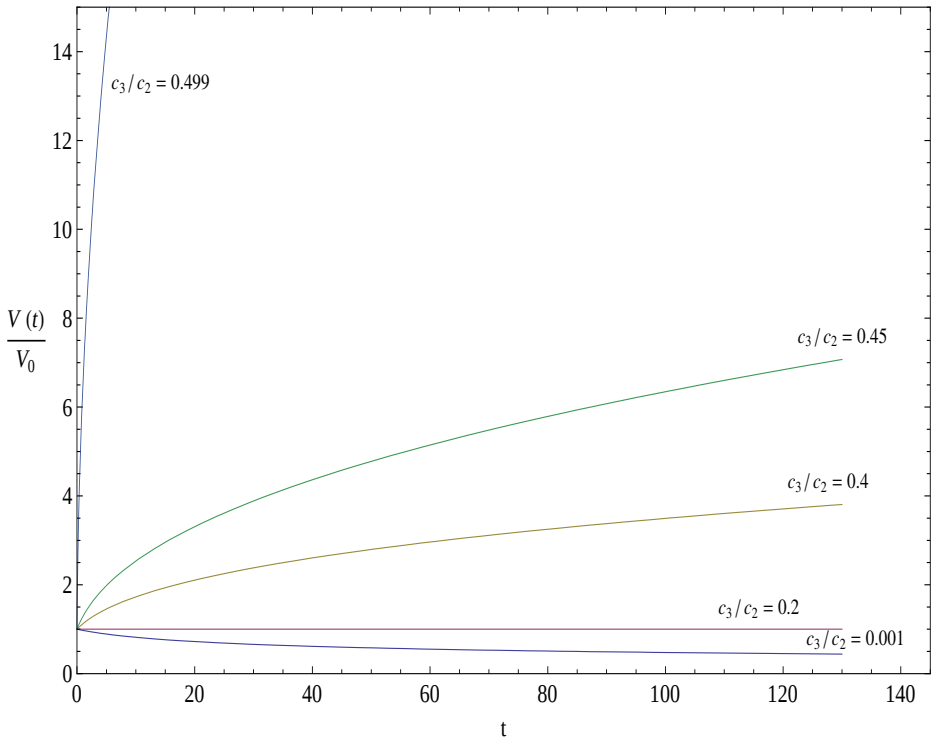


Figure 5.3.3: Leak-off velocity proportional to gradient of fracture half-width: Graph of fracture volume $\frac{V(t)}{V_0}$ given by (5.3.15) plotted against t for a selection of values of the parameter $\frac{c_3}{c_2}$ and for $\frac{V_0}{I} = 1$.

5.3.2 Fracture half-width and leak-off velocity

Consider now $h(x,t)$ which is given by (5.3.17) and plotted in Figures 5.3.4 to 5.3.8. For all Figures 5.3.4 to 5.3.8 there is no fluid injection at the fracture entry. Fluid can therefore only enter or leave the fracture at the fluid/rock interface. Figures (5.3.4) and (5.3.5) clearly show that the length of the fracture increases even if there is leak-off at the fluid/rock interface or if the rock is impermeable. When there is injection of fluid at the fluid/rock interface, Figures

(5.3.6) to (5.3.8) show that the rate of increase in the length of the fracture increases as the rate of fluid injection at interface increases and tends to infinity as $\frac{c_3}{c_2} \to 0.5$. Most of the fluid injection occurs in the neighbourhood of the fracture tip.

From (5.3.17),

$$h(0,t) = \frac{V_0}{2I}\left[1 + \frac{\Lambda t}{24\left(\frac{1}{2} - \frac{c_3}{c_2}\right)}\left(\frac{V_0}{I}\right)^3\right]^{\frac{2}{3}\left(\frac{c_3}{c_2} - \frac{1}{2}\right)}. \tag{5.3.26}$$

In this section, the analytical solution exists only for $0 < \frac{c_3}{c_2} < 0.5$ and therefore $h(0,t)$ always decreases as t increases and the width of the fracture at the entry decreases as t increases. The gradient of the fracture half-width is

$$\frac{\partial h}{\partial x}(x,t) = -\frac{V_0 x}{3I}\left[1 + \frac{\Lambda t}{24\left(\frac{1}{2} - \frac{c_3}{c_2}\right)}\left(\frac{V_0}{I}\right)^3\right]^{-\frac{4}{3}\left(\frac{c_3}{c_2} + \frac{1}{4}\right)}\left(1 - \frac{x^2}{L^2}\right)^{-\frac{2}{3}}. \tag{5.3.27}$$

Therefore $\frac{\partial h}{\partial x} \to -\infty$ as $x \to L(t)$. Lubrication theory breaks down in the neighbourhood of the tip of the fracture, $x = L(t)$.

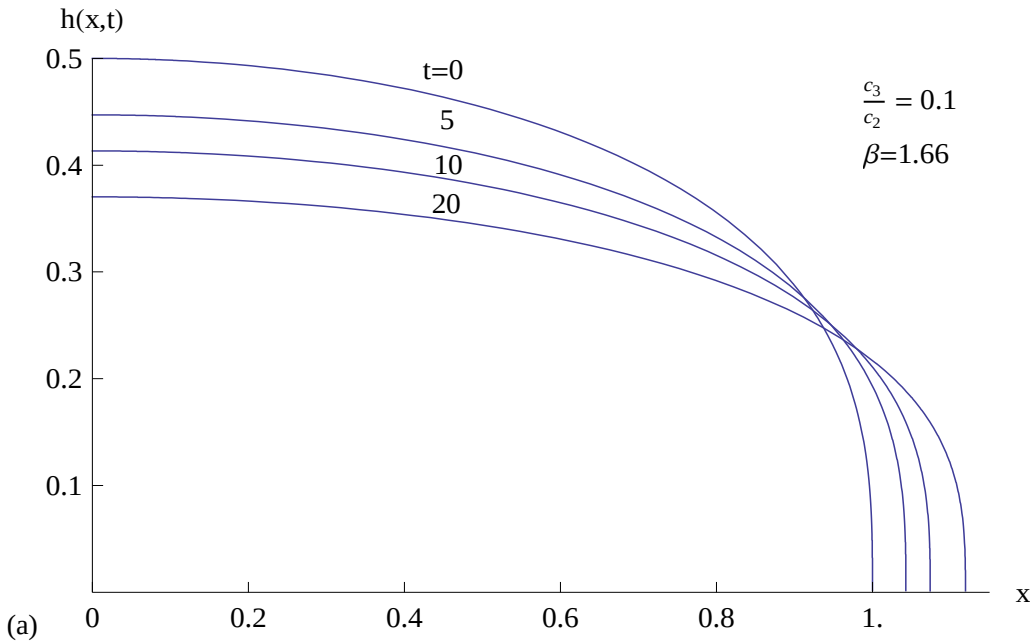
Finally, consider $v_n(x,t)$ which is given by (5.3.18) and is plotted in Figures 5.3.4 to 5.3.8. From (5.3.18),

$$v_n(0,t) = 0, \tag{5.3.28}$$

and

$$v_n(L,t) = \begin{cases} +\infty, & 0 < \frac{c_3}{c_2} < 0.2, \\ -\infty, & 0.2 < \frac{c_3}{c_2} < 0.5. \end{cases} \tag{5.3.29}$$

For all values, $0 < \frac{c_3}{c_2} < 0.5$, $v_n(x,t)$ is approximately zero at the interface in the neighbourhood of the fracture entry and $v_n = \pm\infty$ at the fracture tip depending on whether $\beta > 0$ or $\beta < 0$. For $0 < \frac{c_3}{c_2} < 0.2$, $\beta > 0$ and $v_n(x,t) > 0$. There is therefore fluid leak-off in the region $0 < x \leq L(t)$. When $0.2 < \frac{c_3}{c_2} < 0.5$, $\beta < 0$ and $v_n(x,t) < 0$. Fluid injection at the fluid/rock interface takes place in the region $0 < x \leq L(t)$.



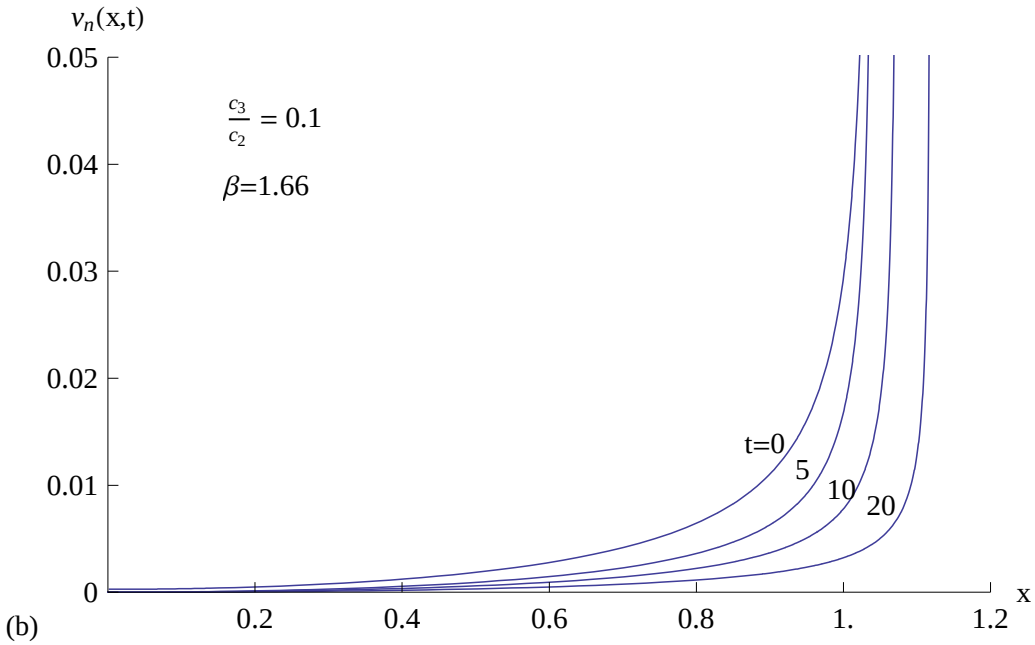


Figure 5.3.4: (a) Fracture half-width, $h(x,t)$, given by (5.3.17) and (b) leak-off velocity at the fluid/rock interface, $v_n(x,t)$, given by (5.3.18), plotted against x for a range of values of t and for $\frac{c_3}{c_2} = 0.1$, $\beta = 1.66$.

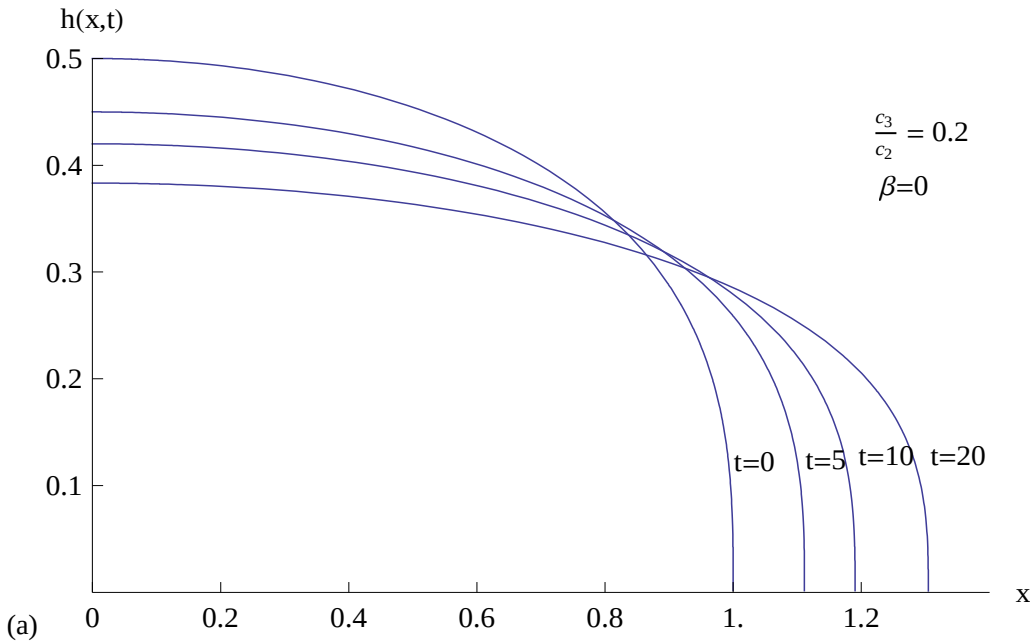


Figure 5.3.5: (a) Fracture half-width, $h(x,t)$, given by (5.3.17) plotted against x for a range of values of t and for $\frac{c_3}{c_2} = 0.2$, $\beta = 0$. The leak-off velocity at the fluid/rock interface, $v_n(x,t)$, given by (5.3.18) is zero.

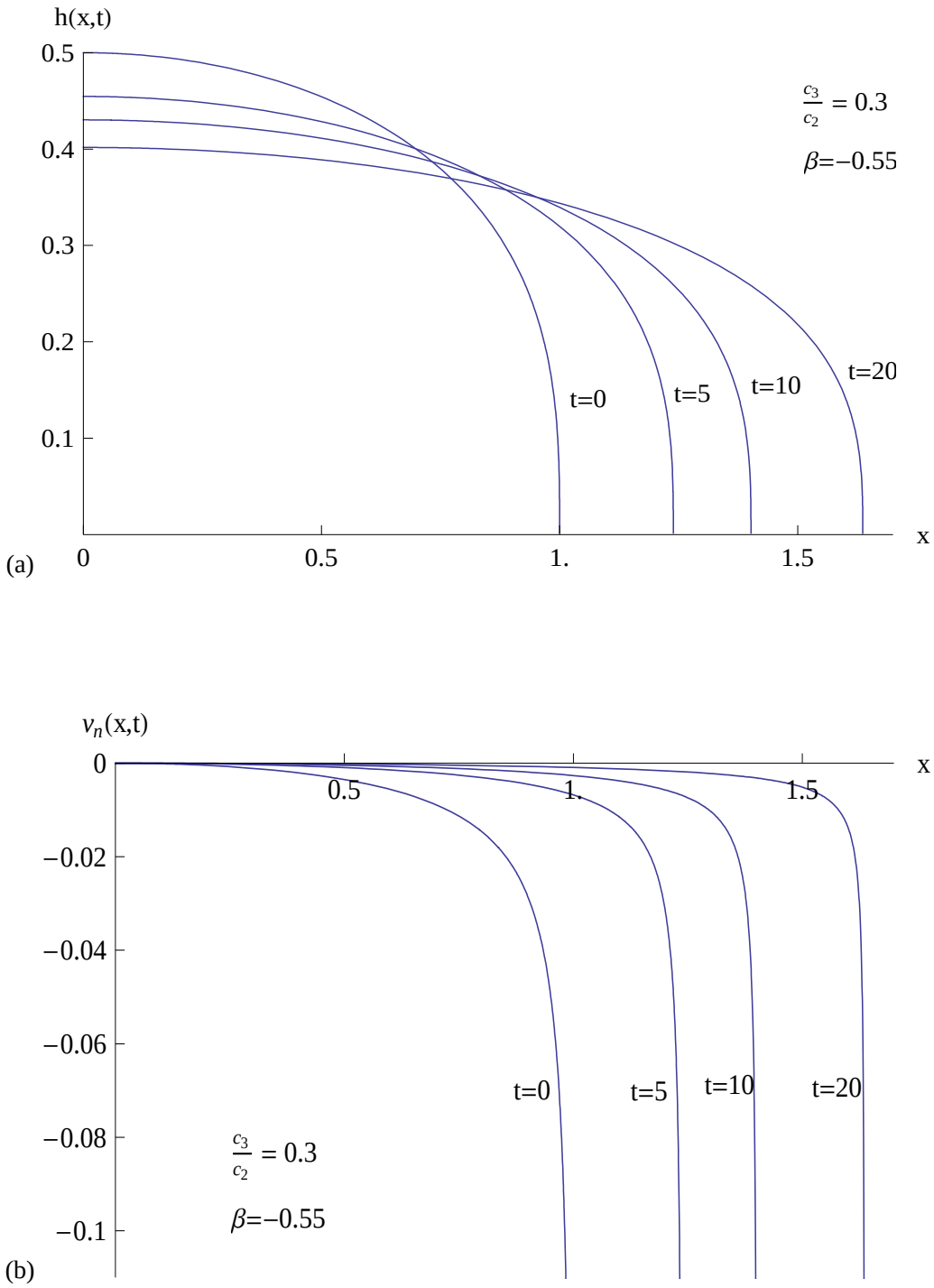
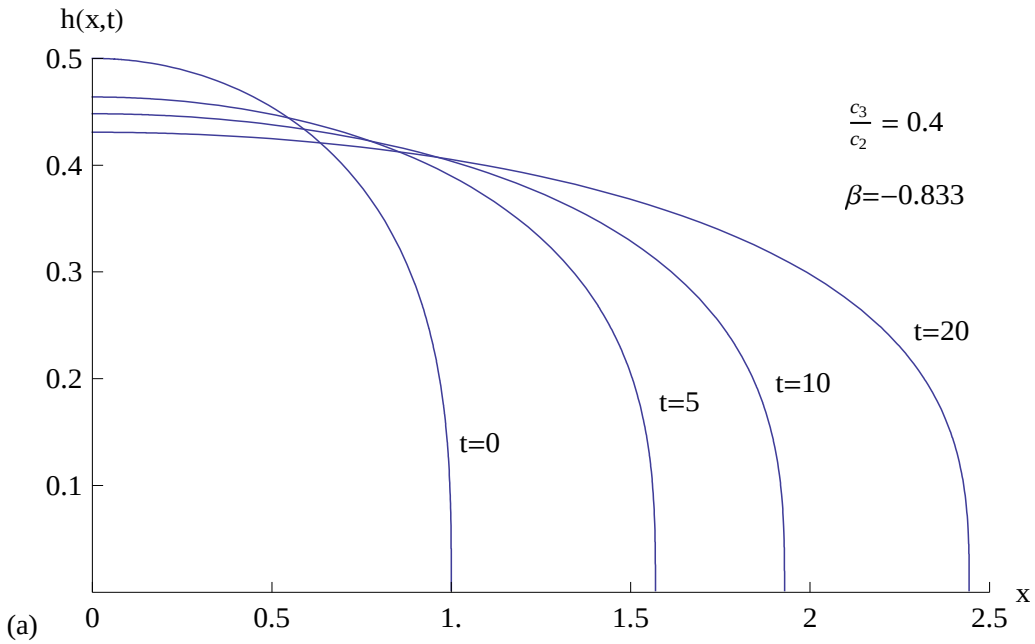


Figure 5.3.6: (a) Fracture half-width, $h(x,t)$, given by (5.3.17) and (b) leak-off velocity at the fluid/rock interface, $v_n(x,t)$, given by (5.3.18), plotted against x for a range of values of t and for $\frac{c_3}{c_2} = 0.3$, $\beta = -0.55$.



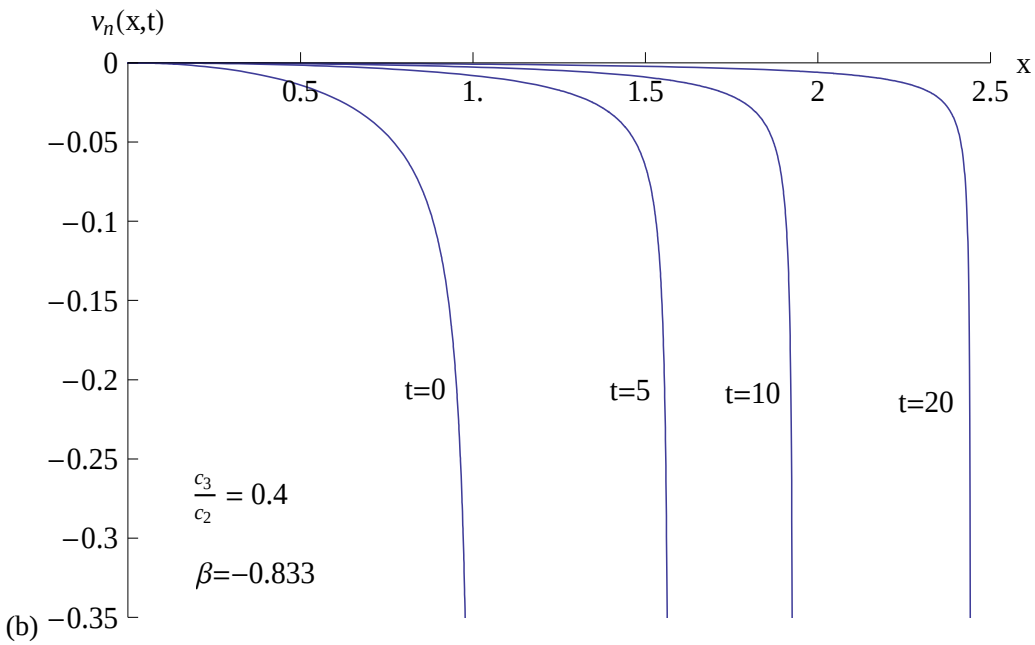


Figure 5.3.7: (a) Fracture half-width, $h(x,t)$, given by (5.3.17) and (b) leak-off velocity at the fluid/rock interface, $v_n(x,t)$, given by (5.3.18), plotted against x for a range of values of t and for $\frac{c_3}{c_2} = 0.4$, $\beta = -0.833$.

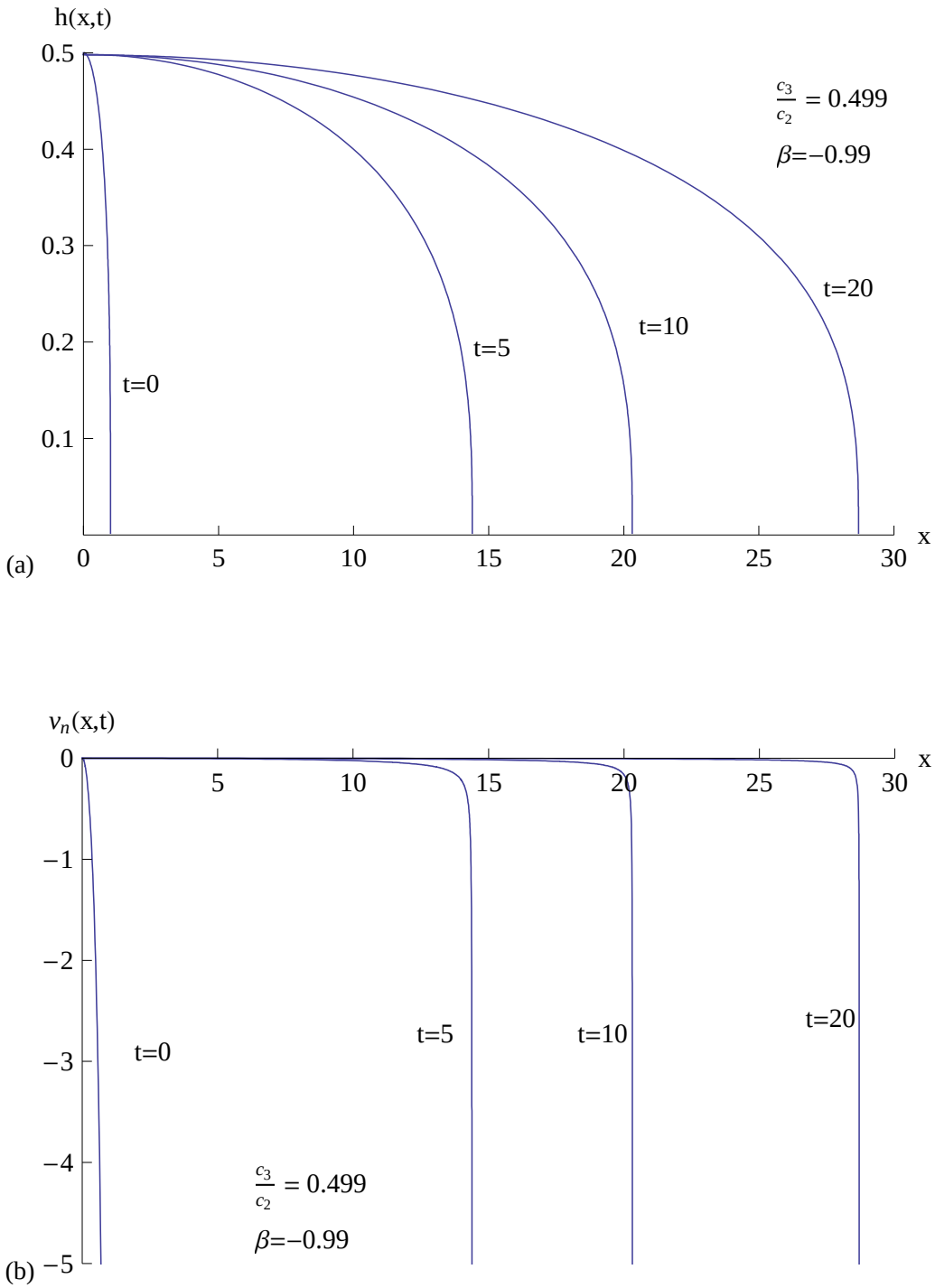


Figure 5.3.8: (a) Fracture half-width, $h(x,t)$, given by (5.3.17) and (b) leak-off velocity at the fluid/rock interface, $v_n(x,t)$, given by (5.3.18), plotted against x for a range of values of t and for $\frac{c_3}{c_2} = 0.499$, $\beta = -0.99$.

5.4 Exact analytical solutions: Case 2

We now look for a solution of (5.2.3) subject to (5.2.4) and (5.2.5) which is of the form

$$F(u) = a(1-u)^n, \tag{5.4.1}$$

where a and n are constants to be determined such that $a \neq 0$ and $n > 0$. The boundary condition (5.2.4) is satisfied by (5.4.1). We substitute (5.4.1) into (5.2.3) to obtain

$$\Lambda a^4 n(4n-1)(1-u)^{4n-2} - 3a(1+\beta)n(1-u)^{n-1} + a\left(3n(1+\beta) + \frac{c_2}{c_3} - 2\right)(1-u)^n = 0. \tag{5.4.2}$$

The equation (5.4.2) will be satisfied if

$$\Lambda a^4 n(4n-1)(1-u)^{4n-2} - 3a(1+\beta)n(1-u)^{n-1} = 0 \tag{5.4.3}$$

and

$$3n(1+\beta) + \frac{c_2}{c_3} - 2 = 0. \tag{5.4.4}$$

Equating the powers of $(1-u)$ in (5.4.3) gives

$$n = \frac{1}{3}. \tag{5.4.5}$$

By substituting (5.4.5) into (5.4.3) and (5.4.4) we obtain

$$\frac{\Lambda}{9}a^4 - a(1+\beta) = 0, \tag{5.4.6}$$

$$\beta = 1 - \frac{c_2}{c_3}. \tag{5.4.7}$$

Solving (5.4.6) for a gives

$$a = \left(\frac{9}{\Lambda}(1+\beta)\right)^{\frac{1}{3}}. \tag{5.4.8}$$

Hence, the solution of (5.2.3) of the form (5.4.1) is

$$F(u) = \left(\frac{9}{\Lambda}\left(2 - \frac{c_2}{c_3}\right)\right)^{\frac{1}{3}}(1-u)^{\frac{1}{3}}. \tag{5.4.9}$$

A non-zero real solution exists for $-\infty < \frac{c_2}{c_3} < 2$.

Equation (5.4.9) must satisfy the second boundary condition (5.2.5). We now show that the boundary condition (5.2.5) is identically satisfied. Substituting (5.4.9) into the left hand side of (5.2.5) gives

$$\Lambda F^3(0)\frac{dF}{du}(0) = -3\left(\frac{9}{\Lambda}\right)^{\frac{1}{3}}\left(2-\frac{c_2}{c_3}\right)^{\frac{4}{3}}, \tag{5.4.10}$$

while substituting (5.4.9) into the right hand side of (5.2.5) gives

$$\left(\frac{c_2}{c_3}-5-3\beta\right)\int_0^1 F(u)du = \frac{3}{4}\left(\frac{c_2}{c_3}-5-3\beta\right)\left(\frac{9}{\Lambda}\left(2-\frac{c_2}{c_3}\right)\right)^{\frac{1}{3}}. \tag{5.4.11}$$

On using (5.4.7) for β it is readily verified that the boundary condition (5.2.5) is satisfied.

By substituting (5.4.9) into (5.2.6) we obtain

$$\frac{c_3}{c_1} = \frac{8}{243}\frac{\Lambda V_0^3}{\left(2-\frac{c_2}{c_3}\right)} \tag{5.4.12}$$

and hence from (5.2.7),

$$\frac{c_2}{c_1} = \frac{4}{243}\frac{\Lambda V_0^3}{\left(\frac{c_3}{c_2}-\frac{1}{2}\right)}. \tag{5.4.13}$$

We will express the results in terms of the parameter $\frac{c_3}{c_2}$.

From (5.2.8) to (5.2.12),

$$L(t) = \left[1+\frac{4}{243}\frac{V_0^3}{\left(\frac{c_3}{c_2}-\frac{1}{2}\right)}\Lambda t\right]^{\frac{c_3}{c_2}}, \tag{5.4.14}$$

$$V(t) = V_0\left[1+\frac{4}{243}\frac{V_0^3}{\left(\frac{c_3}{c_2}-\frac{1}{2}\right)}\Lambda t\right]^{\frac{5}{3}\frac{c_3}{c_2}-\frac{1}{3}}, \tag{5.4.15}$$

$$h(x,t) = \frac{2}{3}V_0\left[1+\frac{4}{243}\frac{V_0^3}{\left(\frac{c_3}{c_2}-\frac{1}{2}\right)}\Lambda t\right]^{\frac{2}{3}\frac{c_3}{c_2}-\frac{1}{3}}\left(1-\frac{x}{L(t)}\right)^{\frac{1}{3}}, \tag{5.4.16}$$

$$v_n(x,t) = \frac{8\Lambda V_0}{2187}\left(\frac{\frac{c_3}{c_2}-1}{\frac{c_3}{c_2}-\frac{1}{2}}\right)\left[1+\frac{4}{243}\frac{V_0^3}{\left(\frac{c_3}{c_2}-\frac{1}{2}\right)}\Lambda t\right]^{-\frac{1}{3}\left(\frac{c_3}{c_2}+4\right)} \times x\left(1-\frac{x}{L(t)}\right)^{-\frac{2}{3}}, \tag{5.4.17}$$

$$p(x,t) = \Lambda h(x,t). \tag{5.4.18}$$

The solution exists provided the values of $\frac{c_3}{c_2}$ do not lie in the range $0 < \frac{c_3}{c_2} \leq 0.5$. This is shown in Figure 5.3.1. In the limit $\frac{c_3}{c_2} \to \infty$, $\beta \to 1$ and the group invariant solutions for $L(t)$, $V(t)$, $h(x,t)$ and $p(x,t)$ have an exponential time-dependence given by

$$L(t) = \exp\left(\frac{4V_0^3}{243}\Lambda t\right), \tag{5.4.19}$$

$$V(t) = V_0 \exp\left(\frac{20V_0^3}{729}\Lambda t\right), \tag{5.4.20}$$

$$h(x,t) = \frac{2V_0}{3}\exp\left(\frac{8V_0^3}{729}\Lambda t\right)\left[1 - \frac{x}{L(t)}\right]^{\frac{1}{3}}, \tag{5.4.21}$$

$$v_n(x,t) = \frac{8\Lambda V_0}{2187}\exp\left(\frac{-4V_0^3}{729}\Lambda t\right) x \left(1 - \frac{x}{L(t)}\right)^{-\frac{2}{3}} \tag{5.4.22}$$

and $p(x,t)$ is given by (5.4.18) and (5.4.21).

5.5 Discussion of results for $\beta = 1 - \frac{c_2}{c_3}$

When (5.4.7), (5.4.9), (5.4.12) and (5.4.13) are substituted into (5.2.25) and (5.2.26) it is found that the rate of fluid injection at the fracture entry is

$$q_1(t) = \frac{32}{729}\Lambda V_0^4\left[1 + \frac{4}{243}\frac{V_0^3}{\left(\frac{c_3}{c_2} - \frac{1}{2}\right)}\Lambda t\right]^{\frac{5}{3}\left(\frac{c_3}{c_2} - \frac{4}{5}\right)} \tag{5.5.1}$$

and the rate of fluid leak-off at the fluid/rock interface is

$$q_2(t) = \frac{4}{243}\left(\frac{\frac{c_3}{c_2} - 1}{\frac{c_3}{c_2} - \frac{1}{2}}\right)\Lambda V_0^4\left[1 + \frac{4}{243}\frac{V_0^3}{\left(\frac{c_3}{c_2} - \frac{1}{2}\right)}\Lambda t\right]^{\frac{5}{3}\left(\frac{c_3}{c_2} - \frac{4}{5}\right)}. \tag{5.5.2}$$

Therefore $q_1(t) > 0$ and fluid is always injected into the fracture at entry. The rate of fluid leak-off satisfies

$$q_2(t)\begin{cases} > 0 & \text{if} \quad \frac{c_3}{c_2} > 1 \\ < 0 & \text{if} \quad \frac{1}{2} < \frac{c_3}{c_2} < 1. \end{cases} \tag{5.5.3}$$

Equation (5.5.1) is plotted in Figure 5.5.1 and (5.5.2) is plotted in Figure 5.5.2. The rate of fluid injection at the fracture entry is always positive. The rate of fluid inflow at the fluid/rock

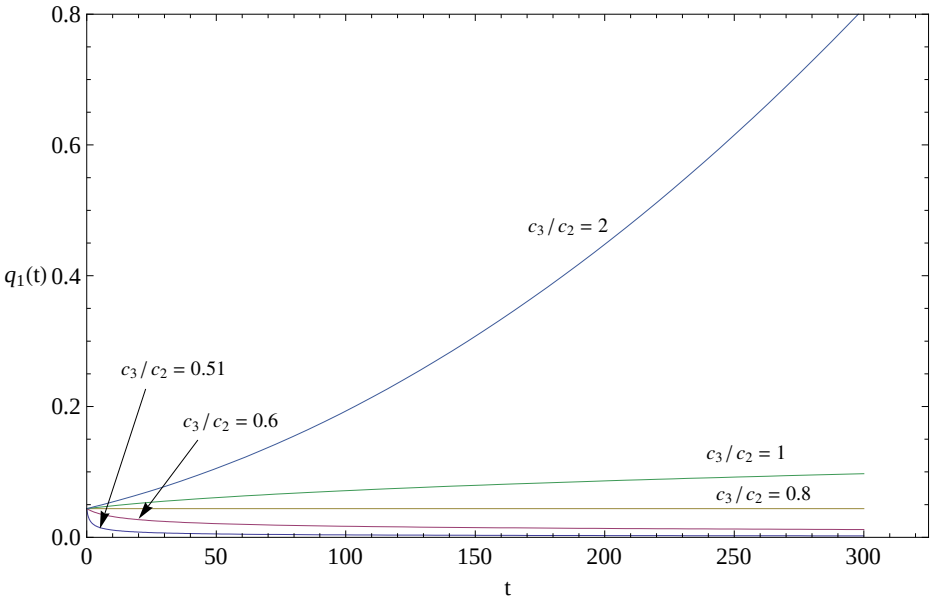


Figure 5.5.1: Leak-off velocity proportional to gradient of fracture half-width and $\beta = 1 - \frac{c_2}{c_3}$. Rate of fluid injection at entry, $q_1(t)$, given by (5.5.1) plotted against t for $\frac{c_3}{c_2} = 0.51, 0.6, 0.8, 1, 2$ and for $V_0 = 1$ and $\Lambda = 1$.

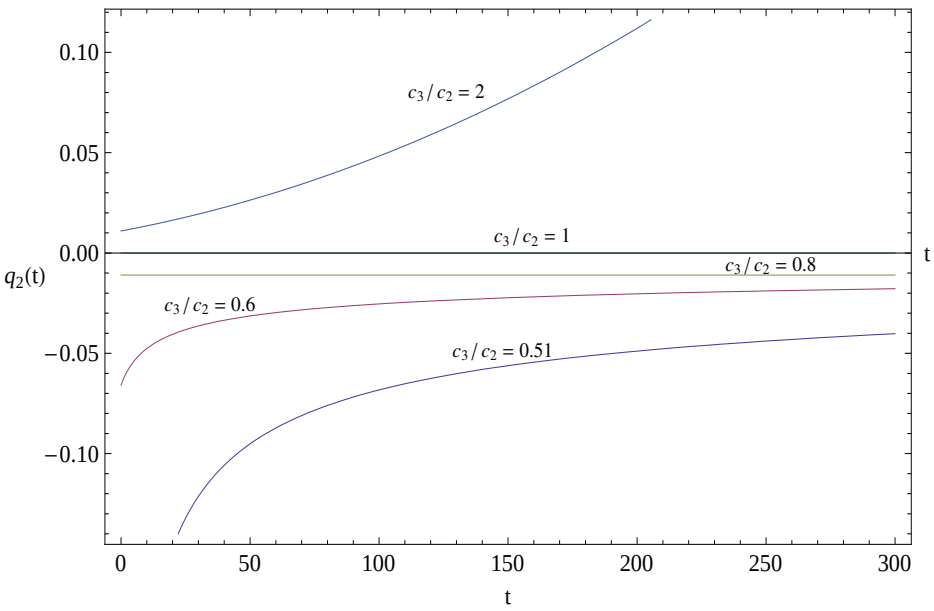


Figure 5.5.2: Leak-off velocity proportional to gradient of fracture half-width and $\beta = 1 - \frac{c_2}{c_3}$. Rate of fluid leak-off at fluid/rock interface, $q_2(t)$, given by (5.5.2) plotted against t for $\frac{c_3}{c_2} = 0.51, 0.6, 0.8, 1, 2$ and for $V_0 = 1$ and $\Lambda = 1$.

interface tends to negative infinity as $\frac{c_3}{c_2} \to \frac{1}{2}$ which is a point on the limiting curve for solutions.

Condition (5.4.7) can be written as

$$\beta = \frac{\frac{c_3}{c_2} - 1}{\frac{c_3}{c_2}} \tag{5.5.4}$$

and as

$$\frac{c_3}{c_2} = \frac{1}{1-\beta}. \tag{5.5.5}$$

In Figure 5.3.1, β given by (5.5.4) is plotted against $\frac{c_3}{c_2}$ for the whole range $-\infty < \frac{c_3}{c_2} < \infty$. In Figures 5.5.3 to 5.5.10 which follow, β is given by (5.5.4), $V_0 = 1$ and t is as defined by (4.4.9).

5.5.1 Fracture length and volume

Consider first the length of the fracture $L(t)$ given by (5.4.14) and plotted in Figure 5.5.3. The values of the parameter $\frac{c_3}{c_2}$ for which the solution exists satisfy $-\infty < \frac{c_3}{c_2} < 0\,(1 < \beta < \infty)$ and $0.5 < \frac{c_3}{c_2} < \infty\,(-1 < \beta < 1)$. When $0.5 < \frac{c_3}{c_2} < 1$, $-1 < \beta < 0$ and there is always fluid inflow at the fluid/rock interface. We see from Figure 5.5.3 that for $\frac{c_3}{c_2} = 0.51$ the length of the fracture grows strongly due to the inflow of fluid at the interface. For $\frac{c_3}{c_2} = 1$, $\beta = 0$ and no fluid leaves or enters the fracture through the interface. For $1 < \frac{c_3}{c_2} < \infty$, $0 < \beta \leq 1$ and fluid leaks off into the rock formation through the interface. As $\frac{c_3}{c_2}$ increases from $-\infty$ to 0, β increases from 1 to $+\infty$. Therefore there is leak-off of fluid at the interface and $L(t) \to \infty$ in the finite time

$$\Lambda t = \frac{243\left(\frac{1}{2} - \frac{c_3}{c_2}\right)}{4V_0^3}. \tag{5.5.6}$$

Consider next the total volume of the fracture given by equation (5.4.15) and plotted in Figure 5.5.4. When $0.5 < \frac{c_3}{c_2} < 1$, then $-1 < \beta < 0$ and fluid is always injected at the interface in the region $0 < x < L(t)$. For $1 < \frac{c_3}{c_2} < \infty$, $0 < \beta < 1$ and there is fluid leak-off at the interface in the region $0 < x < L(t)$. When $\beta = 0$, there is no exchange of fluid at the interface. For $0.5 < \frac{c_3}{c_2} < \infty$, the time rate of change of fracture volume is positive, $\frac{dV}{dt} > 0$, and $V(t) \to \infty$ as $t \to \infty$. For $-\infty < \frac{c_3}{c_2} < 0$, $\frac{dV}{dt} > 0$ and $V(t) \to \infty$ in the finite time (5.5.6). In Figure 5.5.4, when $\frac{c_3}{c_2} = -1$ and $V_0 = 1$, $V(t) \to \infty$ in the finite $t' = \Lambda t = 91.125$.

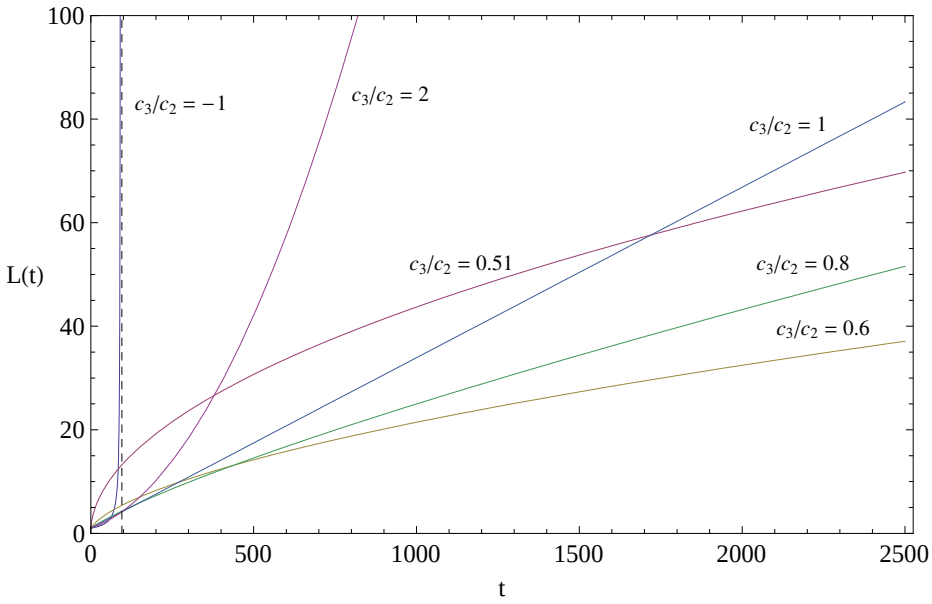


Figure 5.5.3: Leak-off velocity proportional to gradient of fracture half-width: Graph of fracture length $L(t)$ given by (5.4.14) plotted against t for a selection of values of the parameter $\frac{c_3}{c_2}$ and for $V_0 = 1$.

The total volume of the fracture always increases for all the values of $\frac{c_3}{c_2}$ for which $V(t)$ exists.

5.5.2 Fracture half-width and leak-off velocity

Consider now the fracture half-width given by (5.4.16) and plotted in Figures 5.5.5 to 5.5.10. There is always inflow of fluid at the fracture entry for all cases presented in Figures 5.5.5 to 5.5.10. Fluid inflow at the fluid/rock interface occurs in Figures 5.5.5 to 5.5.9 and we see that the fracture length at time $t = 20$ decreases as the rate of fluid injection at the interface, $q_2(t)$, decreases and as the rate of fluid injection at the fracture entry, $q_1(t)$, increases. This seems to imply that fluid inflow at the interface is more important than fluid injection at the entry to the fracture. But as t becomes sufficiently large, fluid injection at the entry becomes gradually more effective than fluid inflow at interface. This is shown in Figure 5.5.3. In Figure 5.5.10 for which the rate of fluid inflow at the interface, q_2, vanishes, the fracture length, $L(t)$, grows linearly due entirely to injection at the fracture entry.

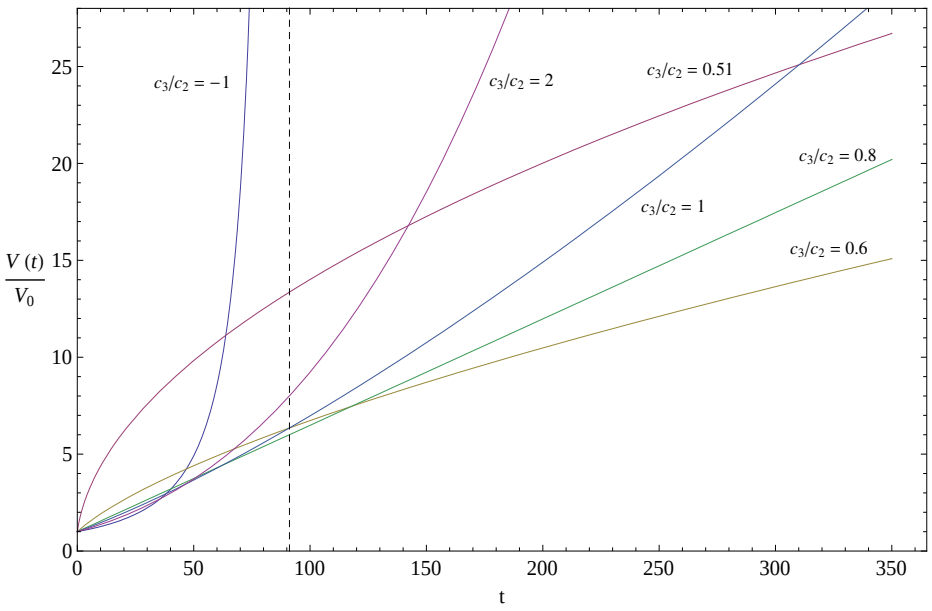


Figure 5.5.4: Leak-off velocity proportional to gradient of fracture half-width: Total volume of the fracture $\frac{V(t)}{V_0}$ given by (5.4.15) plotted against t for a selection of values of the parameter $\frac{c_3}{c_2}$ and for $V_0 = 1$.

From (5.4.16),

$$h(0,t) = \frac{2}{3}V_0\left[1 + \frac{4}{243}\frac{V_0^3}{\left(\frac{c_3}{c_2} - \frac{1}{2}\right)}\Lambda t\right]^{\frac{2}{3}\left(\frac{c_3}{c_2} - \frac{1}{2}\right)}. \tag{5.5.7}$$

For $0.5 < \frac{c_3}{c_2} < \infty$, $h(0,t)$ increases as t increases and the width of the fracture at the entry increases as t increases. This result is illustrated in Figures 5.5.5 to 5.5.10. Also,

$$\frac{\partial h}{\partial x}(x,t) = -\frac{2}{9}V_0\left[1 + \frac{4}{243}\frac{V_0^3}{\left(\frac{c_3}{c_2} - \frac{1}{2}\right)}\Lambda t\right]^{-\frac{1}{3}\left(\frac{c_3}{c_2}+1\right)}\left(1 - \frac{x}{L(t)}\right)^{-\frac{2}{3}}. \tag{5.5.8}$$

and therefore $\frac{\partial h}{\partial x}(x,t) \to -\infty$ as $x \to L(t)$. Lubrication theory therefore breaks down in the neighbourhood of the fracture tip.

The graphs of the leak-off velocity, $v_n(x,t)$, given by (5.4.17), are shown in Figures 5.5.5b to 5.5.10b. On the interface at the fracture entry,

$$v_n(0,t) = 0 \tag{5.5.9}$$

for all values $0.5 < \frac{c_3}{c_2} < \infty$. In the neighbourhood of the fracture tip,

$$v_n(L,t) = \begin{cases} -\infty & 0.5 < \frac{c_3}{c_2} < 1 \\ +\infty & 1 < \frac{c_3}{c_2} < \infty \end{cases} . \tag{5.5.10}$$

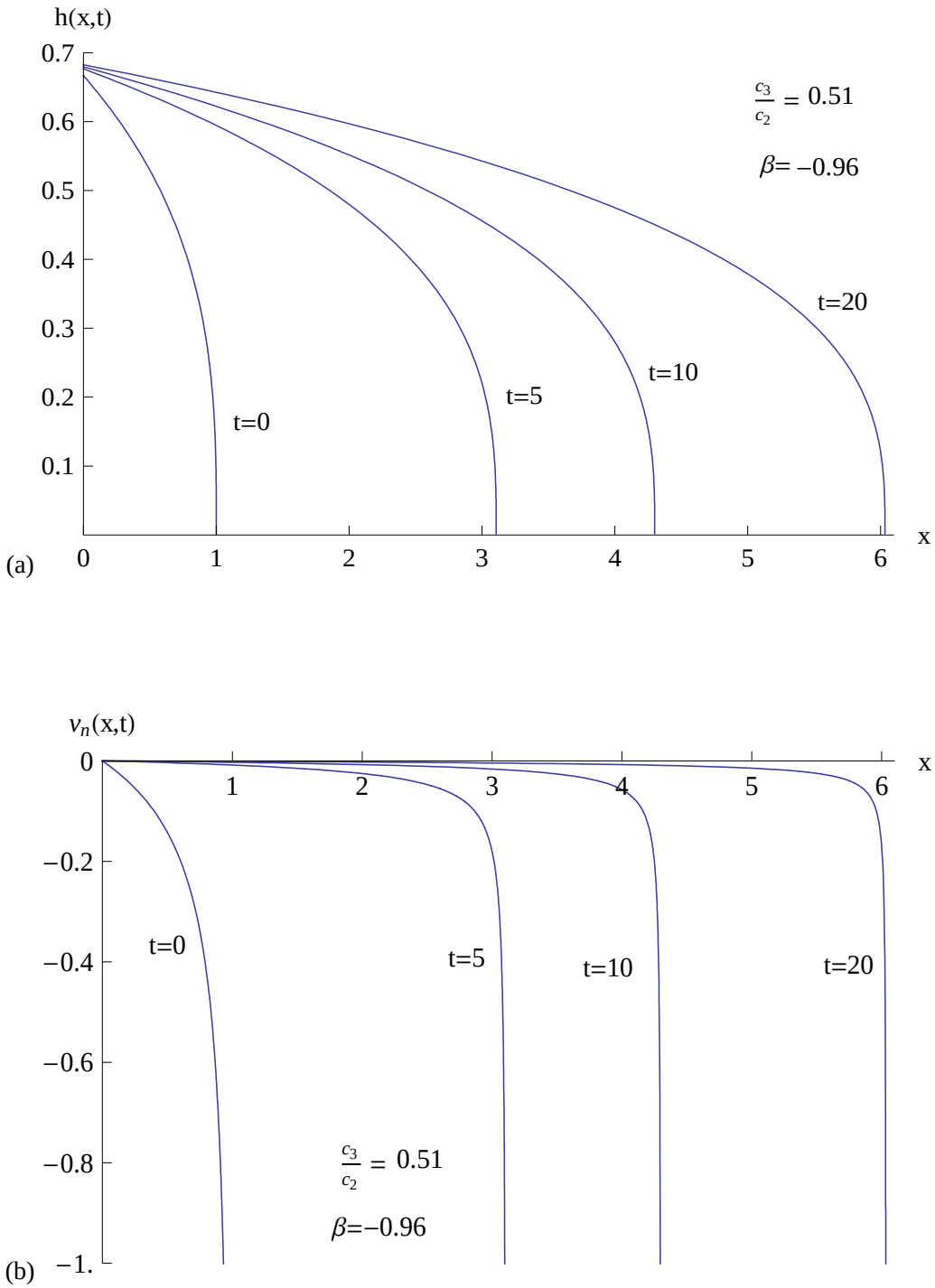


Figure 5.5.5: (a) Fracture half-width, $h(x,t)$, given by (5.4.16) and (b) leak-off velocity at the fluid/rock interface, $v_n(x,t)$, given by (5.4.17), plotted against x for a range of values of t and for $\frac{c_3}{c_2} = 0.51$, $\beta = -0.96$.

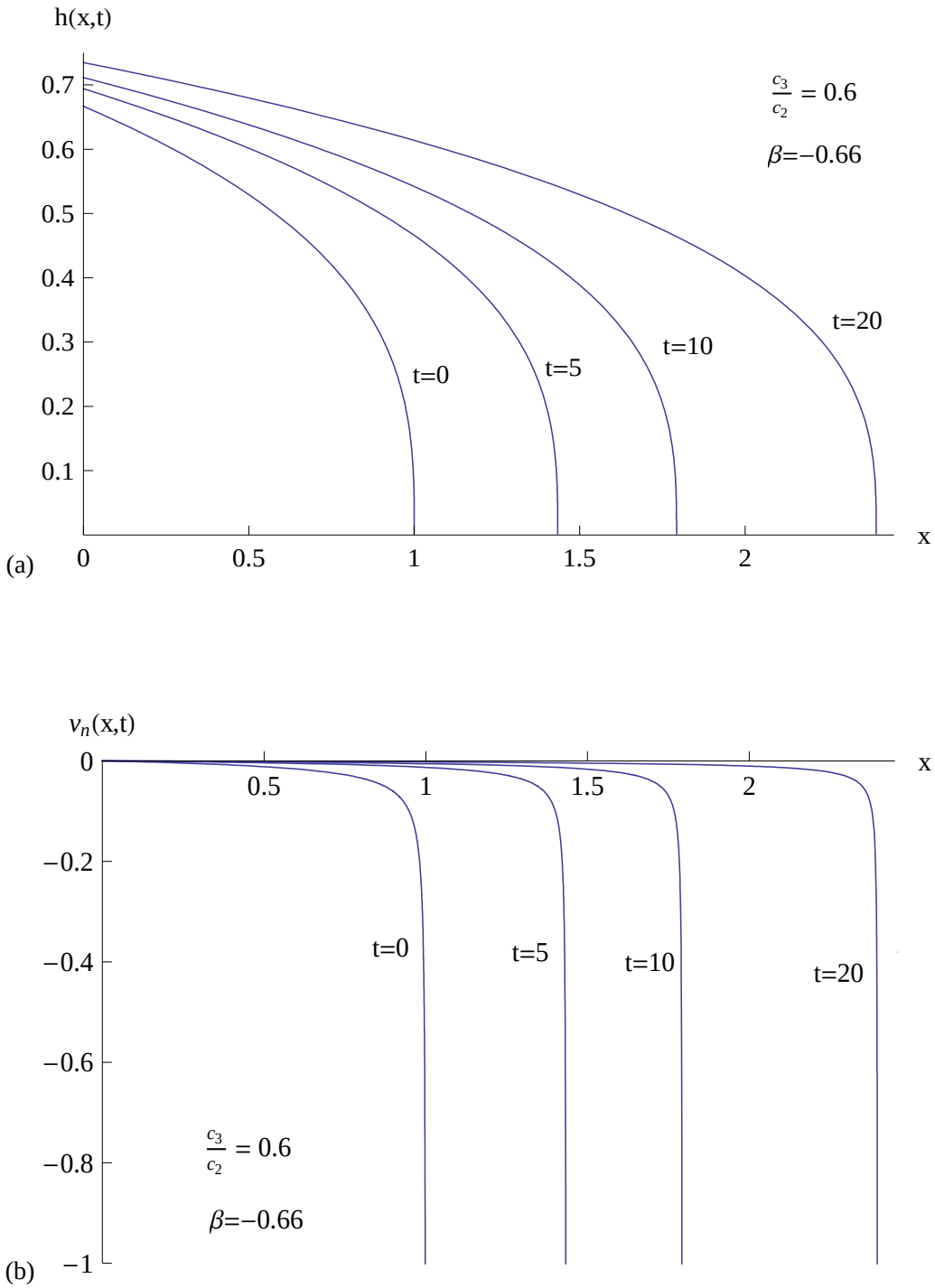


Figure 5.5.6: (a) Fracture half-width, $h(x,t)$, given by (5.4.16) and (b) leak-off velocity at the fluid/rock interface, $v_n(x,t)$, given by (5.4.17), plotted against x for a range of values of t and for $\frac{c_3}{c_2} = 0.6$, $\beta = -0.66$.

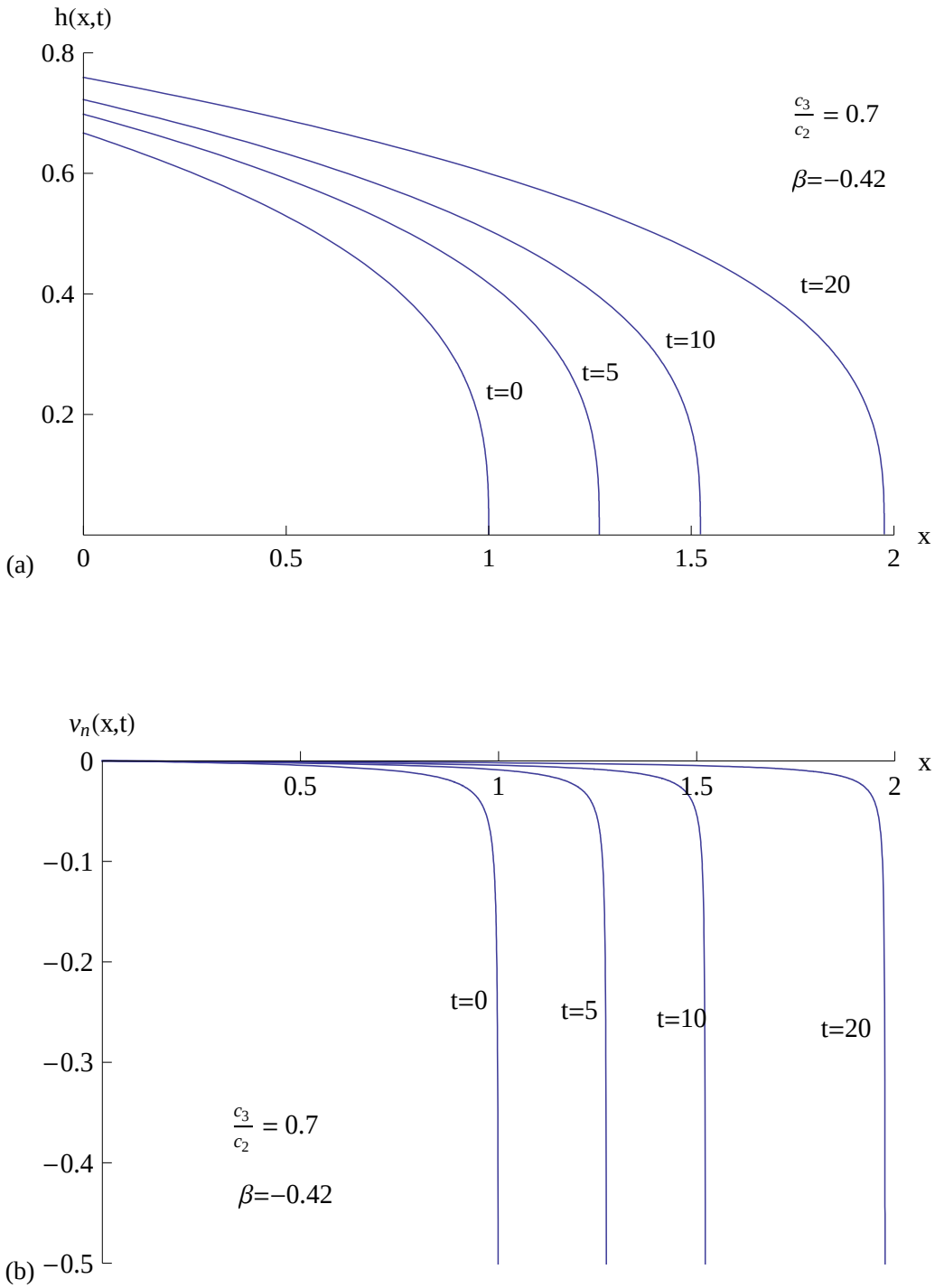


Figure 5.5.7: (a) Fracture half-width, $h(x,t)$, given by (5.4.16) and (b) leak-off velocity at the fluid/rock interface, $v_n(x,t)$, given by (5.4.17), plotted against x for a range of values of t and for $\frac{c_3}{c_2} = 0.7$, $\beta = -0.42$.

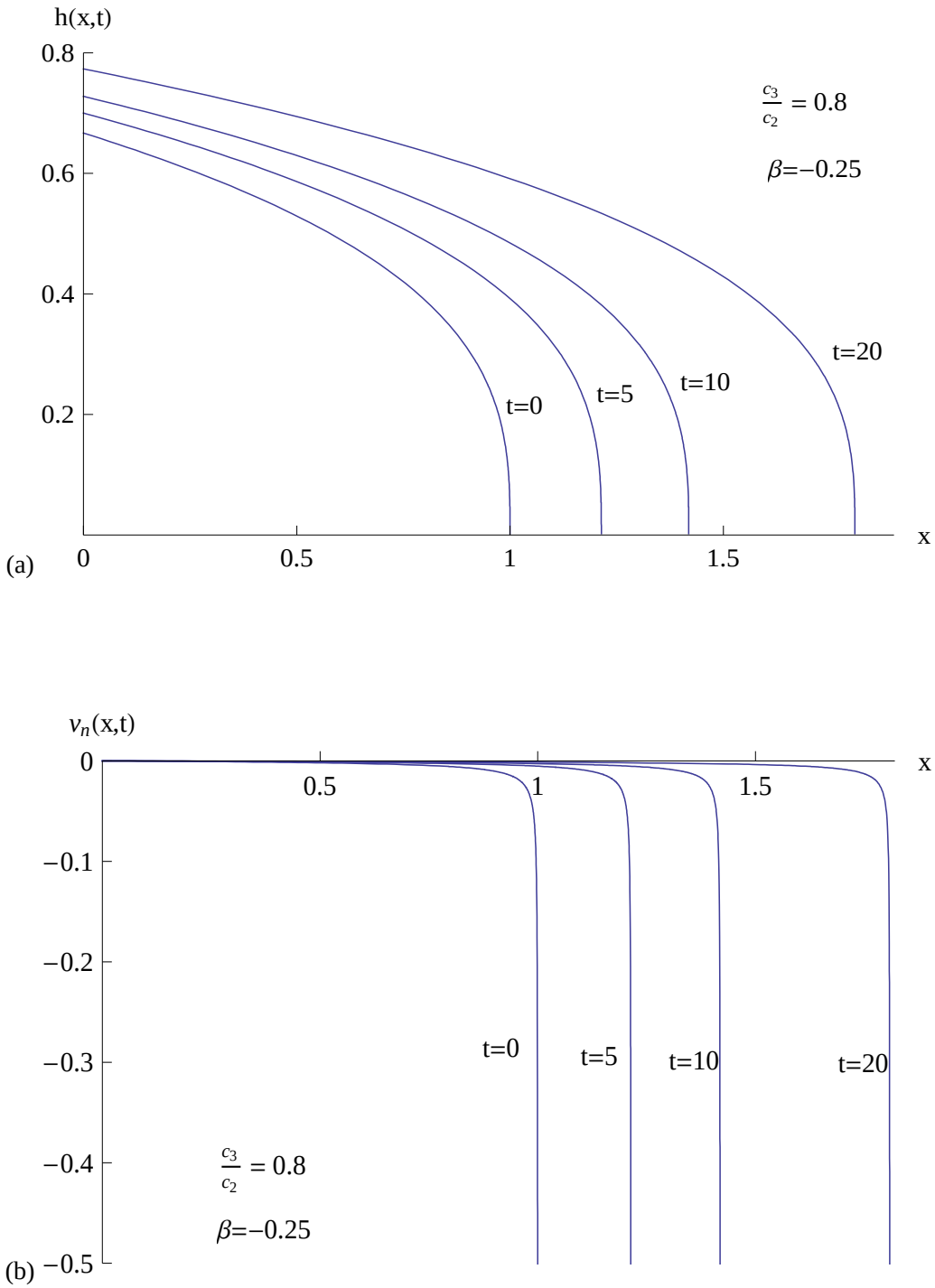


Figure 5.5.8: (a) Fracture half-width, $h(x,t)$, given by (5.4.16) and (b) leak-off velocity at the fluid/rock interface, $v_n(x,t)$, given by (5.4.17), plotted against x for a range of values of t and for $\frac{c_3}{c_2} = 0.8$, $\beta = -0.25$.

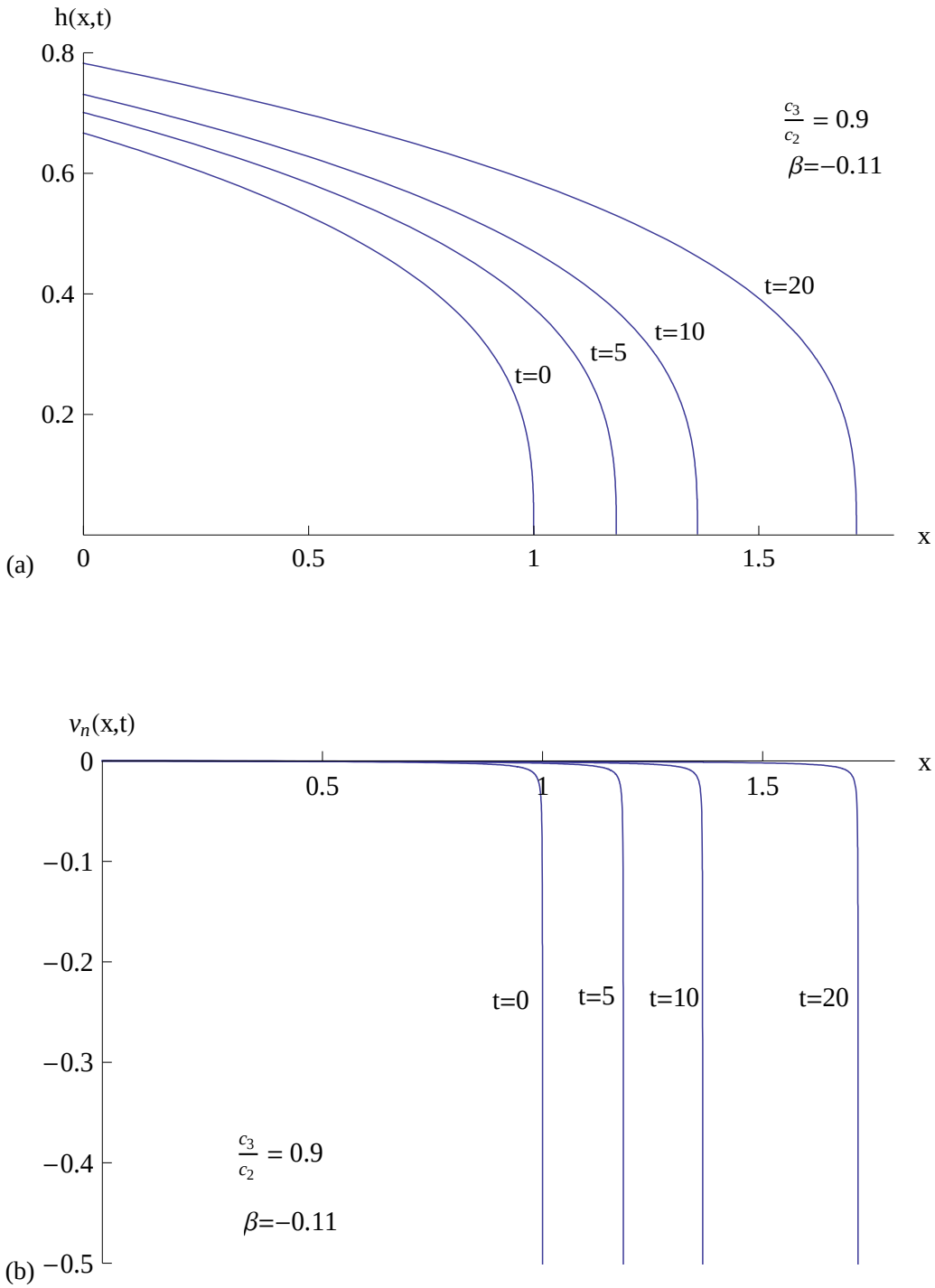


Figure 5.5.9: (a) Fracture half-width, $h(x,t)$, given by (5.4.16) and (b) leak-off velocity at the fluid/rock interface, $v_n(x,t)$, given by (5.4.17), plotted against x for a range of values of t and for $\frac{c_3}{c_2} = 0.9$, $\beta = -0.11$.

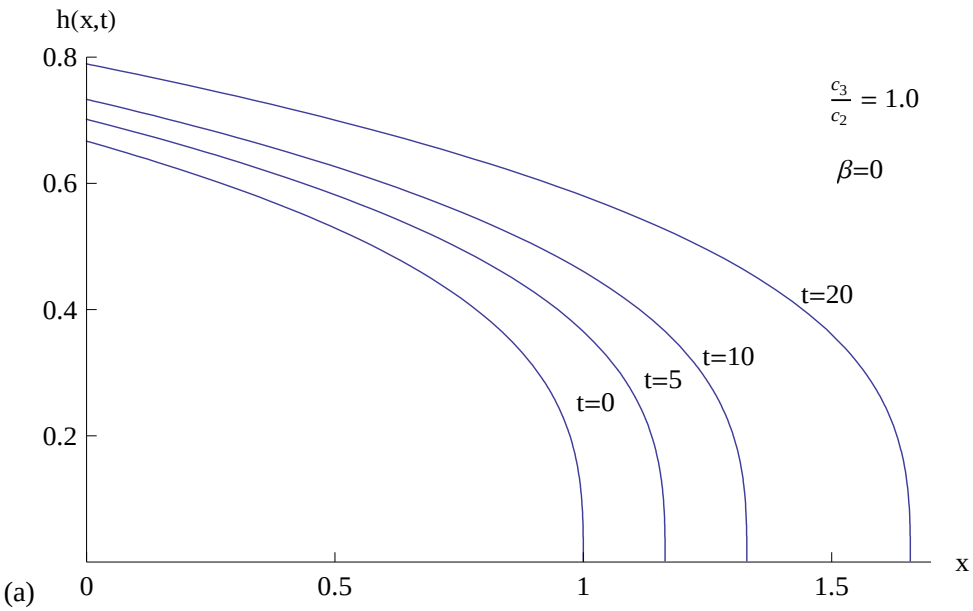


Figure 5.5.10: (a) Fracture half-width, $h(x,t)$, given by (5.4.16) plotted against x for a range of values of t and for $\frac{c_3}{c_2} = 1.0$, $\beta = 0$. The leak-off velocity $v_n = 0$ and the rock is impermeable.

5.6 Transformation of boundary value problem to two initial value problems

In this section we present a method for numerically solving the boundary value problem (5.2.3), (5.2.4) and (5.2.5) by transforming it to two initial value problems as discussed in Chapter 4. Equation (5.2.3) is of the form

$$\Lambda \frac{d}{du}\left(F^3 \frac{dF}{du}\right) + A\frac{d}{du}(uF) + BF = 0, \tag{5.6.1}$$

with $A = 3(1+\beta)$ and $B = \left(\frac{c_2}{c_3} - 3\beta - 5\right)$ and it admits only one Lie point symmetry generator. Equation (5.2.3) is not completely integrable to yield an analytical solution and hence it is solved numerically for some values of $\frac{c_3}{c_2}$ and β which are of clear physical significance. Equation (5.2.3) is invariant under the scaling transformation

$$\overline{u} = \lambda u, \qquad \overline{F} = \lambda^{\frac{2}{3}} F, \tag{5.6.2}$$

as discussed in Section 4.7.

The boundary value problem (5.2.3) to (5.2.5) is

$$\Lambda\frac{d}{du}\left(F^3\frac{dF}{du}\right)+3(1+\beta)\frac{d}{du}\left(uF\right)+\left(\frac{c_2}{c_3}-5-3\beta\right)F=0, \tag{5.6.3}$$

$$F(1)=0, \tag{5.6.4}$$

$$\Lambda F^3(0)\frac{dF}{du}(0)=\left(\frac{c_2}{c_3}-5-3\beta\right)\int_0^1 F(u)du. \tag{5.6.5}$$

Under the transformation (5.6.2), equations (5.6.3) to (5.6.5) become

$$\Lambda\frac{d}{d\overline{u}}\left(\overline{F}^3\frac{d\overline{F}}{d\overline{u}}\right)+3(1+\beta)\frac{d}{d\overline{u}}\left(\overline{u}\overline{F}\right)+\left(\frac{c_2}{c_3}-5-3\beta\right)\overline{F}(\overline{u})=0, \tag{5.6.6}$$

$$\overline{F}(\lambda)=0, \tag{5.6.7}$$

$$\Lambda\overline{F}^3(0)\frac{d\overline{F}}{d\overline{u}}(0)=\left(\frac{c_2}{c_3}-5-3\beta\right)\int_0^\lambda \overline{F}(\overline{u})d\overline{u}. \tag{5.6.8}$$

We now choose

$$\overline{F}(0)=1. \tag{5.6.9}$$

Then from (5.6.2),

$$F(0)=\frac{1}{\lambda^{\frac{2}{3}}} \tag{5.6.10}$$

where λ is defined by (5.6.7). The boundary value problem (5.2.3) to (5.2.5) can therefore be transformed to the following two Initial Value Problems:

Initial Value Problem 1:

$$\Lambda\frac{d}{d\overline{u}}\left(\overline{F}^3\frac{d\overline{F}}{d\overline{u}}\right)+3\left(1+\beta\right)\frac{d}{d\overline{u}}\left(\overline{u}\overline{F}(\overline{u})\right)+\left(\frac{c_2}{c_3}-5-3\beta\right)\overline{F}(\overline{u})=0, \tag{5.6.11}$$

$$\overline{F}(0)=1,\qquad \Lambda\frac{d\overline{F}}{d\overline{u}}(0)=\left(\frac{c_2}{c_3}-5-3\beta\right)\int_0^\lambda \overline{F}(\overline{u})d\overline{u}, \tag{5.6.12}$$

where $0\le\overline{u}\le\lambda$ and λ is defined by

$$\overline{F}(\lambda)=0. \tag{5.6.13}$$

Initial Value Problem 2:

$$\Lambda\frac{d}{du}\left(F^3\frac{dF}{du}\right)+3\left(1+\beta\right)\frac{d}{du}\left(uF(u)\right)+\left(\frac{c_2}{c_3}-5-3\beta\right)F(u)=0, \tag{5.6.14}$$

$$F(0)=\lambda^{-\frac{2}{3}},\qquad \Lambda\frac{dF}{du}(0)=\lambda^2\left(\frac{c_2}{c_3}-5-3\beta\right)\int_0^1 F(u)du, \tag{5.6.15}$$

where $0 \leq u \leq 1$.

The value of λ is obtained from the Initial Value Problem 1. The solution $F(u)$ is obtained from the Initial Value Problem 2. The remainder of the solution is then given by (5.2.6) to (5.2.12). We will transform the boundary value problems for the cases (5.3.1) and (5.4.7) in which exact analytical solutions exist to two Initial Value Problems. These Initial Value Problems will be solved for $F(u)$ to obtained the results found in Sections 5.3 and 5.4. This was done in Section 4.7 and it gives a check on the numerical method.

***Special Case 1*:** $\beta = \frac{1}{3}\left(\frac{c_2}{c_3} - 5\right)$

For this special case the boundary value problem (5.6.3) to (5.6.5) is transformed into the following two Initial Value Problems:

Initial Value Problem 1:

$$\Lambda \frac{d}{d\overline{u}}\left(\overline{F}^3 \frac{d\overline{F}}{d\overline{u}}\right) + \left(\frac{c_2}{c_3} - 2\right)\frac{d}{d\overline{u}}\left(\overline{u}\overline{F}(\overline{u})\right) = 0, \tag{5.6.16}$$

$$\overline{F}(0) = 1, \qquad \frac{d\overline{F}}{d\overline{u}}(0) = 0, \tag{5.6.17}$$

where $0 \leq \overline{u} \leq \lambda$ and λ is defined by

$$\overline{F}(\lambda) = 0. \tag{5.6.18}$$

Initial Value Problem 2:

$$\Lambda \frac{d}{du}\left(F^3 \frac{dF}{du}\right) + \left(\frac{c_2}{c_3} - 2\right)\frac{d}{du}\left(uF(u)\right) = 0, \tag{5.6.19}$$

$$F(0) = \lambda^{-\frac{2}{3}}, \qquad \frac{dF}{du}(0) = 0, \tag{5.6.20}$$

where $0 \leq u \leq 1$ and the parameter λ is obtained from Problem 1.

Integrating (5.6.16) once with respect to $\overline{u}$ gives

$$\Lambda \overline{F}^3 \frac{d\overline{F}}{d\overline{u}} + \left(\frac{c_2}{c_3} - 2\right)\overline{u}\overline{F}(\overline{u}) = A, \tag{5.6.21}$$

where A is a constant. Applying the initial conditions (5.6.17a) and (5.6.17b) at $\overline{u} = 0$ gives $A = 0$. Equation (5.6.21) becomes

$$\Lambda \overline{F}^2 \frac{d\overline{F}}{d\overline{u}} = -\left(\frac{c_2}{c_3} - 2\right)\overline{u}, \tag{5.6.22}$$

which is variables separable. Thus

$$\Lambda\overline{F}^3(\overline{u}) = -\frac{3}{2}\left(\frac{c_2}{c_3} - 2\right)\overline{u}^2 + B \tag{5.6.23}$$

where B is a constant. Using (5.6.17a) it follows from (5.6.23) that $B = \Lambda$ and therefore

$$\overline{F}(\overline{u}) = \left(1 - \frac{3}{2\Lambda}\left(\frac{c_2}{c_3} - 2\right)\overline{u}^2\right)^{\frac{1}{3}}. \tag{5.6.24}$$

By using (5.6.18), λ is obtained as

$$\lambda = \left(\frac{2\Lambda}{3\left(\frac{c_2}{c_3} - 2\right)}\right)^{\frac{1}{2}}, \tag{5.6.25}$$

provided $\frac{c_2}{c_3} > 2$.

Similarly, equation (5.6.19) of the Initial Value Problem 2 is solved for $F(u)$ to obtain

$$F(u) = \left[\frac{3}{2\Lambda}\left(\frac{c_2}{c_3} - 2\right)\right]^{\frac{1}{3}}\left(1 - u^2\right)^{\frac{1}{3}}, \tag{5.6.26}$$

provided $\frac{c_2}{c_3} > 2$. Equation (5.6.26) agrees with (5.3.10) derived for $F(u)$ in Section 5.3.

***Special Case 2*: $\beta = 1 - \frac{c_2}{c_3}$**

For this special case the boundary value problem (5.6.3) to (5.6.5) is transformed into the following two Initial Value Problems:

Initial Value Problem 1

$$\Lambda\frac{d}{d\overline{u}}\left(\overline{F}^3\frac{d\overline{F}}{d\overline{u}}\right) - 3\left(\frac{c_2}{c_3} - 2\right)\overline{u}\frac{d\overline{F}}{d\overline{u}} + \left(\frac{c_2}{c_3} - 2\right)\overline{F} = 0, \tag{5.6.27}$$

$$\overline{F}(0) = 1, \qquad \Lambda\frac{d\overline{F}}{d\overline{u}}(0) = 4\left(\frac{c_2}{c_3} - 2\right)\int_0^{\lambda}\overline{F}(u)d\overline{u}, \tag{5.6.28}$$

where $0 \leq \overline{u} \leq \lambda$ and λ is defined by

$$\overline{F}(\lambda) = 0. \tag{5.6.29}$$

Initial Value Problem 2

$$\Lambda\frac{d}{du}\left(F^3\frac{dF}{du}\right) - 3\left(\frac{c_2}{c_3} - 2\right)u\frac{dF}{du} + \left(\frac{c_2}{c_3} - 2\right)F = 0, \tag{5.6.30}$$

$$F(0) = \lambda^{-\frac{2}{3}}, \qquad \Lambda\frac{dF}{du}(0) = 4\lambda^2\left(\frac{c_2}{c_3} - 2\right)\int_0^1 F(u)du. \tag{5.6.31}$$

where $0 \leq u \leq 1$ and the parameter λ is obtained from Problem 1.

In order to solve Problem 1 look for a solution of (5.6.27) of the form

$$\overline{F}(\overline{u}) = A\left(B - \overline{u}\right)^n, \tag{5.6.32}$$

where A, B and n are constants to be determined such that $A \neq 0$ and $n > 0$. Using (5.6.28a) we have

$$1 = AB^n. \tag{5.6.33}$$

Substituting (5.6.32) into (5.6.27) and solving as described in Section 5.4 gives

$$n = \frac{1}{3}, \qquad \frac{\Lambda}{9}A^3 = \left(2 - \frac{c_2}{c_3}\right)B \tag{5.6.34}$$

and therefore using (5.6.33),

$$A = \left[\frac{9}{\Lambda}\left(2 - \frac{c_2}{c_3}\right)\right]^{\frac{1}{6}}, \qquad B = \left[\frac{\Lambda}{9\left(2 - \frac{c_2}{c_3}\right)}\right]^{\frac{1}{2}}, \tag{5.6.35}$$

provided $\frac{c_2}{c_3} < 2$. Thus

$$\overline{F}(\overline{u}) = \left[\frac{9}{\Lambda}\left(2 - \frac{c_2}{c_3}\right)\right]^{\frac{1}{6}}\left[\left(\frac{\Lambda}{9\left(2 - \frac{c_2}{c_3}\right)}\right)^{\frac{1}{2}} - \overline{u}\right]^{\frac{1}{3}} \tag{5.6.36}$$

and hence from (5.6.29),

$$\lambda = \left(\frac{\Lambda}{9\left(2 - \frac{c_2}{c_3}\right)}\right)^{\frac{1}{2}}. \tag{5.6.37}$$

It can be verified that the boundary condition (5.6.28b) is identically satisfied by (5.6.36). The solution of the Initial Value Problem 2 is performed in a similar way by looking for a solution of (5.6.30) of the form $F(u) = A\left(B - u\right)^n$. It is found that

$$F(u) = \left[\frac{9}{\Lambda}\left(2 - \frac{c_2}{c_3}\right)\right]^{\frac{1}{3}}\left(1 - u\right)^{\frac{1}{3}}, \tag{5.6.38}$$

where $\frac{c_2}{c_3} < 2$ for a non-zero real solution to exist. Equation (5.6.38) agrees with (5.4.9) derived for $F(u)$ in Section 5.4.

5.7 Numerical solution

Using 4.8.1, the boundary value problem (5.2.3) to (5.2.5) is transformed to the two Initial Value Problems (5.6.11) to (5.6.13) and (5.6.14) to (5.6.15) with $\Lambda = 1$.

Initial value Problem 1:

$$\frac{d}{d\overline{u}}\left(\overline{F}^3\frac{d\overline{F}}{d\overline{u}}\right) + 3\left(1+\beta\right)\frac{d}{d\overline{u}}\left(\overline{u}\overline{F}(\overline{u})\right) + \left(\frac{c_2}{c_3} - 5 - 3\beta\right)\overline{F}(\overline{u}) = 0, \tag{5.7.1}$$

$$\overline{F}(0) = 1, \qquad \frac{d\overline{F}}{d\overline{u}}(0) = \left(\frac{c_2}{c_3} - 5 - 3\beta\right)\int_0^{\lambda}\overline{F}(\overline{u})d\overline{u}, \tag{5.7.2}$$

where $0 \leq \overline{u} \leq \lambda$ and λ is defined by

$$\overline{F}(\lambda) = 0. \tag{5.7.3}$$

Initial value Problem 2:

$$\frac{d}{du}\left(F^3\frac{dF}{du}\right) + 3\left(1+\beta\right)\frac{d}{du}\left(uF(u)\right) + \left(\frac{c_2}{c_3} - 5 - 3\beta\right)F(u) = 0, \tag{5.7.4}$$

$$F(0) = \lambda^{-\frac{2}{3}}, \qquad \frac{dF}{du}(0) = \lambda^{\frac{1}{3}}\frac{d\overline{F}}{d\overline{u}}(0). \tag{5.7.5}$$

We will solve numerically equations (5.7.1) to (5.7.3) of the Initial Value Problem 1 and equations (5.7.4) and (5.7.5) of the Initial Value Problem 2 using the computer algebra package MATHEMATICA. Firstly, we rewrite the second order differential equation (5.7.1) as the coupled first order differential equations

$$\frac{d\overline{F}}{d\overline{u}} = y_2, \tag{5.7.6}$$

$$\frac{dy_2}{d\overline{u}} = -\frac{1}{\overline{F}^3}\left[3\overline{F}^2y_2^2 + 3(1+\beta)\overline{u}y_2 + \left(\frac{c_2}{c_3} - 2\right)\overline{F}\right]. \tag{5.7.7}$$

subject to the initial and boundary conditions

$$\overline{F}(0) = 1, \quad y_2(0) = k, \quad \overline{F}(\lambda) = 0, \tag{5.7.8}$$

where k is to be determined from the algorithm outlined in Section 4.8. The second order differential equation (5.7.4) is rewritten as the set of coupled differential equations

$$\frac{dF}{du} = y_3, \tag{5.7.9}$$

$$\frac{dy_3}{du} = -\frac{1}{F^3}\left[3F^2y_3^2 + 3(1+\beta)uy_3 + \left(\frac{c_2}{c_3} - 2\right)F\right], \tag{5.7.10}$$

subject to the initial conditions

$$F(0) = \lambda^{-\frac{2}{3}}, \quad y_3(0) = \lambda^{\frac{1}{3}} y_2(0). \tag{5.7.11}$$

As also outlined in Section 4.8, we first determine the value of λ, starting the backward integration of the system of first order equations (5.7.6) and (5.7.7) with the asymptotic representations

$$\overline{F}(\overline{u}) \sim (9\lambda(1+\beta))^{\frac{1}{3}} (\lambda - \overline{u})^{\frac{1}{3}} \quad \text{as} \quad \overline{u} \to \lambda, \tag{5.7.12}$$

$$y_2(\overline{u}) \sim -\frac{1}{3}(9\lambda(1+\beta))^{\frac{1}{3}} (\lambda - \overline{u})^{-\frac{2}{3}} \quad \text{as} \quad \overline{u} \to \lambda, \tag{5.7.13}$$

which are obtained from (5.2.21) using the scaling transformation (5.6.2). The algorithm for solving the coupled systems (5.7.6) to (5.7.7) and (5.7.9) to (5.7.10) of first order ordinary differential equations subject to (5.7.8) and (5.7.11), respectively, is similar to that described in Section 4.8. Tables 5.8.1 and 5.8.2 compare the numerical and analytical solutions for $F(u)$ for the two cases in which analytical solutions were derived in Sections 5.3 and 5.4. The results shown are obtained for $\varepsilon_3 = 10^{-7}$ and the analytical and numerical solutions agree to six decimal place everywhere except in the neighbourhood of the fracture tip where the solutions agree to 3 decimal places.

5.8 Numerical Results

We analyse the results obtained for the numerical solution of the two Initial Value Problems for a selection of values of $\frac{c_3}{c_2}$ and β. We found that the set of values of $(\frac{c_3}{c_2}, \beta)$ for which a solution exists of the two Initial Value Problems is bounded below by a limit curve in the $(\frac{c_3}{c_2}, \beta)$ plane.

The limiting curve for solutions is described by

$$\beta_{min} = \begin{cases} \frac{4\left(\frac{1}{8} - \frac{c_3}{c_2}\right)}{3\frac{c_3}{c_2}}, & 0 < \frac{c_3}{c_2} \leq 0.5, \\ -1, & 0.5 \leq \frac{c_3}{c_2} < \infty, \end{cases} \tag{5.8.1}$$

where β_{min} is the minimum value of β for a given value of $\frac{c_3}{c_2}$. The limiting curve (5.8.1) is plotted in Figure 5.3.1. No solution exists for values of $(\frac{c_3}{c_2}, \beta)$ below the limiting curve.

Special Case $\frac{c_2}{c_3} - 3\beta - 5$ =0		
u	Exact Solution	Numerical Solution
0.000	2.289430	2.289430
0.200	2.258490	2.258490
0.400	2.160160	2.160160
0.600	1.972970	1.972970
0.800	1.628650	1.628650
0.900	1.316170	1.316170
0.920	1.226100	1.226100
0.940	1.117840	1.117840
0.960	0.979864	0.979864
0.980	0.780355	0.780355
0.982	0.753678	0.753678
0.984	0.724905	0.724905
0.986	0.693579	0.693580
0.988	0.659062	0.659062
0.990	0.620409	0.620409
0.992	0.576130	0.576130
0.994	0.523624	0.523624
0.996	0.457580	0.457581
0.998	0.363303	0.363303
1.000	0.000000	0.000838

Table 5.8.1: Comparison of the numerical and analytical solution for $F(u)$ for the special case $\frac{c_2}{c_3} - 3\beta - 5$ =0.

Special Case $\beta = 1 - \frac{c_2}{c_3}$		
u	Exact Solution	Numerical Solution
0.000	1.889880	1.889880
0.200	1.754410	1.754410
0.400	1.593990	1.593990
0.600	1.392480	1.392480
0.800	1.105210	1.105210
0.900	0.877205	0.877205
0.920	0.814325	0.814325
0.940	0.739864	0.739863
0.960	0.646330	0.646330
0.980	0.512993	0.512992
0.982	0.495289	0.495289
0.984	0.476220	0.476220
0.986	0.455488	0.455488
0.988	0.432675	0.432674
0.990	0.407163	0.407162
0.992	0.377976	0.377976
0.994	0.343414	0.343414
0.996	0.300000	0.299999
0.998	0.238110	0.238110
1.000	0.000000	0.000884

Table 5.8.2: Comparison of the numerical and analytical solution for $F(u)$ for the special case $\beta = 1 - \frac{c_2}{c_3}$.

Equation (5.8.1) was found numerically and no analytical proof has been found that no solution exists for values of $(\frac{c_3}{c_2}, \beta)$ below the limiting curve. For the two special cases for which analytical solutions were derived in Sections 5.3 and 5.4, we found that the solutions did not exist for $\beta < -1$. The special analytical results are therefore consistent with the general numerical result for non-existence of solutions. The values of $(\frac{c_3}{c_2}, \beta)$ in the region bounded by the curves (5.8.1) and (5.3.1) in the $(\frac{c_3}{c_2}, \beta)$ plane describe operating conditions in which fluid is extracted out of the fracture at the entry to the fracture. Solutions in this region could have application in the extraction of oil from a fracture. The physical significance of the curve (5.8.1) is not known.

5.8.1 Graphical results for fixed $\frac{c_3}{c_2}$ and varying values of β

We present in this section a discussion on the graphs obtained from the numerical solution of the two Initial Value Problems in Section 5.7. The graphs are those for which $\frac{c_3}{c_2}$ is fixed and β is varied. Hence the effect of β on $h(x,t)$, $L(t)$ and $v_n(x,t)$ can be studied.

In Figure 5.8.1, $\frac{c_3}{c_2} = 0.1$ and the numerical solution exists for $0.33 \leq \beta < \infty$. Solutions describing fluid extraction at the fracture entry occur for $0.33 \leq \beta < 1.66$. For $1.66 \leq \beta < \infty$, solutions for fluid injection into the fracture at the entry are obtained. When $\beta = 1.66$, we have a particular case of the exact solution for which the fluid injection rate, q_1, is zero. When $\beta = 0.4$, the shape of $h(x,t)$ was unexpected since the half-width first increases with x before decreasing. This may be due to fluid extraction at the fracture entry. Fluid inflow at the interface occurs for $0 < x < 0.6$ due to $\frac{\partial h}{\partial x} > 0$ and leak-off occurs in the remaining region $0.6 < x \leq L(t)$.

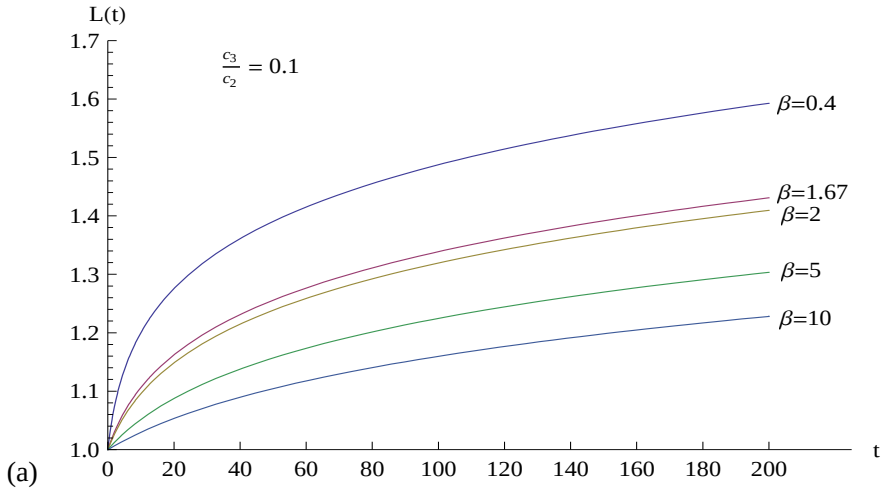
In Figure 5.8.2, $\frac{c_3}{c_2} = 0.125$ and the numerical solution exists for $0 \leq \beta < \infty$. All solutions have leak-off at the interface except when $\beta = 0$ in which case no fluid exchange occurs at the interface. For $0 < \beta < 1$, we obtain solutions describing fluid extraction out of the fracture at the entry and fluid injection into the fracture at the entry occurs for $1 < \beta < \infty$. The analytical solution for which the rate of fluid injection at the entry, q_1, is zero exists when $\beta = 1$. In Figure 5.8.2a, we see that as the leak-off parameter, β, increases, the increase in length decreases.

In Figure 5.8.3, $\frac{c_3}{c_2} = 0.2$ and the numerical solution exists for $-0.5 \leq \beta < \infty$. The volume of the fracture is always conserved when $\frac{c_3}{c_2} = 0.2$. Solutions describing fluid extraction at the entry occur for $-0.5 \leq \beta < 0$ while solutions that describe fluid injection at the entry occur for $0 < \beta < \infty$. When $\beta = 0$, $v_n(x,t) = 0$ and there is no fluid leak-off at interface. An analytical solution exists for this case. In all cases the length of the fracture increases. The increase is greater than for an impermeable rock when there is fluid injection at the interface ($\beta < 0$) and is less than for an impermeable rock when there is fluid leak-off at the interface ($\beta > 0$).

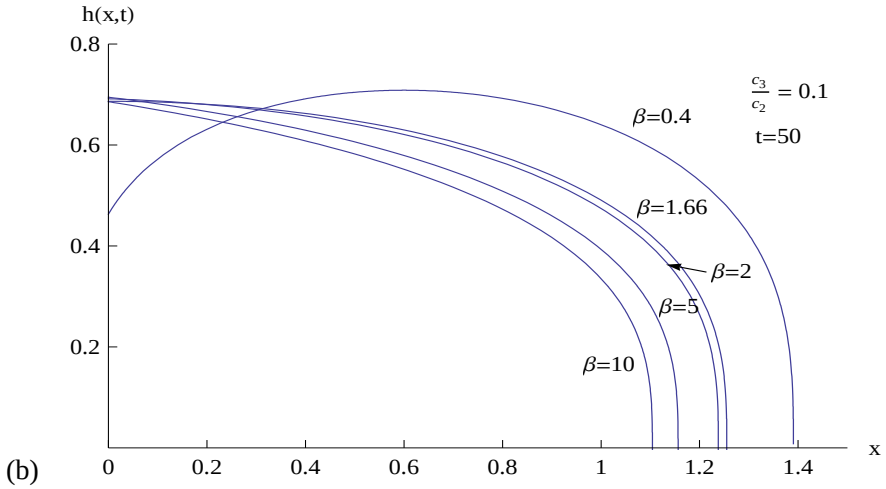
In Figure 5.8.4, $\frac{c_3}{c_2} = 0.5$ and the numerical solution exists for $-1 \leq \beta < \infty$. The fluid pressure at the fracture entry is always constant when $\frac{c_3}{c_2} = 0.5$. All solutions have fluid injection at the fracture entry. No solution exist for fluid extraction out of the fracture at the entry. When $\beta = -0.9$ and $\beta = -0.5$, fluid injection occurs at the interface while for $\beta = 5$ and $\beta = 10$, there is fluid leak-off at the interface. For $\beta = 0$, no fluid exchange occurs at the interface. In all cases the length of the fracture increases and the rate of increase decreases as β increases from negative to positive values.

In Figure 5.8.5, $\frac{c_3}{c_2} = 0.8$ and the numerical solution exists for $-1 \leq \beta < \infty$. The rate of fluid injection at the fracture entry, q_1, is always constant for $\frac{c_3}{c_2} = 0.8$. All solutions have fluid injection at entry. When $\beta = -0.25$, the analytical solutions (5.4.14) to (5.4.18) applies. No leak-off occurs for $\beta = 0$.

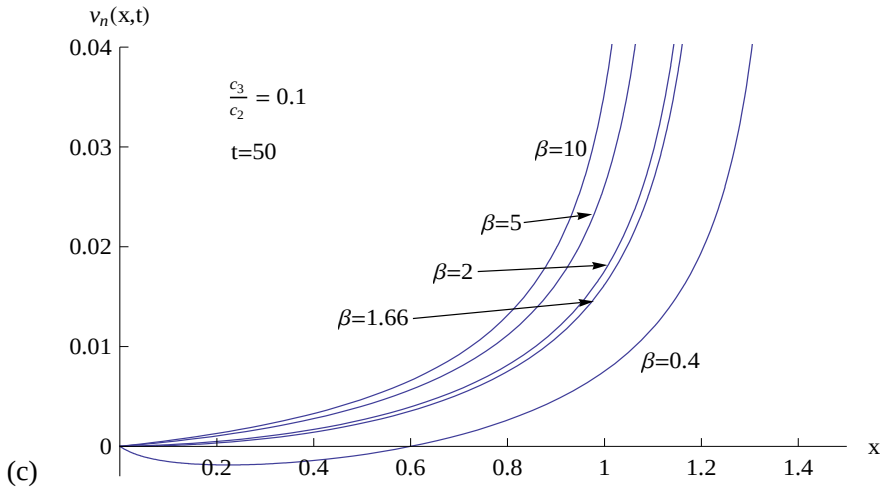
In Figure 5.8.6, $\frac{c_3}{c_2} = 1$ and the numerical solution exists for $-1 \leq \beta < \infty$. The length of the fracture, $L(t)$, always grows linearly with time when $\frac{c_3}{c_2} = 1$ and the velocity of propagation of the fracture is constant. The graphs of $L(t)$ against t in Figure 5.8.6a are straight lines. When $\beta = 0$, the exact solution (5.4.14) to (5.4.18) is satisfied.



(a)

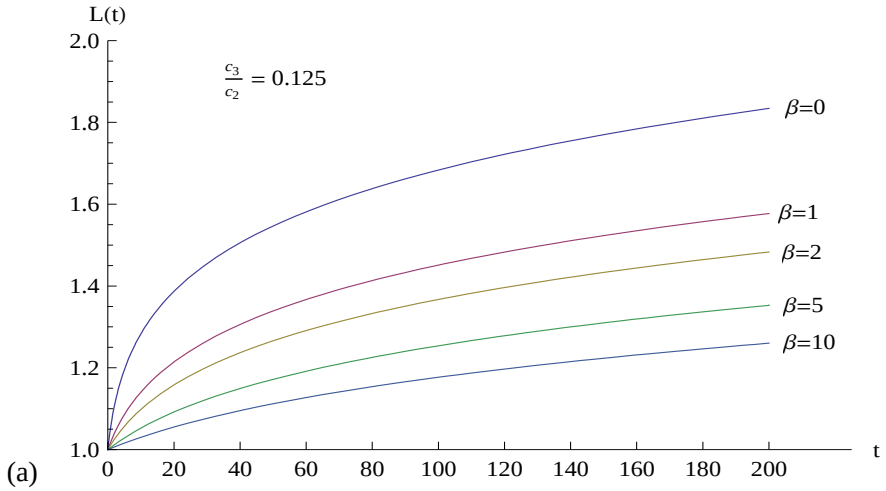


(b)

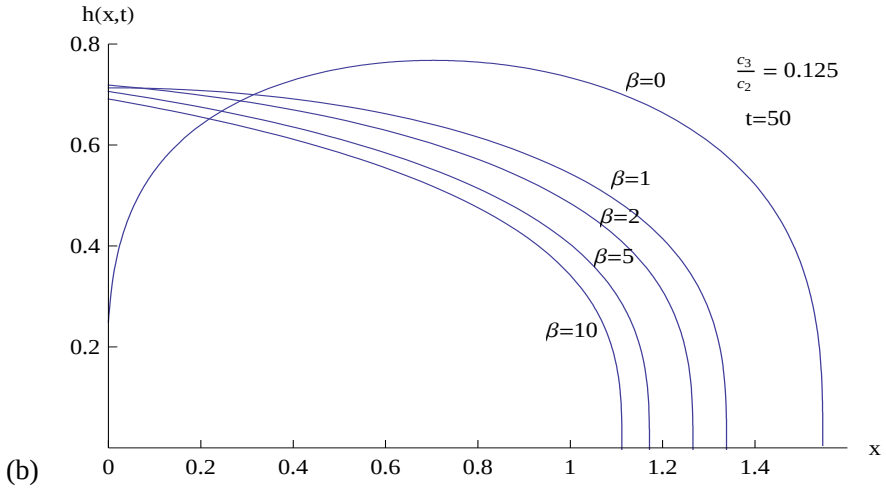


(c)

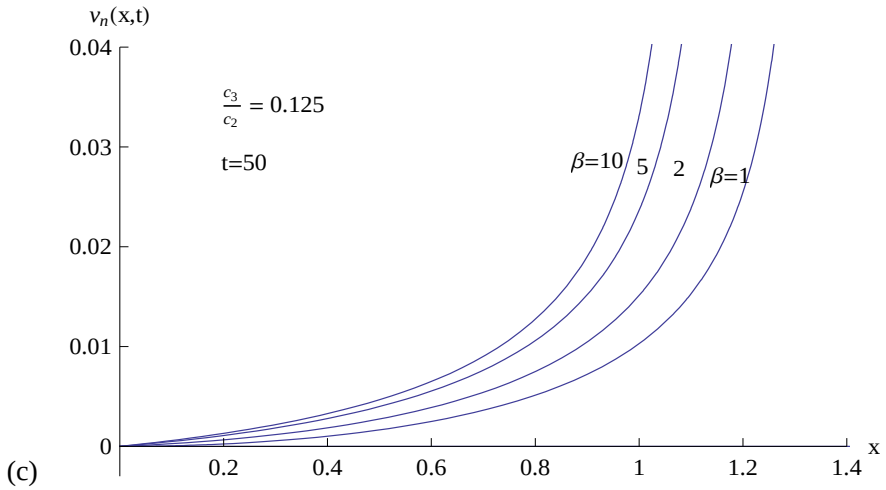
Figure 5.8.1: Graphs for $\frac{c_3}{c_2} = 0.1$ and a selection of values of β : (a) Fracture length $L(t)$ plotted against time; (b) Fracture half-width $h(x,t)$ plotted against x at time $t = 50$; (c) Leak-off fluid velocity $v_n(x,t)$ plotted against x at time $t = 50$.



(a)



(b)



(c)

Figure 5.8.2: Graphs for $\frac{c_3}{c_2} = 0.125$ and a selection of values of β : (a) Fracture length $L(t)$ plotted against time; (b) Fracture half-width $h(x,t)$ plotted against x at time $t = 50$; (c) Leak-off fluid velocity $v_n(x,t)$ plotted against x at time $t = 50$.

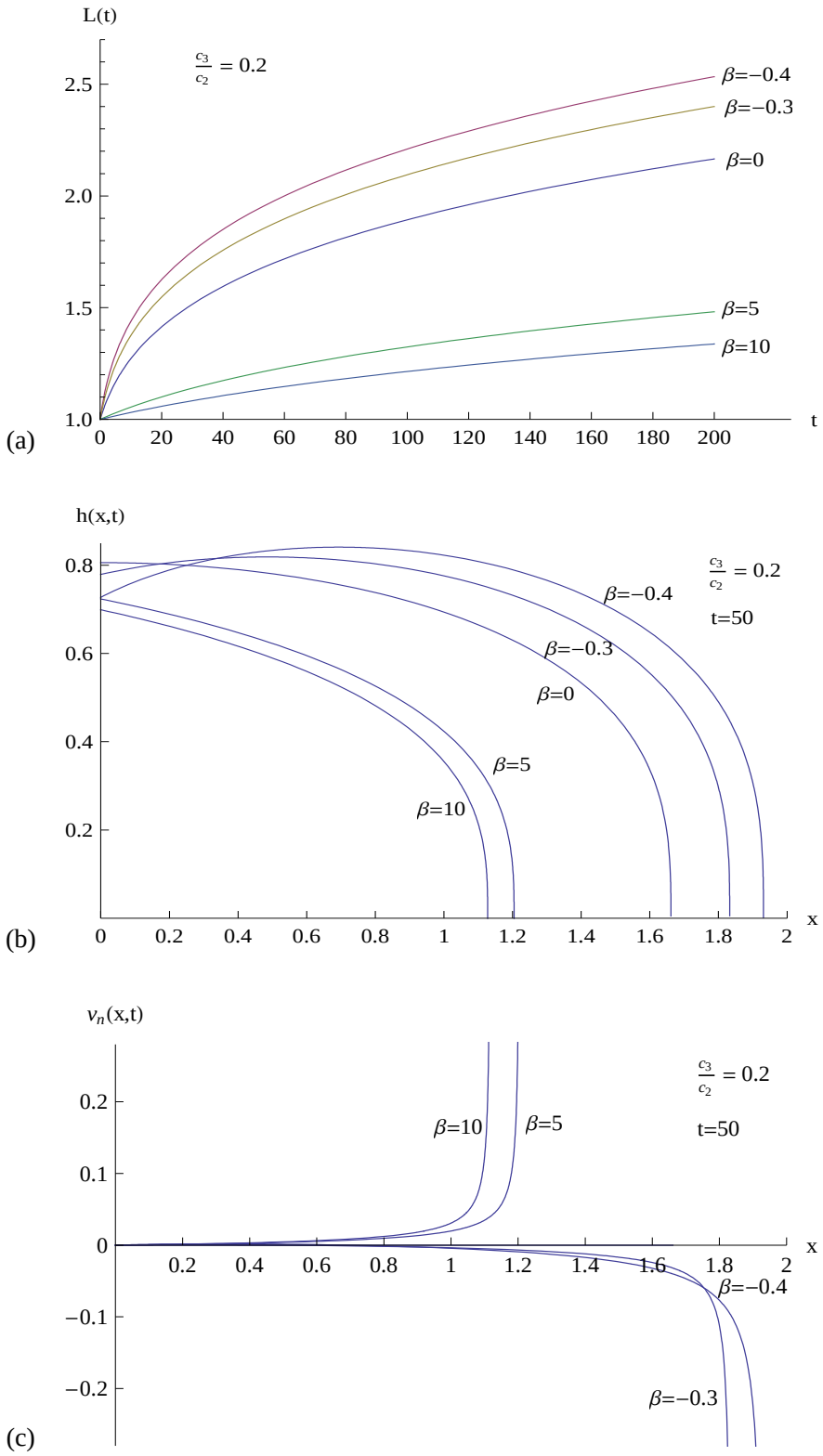
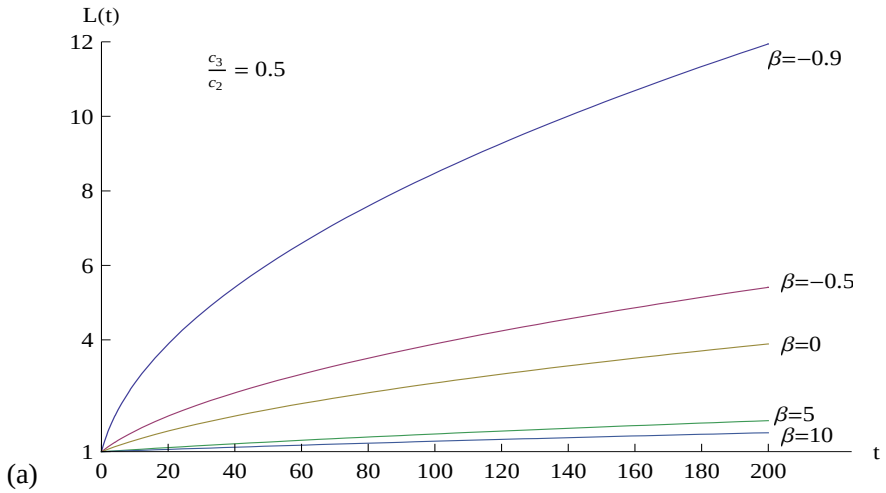
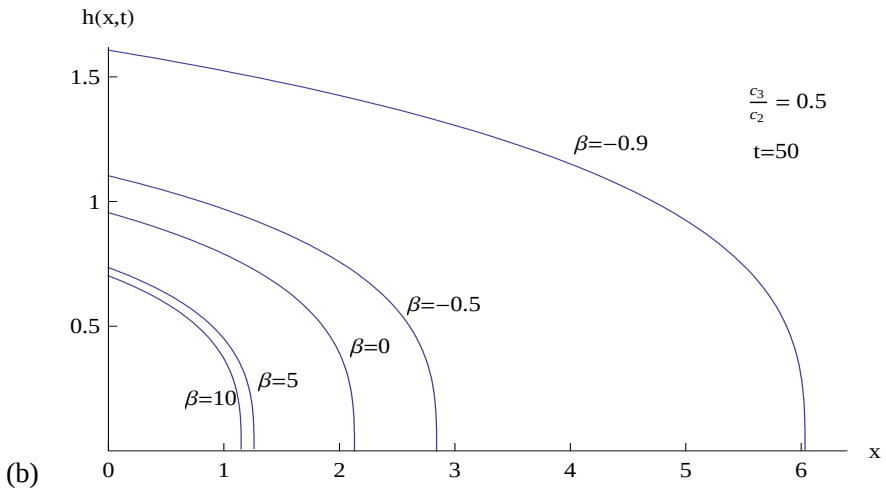


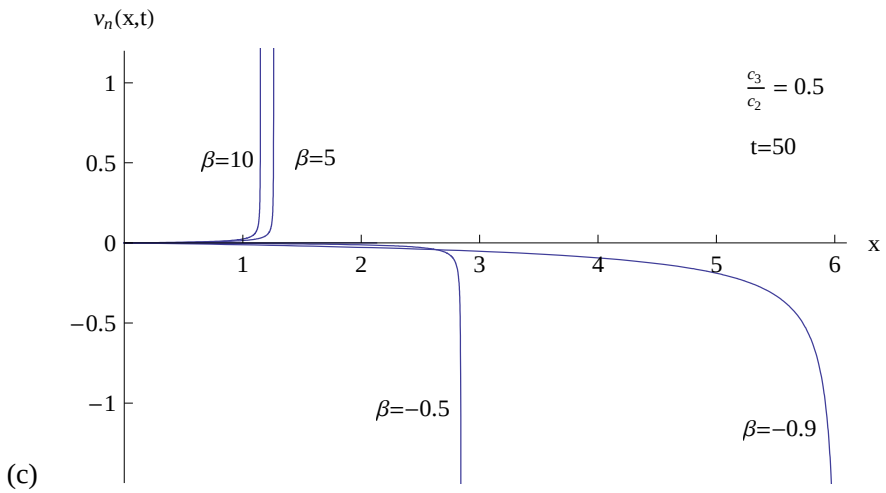
Figure 5.8.3: Graphs for $\frac{c_3}{c_2} = 0.2$ and a selection of values of β : (a) Fracture length $L(t)$ plotted against time; (b) Fracture half-width $h(x,t)$ plotted against x at time $t = 50$; (c) Leak-off fluid velocity $v_n(x,t)$ plotted against x at time $t = 50$.



(a)

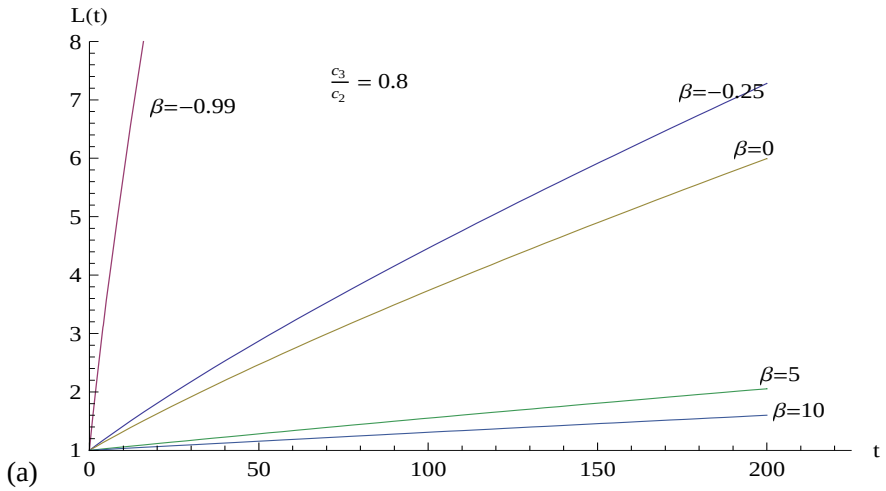


(b)

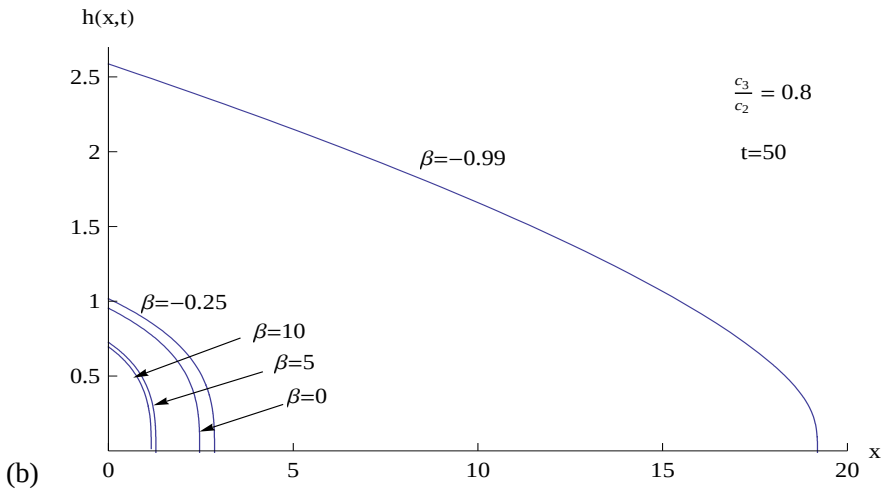


(c)

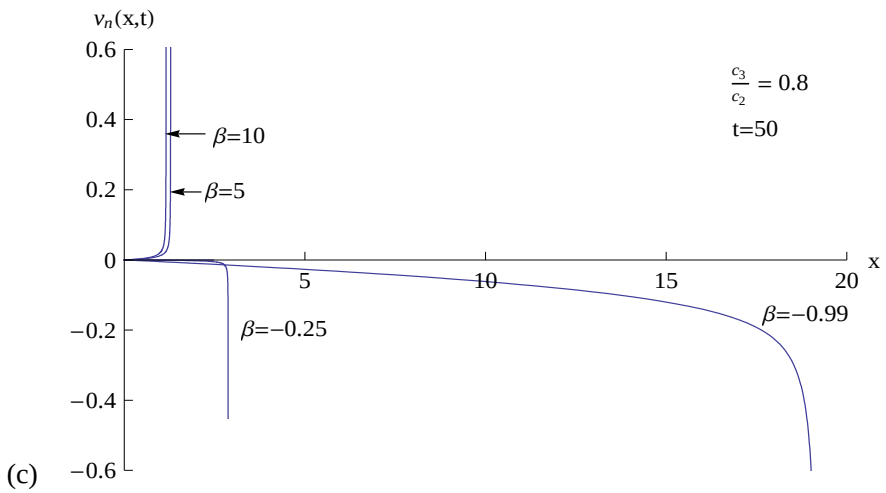
Figure 5.8.4: Graphs for $\frac{c_3}{c_2} = 0.5$ and a selection of values of β : (a) Fracture length $L(t)$ plotted against time; (b) Fracture half-width $h(x,t)$ plotted against x at time $t = 50$; (c) Leak-off fluid velocity $v_n(x,t)$ plotted against x at time $t = 50$.



(a)

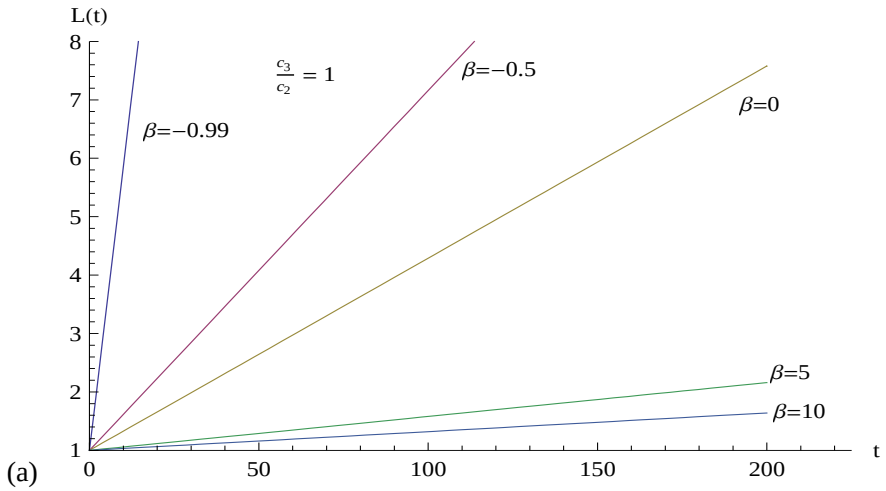


(b)

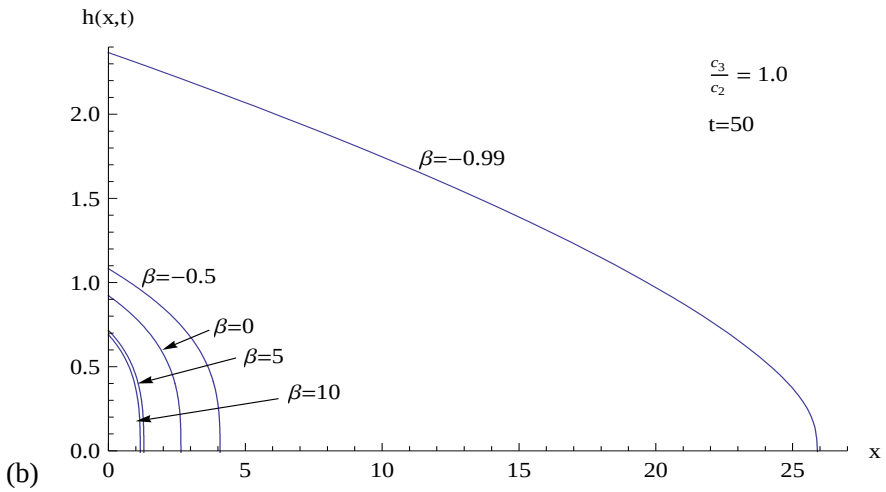


(c)

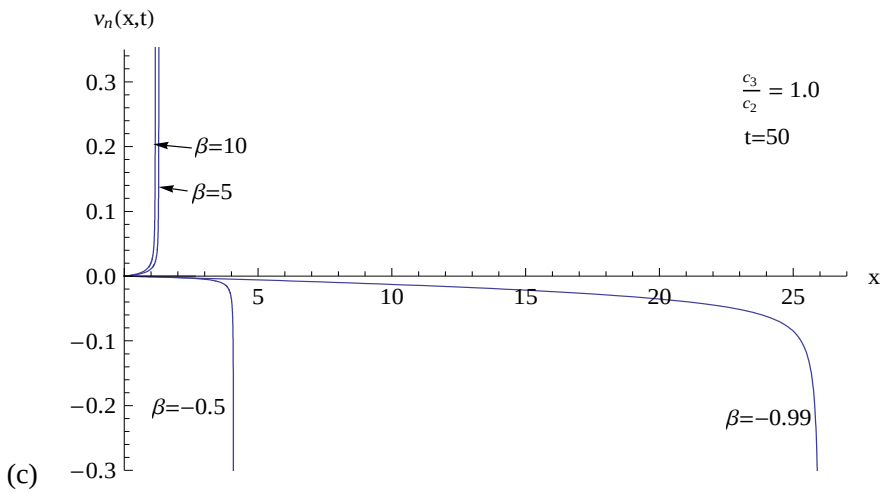
Figure 5.8.5: Graphs for $\frac{c_3}{c_2} = 0.8$ and a selection of values of β : (a) Fracture length $L(t)$ plotted against time; (b) Fracture half-width $h(x,t)$ plotted against x at time $t = 50$; (c) Leak-off fluid velocity $v_n(x,t)$ plotted against x at time $t = 50$.



(a)



(b)



(c)

Figure 5.8.6: Graphs for $\frac{c_3}{c_2} = 1$ and a selection of values of β : (a) Fracture length $L(t)$ plotted against time; (b) Fracture half-width $h(x,t)$ plotted against x at time $t = 50$; (c) Leak-off fluid velocity $v_n(x,t)$ plotted against x at time $t = 50$.

5.8.2 Graphical results for fixed β and varying values of $\frac{c_3}{c_2}$

In this section we will discuss the graphs obtained from the numerical solution of the two Initial Value Problems of Section 5.7. The graphs are those for which $\frac{c_3}{c_2}$ is varied and β is kept fixed. This allows us to study the effect of $\frac{c_3}{c_2}$ on the evolution of the fracture half-width and propagation of the fracture length. The physical significance of the parameter $\frac{c_3}{c_2}$ for $0 \leq \frac{c_3}{c_2} \leq 1$ is given in Table 3.7.1.

In Figure 5.8.7, $\beta = -0.9$ and the solution exists for $0.38 \leq \frac{c_3}{c_2} < \infty$. The solutions obtained using the values of $\frac{c_3}{c_2}$ in the range $0.38 \leq \frac{c_3}{c_2} < 0.43$ describe fluid extraction out of the fracture at the entry. For $0.43 < \frac{c_3}{c_2} < \infty$, the solutions obtained describe fluid injection into the fracture at the fracture entry. When $\frac{c_3}{c_2} = 0.43$, the fluid injection rate at the fracture entry vanishes and the analytical solution, (5.3.15) to (5.3.19), applies. All solutions have fluid injection at the fluid/rock interface. For all solutions presented, $L(t)$ increases with time and the increase is greater for larger values of $\frac{c_3}{c_2}$.

In Figure 5.8.8, $\beta = -0.5$ and the solution exists for $0.2 \leq \frac{c_3}{c_2} < \infty$. For $0.2 \leq \frac{c_3}{c_2} < 0.285$, the solutions describe fluid extraction out of fracture at the fracture entry while for $0.285 < \frac{c_3}{c_2} < \infty$, solutions for which fluid is injected into the fracture at the entry are obtained. When $\frac{c_3}{c_2} = 0.285$, equation (5.3.1) for which the rate of fluid injection, q_1, is zero is satisfied and the analytical solution (5.3.15) to (5.3.19) is valid. Equation (5.4.7) is satisfied when $\frac{c_3}{c_2} = 0.67$ and the second analytical solution (5.4.14) to (5.4.18) applies. When $\frac{c_3}{c_2} = 0.2$, the total volume of the fluid in the fracture is constant and the graph of $h(x,t)$ against x shows that the half-width first increases with x before decreasing. This may be as a result of the extraction of fluid at the fracture entry.

In Figure 5.8.9, $\beta = 0$ and the solution exists for $0.125 \leq \frac{c_3}{c_2} < \infty$. The solutions describing fluid extraction at the entry occur for $0.125 \leq \frac{c_3}{c_2} < 0.2$ and those describing fluid injection at the entry occur for $0.2 < \frac{c_3}{c_2} < \infty$. Since $\beta = 0$, all solutions have no fluid exchange at the fluid/rock interface and therefore the rock mass is impermeable. When $\frac{c_3}{c_2} = 0.2$, equation (5.3.1) for which the rate of fluid injection, q_1, vanishes is satisfied and the total volume of the fracture remains constant. When $\frac{c_3}{c_2} = 0.125$, fluid is extracted at the fracture entry and the graph of $h(x,t)$ against x again increases with x before decreasing.

In Figure 5.8.10, $\beta = 1$ and the solution exists for $0.0714 \leq \frac{c_3}{c_2} < \infty$. Solutions that describe fluid extraction at the fracture entry occur for $0.0714 \leq \frac{c_3}{c_2} < 0.125$ while solutions describing fluid injection at the entry occur for $0.125 < \frac{c_3}{c_2} < \infty$. Since $\beta = 1$, all solutions have leak-off at the fluid/rock interface. When $\frac{c_3}{c_2} = 0.125$, equation (5.3.1), for which the rate of fluid injection at the fracture entry vanishes, is satisfied. The line $\beta = 1$ is an asymptote for (5.4.7) in the $(\frac{c_3}{c_2}, \beta)$ plane. Hence no numerical solution exists when (5.4.7) is satisfied because $\beta = 1$ is only attained asymptotically. When $\frac{c_3}{c_2} = 0.0714$, $h(x,t)$ initially increases with x before decreasing. The smaller half-width at the fracture entry is due to the extraction of fluid at the entry.

In Figure 5.8.11, $\beta = 5$ and the solution exists for $0.026 \leq \frac{c_3}{c_2} < \infty$. Solutions that describe fluid extraction at the fracture entry occur for $0.026 \leq \frac{c_3}{c_2} < 0.05$ while for $0.05 < \frac{c_3}{c_2} < \infty$, there is always fluid injection at the entry. When $\frac{c_3}{c_2} = 0.05$, the rate of fluid injection at the fracture entry vanishes and the analytical solution, (5.3.15) to (5.3.19), applies. The fracture length increases as $\frac{c_3}{c_2}$ increases and when $\frac{c_3}{c_2} = 0.026$ the graph of $h(x,t)$ against x has a smaller half-width at the fracture entry due to the extraction of fluid at the entry.

We see that as β increases corresponding to larger leak-off velocity, the growth of the fracture length in Figures 5.8.7a to 5.8.11a decreases.

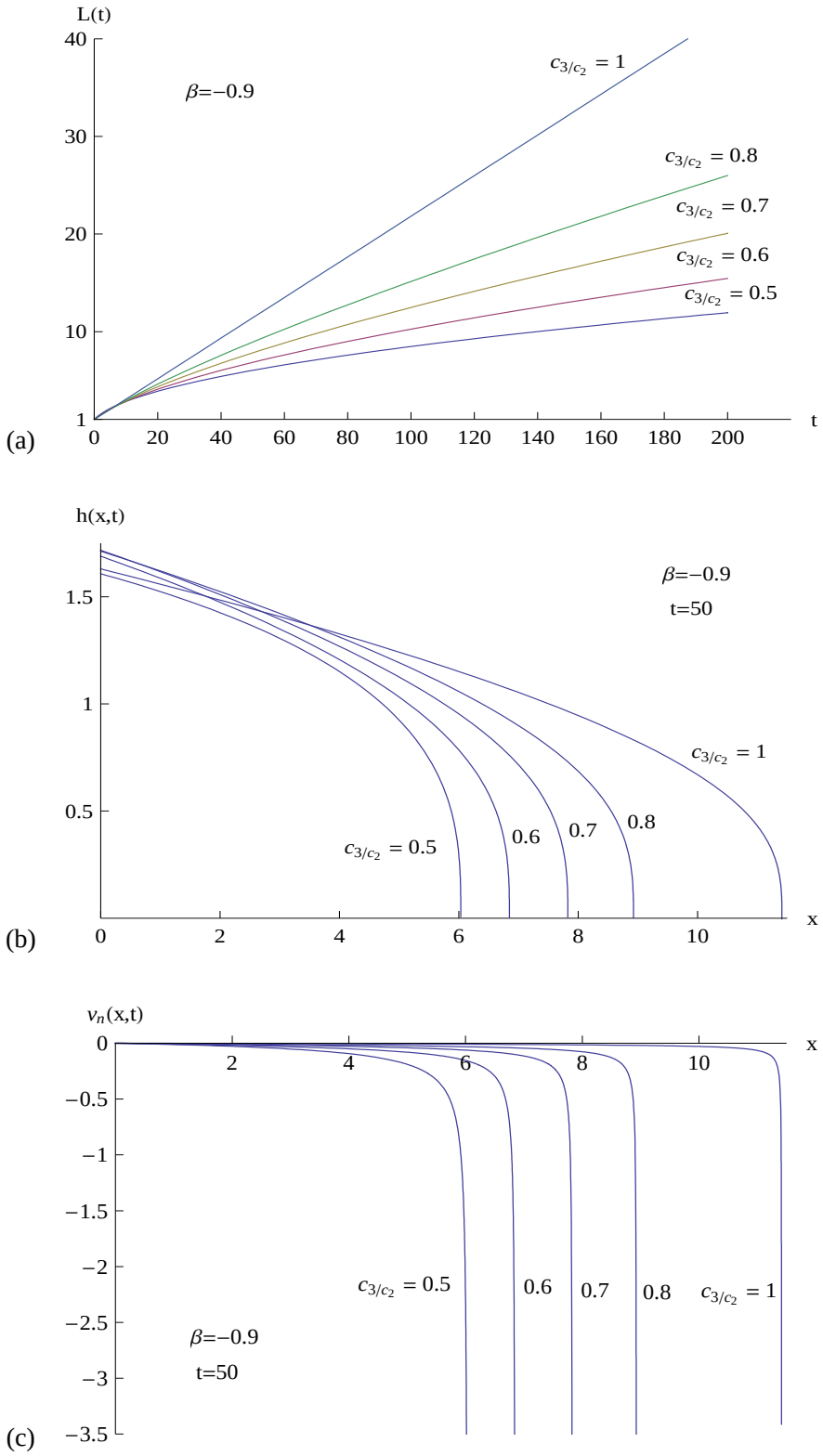


Figure 5.8.7: Graphs for $\beta = -0.9$ and a selection of values of $\frac{c_3}{c_2}$: (a) Fracture length $L(t)$ plotted against time; (b) Fracture half-width $h(x,t)$ plotted against x at time $t = 50$; (c) Leak-off fluid velocity $v_n(x,t)$ plotted against x at time $t = 50$.

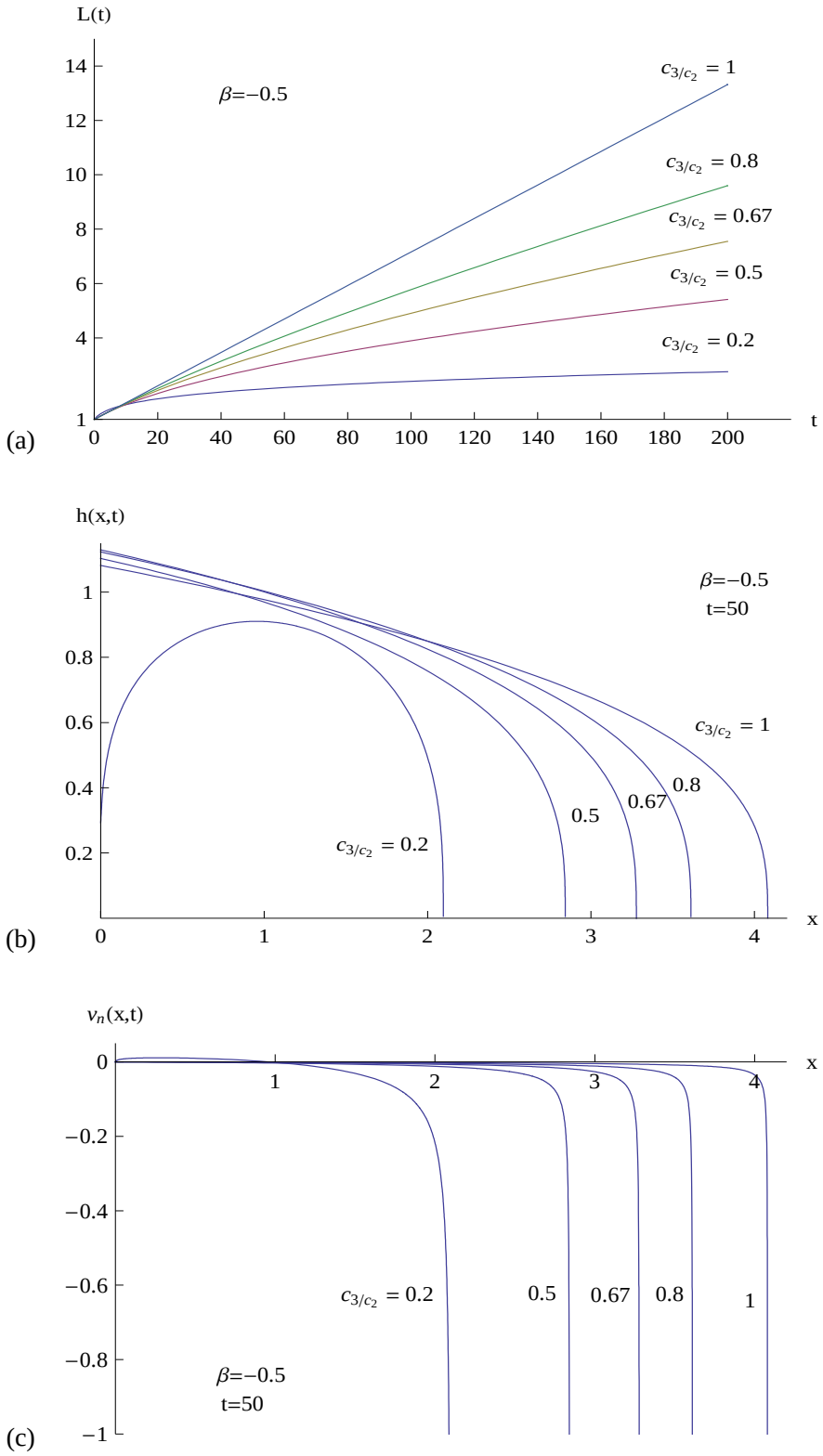


Figure 5.8.8: Graphs for $\beta = -0.5$ and a selection of values of $\frac{c_3}{c_2}$: (a) Fracture length $L(t)$ plotted against time; (b) Fracture half-width $h(x,t)$ plotted against x at time $t = 50$; (c) Leak-off fluid velocity $v_n(x,t)$ plotted against x at time $t = 50$.

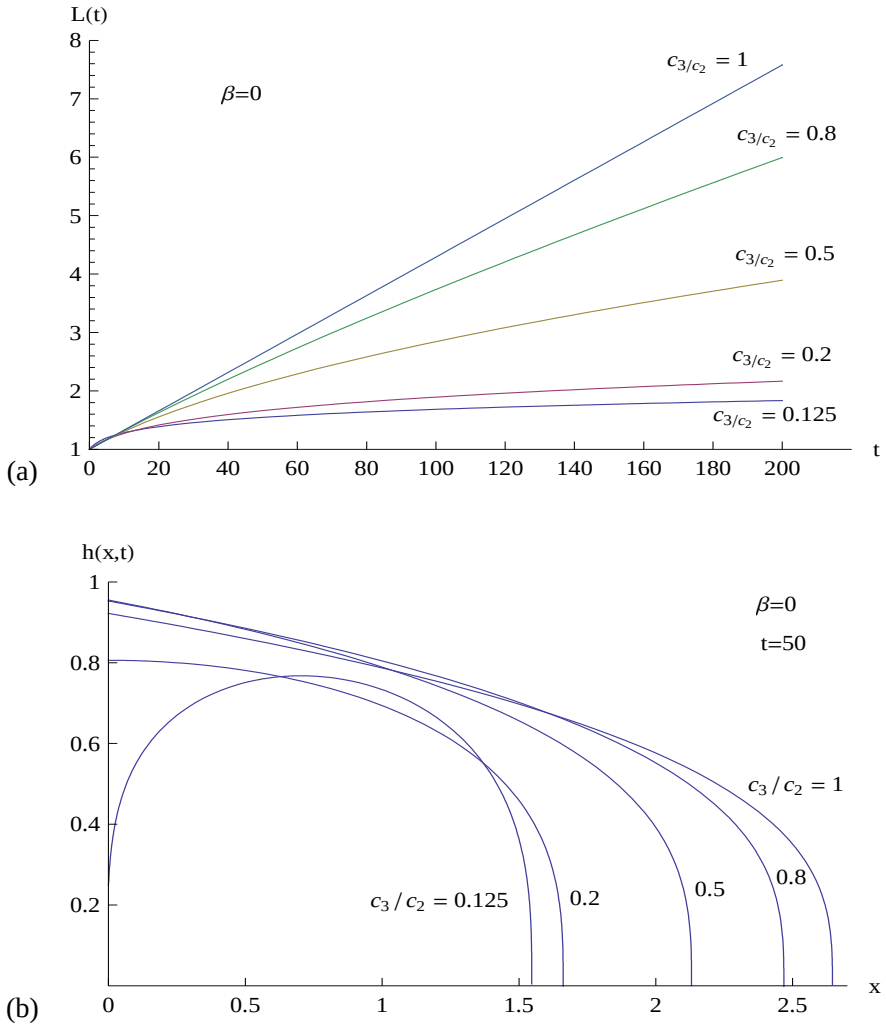
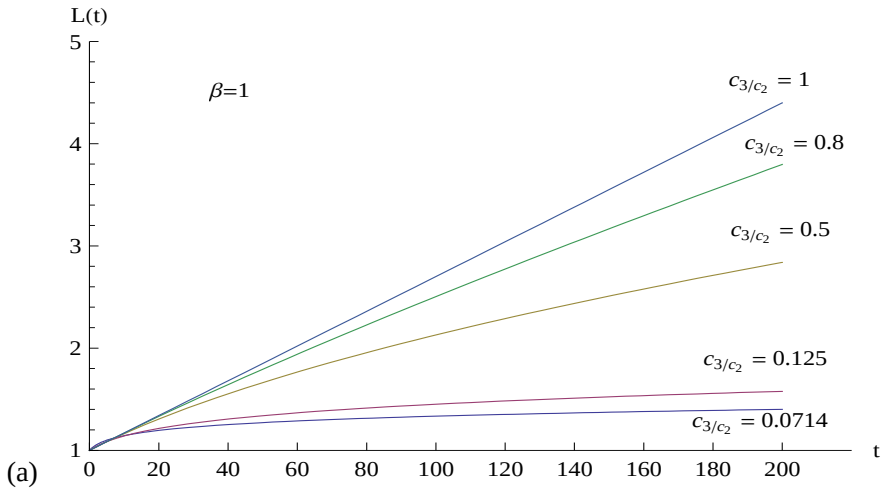
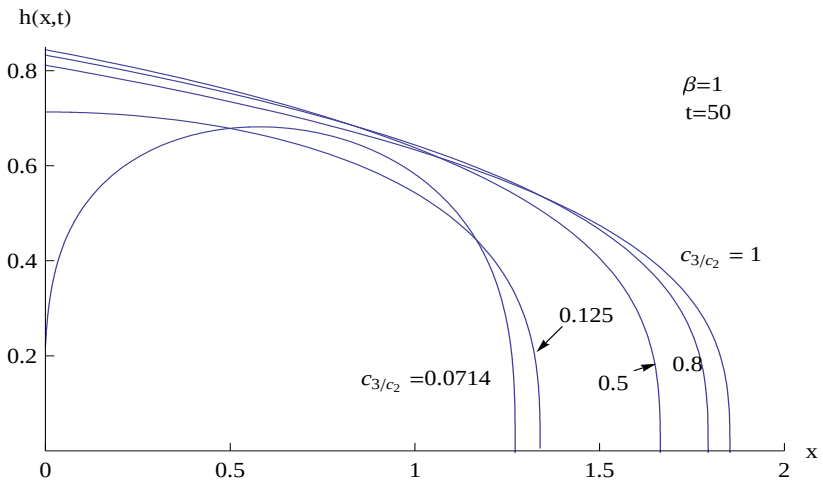


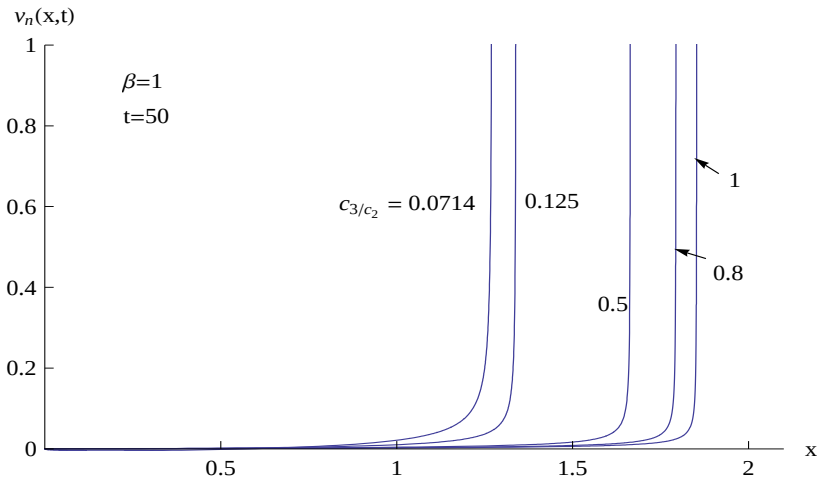
Figure 5.8.9: Graphs for $\beta = 0$ and a selection of values of $\frac{c_3}{c_2}$: (a) Fracture length $L(t)$ plotted against time; (b) Fracture half-width $h(x,t)$ plotted against x at time $t = 50$. The leak-off velocity, $v_n(x,t)$, is zero for all values of $\frac{c_3}{c_2}$ and the rock is impermeable.



(a)

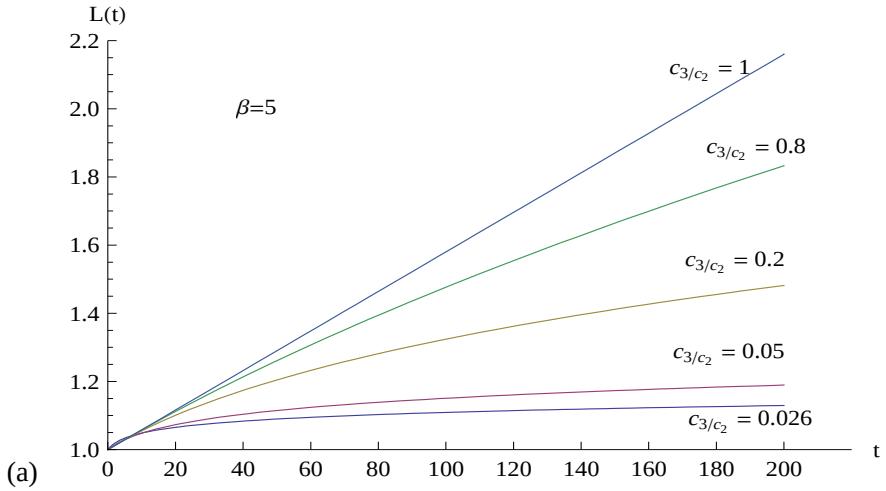


(b)

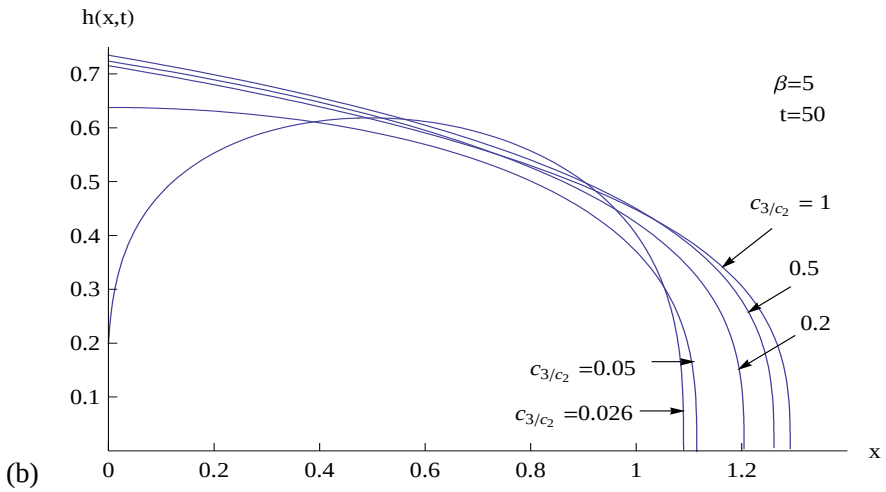


(c)

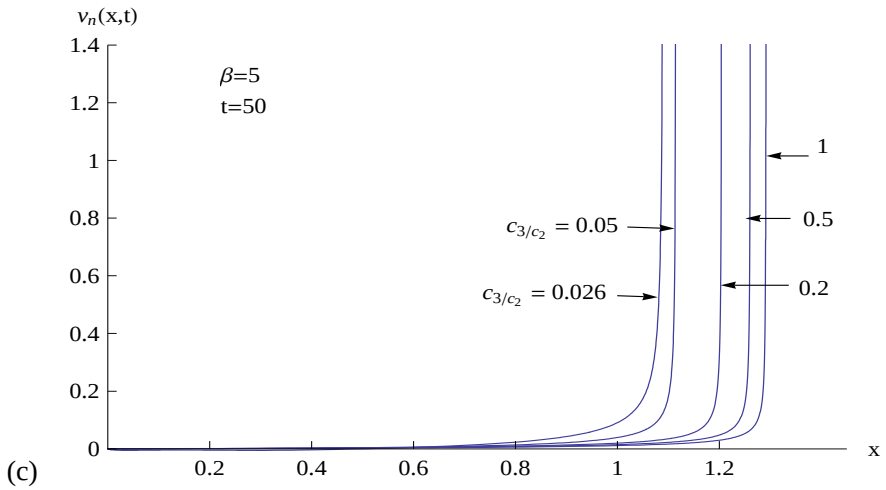
Figure 5.8.10: Graphs for $\beta = 1$ and a selection of values of $\frac{c_3}{c_2}$: (a) Fracture length $L(t)$ plotted against time; (b) Fracture half-width $h(x,t)$ plotted against x at time $t = 50$; (c) Leak-off fluid velocity $v_n(x,t)$ plotted against x at time $t = 50$.



(a)



(b)



(c)

Figure 5.8.11: Graphs for $\beta = 5$ and a selection of values of $\frac{c_3}{c_2}$: (a) Fracture length $L(t)$ plotted against time; (b) Fracture half-width $h(x,t)$ plotted against x at time $t = 50$; (c) Leak-off fluid velocity $v_n(x,t)$ plotted against x at time $t = 50$.

5.9 Conclusions

When the leak-off velocity v_n is proportional to the gradient of the fracture half-width, solutions depending essentially on the parameters $\frac{c_3}{c_2}$ and β are obtained.

Numerical and analytical solutions were found for the volume of the fracture, $V(t)$, fracture length, $L(t)$, fracture half-width, $h(x,t)$, leak-off velocity, $v_n(x,t)$ and the fluid presssure $p(x,t)$ for values of $\frac{c_3}{c_2}$ and β of physical significance in the range $-\infty < \frac{c_3}{c_2} < \infty$ and $-1 < \beta < \infty$. Unlike in Chapter 4 where exponential solutions were obtained for the two special cases leading to exact analytical solutions, exponential solutions exist only for the second special case which was derived in Section 5.4. They do not exist for the first special case which was derived in Section 5.3. The non-existence of exponential solutions in Section 5.3 is because the exact analytical solutions obtained are valid only for values of the parameter $\frac{c_3}{c_2}$ satisfying $0 < \frac{c_3}{c_2} < 0.5$. Exponential solutions exists only in the limit $\frac{c_3}{c_2} \to \infty$. Approximate power law solutions for $L(t)$ and $V(t)$ which exist for large times can be found for the two special cases.

Three regions of the $(\frac{c_3}{c_2}, \beta)$ plane were found for $\frac{c_3}{c_2} > 0$. The role of the curve

$$\beta = \frac{5\left(\frac{1}{5} - \frac{c_3}{c_2}\right)}{3\frac{c_3}{c_2}} \tag{5.9.1}$$

as a dividing curve between solutions for which fluid is injected at the fracture entry and for which fluid is extracted at the fracture entry was explained in Chapter 4. The rate of fluid injection or extraction at the entry vanishes when (5.9.1) is satisfied. The curve

$$\beta = \frac{4\left(\frac{1}{8} - \frac{c_3}{c_2}\right)}{3\frac{c_3}{c_2}} \tag{5.9.2}$$

separates the solution space from the space for which solutions do not exist.

In Figures 5.8.1a to 5.8.6a, the length of the fracture increases when there is leak-off or fluid injection at the fluid/rock interface and also when the rock is impermeable. When there is leak-off the increase in length is less than when the rock is impermeable while when there is fluid injection at the interface the length is greater than when the rock is impermeable.

We saw from Figures 5.8.7a to 5.8.11a that an increase in the parameter $\frac{c_3}{c_2}$ is associated with an increase in fracture length. This applies both when there is leak-off and when there is

fluid injection at the interface. It also applies when the rock is impermeable. As β is increased, corresponding to weaker fluid injection at interface or stronger leak-off, the extent of growth of the length of the fracture decreased.

The graphs of the leak-off velocity in Figures 5.8.1c to 5.8.11c reflect the fact that v_n is proportional to $-\beta\frac{\partial h}{\partial x}$.

The gradient of the fracture half-width, $\frac{\partial h}{\partial x}$, tends to $-\infty$ as $x \to L(t)$ for all the numerical and analytical solutions. Hence the thin film theory breaks down in the neighbourhood of the tip of the fracture.

By solving the two Initial Value Problems for the special cases (5.3.1) and (5.4.7) which yield exact analytical solutions, we were able to check the accuracy of the numerical solution. We found that for the two special cases the agreement between the analytical and numerical solutions was to five decimal places except near the fracture tip where the agreement was to three decimal places. The graphs of the numerical and analytical solutions overlap.

Chapter 6

Conclusions

We have shown in this work that similarity solutions can be derived for a fluid-driven pre-existing fracture in permeable rock in a similar way to that in an impermeable rock (Fitt et al, 2007) by the adoption of the PKN elasticity hypothesis, lubrication theory and using the Lie point symmetries of the resulting nonlinear diffusion equation. Numerical results were also obained by reformulating the boundary value problem as a pair of initial value problems which are easier to solve than the original boundary value problem. The pair of initial value problems was solved using a shooting method. The boundary value problem obtained in this work was in terms of two dependent variables F and G. In order to solve completely the problem, two special relations between F and G were considered. In the first relation, G is proportional to F and in the second relation, G is proportional to $\frac{dF}{du}$. The proportionality constant β plays a key role in understanding flow conditions at the fluid/rock interface. Similarity solutions were obtained for each of these relations.

The similarity solutions have several features. They describe the fluid-driven propagation of a pre-existing fracture under varying operating conditions shown in Table 3.7.1. Pre-existing fractures play a key role in the success of hydraulic fracturing as a means of fracturing rock in the mining and petroleum industries. The solutions depend essentially on two undetermined parameters, $\frac{c_3}{c_2}$ and β, which can be chosen to impose a range of operating conditions at the fracture entry and at the fluid/rock interface. These parameters were varied to obtain a range of models which were solved numerically. For each of the two special relations between F and G two sets of analytical solutions were derived and each set of analytical solutions sat-

isfies a special relation between the parameters $\frac{c_3}{c_2}$ and β.

Solutions were also found for a two-dimensional fluid-driven pre-existing fracture with length and volume proportional to $\exp(\alpha t)$ where α is a constant. For large times the fracture length and volume behave approximately as power law solutions of the form at^b where a and b are constants.

Various operating conditions were considered. For example, constant rate of fluid injection into the fracture at the entry as well as constant rate of fluid leak-off at the fluid/rock interface occur when $\frac{c_3}{c_2} = 0.8$ while constant pressure at the entry, $p(0,t)$, occurs for $\frac{c_3}{c_2} = 0.5$. Operating conditions resulting in a constant growth rate of the fracture volume occur for $\frac{c_3}{c_2} = 0.2$.

In our model, fluid can enter into the fracture at the fluid/rock interface. This is possible when the rock mass is saturated with fluid. We assumed that the fluid in the rock mass is the same as the fluid in the fracture. When $v_n \propto h$, the velocity at which fluid enters the fracture through the interface is bounded since $F(u)$ is bounded and β has a minimum value of -2.66.

The discovery of an n-shaped fracture due to fluid extraction at the entry was unexpected. Fluid extraction at the entry reduces the speed of evolution of the interface near the entry relative to the interface away from the fracture entry.

When $G(u) = \beta F(u)$ the n-shaped fracture exists when

$$\frac{8\left(\frac{1}{8} - \frac{c_3}{c_2}\right)}{3\frac{c_3}{c_2}} < \beta < \frac{5\left(\frac{1}{5} - \frac{c_3}{c_2}\right)}{3\frac{c_3}{c_2}}, \quad \frac{c_3}{c_2} > 0, \tag{6.0.1}$$

or equivalently when

$$\frac{1}{(8+3\beta)} < \frac{c_3}{c_2} < \frac{1}{(5+3\beta)}, \quad \beta > -\frac{8}{3}, \tag{6.0.2}$$

which is the range for extraction of fluid at the fracture entry to exist when $\frac{c_3}{c_2} > 0$. When $G(u) = -\beta u \frac{dF}{du}$ the corresponding ranges are

$$\frac{4\left(\frac{1}{8} - \frac{c_3}{c_2}\right)}{3\frac{c_3}{c_2}} < \beta < \frac{5\left(\frac{1}{5} - \frac{c_3}{c_2}\right)}{3\frac{c_3}{c_2}}, \quad 0 < \frac{c_3}{c_2} < \frac{1}{2} \tag{6.0.3}$$

and

$$\frac{1}{2\,(4+3\beta)} < \frac{c_3}{c_2} < \frac{1}{(5+3\beta)}, \quad \beta > -1. \tag{6.0.4}$$

The n-shape is maximum at the lower limit and vanishes at the upper limit since

$$\frac{\partial h}{\partial x}(0,t) = 0 \quad \text{when} \quad \beta = \frac{5\left(\frac{1}{5} - \frac{c_3}{c_2}\right)}{3\frac{c_3}{c_2}}. \tag{6.0.5}$$

The lubrication theory velocity profile

$$v_x(x,z,t) = -\frac{1}{2}\left(h^2 - z^2\right)\frac{\partial p}{\partial x}, \tag{6.0.6}$$

which was derived using the thin film approximation and which represents parallel flow is totally incorrect in the neighbourhood of the fracture tip. Yet by using it, solutions to the governing equations can be obtained without invoking any further condition at the fracture tip. The asymptotic relation used to commence the numerical integration of the differential equation was obtained from (6.0.6) and is not an externally imposed condition. Also, at the tip of the fracture, the gradient of the half-width satisfies $\frac{\partial h}{\partial x} = -\infty$. Lubrication theory breaks down only in the neighbourhood of the tip of the fracture.

In the solutions which were considered the length of the fracture always increased even when there was extraction of fluid at the fracture entry or leak-off of fluid at the fluid/rock interface. When there is leak-off of fluid the increase in length is less than in an impermeable rock while when there is injection of fluid at the interface the increase in length is greater than in an impermeable rock.

The two exact analytical solutions which were derived for

$$\beta = \frac{5\left(\frac{1}{5} - \frac{c_3}{c_2}\right)}{3\frac{c_3}{c_2}}, \tag{6.0.7}$$

one when $G(u) = \beta F(u)$ and the other when $G(u) = -\beta u\frac{dF}{du}$, describe the evolution of the fluid-filled fracture when there is no injection of fluid at the entry. They may be useful in modelling the evolution of the fracture when the entrance is sealed and it evolves as a result of leak-off or fluid inflow at the fluid/rock interface

For both $G(u) = \beta F(u)$ and $G(u) = -\beta u\frac{dF}{du}$ regions of the $\left(\frac{c_3}{c_2}, \beta\right)$ plane were found which describe solutions with fluid extraction at the fracture entry. These solutions may be useful in industries such as the oil industry in which fluid is extracted from the fracture.

In the PKN model, the excess fluid pressure, $p(x,t)$, is proportional to the half-width, $h(x,t)$, of the fracture. Hence operating conditions based on pressure can be imposed at the fracture entry to obtain models which are solved either analytically or, in general, numerically. However, the shortcoming of this model is that the excess pressure necessarily vanishes at the fracture tip and therefore no stress intensity factor can be defined.

Conservation laws for the nonlinear diffusion equations were not investigated in this work. Further work can be done, for example in the case when the fluid is non-Newtonian. Flow of non-Newtonian fluids in fractures is of interest in several geophysical and industrial applications. At ultra-high pressure the dependence of viscosity on pressure can be important. Finally, the problem of a fluid-driven fracture in which the fluid flow in the fracture is turbulent can be investigated.

APPENDIX A

Derivation of the Lie point symmetries of the nonlinear diffusion equation for fluid driven fracture of permeable rock

In this section we will show completely the derivation of the Lie point symmetries of the nonlinear diffusion equation

$$\frac{\partial h}{\partial t} = \frac{\Lambda}{3}\frac{\partial}{\partial x}\left(h^3\frac{\partial h}{\partial x}\right) - v_n(x,t). \tag{A.1}$$

The diffusion equation (A.1) describes the evolution of the fracture half-width during the process of hydraulic fracturing in a permeable rock. Since the rock is permeable fluid leaks off into the surrounding rock formation. The leak off velocity relative to the fluid/rock interface is $v_n(x,t)$.

Equation (A.1) is rewritten as

$$h_t - \frac{\Lambda}{3}h^3h_{xx} - \Lambda h^2h_x^2 + v_n = 0. \tag{A.2}$$

The Lie point symmetry generator

$$X = \xi^1(t,x,h)\frac{\partial}{\partial t} + \xi^2(t,x,h)\frac{\partial}{\partial x} + \eta(t,x,h)\frac{\partial}{\partial h} \tag{A.3}$$

of equation (A.1) is derived by solving the determining equation

$$X^{[2]}[h_t - \frac{\Lambda}{3}h^3h_{xx} - \Lambda h^2h_x^2 + v_n]\Big|_{h_t=\frac{\Lambda}{3}h^3h_{xx}+\Lambda h^2h_x^2-v_n} = 0, \tag{A.4}$$

for $\xi^1(t,x,h)$, $\xi^2(t,x,h)$ and $\eta(t,x,h)$ where $X^{[2]}$, the second prolongation of X, is given by

$$X^{[2]} = X + \zeta_1 \frac{\partial}{\partial h_t} + \zeta_2 \frac{\partial}{\partial h_x} + \zeta_{11} \frac{\partial}{\partial h_{tt}} + \zeta_{12} \frac{\partial}{\partial h_{tx}} + \zeta_{22} \frac{\partial}{\partial h_{xx}} \tag{A.5}$$

and ζ_i and ζ_{ij} are defined by

$$\zeta_i = D_i(\eta) - h_k D_i(\xi^k), \qquad i = 1,2, \tag{A.6}$$

$$\zeta_{ij} = D_j(\zeta_i) - h_{ik} D_j(\xi^k), \qquad i,j = 1,2, \tag{A.7}$$

with summation over the repeated index k from 1 to 2. The total derivatives with respect to the independent variables t and x are given by

$$D_1 = D_t = \frac{\partial}{\partial t} + h_t \frac{\partial}{\partial h} + h_{tt} \frac{\partial}{\partial h_t} + h_{xt} \frac{\partial}{\partial h_x} + \ldots \,, \tag{A.8}$$

$$D_2 = D_x = \frac{\partial}{\partial x} + h_x \frac{\partial}{\partial h} + h_{tx} \frac{\partial}{\partial h_t} + h_{xx} \frac{\partial}{\partial h_x} + \ldots . \tag{A.9}$$

The leak-off velocity v_n is treated as an arbitrary function of the independent variables t and x.

From the determining equation (A.4), we obtain

$$\begin{aligned} &\xi^1 \frac{\partial v_n}{\partial t} + \xi^2 \frac{\partial v_n}{\partial x} + \eta\left(-\Lambda h^2 h_{xx} - 2\Lambda h h_x^2\right) + \zeta_1 \\ &+\zeta_2\left(-2\Lambda h^2 h_x\right) + \zeta_{22}\left(-\frac{\Lambda}{3}h^3\right)\Big|_{h_t = \frac{\Lambda}{3}h^3 h_{xx} + \Lambda h^2 h_x^2 - v_n} = 0. \end{aligned} \tag{A.10}$$

We now calculate the expressions for ζ_1, ζ_2, and ζ_{22} according to equations (A.6) and (A.7):

$$\zeta_1 = D_t(\eta) - h_t D_t(\xi^1) - h_x D_t(\xi^2), \tag{A.11}$$

$$\zeta_2 = D_x(\eta) - h_t D_x(\xi^1) - h_x D_x(\xi^2), \tag{A.12}$$

$$\zeta_{22} = D_x(\zeta_2) - h_{xt} D_x(\xi^1) - h_{xx} D_x(\xi^2). \tag{A.13}$$

Expanding equations (A.11), (A.12) and (A.13) using (A.8) and (A.9), we obtain

$$\zeta_1 = \eta_t + h_t\eta_h - h_t\left(\xi^1_t + h_t\xi^1_h\right) - h_x\left(\xi^2_t + h_t\xi^2_h\right), \tag{A.14}$$

$$\zeta_2 = \eta_x + h_x\eta_h - h_t\left(\xi^1_x + h_x\xi^1_h\right) - h_x\left(\xi^2_x + h_x\xi^2_h\right), \tag{A.15}$$

$$\begin{aligned}\zeta_{22} &= D_x\left(D_x(\eta) - h_tD_x(\xi^1) - h_xD_x(\xi^2)\right) - h_{xt}D_x(\xi^1) - h_{xx}D_x(\xi^2)\\ &= D^2_x(\eta) - h_tD^2_x(\xi^1) - 2h_{xt}D_x(\xi^1) - 2h_{xx}D_x(\xi^2) - h_xD^2_x(\xi^2)\\ &= \eta_{xx} + 2h_x\eta_{xh} + h^2_x\eta_{hh} + h_{xx}\eta_h - h_t\xi^1_{xx} - 2h_xh_t\xi^1_{xh} - h_th^2_x\xi^1_{hh} - h_th_{xx}\xi^1_h\\ &\quad -2h_{xt}\xi^1_x - 2h_xh_{xt}\xi^1_h - 2h_{xx}\xi^2_x - 3h_xh_{xx}\xi^2_h - h_x\xi^2_{xx} - 2h^2_x\xi^2_{xh} - h^3_x\xi^2_{hh}.\end{aligned} \tag{A.16}$$

The expressions for ζ_1, ζ_2 and ζ_{22} are substituted into the determining equation (A.10) to obtain

$$\begin{aligned}&\xi^1\frac{\partial v_n}{\partial t} + \xi^2\frac{\partial v_n}{\partial x} + \eta\left(-\Lambda h^2h_{xx} - 2\Lambda hh^2_x\right) + \eta_t + h_t\eta_h - h_t\left(\xi^1_t + h_t\xi^1_h\right)\\ &-h_x\left(\xi^2_t + h_t\xi^2_h\right) - 2\Lambda h^2h_x\left(\eta_x + h_x\eta_h - h_t\left(\xi^1_x + h_x\xi^1_h\right) - h_x\left(\xi^2_x + h_x\xi^2_h\right)\right)\\ &-\frac{\Lambda}{3}h^3\Big(\eta_{xx} + 2h_x\eta_{xh} + h^2_x\eta_{hh} + h_{xx}\eta_h - h_t\xi^1_{xx} - 2h_xh_t\xi^1_{xh}\\ &-h_th^2_x\xi^1_{hh} - h_th_{xx}\xi^1_h - 2h_{xt}\xi^1_x - 2h_xh_{xt}\xi^1_h - 2h_{xx}\xi^2_x\\ &-3h_xh_{xx}\xi^2_h - h_x\xi^2_{xx} - 2h^2_x\xi^2_{xh} - h^3_x\xi^2_{hh}\Big)\Big|_{h_t=\frac{\Lambda}{3}h^3h_{xx}+\Lambda h^2h^2_x-v_n} = 0.\end{aligned} \tag{A.17}$$

We now expand equation (A.17), replacing h_t using the partial differential equation. This gives a linear homogenous partial differential equation of order 2 for the unknown functions

$\xi^1(t,x,h)$, $\xi^2(t,x,h)$ and $\eta(t,x,h)$:

$$
\begin{aligned}
&\xi^1\frac{\partial v_n}{\partial t}+\xi^2\frac{\partial v_n}{\partial x}-\Lambda h^2h_{xx}\eta-2\Lambda hh_x^2\eta+\eta_t+\frac{\Lambda}{3}h^3h_{xx}\eta_h+\Lambda h^2h_x^2\eta_h\\
&-v_n\eta_h-\frac{\Lambda}{3}h^3h_{xx}\xi_t^1-\Lambda h^2h_x^2\xi_t^1+v_n\xi_t^1-\frac{\Lambda^2}{9}h^6h_{xx}^2\xi_h^1-\frac{\Lambda^2}{3}h^5h_x^2h_{xx}\xi_h^1\\
&+\frac{\Lambda}{3}h^3h_{xx}v_n\xi_h^1-\frac{\Lambda^2}{3}h^5h_x^2h_{xx}\xi_h^1-\Lambda^2h^4h_x^4\xi_h^1+\Lambda h^2h_x^2v_n\xi_h^1+\frac{\Lambda}{3}h^3h_{xx}v_n\xi_h^1+\Lambda h^2h_x^2v_n\xi_h^1\\
&-v_n^2\xi_h^1-h_x\xi_t^2-\frac{\Lambda}{3}h^3h_xh_{xx}\xi_h^2-\Lambda h^2h_x^3\xi_h^2+v_nh_x\xi_h^2-2\Lambda h^2h_x\eta_x\\
&-2\Lambda h^2h_x^2\eta_h+\frac{2\Lambda^2}{3}h^5h_xh_{xx}\xi_x^1+\frac{2\Lambda^2}{3}h^5h_x^2h_{xx}\xi_h^1+2\Lambda^2h^4h_x^3\xi_x^1+2\Lambda^2h^4h_x^4\xi_h^1-2\Lambda h^2h_xv_n\xi_x^1\\
&-2\Lambda h^2h_x^2v_n\xi_h^1+2\Lambda h^2h_x^2\xi_x^2+2\Lambda h^2h_x^3\xi_h^2-\frac{\Lambda}{3}h^3\eta_{xx}-\frac{2\Lambda}{3}h^3h_x\eta_{xh}-\frac{\Lambda}{3}h^3h_x^2\eta_{hh}\\
&-\frac{\Lambda}{3}h^3h_{xx}\eta_h+\frac{\Lambda^2}{9}h^6h_{xx}\xi_{xx}^1+\frac{\Lambda^2}{9}h^6h_{xx}\xi_{xx}^1+\frac{\Lambda^2}{3}h^5h_x^2\xi_{xx}^1-\frac{\Lambda}{3}h^3v_n\xi_{xx}^1+\frac{2\Lambda^2}{9}h^6h_xh_{xx}\xi_{xh}^1\\
&+\frac{2\Lambda^2}{3}h^5h_x^3\xi_{xh}^1-\frac{2\Lambda}{3}h^3h_xv_n\xi_{xh}^1+\frac{\Lambda^2}{9}h^6h_x^2h_{xx}\xi_{hh}^1+\frac{\Lambda^2}{3}h^5h_x^4\xi_{hh}^1-\frac{\Lambda}{3}h^3h_x^2v_n\xi_{hh}^1+\frac{\Lambda^2}{9}h^6h_{xx}^2\xi_h^1\\
&+\frac{\Lambda^2}{3}h^5h_x^2h_{xx}\xi_h^1-\frac{\Lambda}{3}h^3h_{xx}v_n\xi_h^1+\frac{2\Lambda}{3}h^3h_{xt}\xi_x^1+\frac{2\Lambda}{3}h^3h_xh_{xt}\xi_h^1+\frac{2\Lambda}{3}h^3h_{xx}\xi_x^2\\
&+\Lambda h^3h_xh_{xx}\xi_h^2+\frac{\Lambda}{3}h^3h_x\xi_{xx}^2+\frac{2\Lambda}{3}h^3h_x^2\xi_{xh}^2+\frac{\Lambda}{3}h^3h_x^3\xi_{hh}^2=0.
\end{aligned}
\tag{A.18}
$$

Since the functions to be determined do not depend on the derivatives of h, equation (A.18) is separated according to partial derivatives of h. One then equates the coefficients of the partial derivatives of h to zero. In this manner, (A.18) decomposes into an overdetermined system of equations in which there are more equations than unknown variables.

Equating the coefficients of the partial derivatives of h to zero yields

$$h_x^2 h_{xx}: \ \frac{h}{3}\xi_{hh}^1 + \xi_h^1 = 0, \tag{A.19}$$

$$h_x h_{xx}: \ \xi_h^2 + \Lambda h^2 \xi_x^1 + \frac{\Lambda}{3} h^3 \xi_{xh}^1 = 0, \tag{A.20}$$

$$h_x h_{xt}: \ \xi_h^1 = 0. \tag{A.21}$$

$$h_{xt}: \ \xi_x^1 = 0, \tag{A.22}$$

$$h_{xx}^2: \ 0 = 0 \tag{A.23}$$

$$h_{xx}: \ \eta + \frac{h}{3}\xi_t^1 - \frac{\Lambda}{9} h^4 \xi_{xx}^1 - \frac{2h}{3}\xi_x^2 - \frac{h}{3}\xi_h^1 v_n = 0, \tag{A.24}$$

$$h_x^4: \ \xi_h^1 + \frac{1}{3} h \xi_{hh}^1 = 0, \tag{A.25}$$

$$h_x^3: \ \xi_h^2 + 2\Lambda h^2 \xi_x^1 + \frac{2\Lambda}{3} h^3 \xi_{xh}^1 + \frac{1}{3} h \xi_{hh}^2 = 0, \tag{A.26}$$

$$\begin{aligned} h_x^2: \ & 2\eta + h\eta_h + h\xi_t^1 - 2h\xi_x^2 + \frac{1}{3} h^2 \eta_{hh} \\ & -\frac{\Lambda}{3} h^4 \xi_{xx}^1 + \frac{1}{3} h^2 \xi_{hh}^1 v_n - \frac{2}{3} h^2 \xi_{xh}^2 = 0, \end{aligned} \tag{A.27}$$

$$h_x: \ \xi_t^2 - \xi_h^2 v_n + 2\Lambda h^2 \eta_x + 2\Lambda h^2 \xi_x^1 v_n + \frac{2\Lambda}{3} h^3 \eta_{xh} + \frac{2\Lambda}{3} h^3 \xi_{xh}^1 v_n - \frac{\Lambda}{3} h^3 \xi_{xx}^2 = 0, \tag{A.28}$$

$$1: \ \xi^1 \frac{\partial v_n}{\partial t} + \xi^2 \frac{\partial v_n}{\partial x} + \eta_t - v_n \eta_h + v_n \xi_t^1 - v_n^2 \xi_h^1 - \frac{\Lambda}{3} h^3 \eta_{xx} - \frac{\Lambda}{3} h^3 v_n \xi_{xx}^1 = 0. \tag{A.29}$$

From (A.21) and (A.22),

$$\xi_h^1 = 0 \quad \text{and} \quad \xi_x^1 = 0. \tag{A.30}$$

It then follows from (A.30) that

$$\xi^1 = \xi^1(t) \tag{A.31}$$

Equation (A.20) reduces to

$$\xi_h^2 = 0, \tag{A.32}$$

which implies that

$$\xi^2 = \xi^2(x, t). \tag{A.33}$$

Equations (A.19) to (A.29) reduce to

$$h_{xx}: \ \eta + \frac{1}{3}h\xi_t^1 - \frac{2}{3}h\xi_x^2 = 0, \tag{A.34}$$

$$h_x^2: \ 2\eta + h\eta_h + h\xi_t^1 - 2h\xi_x^2 + \frac{1}{3}h^2\eta_{hh} = 0, \tag{A.35}$$

$$h_x: \ \xi_t^2 + 2\Lambda h^2\eta_x + \frac{2\Lambda}{3}h^3\eta_{xh} - \frac{\Lambda}{3}h^3\xi_{xx}^2 = 0. \tag{A.36}$$

$$1: \ \xi^1\frac{\partial v_n}{\partial t} + \xi^2\frac{\partial v_n}{\partial x} + \eta_t - \eta_h v_n + \xi_t^1 v_n - \frac{\Lambda}{3}h^3\eta_{xx} = 0. \tag{A.37}$$

From (A.34), we have

$$\eta = \frac{h}{3}\left(2\xi_x^2 - \xi_t^1\right). \tag{A.38}$$

Differentiating η with respect to x and then with respect to h, we obtain

$$\eta_x = \frac{2}{3}h\xi_{xx}^2 \quad \text{and} \quad \eta_{xh} = \frac{2}{3}\xi_{xx}^2. \tag{A.39}$$

We substitute η_x and η_{xh} given by (A.39) into (A.36) to obtain

$$\xi_t^2 + \frac{13\Lambda}{9}h^3\xi_{xx}^2 = 0. \tag{A.40}$$

Since ξ^2 is independent of h, we equate the coefficients of the powers of h to zero:

$$h^0: \ \xi_t^2 = 0, \tag{A.41}$$

$$h^3: \ \xi_{xx}^2 = 0. \tag{A.42}$$

Hence, we conclude from (A.41) and (A.32) that

$$\xi^2 = \xi^2(x) \tag{A.43}$$

and from (A.42) we have

$$\xi^2(x) = c_4 + c_3 x, \tag{A.44}$$

where c_3 and c_4 are constants. Substitute (A.44) into (A.38). Hence (A.38) becomes

$$\eta(t,h) = \frac{1}{3}h\left(2c_3 - \xi_t^1\right). \tag{A.45}$$

If (A.45) for $\eta(t,h)$ is substituted into (A.35) then (A.35) is identically satisfied. If (A.45) for $\eta(t,h)$ is substituted into (A.37) then (A.37) becomes

$$\xi^1\frac{\partial v_n}{\partial t}+\xi^2\frac{\partial v_n}{\partial x}+\frac{2}{3}\left(2\xi_t^1-c_3\right)v_n-\frac{1}{3}h\xi_{tt}^1=0. \tag{A.46}$$

The functions ξ^1, ξ^2, v_n are all independent of h. Hence equating the coefficients of powers of h on each side of (A.46) gives

$$h:\ \xi_{tt}^1=0, \tag{A.47}$$

$$h^0:\ \xi^1\frac{\partial v_n}{\partial t}+\xi^2\frac{\partial v_n}{\partial x}+\frac{2}{3}\left(2\xi_t^1-c_3\right)v_n=0. \tag{A.48}$$

From (A.47), we obtain

$$\xi^1=c_1+c_2t. \tag{A.49}$$

On substituting (A.44) and (A.49) into (A.48), we obtain

$$\left(c_1+c_2t\right)\frac{\partial v_n}{\partial t}+\left(c_4+c_3x\right)\frac{\partial v_n}{\partial x}=\frac{2}{3}\left(c_3-2c_2\right)v_n. \tag{A.50}$$

Finally, substituting (A.49) into (A.45) gives

$$\eta=\frac{1}{3}\left(2c_3-c_2\right)h. \tag{A.51}$$

The Lie point symmetry generator is therefore of the form

$$\begin{aligned}X &= \left(c_1+c_2t\right)\frac{\partial}{\partial t}+\left(c_4+c_3x\right)\frac{\partial}{\partial x}+\frac{1}{3}\left(2c_3-c_2\right)h\frac{\partial}{\partial h}\\ &= c_1X_1+c_2X_2+c_3X_3+c_4X_4,\end{aligned} \tag{A.52}$$

where

$$X_1 = \frac{\partial}{\partial t}, \tag{A.53}$$

$$X_2 = t\frac{\partial}{\partial t}-\frac{1}{3}h\frac{\partial}{\partial h}, \tag{A.54}$$

$$X_3 = x\frac{\partial}{\partial x}+\frac{2}{3}h\frac{\partial}{\partial h}, \tag{A.55}$$

$$X_4 = \frac{\partial}{\partial x}, \tag{A.56}$$

$$\tag{A.57}$$

provided that the leak-off velocity $v_n(x,t)$ satisfies the first order linear partial differential equation (A.50).

APPENDIX B

Derivation of the Lie point symmetries of a nonlinear second order ordinary differential equation

We derive the Lie point symmetry of the second order nonlinear differential equation

$$\Lambda \frac{d}{du}\left(F^3 \frac{dF}{du}\right) + A\frac{d}{du}(uF) + BF = 0, \tag{B.1}$$

where A, B are constants. We will require that $A \neq 0$ but we will see that there is no condition on B.

Equation (B.1) can be written in the form

$$H(u, F, F_u, F_{uu}) = 0, \tag{B.2}$$

where

$$H = \Lambda F^3 \frac{d^2F}{du^2} + 3\Lambda F^2 \left(\frac{dF}{du}\right)^2 + Au\frac{dF}{du} + (A+B)F. \tag{B.3}$$

The Lie point symmetry generator,

$$X = \xi(u, F)\frac{\partial}{\partial u} + \eta(u, F)\frac{\partial}{\partial F}, \tag{B.4}$$

of equation (B.1) is derived by solving the determining equation,

$$X^{[2]}H\Big|_{H=0} = 0, \tag{B.5}$$

for the unknown functions $\xi(u, F)$ and $\eta(u, F)$ where $X^{[2]}$, the second prolongation of X, is given by

$$X^{[2]} = X + \zeta_1(u, F, F_u)\frac{\partial}{\partial F_u} + \zeta_2(u, F, F_u, F_{uu})\frac{\partial}{\partial F_{uu}}, \tag{B.6}$$

where

$$\zeta_1 = D(\eta) - F_u D(\xi), \tag{B.7}$$

$$\zeta_2 = D(\zeta_1) - F_{uu} D(\xi) \tag{B.8}$$

and

$$D = \frac{d}{du} + F_u \frac{d}{dF} + F_{uu} \frac{d}{dF_u} + \cdots . \tag{B.9}$$

The expanded form of ζ_1 and ζ_2 is

$$\zeta_1 = \eta_u + F_u \left(\eta_F - \xi_u\right) - F_u^2 \xi_F, \tag{B.10}$$

$$\begin{aligned} \zeta_2 = {} & \eta_{uu} + 2\eta_{uF} F_u + \eta_{FF} F_u^2 + \eta_F F_{uu} - \xi_{uu} F_u \\ & -2F_u^2 \xi_{uF} - F_u^3 \xi_{FF} - 2\xi_u F_{uu} - 3\xi_F F_u F_{uu}. \end{aligned} \tag{B.11}$$

The determining equation (B.5) becomes

$$\xi(AF_u) + \eta\left(3\Lambda F^2 F_{uu} + 6\Lambda F F_u^2 + A + B\right) + \zeta_1\left(6\Lambda F^2 F_u + Au\right) + \zeta_2(\Lambda F^3)\Big|_{H=0} = 0. \tag{B.12}$$

We now substitute the expressions (B.10) and (B.11) for ζ_1 and ζ_2 into (B.12) to obtain the determining equation

$$\begin{aligned} & A\xi F_u + 3\eta\Lambda F^2 F_{uu} + 6\eta\Lambda F F_u^2 + (A+B)\eta + 6\Lambda F^2 F_u \eta_u + Au\eta_u \\ & +6\Lambda F^2 F_u^2 \eta_F + AuF_u\eta_F - 6\Lambda F^2 F_u^2 \xi_u - AuF_u\xi_u - 6\Lambda F^2 F_u^3 \xi_F \\ & -AuF_u^2\xi_F + \Lambda F^3\eta_{uu} + 2\Lambda F_u F^3 \eta_{uF} + \Lambda F^3 F_u^2 \eta_{FF} + \Lambda F^3 F_{uu}\eta_F - \Lambda F^3 F_u \xi_{uu} \\ & -2\Lambda F^3 F_u^2 \xi_{uF} - \Lambda F^3 F_u^3 \xi_{FF} - 3\Lambda F_u F_{uu} F^3 \xi_F - 2\Lambda F^3 F_{uu}\xi_u\Big|_{H=0} = 0. \end{aligned} \tag{B.13}$$

To impose the condition $H = 0$ on (B.13) we use (B.3) for H to give

$$\Lambda F^3 F_{uu} = -\left(3\Lambda F^2 F_u^2 + AuF_u + (A+B)F\right) \tag{B.14}$$

and replace F_{uu} in (B.13) by (B.14). The determining equation (B.13) then becomes

$$A\xi FF_u - 9\Lambda F^2F_u^2\eta - 3AuF_u\eta - 3(A+B)F\eta + 6\Lambda F^2F_u^2\eta + (A+B)F\eta$$

$$+6\Lambda F^3F_u\eta_u + AuF\eta_u + 6\Lambda F^3F_u^2\eta_F + AuFF_u\eta_F - 6\Lambda F^3F_u^2\xi_u$$

$$-AuFF_u\xi_u - 6\Lambda F^3F_u^3\xi_F - AuFF_u^2\xi_F + \Lambda F^4\eta_{uu} + 2\Lambda F_uF^4\eta_{uF}$$

$$+\Lambda F^4F_u^2\eta_{FF} - 3\Lambda F^3F_u^2\eta_F - AuFF_u\eta_F - (A+B)F^2\eta_F - \Lambda F^4F_u\xi_{uu}$$

$$-2\Lambda F^4F_u^2\xi_{uF} - \Lambda F^4F_u^3\xi_{FF} + 9\Lambda F^3F_u^3\xi_F + 3AuFF_u^2\xi_F$$

$$+3(A+B)F^2F_u\xi_F + 6\Lambda F^3F_u^2\xi_u + 2AuFF_u\xi_u + 2(A+B)F^2\xi_u = 0. \tag{B.15}$$

Since ξ and η do not depend on the derivatives of F, equation (B.15) is separated according to the coefficients of the derivatives of F. Setting each of these coefficients to zero, we obtain

$$F_u^3: \quad F\xi_{FF} - 3\xi_F = 0, \tag{B.16}$$

$$F_u^2: \quad -3\Lambda F\eta + \Lambda F^3\eta_{FF} + 3\Lambda F^2\eta_F + 2Au\xi_F - 2\Lambda F^3\xi_{uF} = 0, \tag{B.17}$$

$$F_u: \quad AF\xi - 3Au\eta + 6\Lambda F^3\eta_u + AuF\xi_u + 2\Lambda F^4\eta_{uF}$$
$$-\Lambda F^4\xi_{uu} + 3(A+B)F^2\xi_F = 0, \tag{B.18}$$

$$1: \quad -2(A+B)\eta + Au\eta_u + \Lambda F^3\eta_{uu} - (A+B)F\eta_F + 2(A+B)F\xi_u = 0. \tag{B.19}$$

Integrate (B.16) to obtain

$$\xi(u,F) = F^4G(u) + H(u). \tag{B.20}$$

Substitute (B.20) into (B.17) to obtain

$$\frac{\partial^2\eta}{\partial F^2} + \frac{3}{F}\frac{\partial\eta}{\partial F} - \frac{3}{F^2}\eta = 8F^3\frac{dG}{du} - \frac{8A}{\Lambda}uG(u), \tag{B.21}$$

which may be rewritten as

$$\frac{\partial^2\eta}{\partial F^2} + 3\frac{\partial}{\partial F}\left(\frac{\eta}{F}\right) = 8F^3\frac{dG}{du} - \frac{8A}{\Lambda}uG(u). \tag{B.22}$$

Integrating (B.22) once with respect to F gives

$$\frac{\partial\eta}{\partial F} + \frac{3}{F}\eta = 2\frac{dG}{du}F^4 - \frac{8A}{\Lambda}uG(u)F + 4D(u) \tag{B.23}$$

where $4D(u)$ is used instead of $D(u)$ to simplify the result for η. The integrating factor for (B.23) is F^3. Integrating (B.23) with respect to F gives

$$\eta(u,F) = \frac{1}{4}\frac{dG}{du}F^5 - \frac{8}{5\Lambda}AuG(u)F^2 + D(u)F + \frac{E(u)}{F^3}. \tag{B.24}$$

Substitute (B.20) and (B.24) into (B.18) and separate the resulting equation according to powers of F. This gives

$$F^8: \ \frac{d^2G}{du^2} = 0, \tag{B.25}$$

$$F^5: \ \frac{21}{4}Au\frac{dG}{du} + (A-4B)\,G(u) = 0, \tag{B.26}$$

$$F^4: \ \frac{d^2H}{du^2} - 8\frac{dD}{du} = 0, \tag{B.27}$$

$$F^2: \ A^2u^2G(u) = 0, \tag{B.28}$$

$$F: \ A\left(u\frac{dH}{du} + H(u) - 3uD(u)\right) = 0, \tag{B.29}$$

$$F^{-3}: \ AuE(u) = 0, \tag{B.30}$$

$$1: \ 0 = 0. \tag{B.31}$$

Assume that $A \neq 0$. Equations (B.28) and (B.30) then gives

$$G(u) = 0, \tag{B.32}$$

$$E(u) = 0. \tag{B.33}$$

When (B.32) and (B.33) are substituted into (B.20) and (B.24), we obtain

$$\xi(u,F) = H(u), \tag{B.34}$$

$$\eta(u,F) = D(u)F, \tag{B.35}$$

subject to the conditions (B.27) and (B.29) which are

$$\frac{d^2H}{du^2} - 8\frac{dD}{du} = 0, \tag{B.36}$$

$$u\frac{dH}{du} + H(u) - 3uD(u) = 0. \tag{B.37}$$

Equations (B.25) and (B.26) are identically satisfied by (B.32). Substituting (B.34) and (B.35) into (B.19), we obtain

$$\Lambda F^4 \frac{d^2D}{du^2} + AuF\frac{dD}{du} - 3(A+B)FD(u) + 2(A+B)F\frac{dH}{du} = 0. \tag{B.38}$$

We separate (B.38) according to powers of F :

$$F^4 : \frac{d^2D}{du^2} = 0, \tag{B.39}$$

$$F : Au\frac{dD}{du} - 3(A+B)D(u) + 2(A+B)\frac{dH}{du} = 0. \tag{B.40}$$

Integrate (B.39) to obtain

$$D = d_1u + d_2, \tag{B.41}$$

where d_1 and d_2 are constants. We substitute (B.41) into (B.36) and on integrating we have

$$H = 4d_1u^2 + h_1u + h_2. \tag{B.42}$$

where h_1 and h_2 are constants. We now substitute (B.41) and (B.42) into (B.37) and (B.40) to obtain

$$9d_1u^2 + (2h_1 - 3d_2)u + h_2 = 0, \tag{B.43}$$

$$(14Ad_1 + 13Bd_1)\,u + 2h_1(A+B) - 3d_2(A+B) = 0. \tag{B.44}$$

We separate (B.43) according to powers of u to obtain

$$u^2 : \ d_1 = 0, \tag{B.45}$$

$$u : \ 2h_1 - 3d_2 = 0, \tag{B.46}$$

$$1 : \ h_2 = 0. \tag{B.47}$$

Equation (B.44) reduces to

$$(A+B)(2h_1 - 3d_2) = 0 \tag{B.48}$$

which is identically satisfied. From (B.46), we obtain

$$h_1 = \frac{3}{2}d_2. \tag{B.49}$$

Hence (B.34) and (B.35) become

$$\xi(u,F)=\frac{3}{2}ud_2, \qquad \eta(u,F)=d_2F \tag{B.50}$$

and therefore

$$X=\frac{d_2}{2}\left(3u\frac{\partial}{\partial u}+2F\frac{\partial}{\partial F}\right).$$

Hence if $A\neq 0$, equation (B.1) admits one Lie point symmetry generator

$$X=3u\frac{\partial}{\partial u}+2F\frac{\partial}{\partial F}. \tag{B.51}$$

Bibliography

[1] D.A. Spence and D.L. Turcotte. Magma-driven propagation of cracks. *Journal of Geophysics*, 90:575–580, 1985.

[2] Birch Francis, editor. *Handbook of Physical Constants*. Number 36. Jan. 31 1942. GSA Special Paper.

[3] M.K. Hubbert and D.G. Willis. Mechanics of Hydraulic Fracturing. *Trans AIME*, 210:153, 1957.

[4] J.C. Jaeger, N.G.W. Cook, and R.W. Zimmerman. *Fundamentals of Rock Mechanics*. Blackwell Publishing, Oxford, fourth edition, 2007.

[5] A.D. Fitt, D.P. Mason, and E.A. Moss. Group invariant solution for a pre-existing fluid-driven fracture in impermeable rock. *Zeitschrift fur Angewandte Mathematik und Physik (ZAMP)*, 58:1049–1067, 2007.

[6] T. Perkins and L. Kern. Widths of hydraulic fractures. *Journal of Petroleum Technology*, 222:937–949, 1961.

[7] R. Nordgren. Propagation of vertical hydraulic fractures. *Journal of Petroleum Technology*, 253:306–314, 1972.

[8] S. Khristianovic and Y. Zheltov. Formation of vertical fractures by means of highly viscous fluids. In *4th World Petroleum Congress*, pages 579–586, Rome, 1955.

[9] S.H. Advani and J.K. Lee. Three-dimensional modelling of hydraulic fractures in layered media: Finite element formulations. *ASME J. Energy Res. Technol*, 112:1–18, 1990.

[10] J.I. Adachi, E. Siebrits, A.P. Pierce, and J Desroches. Computer simulation of hydraulic fractures. *International Journal of Rock Mechanics and Mining Sciences*, 44:739–757, 2007.

[11] I.N. Sneddon and H.A. Elliot. The opening of a Griffith crack under internal pressure. *Quart. App. Math.*, 4:262–267, 1946.

[12] J. Geertsma and F. de Klerk. A rapid method of predicting width and extent of hydraulic induced fractures. *Journal of Petroleum Technology*, 246:1571–1581, 1969.

[13] D.A. Spence and P.W. Sharp. Self similar solution for elasto-hydrodynamic cavity flow. *Proc. R. Soc. London, Ser. A*, 400:289–313, 1985.

[14] B. Cotterell and J.R. Rice. Slightly curved or kinked cracks. *International Journal of Fracture*, 16:155–169, 1980.

[15] P.A. Martin. Perturbed cracks in two dimensions:An integral-equation approach. *International Journal of Fracture*, 104:317–327, 2000.

[16] P.A. Martin. On wrinkled penny-shaped cracks. *Journal of Mechanics and Physics of Solids*, 49:1481–1495, 2001.

[17] D.J. Acheson. *Elementary Fluid Dynamics*. Clarendon Press, Oxford, 1990.

[18] N.H. Ibragimov and R.L. Anderson. One-parameter transformation groups. In N.H. Ibragimov, editor, *CRC Handbook of Lie Group Analysis of Differential Equations*, volume 1:Symmetries, Exact Solutions and Conservation Laws, pages 7–14. CRC Press, Boca Raton, 1994.

[19] N.H. Ibragimov. *Elementary Lie Group Analysis and Ordinary Differential Equations*, volume 4. John Wiley and Sons, Chichester, 1999.

[20] G. Bluman and J. Cole. *Similarity Methods for Differential Equations*. Springer-Verlag, New York, 1974.

[21] G. Bluman and S. Kumei. *Symmetries and Differential Equations*. Springer-Verlag, New York, 1989.

[22] G. Bluman and S. Anco. *Symmetries and Integration Methods for Differential Equations*. Springer-Verlag, New York, 2002.

[23] D.A. Mendelsohn. A review of hydraulic fracture modelling - Part I: General concepts, 2D models and motivation for 3D modelling. *ASME J. Energy Res. Tech*, 106:369–376, 1984.

[24] R.P. Gillespie. *Integration*. Oliver and Boyd, Edinburgh, 1959.

[25] W.F. Ames. Applications of group theory in computation - a survey. In N.H. Ibragimov, editor, *CRC Handbook of Lie Group Analysis of Differential Equations*, volume 1:Symmetries, Exact Solutions and Conservation Laws, pages 350–355. CRC Press, Boca Raton, 1994.

[26] M.S. Klamkin. On the transformation of a class of boundary value problems into initial value problems for ordinary differential equations. *SIAM Review*, 4:43–47, 1962.

[27] M.S. Klamkin. Transformation of boundary value problems into initial value problems. *J. Math. Anal. Applic*, 32:308–330, 1970.

[28] T.Y. Na. Transforming boundary conditions into initial conditions for ordinary differential equations. *SIAM Rev*, 10:85–87, 1968.

[29] T.Y. Na. Further extensions on transforming from boundary value to initial value problems. *SIAM Rev*, 10:85–87, 1968.